THEORETICAL INVESTIGATION OF VARIABLE INFRA-RED EMISSION BY COSMIC DUST SOURCES

by

MICHAEL F. BODE B.Sc.

A thesis submitted to the University of Keele
for the Degree of Doctor of Philosophy

Department of Physics,
University of Keele,
Keele,
Staffordshire.

December 1979

TO MY PARENTS

Acknowledgements

The author would like to express his grateful thanks to:-

Dr. A. Evans for his guidance and enthusiastic encouragement throughout the course of the work described herein.

Dr. R. C. Maddison for his supervision during the early stages of this work.

Professor W. Fuller for his advice and encouragement and for the provision of office space and facilities.

Drs. P. Collis and F. Grundy and the staff of the Computer Centre for their guidance in the early stages of the computational work.

Messrs. N. Banks and S. Cartledge for their help in the preparation of the figures.

Mr. M. Daniels for his photographic copying of some of the figures taken from the literature.

Mrs. S. Cooper for her accurate typing of this thesis.

Mrs. S. Jackson and Mrs. E. Durant for their assistance with secretarial work.

All the staff of the Physics department and others of the University of Keele in general for their many useful discussions.

The University of Keele for the provision of a Research Studentship, travel funds and computer time.

The referees of our published and submitted papers, Dr. E. L. Wright and Professor J. M. Greenberg as well as anonymous referees of Bode and Evans (1979b) and some of the work outlined in Chapter 6.

My parents and family for their foresight and forebearance.

Abstract

Light travel time considerations are applied to the development of the infra-red flux from a cloud of dust grains surrounding a variable cosmic source of heating radiation. The properties of individual grains are explored, and the equation of radiative transfer is solved for the case of a spherically symmetric thermal source observed at a large distance. Models of specific novae are developed from the standpoint of grains existing prior to nova outburst. The situation in which a variable primary source is surrounded by a disc of dust grains is explored, as is that in which an expanding central cavity is formed by grain evaporation. In both cases qualitative comparisons are made with observations of cosmic sources of variable thermal emission from dust grains.

"Empodocles ... says that the light from the Sun reaches the intervening space before it reaches the eye ... For when a thing is moved it is moved from one place to another and hence a certain time must elapse during which it is being moved ... But every period is divisible, therefore there was a time when the ray was not yet seen but was being transmitted through the medium"

Aristotle, De Sensu, 6, 446a 25-b2

CONTENTS

CHAPTER 1

Introduction

1.1.1 General Summary

Over the last two decades observational astronomy has benefitted from the broadening of the range of wavelengths accessible to observation and among the 'new' wavelengths to be explored were those of the infra-red. Infra-red astronomy has since blossomed to become a major component of the whole astrophysical information-gathering machine. It is particularly well suited to the study of thermal emission from cosmic dust grains and it has revealed that many astrophysical objects have dust associated with them by virtue of their strong thermal infra-red emission.

Many thermally emitting infra-red objects are intrinsically variable both at short wavelengths(from the central source) and hence also at long wavelengths (the dust shell). However it appears that little theoretical work has been previously undertaken into this situation. This work seeks to develop the theory of thermal emission from dust grains surrounding a variable high frequency source.

The problem which seemed at first sight to be straighforward turns out to be complex. This is because emission at any given instant will be seen to be different for observers depending on their locations relative to the dust shell. Due to finite light travel times the observed emitting region will contain grains heated by various phases of the central source light curve. These phase effects will depend upon the relative positions of the central source, grains, and observer.

It was soon realised that any detailed work would have to take into account the dependence of the absorption and scattering efficiencies of grains on their size, shape, composition, temperature etc.. However in order to make the analysis at all feasible many reasonable assumptions

both about the grains themselves and the dust clouds in which they are situated had to be made. Generally therefore we deal with spherical graphite grains in clouds which are symmetrically positioned about the central object.

Although, as has been stated above, many types of object may be of interest, this work concentrates on novae for which it is known that thermal emission from grains is associated with the sudden rise in luminosity of the central object.

Our models differ from those described by other authors in that the late development of a substantial thermal excess is attributed to emission from grains extant before the concurrent outburst.

Application of the work described herein to other astrophysical objects has been briefly explored although the detail is not as great as for novae. However this work does include very general models of sources similar to certain Seyfert galaxies and Mira variables.

It is hoped that this work and subsequent research stemming directly or indirectly from it will aid our understanding of cosmic dust sources and processes involved in their variable thermal emission.

1.2.1 Detailed Summary

Observational data on objects which possibly comprise a variable central source of high frequency radiation surrounded by a distribution of dust grains are given in chapter 2. As with much of this work the main emphasis is on the observations made of classical novae with late developing thermal excesses. The three main examples of this type of nova with which we are concerned are Novae Serpentis 1970, Aquilae 1975 and Vulpeculae 1976. Other classical novae, particularly Nova Cygni 1975, are described in less detail as are recurrent novae, Mira variables, Seyfert galaxies and a few other variable infra-red sources of interest.

Chapter 3 describes the theoretical work which has previously been carried out in fields directly related to this work. The first sections of this chapter deal briefly with the scattering and absorption of radiation by dust grains and the processes of formation, growth and destruction of those grains. We then proceed to consider grain temperature and radiation transfer; the geometry of sources and phase relationships within sources and the theoretical background on classical novae. The work on grain formation processes which we describe will be of particular importance in relation to chapter 5. Finally we briefly detail the various methods of determining theoretically certain parameters of the dust shells of thermal sources.

In chapter 4 the basic theoretical background to the problem is explored. Later specific and detailed models are based upon this chapter, which begins with a discussion of the derivation of graphite grain temperatures.

It will become apparent that the analysis of reaction time of grains to changes in the incident high frequency flux as described here is important when the observed source geometry is considered in subsequent sections.

Finally in chapter 4 the equation of transfer is solved analytically for one simple case and numerically for more general situations, the former serving as a check on the latter. This principle of checking numerical solutions against analytical solutions under limiting conditions is applied several times during this work.

Using the numerical method of solution general models of various cosmic sources are then discussed. Results for light curves, spectra, surface brightness variations, observed temperatures, angular diameters and phase relationships are given.

In chapter 5 the principles developed in chapter 4 are applied to classical novae which have late developing thermal infra-red excesses. After discussing previous theoretical work we incorporate the development of the emission from the central object into the models of emission from the dust shell. This results in relatively good fits of theoretical results to observations. The chapter is concluded with a section on predictions for possible observational verification.

Up to chapter 6 the dust shell is generally assumed to consist of a sphere with an evacuated central cavity. Here a disc of grains, again with a central cavity, is assumed to surround a variable central source. Development of this model enables us to give a qualitative explanation of the infra-red behaviour of Nova Cygni 1975.

Complications in accurately determining the behaviour of a thermal source whose grains are subject to evaporation are discussed in chapter 7. Here the evaporation rate of single isolated grains is studied and applied to the observed development of the central cavity. Again it is shown that observed cavity development as well as flux are dependent upon the relative positions of source and observer. A qualitative comparison with the infra-red behaviour of Nova Vulpeculae 1976 is attempted.

Chapter 8 contains several suggestions for continuation and

furtherance of the work begun here. It also includes a general discussion and conclusion to the whole.

The four appendices contain details of the numerical solution of the equation of transfer computer programme; the algebraic notation used throughout; some independent theoretical work on the determination of the value of the cosmological deceleration parameter, q_0, and the author's published papers.

CHAPTER 2

Observational Data

2.1.1 General Introduction

One aim of this work is to apply the general theoretical models derived largely in chapter 4 to actual physical situations. As will be discussed in the following subsection there are several astro-physical objects which fulfil the conditions of ultraviolet and infra-red variability outlined previously in chapter 1.

The major parts of this chapter, chapter 5 and chapter 6 are devoted to a discussion of novae in which there is evidence that the central eruptive object is associated at some time in the outburst with a nearby distribution of dust grains.

2.1.2 Objects of Interest

There appear to be many objects both galactic and extragalactic in which a variable high frequency source is surrounded by, or situated near to a dust grain distribution. Heating of the grains by photons from the primary then causes them to emit in the infra-red. If the primary object is variable the resulting infra-red flux may also be variable but the relative variabilities are dependent upon several parameters of both the primary source and the dust cloud.

The galaxy contains several objects of interest. For example T Tauri stars very often have variable ultraviolet and thermal infra-red excesses (see e.g. Harvel, 1974 and references therein). Carbon stars have long been known to possess infra-red excesses and they may be sites of extensive grain formation (Hoyle and Wickramasinghe, 1962). They are also intrinsically variable at all wavelengths. Observations of the obscured carbon star CRL 3099 by Gehrz *et al*. (1978) have shown extreme infra-red variability in this object.

Mira variables appear to often have associated dust shells. Mira itself has been observed at wavelengths from 5 to 12.5 μm by McCarthy *et al*. (1978) for example. Here the periodic variation at short wavelengths by the central star is mirrored in a phase shifted variation at infra-red wavelengths which presumably originates in the circumstellar dust shell.

Observations of late type Wolf-Rayet stars have shown many of them to be surrounded by extensive dust shells (e.g. Cohen *et al*., 1975). Williams *et al*. (1978) studied the Wolf-Rayet binary HD193793 and observed infra-red variability which led to the conclusion that extensive grain condensation had taken place.

Other rarer and more difficult to classify objects have been observed. For example the variable HM Sge has been observed to brighten markedly from $m_v \sim +16$ to $m_v \sim +12$in less than 6 months (Ciatti *et al*.

1977). It has also shown the presence of an optically thin dust shell at a temperature of ∿ 1000°K according to Puetter et al. (1978). These observations together with those of Davidson et al. (1978) suggest that HM Sge is similar to the variable symbiotic star V1016 Cyg and that like its counterpart it is also variable at infra-red wavelengths.

The class of galactic objects with which we are most concerned in this work is novae. Both classical and recurrent novae are of course rapidly variable at short wavelengths during outburst. Observations in the infra-red have shown that variability occurs for classical novae due to heating of dust grains near the nova system and that certain recurrent novae display a thermal infra-red excess between outbursts. (see sections 2.2 and 2.3, chapter 5 and references therein).

Amongst extragalactic objects the most interesting from our point of view are Seyfert galaxies. Their infra-red spectra contain 3 components which can be attributed to the emission of the stellar members of the galaxy; a thermal component from heated dust and a non-thermal, power-law spectral component (see for example, Neugebauer, 1978).

Seyfert galaxies are often variable at U,B and V wavelengths in their nuclear regions and observation at infra-red wavelengths has also uncovered variability on timescales of a month or more. The infra-red variability has been observed in some Seyferts to be out of step with the shorter wavelength flux changes. (see for example, Penston et al., 1974). It now appears that in the case of the Seyfert galaxy NGC 1068 at least, the nuclear infra-red flux can be mainly attributed to thermal emission by dust grains (see Jones et al., 1977, and references therein).

2.2.1 Classical Novae

Novae are of great interest in this work for several reasons. For example they are intrinsically variable at all wavelengths. Variability typically over a range of 10 - 12 magnitudes in the V-band

from pre-nova to light maximum, and subsequent return to minimum light at the post-nova stage is often observed.

Novae are also relatively common with an estimated occurrence rate of 26 $\pm$ 4 per year in M31 and probably a similar number in our own Galaxy therefore (Arp, 1956). Of these Galactic novae, only roughly 10% are observed - mainly because these objects belong to the disc population of the Galaxy and are therefore subject to heavy obscuration.

The most important reasons for our interest in novae are that they often show evidence of dust association (see e.g. Malakpour, 1976) and in some cases there is a rapid rise in the infra-red flux some time after the visual light maximum (see e.g. Geisel et al., 1970; Vrba et al., 1977; Ney and Hatfield, 1978 etc.).

Nova light curves vary considerably in individual detail if we plot them on the same extended time scale. If, however, we compressed the scales to overlay the curves we would find that they are qualitatively similar. Figure (2.1) shows the essential features of the nova light curve (from McLaughlin, 1960). The dotted line allows for the alternative behaviour during the transition stage between absorption and emission line spectra.

The spectral development of novae can also be generalised. The stages of this development coincide very often with changes in the V curve. Following McLaughlin (1960) the development of typical novae at essentially visual wavelengths can be categorised as in table (2.1).

Knowledge of the spectral development of a nova is obviously essential if we are to determine conditions within the ejecta and if, as in the case of nova Aquilae 1975, we are unsure of the date of outburst.

From studies of novae in M31, Arp (1956) recognised that the absolute magnitude at peak visual luminosity is related to the rate of decline from peak. His idea was developed by Payne-Gaposchkin (1957)

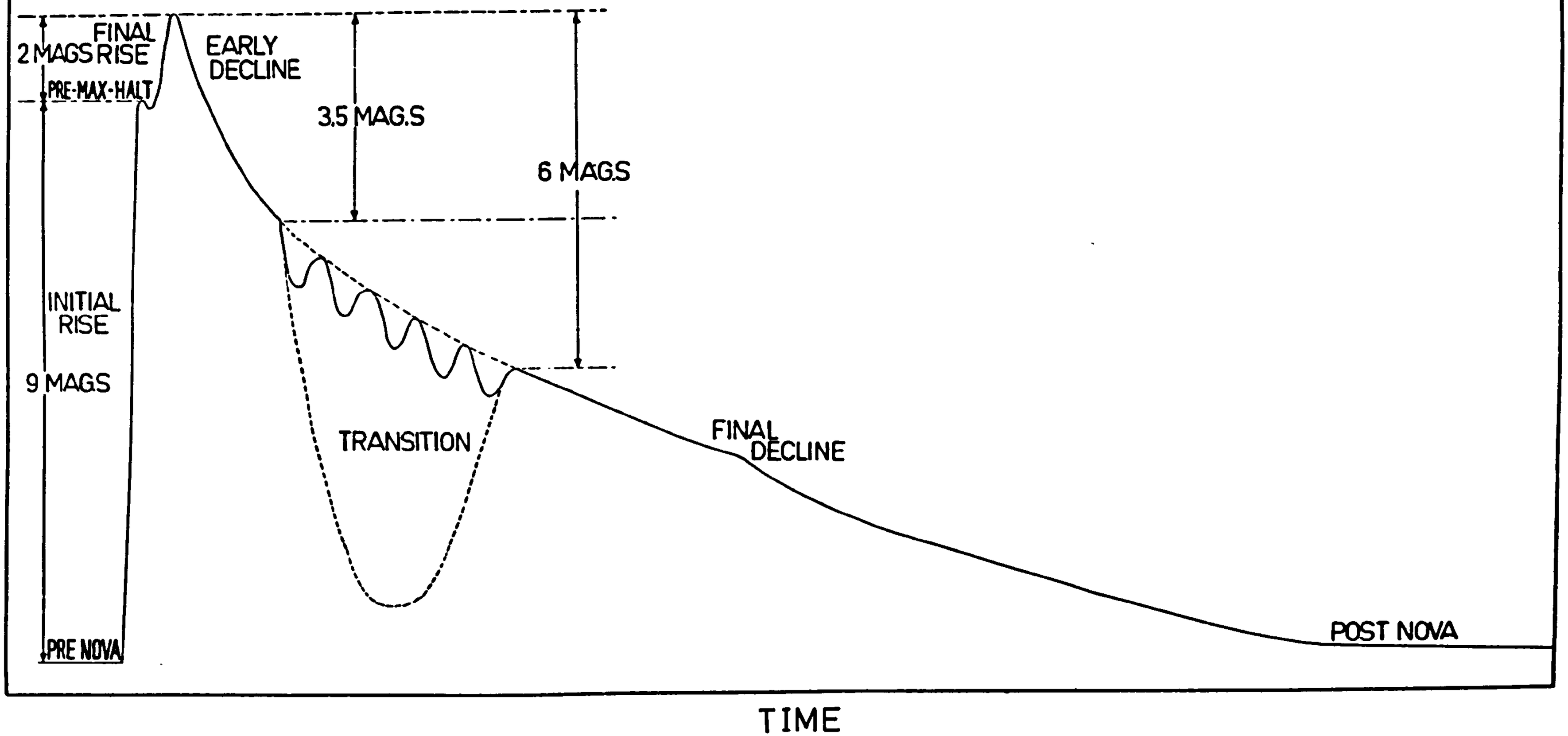

Figure (21) Schematic nova light curve adapted from McLaughlin (1960) by Payne-Gaposchkin (1957). Alternative behaviour during transition is shown as dotted lines.

Text cut off in original

Table 2.1

Generalised Evolutionary Stages of a Classical Nova

Light Curve	Prominent Spectral Systems	Mean Δm From Peak	Emission Lines	Absorption Lines	General Remarks
Prenova	-	-	-	-	Little observational evidence. O-B type stars generally indicated.
Initial Rise	-	-	No Strong Emission	Diffuse Absorption	Rapid rise to ∿2 mag. below max. Type A-F.
Final Rise	-	-	"	Stronger, better defined	Spectrum changes to a later type.
Maximum	-	0.0	Only Hα visible	"	Strengthening continuum. Spectrum similar to A-K supergiant.
Early Decline	Principal Absorption Diffuse-Enhanced Absorption Orion Absorption	0.6 1.2 2.1	CaII, Hα, NaI, FeII	"	Principal spectrum associated with bulk of ejected mass. Diffuse enhanced velocity ∿ 2x principal velocity. Orion velocity $\gtrsim$ Diffuse-enhanced velocity.
Transition (3 often Observed variants shown in figure 2.1)	Principal Absorption '4640' Stage	3.0 3.5 4	 Emission at λ4640 λ4100 Forbidden lines. [NeII] at λ6548, λ6584 strong.	Hydrogen lines only	Sudden change from stellar to nebular spectrum. Emission dominates. Excitation increases with time.
Final Decline	Nebular (Principal)	4-11			Excitation continues to increase. Spectrum Resembles Planetary Nebula.
Postnova		∿ 11	Emission lines disappear		Only continuum of hot O-B type remains.

and presented in its generally accepted form by McLaughlin (1960) as

$$M_v \sim -11.75 + 2.5 \log t_{3,v} \qquad (2.1)$$

where M_v is the absolute visual magnitude and $t_{3,v}$ is the time in days for the visual flux to drop by 3 magnitudes.

2.2.2 Nova Serpentis 1970

Nova Serpentis 1970 is possibly one of the most extensively studied nova events. It was also one of the first to be subjected to very detailed study at infra-red wavelengths. The data presented here are drawn from observations in the ultra-violet, visible, infra-red and radio wavebands over extended periods of time.

The nova was discovered on 1970, February 13 (Hirose, 1970) and reached visual maximum on February 18.46. Subsequently the nova declined steadily in the V-band at a rate of approximately 0.048 mag/day (Borra and Anderson, 1970) until approximately April 17. Here the nova entered the transition region and faded almost exponentially. By 1970 August however the visual luminosity had again increased to a fairly constant level around 6 magnitudes below maximum light. Figure (2.2) is a plot of the UBV data given by Borra and Anderson (1970) drawn from observations made between February and October 1970.

It can clearly be seen from Figure (2.2) that Nova Serpentis became progressively bluer from the first observations until approximately day 60 (i.e. both B-V and U-B decrease). After day 60 however B-V begins to increase again. Confirmation of this fact comes from independent observations made by Burkhead *et al.* (1971). The cause of this anomalous increase is explained by Borra and Anderson (1970) as being the emergence of emission lines in the V-band, as is borne out by their spectral studies.

As B-V increases, U-B continues to decrease to around day 100 from outburst. Borra and Anderson (1970) see this as the result of a

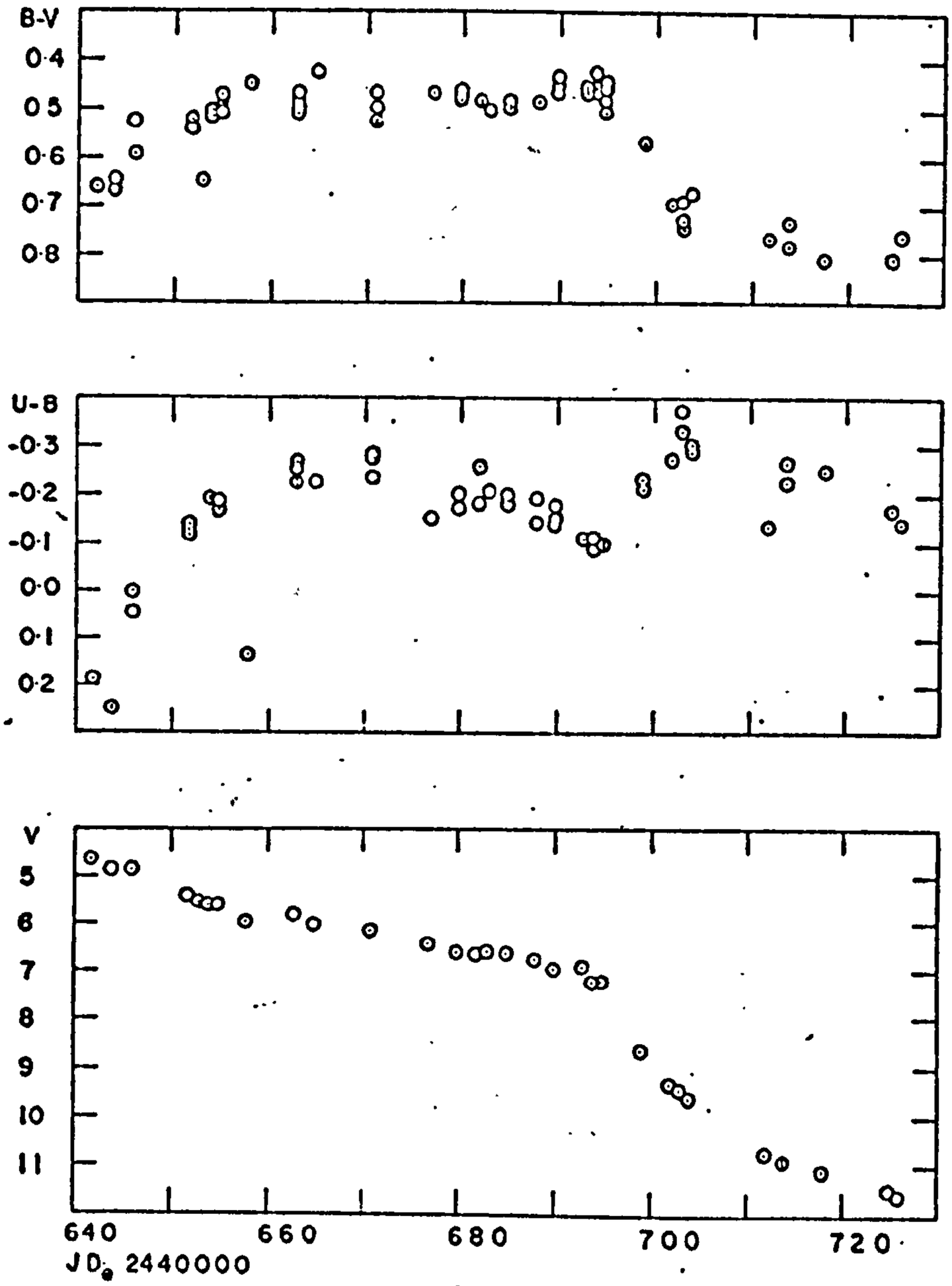

Figure (2.2) UBV observations of Nova Serpentis 1970 from Borra and Andersen (1970). Note the slope break in the V curve at transition and the behaviour of (B-V) and (U-B) at this time.

general fading of the continuum affecting B and V more than U. This suggests that the source is getting progressively bluer (i.e. hotter) with time (an observation consistent with those made at ultra-violet wavelengths by Gallagher and Code, 1974).

Spectra of Nova Serpentis 1970 were obtained by Anderson et al. (1971) and Grygar et al. (1971). The former made observations during the early decline (February/March), just before transition (April 15.4), during the transition minimum (May 29.4) and in the nebular stage (August/September).

The spectrum changed in accordance with that expected for a nova of Serpentis 1970's speed class and light curve. The absorption spectrum of the early decline had given way by May 29.4 to an almost purely emission spectrum with an extremely weak underlying continuum. This latter observation clearly showed the dominance of the [FeII] emission of the so-called η-Carinae stage. By August 13.1 the spectrum was that of emission lines only with [OIII] and helium lines being particularly prominent.

The measured absorption line velocities of February/March 1970 show that the material associated with the principal spectrum can be ascribed a radial velocity $v_p \sim 700$ kms^{-1} whereas that associated with the diffuse enhanced spectrum can be ascribed much higher velocities with a greater scatter from $v_{d.e.} \simeq 1250$ to $v_{d.e.} \simeq 1942$ kms^{-1}.

Grygar et al. (1971) obtained four spectrograms of high dispersion in the transition stage of Nova Serpentis 1970. They noted that the visual light curve slope change of April 16/17 marked the start of rapid changes in the spectral appearance of the nova.

The plates taken on May 9, May 23 and June 13 showed spectra consistent with the findings of Anderson et al. (1971), namely that the nova spectrum was dominated by emission lines and had a very weak continuum. By June 13 the [OIII] emission lines had become dominant

with the blue shifted component much stronger than the red shifted (as was the case with many of the observed lines).

The observed radial velocities of the emission lines were generally less than the earlier spectra of Anderson et al., with typical values of $\simeq 500$ kms^{-1}.

The results of the search for the pre-nova star are given by Burkhead and Seeds (1970). They identified it with an object having Galactic co-ordinates $l^{II} = 32.4^{o}$, $b^{II} = +5.8^{o}$ and magnitude $M_{v} = 16.1$. Following the generally held assumption that all pre-novae are hot, blue stars, Borra and Anderson (1970) conclude that Nova Serpentis 1970 has a large colour excess ($E_{B-V} \simeq 1$). This again agrees with Gallagher and Code's (1974) conclusions and is a subject we will return to below.

The ultra-violet photometry of Nova Serpentis 1970 was carried out by Gallagher and Code using the O-A-O 2 satellite. Their observations covered the period from maximum visible light until approximately the sixtieth day, during which time measurements were made at a number of wavelengths from 1300 Å to 4200 Å (see Figure (2.3)).

It can clearly be seen from Figure (2.3) that at short wavelengths the light curves are very different from those at the longer UBV wavelengths. It appears that the shorter the wavelength the longer it takes the flux at that wavelength to reach a maximum value. Indeed, in the case of the 1550 Å observations (the shortest reliable wavelength in the opinion of Gallagher and Code) there is a dramatic rise in flux around 40 to 50 days. This coupled with the small increase at around 20 days makes this wavelength particularly interesting when compared with the infra-red behaviour of the object.

The increasing delay in the time of maximum flux with decreasing wavelength can perhaps be best explained in terms of the gradual 'uncovering' of the hot central object as the opacity of the ejected matter decreases with expansion (Gallagher and Code, 1974). The peak

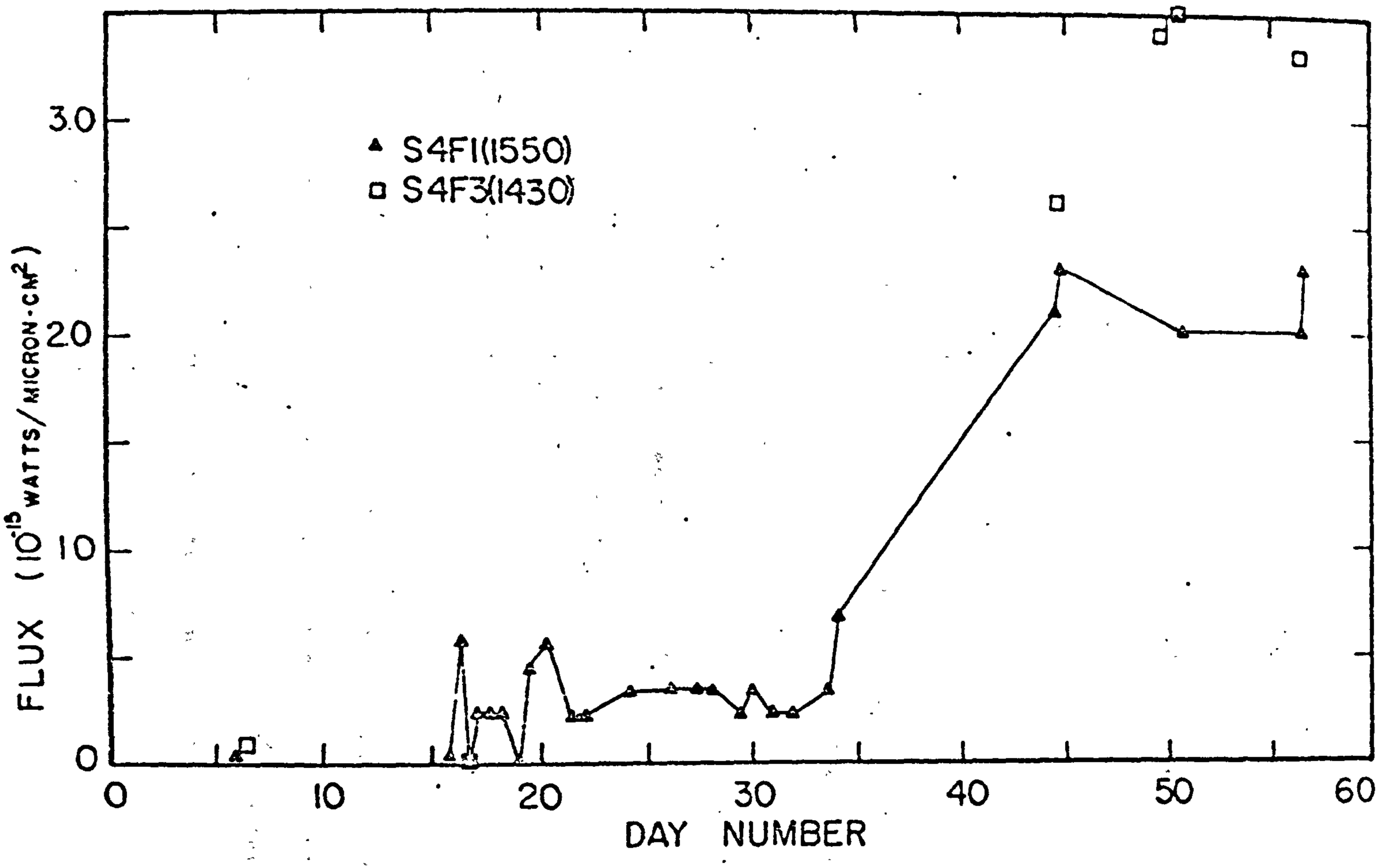

Figure (2.3) Observed flux at 1550Å and 1430Å from reductions made by Gallagher and Code (1974) of O-A-O 2 data for Nova Serpentis 1970.

of emission thus moves to shorter wavelengths with time (see chapter 3).

A major difficulty encountered in ultra-violet observation is that of making reasonable allowance for interstellar (and circumstellar) extinction. Gallagher and Code (1974) found that the colour excess $E_{B-V} \approx 0.8$. Code (1972) suggested that this rather large excess, if explained by the presence of a 'nearby' dust cloud, could also explain the infra-red emission which developed after about 45 days.

Hutchings and Fisher (1973) detected the presence of local reddening in the transition phase of Nova Serpentis 1970 but any change in reddening during the period of their observations is only marginally supported. Malakpour (1976) seemed to find a change in reddening during this period from study of Balmer decrement. Again however the change was small and his conclusion was that grains existed prior to the outburst and grew slightly when the ejecta of the current explosion encountered them.

Zellner (1971) in his studies of the wavelength dependence of the polsarisation of the light from Nova Serpentis 1970 found that the polarisation associated with this object could be explained by the existence of a circumstellar cloud consisting of 0.1μmiron grains (this is acknowledged by Zellner as not being the only possibility however). The observations from which these conclusions were drawn were made during the early stages of the evolution of the nova and therefore provide evidence that grains existed near the nova long before the infra-red rise. The absence of any great increase in polarisation when the infra-red does begin to rise is explained in terms of grains growing to large sizes ($\gtrsim$ 1μm) with the pre-existing grains as condensation nuclei.

If $E_{B-V} \approx 0.8$ is assumed then the corrected fluxes at ultra-violet wavelengths can be derived. Figure (2.4) shows the energy spectra given by Gallagher and Code (1974) for this assumed colour excess. It

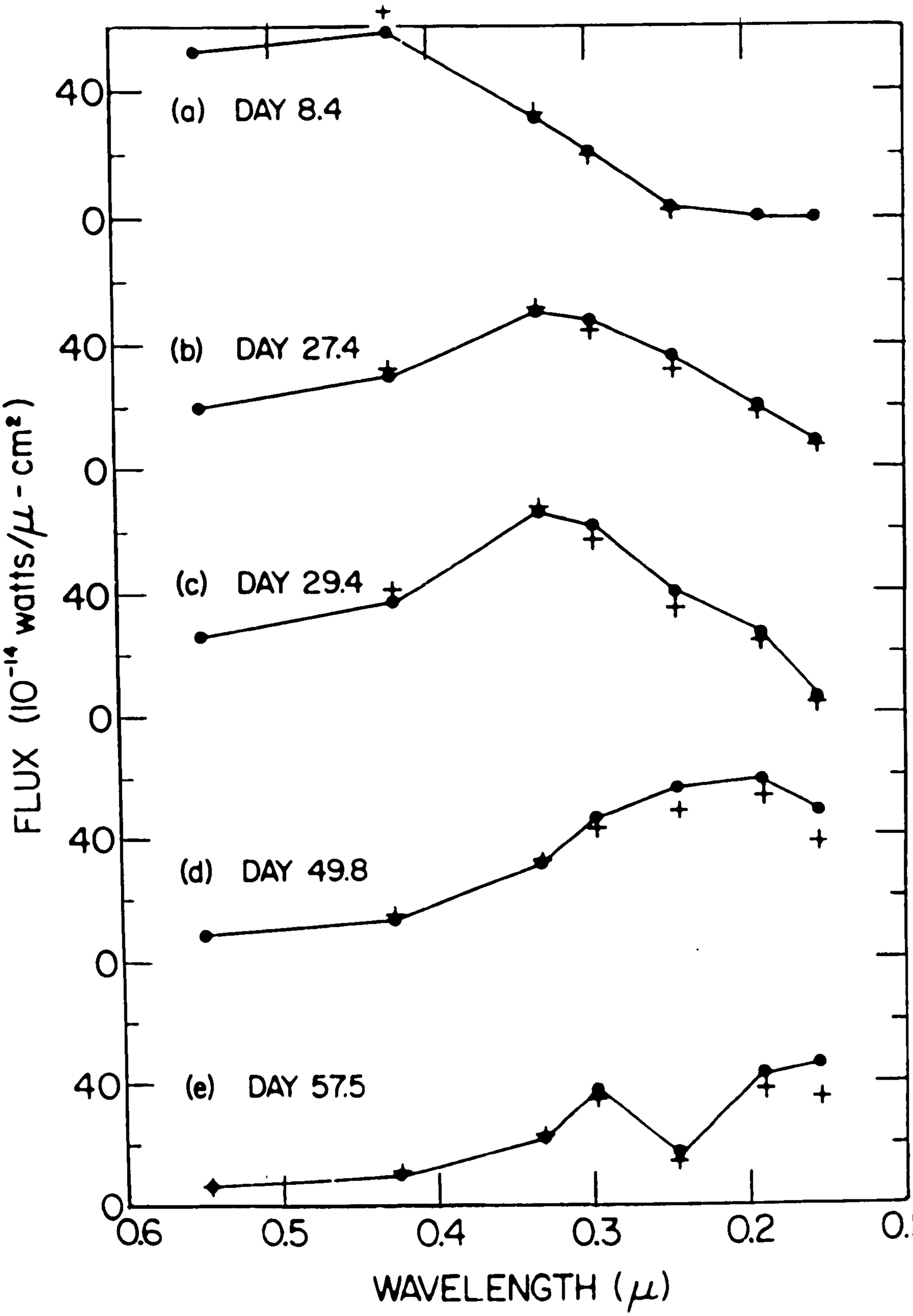

Figure (2.4) The observed variation in spectral distribution with time for Nova Serpentis 1970 (from Gallagher and Code, 1974). Note that the dotted points are for an assumed extinction that is slightly different from that for the points indentified by crosses.

can be seen from Figure (2.4) that the total integrated flux appears to remain almost constant for at least the first 50 days. However the peak of emission moves steadily blueward with time. This situation is of course altered if the assumed E_{B-V} is changed. Indeed Friedjung (1977) suggests that the luminosity decreased slightly over the first 30 days whilst the temperature rose from 5200°K to 9200°K; he notes however the sensitivity of these results to interstellar extinction.

Infra-red observations of Nova Serpentis 1970 began on J.D. 2440651, 19 days after outburst and were continued by Geisel et al. (1970) for approximately 90 days thereafter. Observations were also made at 68, 69 and 70 days by Hyland and Neugebauer (1970). Data at 2.2, 3.4, 5, 10 and 22μm(see Figure (2.5)) all show that a dramatic rise in infra-red luminosity occurred at about day 50. From that point on the infra-red luminosity continued to increase until at least day 111. A study of the spectra confirms that as time progresses the peak wavelength shifts further into the infra-red. If the spectra are taken as approximately black body in form then a temperature of $\sim 900^{o}$K can be ascribed to the source.

From knowledge of the maximum energy flux (i.e. $(\lambda F_{\lambda})_{max}$) together with the black body temperature, T_{BB}, the angular diameter of a black body, Θ_{BB}, can be found using the relationship (Ney and Hatfield, 1978)

$$\Theta_{BB}'' = 2 \times 10^{14} \, (\lambda F_{\lambda})_{max}^{\frac{1}{2}} \, T_{BB}^{-2} \qquad (2.2)$$

Equation (2.2) was used by Geisel et al. (1970) in the calculation of the black body angular diameter of Nova Serpentis 1970 and a figure of 0.07" was arrived at. As we shall see below this is a gross underestimate for an optically thin source and is only approximately true even in the optically thick case unless the individual grains are perfect black bodies forming an effectively 'solid' shell.

Hyland and Neugebauer (1970) found the distance of Nova Serpentis

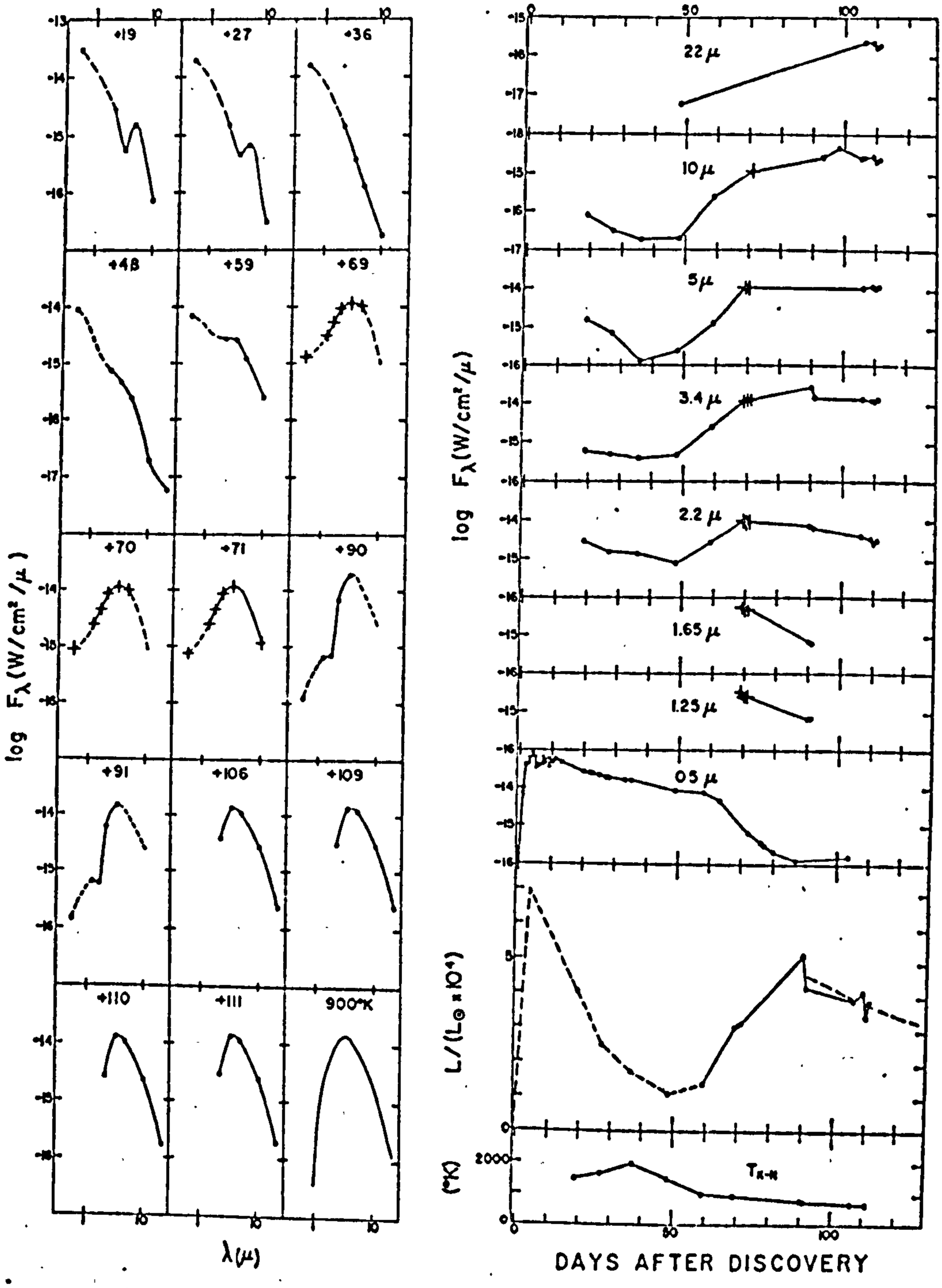

Figure (2.5) Infra-red spectra (left) and light curves from the observations of Nova Serpentis 1970 by Geisel et al. (1970).

1970 to be D = 1.2 ± 0.5 kpc. This was achieved by using the relationship outlined by Payne-Gaposchkin (1957) of the rate of decay of the visual light soon after maximum to absolute visual magnitude (Equation (2.1)) and assuming a colour excess (E_{B-V}) of 0.4.

Using this relationship again, but with a higher value of E_{B-V}, Borra and Anderson found D = 550 pc. Hutchings and Fisher (1973) determined $E_{B-V} \simeq 0.9 \pm 0.1$ and from studies of interstellar line strengths found D to lie in the range 710 pc to 840 pc.

Radio observations of Nova Serpentis 1970 were made by Hjellming and Wade (1970). Details of subsequent observations can be found in Wade and Hjellming (1971). Over the 4 month period of study the radio flux from Nova Serpentis 1970 increased by a factor of 3 as an optically thick emitting region expanded from an equivalent disc diameter of 0.24" at 3.7 cm in June to 0.4" in late October 1970.

2.2.3 Nova Aquilae 1975

At the time of discovery on JD 2442570 Nova Aquilae 1975 had a visual magnitude of + 11.5 (Wild, 1975). Figure (2.6) contains subsequent observations of the nova's steady decline at a rate of 0.095 mag/day^{-1} and U-B and B-V data of Vrba et al. (1977). The behaviour of U-B and B-V is similar to that of Nova Serpentis 1970 at transition (see Figure (2.1)). The date of visual maximum remains uncertain.

The paper by Vrba et al. (1977) contains a spectrum taken by Herbig on July 19 1975. At that time, 43 days from discovery, the continuum was very weak between the extreme wavelengths on the plate of 5700Å and 6800Å. The tracing displays very strong emission lines with nearly rectangular profiles and strong central reversals. The Doppler half-widths are approximately 1000 kms^{-1}. It appears that this is the spectrum of a nova in the nebular stage (comparing the strengths of the Hα and NII lines around 6560Å with detail given in McLaughlin,

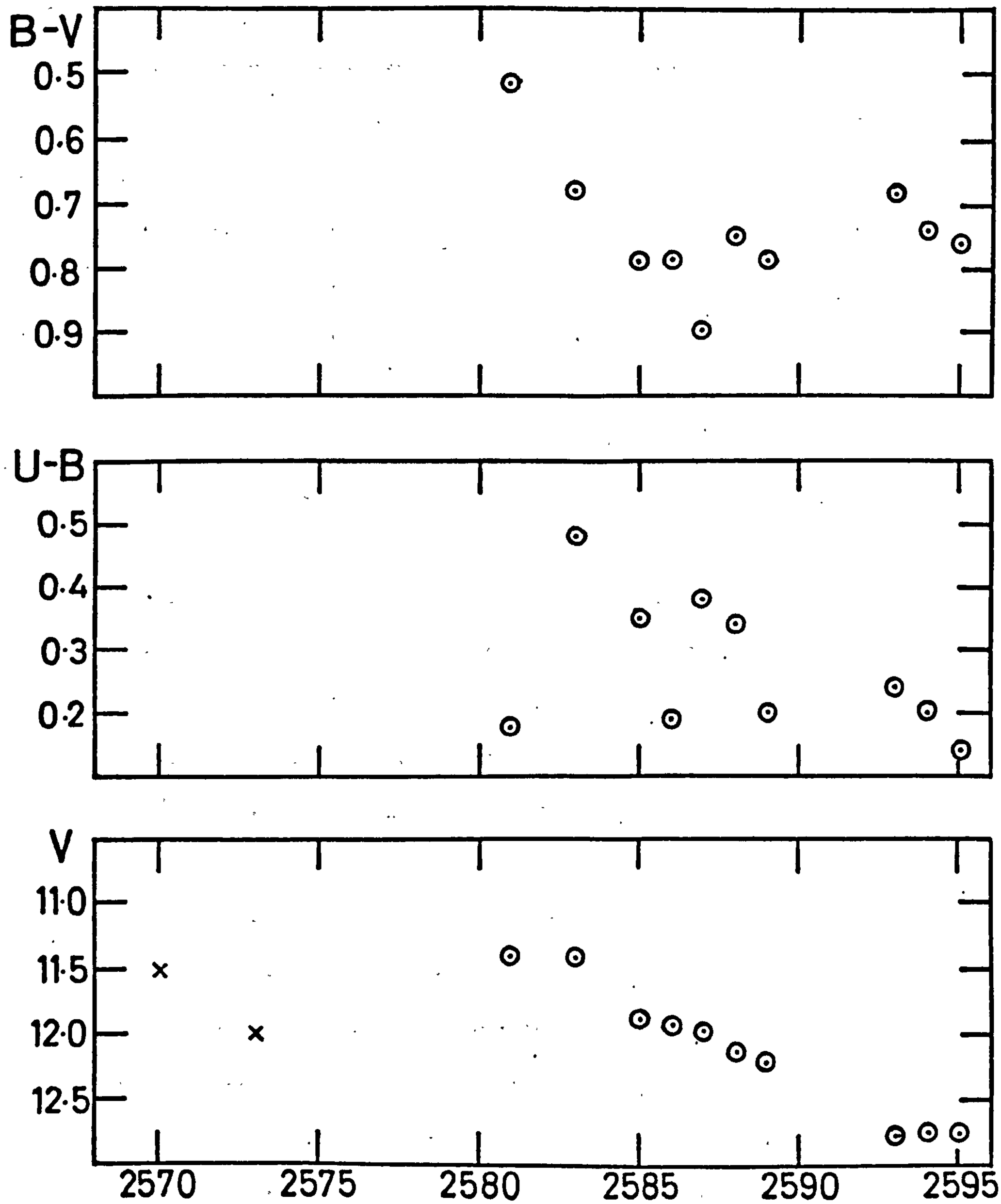

Figure (2.6) UBV observations of Nova Aquilae 1975 from Vrba et al. (1977). Note the similarity with Nova Serpentis 1970 at transition as shown in figure (2.2). Data shown as crosses are Wild's (1975) observations.

1960 and summarised above in table (2.1)). Confirmation of this conclusion comes from another spectrum taken 93 days after outburst by Pesch (1975). Sanduleak and Chen (1975) concluded that the spectrum was characteristic of a nova in the early nebular stage.

The nebular stage generally occurs 4 to 11 magnitudes after maximum. Taking the steady decline rate of 0.095 mag day^{-1} to have been continuous the nova should have reached approximately V = 14.6 by day 43. This is around 3.2 magnitudes below the peak visual magnitude and it would therefore seem unlikely that the first observation caught the nova at maximum visual luminosity. However, it is possible that the maximum occurred only a few days before.

Vrba et al. (1977) observed the nova in the UBJHKL bands as well as the V from 10 to 25 days after discovery (see Figure (2.7)). As with Nova Serpentis 1970 there was a dramatic rise in the infra-red flux. This apparently occurred around 7 days from discovery (by extrapolation). This rise was initially linear in the H K and L bands.

Vrba et al. (1977) concluded that the infra-red rise was due to grain formation in the nova envelope with grains at a characteristic temperature of approximately $1000^{o}K$ (following the work of Clayton and Hoyle, 1976 and Clayton and Wickramasinghe, 1976).

After correcting for thermal emission by grains and interstellar reddening, Vrba et al. (1977) find the V-J colours are consistent with those of an underlying photosphere the spectral type of which changes from B8 to A6 during the 15 days of observation. This is in accordance with the general change in spectral type noted by Payne-Gaposchkin (1957) for novae immediately following the visual maximum. This also suggests, apparently, a spectral type B5 on the discovery date which in turn implies ejection velocities of 1000 kms^{-1}, in agreement with the spectroscopic results of Herbig (Vrba et al., 1977). (Spectral classification from photometry should of course be approached with

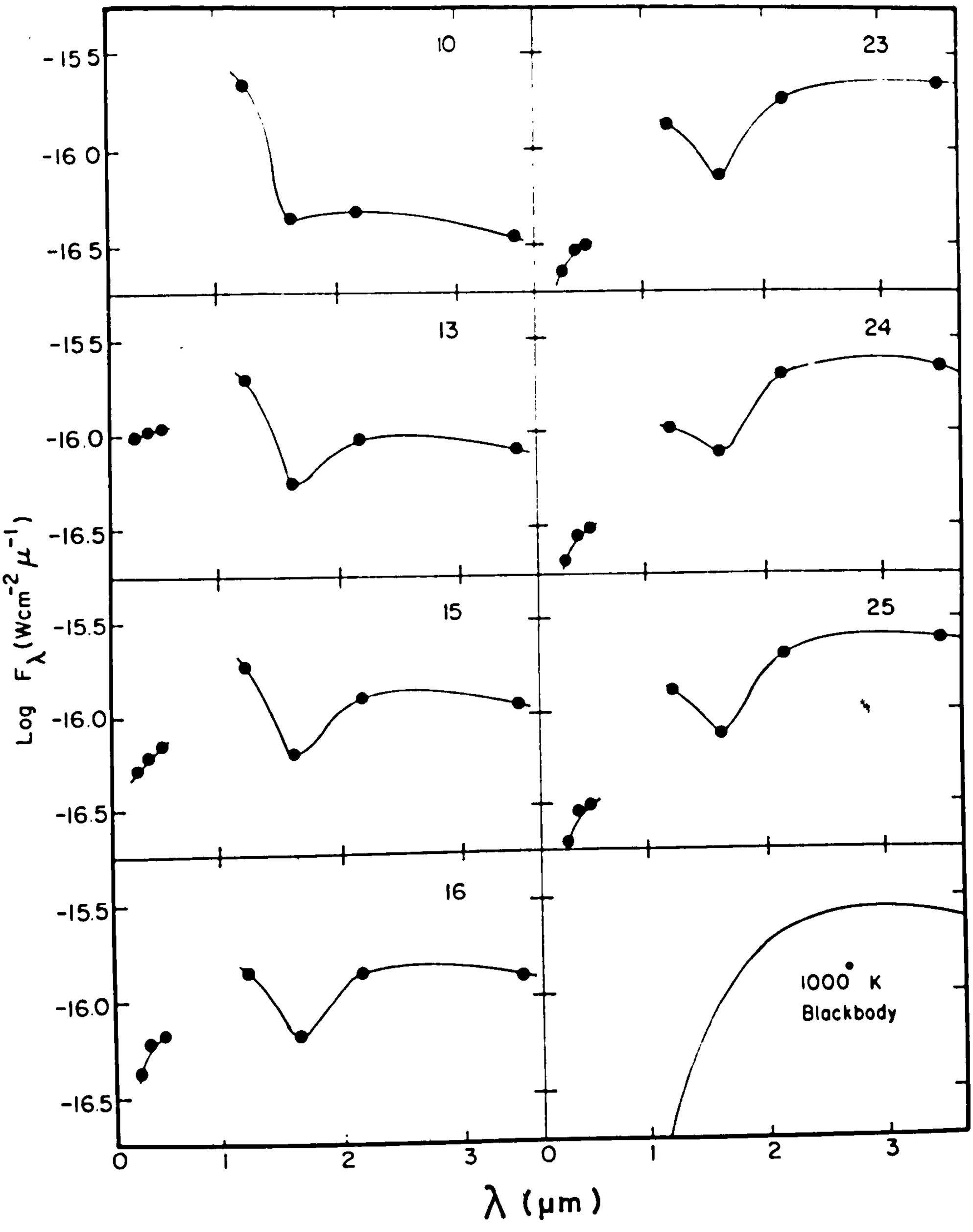

Figure (2.7) Infra-red spectra from the observations of Vrba et al. (1977) of Nova Aquilae 1975.

caution when the object in question may be delivering much of the flux observed through UBV filters in the form of line emission.) They also note that the dereddened U-B and B-V colours indicate that a very strong ultra-violet excess existed at the time of the infra-red rise. This is very significant from our point of view.

From considerations of rate of decline and the interstellar absorption in the direction of Nova Aquilae 1975 Vrba et al. (1977) concluded that the object is at a distance of 3.2 kpc ($(M_V)_{max} \simeq -7.1$). There is however a good deal of uncertainty in this figure due to the unknown nature of the immediately post-maximum light curve and the unevenly distributed interstellar absorption in this region.

Support for the hypothesis that the discovery was not at maximum comes from van Genderen and Uiterwaal (1979) who observed Nova Aquilae 1975 at five wavelengths including the visible from JD 2442575 to 2442624. By construction of two-colour diagrams they concluded that the reddening estimate of Vrba et al. (1977) was much too high. A figure of $A_V \lesssim 2.4$ mag. was suggested. This coupled with the discovery magnitude of 11.5 and their calculated absolute magnitude $M_V = -7.3$ (from equation (2.1)) gave a distance of $\sim$ 20 kpc. As the nova is at Galactic coordinates $l^{II} = 40^o, b^{II} \simeq -4^o$ this would place it outside the Galaxy. A lower value of magnitude at maximum would place the nova at a smaller distance. However even with the suggested peak magnitude of $V \simeq 10.7$ mag. the nova would lie at a distance of > 13 kpc. We will return to this further in Chapter 5.

2.2.4 Nova Vulpeculae 1976

Nova Vulpeculae 1976 was discovered by Alcock (1976) on 1976 October 21.7. An observation by Gorynya (1976) confirmed that it had not reached maximum on October 20.7. The nova was subsequently observed by A.A.V.S.O. and Ney and Hatfield (1978). The latter provide the most

comprehensive record of the infra-red development of a nova to date (see Figure (2.8)).

The observations reported in Ney and Hatfield (1978) cover the period from 3 to 230 days from discovery. During this time the visual light curve displayed behaviour characteristic of a slow nova of the DQ Herculis type. An initial 'plateau' region characterised by irregular fluctuation was followed after approximately 20 days by a fairly steady decline. This continued until around day 60 when the visual light flux went into the rapid decline of the transition stage. This decline coincided with a rapid almost linear rise in the infra-red luminosity. The transition lasted until around day 110 when the nova's magnitude decreased again toward a second maximum approximately 5 magnitudes below the initial peak. Subsequently it assumed a slow and gradual decline toward the quiescent post-nova stage.

The spectral evolution of Nova Vulpeculae 1976 has been observed by Klare and Wolf (1978) and Cottrell and Smith (1978).

The latter observed the nova on several occasions between October 28th and November 20th 1976. They classified the object as a slow nova which at this time had the characteristic absorption and emission lines of a nova at maximum and early postmaximum stages (see Chapter 3). Ejection velocities were found to be $\sim$ 1000 kms^{-1} for the principal spectrum (sic.) and $\sim$ 550 kms^{-1} for the diffuse enhanced (sic.).

Klare and Wolf (1978) observed the nova from October 26th 1976 to October 13th 1977 during which time the object underwent spectral changes characteristic of the principal, diffuse enhanced, Orion and nebular stages.

Five days from discovery the principal absorption spectrum was observed with an expansion velocity $\sim$ 950 kms^{-1}. Eighteen days from discovery the principal absorption had an apparent velocity of $\sim$ 665 kms^{-1} whereas the bright lines of the diffuse enhanced stage now appearing

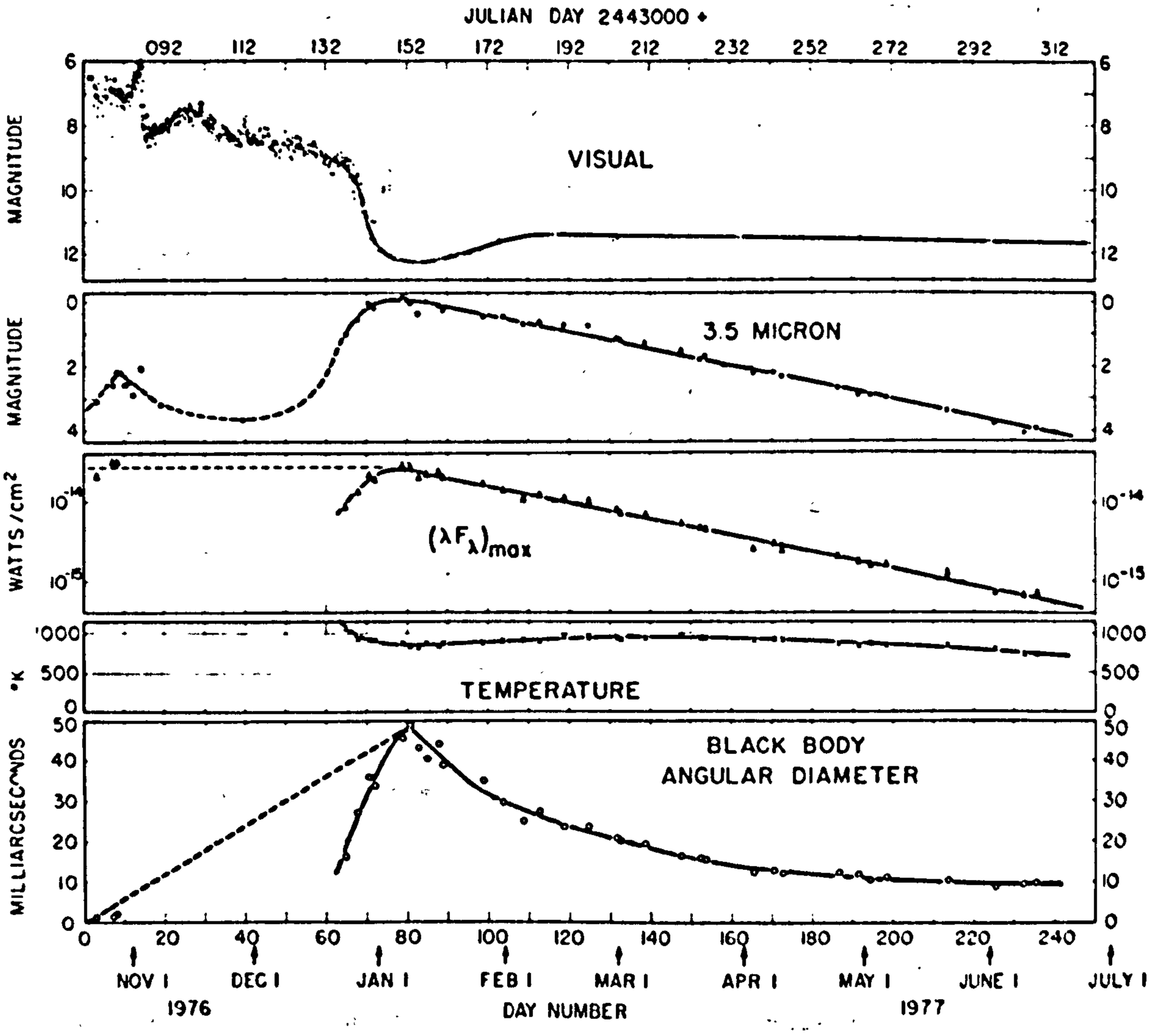

Figure (2.8) Visible and 3.5 μm light curves, energy curve, colour temperature and black body angular diameter measurements for Nova Vulpeculae 1976 from observations by Ney and Hatfield (1978).

seemed to have a velocity of ∿ 1500 kms^{-1}. (Note - the designations of Cottrell and Smith, 1978, would appear to be the wrong way around.)

Spectra taken between days 33 and 51 show that Nova Vulpeculae had entered the Orion stage with the λ4640 feature clearly present. Finally three spectrograms taken on October 13th 1977 (∿ 1 year after peak) showed that the object was well into the nebular stage with a weak continuum underlying bright emission lines.

The infra-red observations of Ney and Hatfield (1978) show that a small infra-red excess existed at around 5μm after about 10 days. This subsequently disappeared to be followed at around 60 days by the emergence of a much larger excess with characteristic temperatures and other time dependent features as shown in Figure (2.8).

Ney and Hatfield (1978) concluded that the nova lies at a distance of 1.5 kpc, although as this is based on calculations of black body angular diameter expansion it is unlikely to be particularly accurate (see Chapter 4).

Unfortunately observations in the U, B and ultra-violet do not appear to have been published.

2.2.5 Other Classical Novae

Nova Delphini 1967 (HR Del) was a very slow nova which maintained an approximately static visual luminosity for ≃ 350 days from outburst. It then underwent a smooth, slow decline ($\dot{m}_v \simeq 0.006$ mag. day^{-1}, Sanyal, 1974).

Observations by Zellner (1971) and Zellner and Morrison (1971) of the polarisation of Nova Delphini 1967 indicated that dust existed near the nova at early times. This is also supported by Malakpour (1973) whose measurement of the Balmer decrement of the nova led him to conclude that dust grains, formed from previous ejecta, existed around the nova prior to the 1967 outburst. Sanyal (1974) detected narrow

emission lines during outburst which are ascribed to a pre-existing circumstellar gas shell.

Infra-red observations in 1970 by Geisel et al. (1970) revealed Nova Delphini to have an infra-red excess 44 days after outburst. About 1150 days later further measurements indicated thermal emission with a temperature of $\sim 300^{o}K$ and luminosity $\sim 30\ L_{\odot}$.

Nova Aquilae 1970 was discovered on April 14th, 1970 and subsequent searches of patrol photographs placed its maximum at around April 9th. The nova declined steadily at around 0.1 mag. day^{-1} until $\sim$ 30 days from peak when it went into transition (Ciatti and Rosino, 1974). Observations by Geisel et al. (1970) revealed that at $\sim$ 55 days Nova Aquilae 1970 was a bright infra-red source ($N \simeq -0.1$) with a spectral distribution characteristic of a $900^{o}K$ black body.

Spectral scans of Nova Aquilae 1970 taken 3 days from discovery by Grenfell (1971) indicated that the nova may have had an infra-red excess at very early times. This conclusion is however sensitive to the assumed interstellar extinction and is not too reliable.

Nova Cephei 1971 was observed at infra-red wavelengths by Sato et al. (1971). Their observations 8 days from discovery ($\sim$ 11 days from peak) showed no infra-red excess at this stage. A slope change suggestive of the onset of transition occurred at $\sim$ 30 days (Kohoutek and Klawittler, 1973). Unfortunately no infra-red observations were made after this time.

One of the most thoroughly observed 'fast' novae was Nova Cygni 1975. This object did not appear as a pre-nova on Palomar Sky Survey prints (Samus, 1975) and yet at peak visual luminosity reached an observed magnitude of $m_v \sim 2$ (Papoušek and Vetešnik, 1977). The subsequent decay rate of the visual light curve was 0.7 mag. day^{-1} (Gallagher and Ney, 1977). Assumption of little reddening in the direction of the nova led Gallagher and Ney (1977) to derive a distance

of ∿ 1.5 kpc. They also proposed that the lack of diffuse-enhanced and Orion absorption spectra during the early decline indicated that the nova explosion itself occurred in rather unusual circumstances.

Infra-red observations of Nova Cygni 1975 were carried out over the first 50 days by Gallagher and Ney (1977). They observed a black-body distribution over the first 3 days but by day 4 the spectrum followed $f_\nu \simeq$ constant. This is characteristic of free-free emission from the expanding nebula. Up to day 50 no late developing infra-red excess was observed.

Ennis et al. (1977) observed the nova at wavelengths from 1 to 20 μm for a period 2 days before maximum light to approximately 1 year after. The characteristic change of spectral appearance from black body to free-free was again apparent during the first few days of observation as the ejecta became optically thin.

The temporal development of the infra-red flux from the nova indicates that the ejecta are in the form of a shell whose thickness increases with time. This would give rise to a t^{-2} decay in free-free flux initially, followed by a t^{-3} decline. The observations closely follow this predicted behaviour except at late times for 1.6, 3.5 and 10 μm when an excess flux to the theoretical free-free emission is evident. Subtraction of the observations from the t^{-3} curve reveals the 'excess' light curves of Figure (2.9).

The development of an excess at 10 μm is undisputed. Those at 1.6 and 3.5 μm are less definite. However Szkody (1977) in observations of the nova at 3 months, 11 months and 1 year after outburst found that an infra-red excess was evident at 3.5 μm for the last two observations at least. When the free-free contribution was subtracted by the present author the Szbody observations were found to agree well with those derived from Ennis et al. (1977).

Ennis et al. ascribed the 10 μm excess to the possible formation

Figure (2.9) The development of the infra-red excess of Nova Cygni 1975 from observations by Ennis et al. (1977) and Szkody (1977). It is assumed that the non-thermal contribution to the observed flux decays as t^{-3} at all wavelengths.

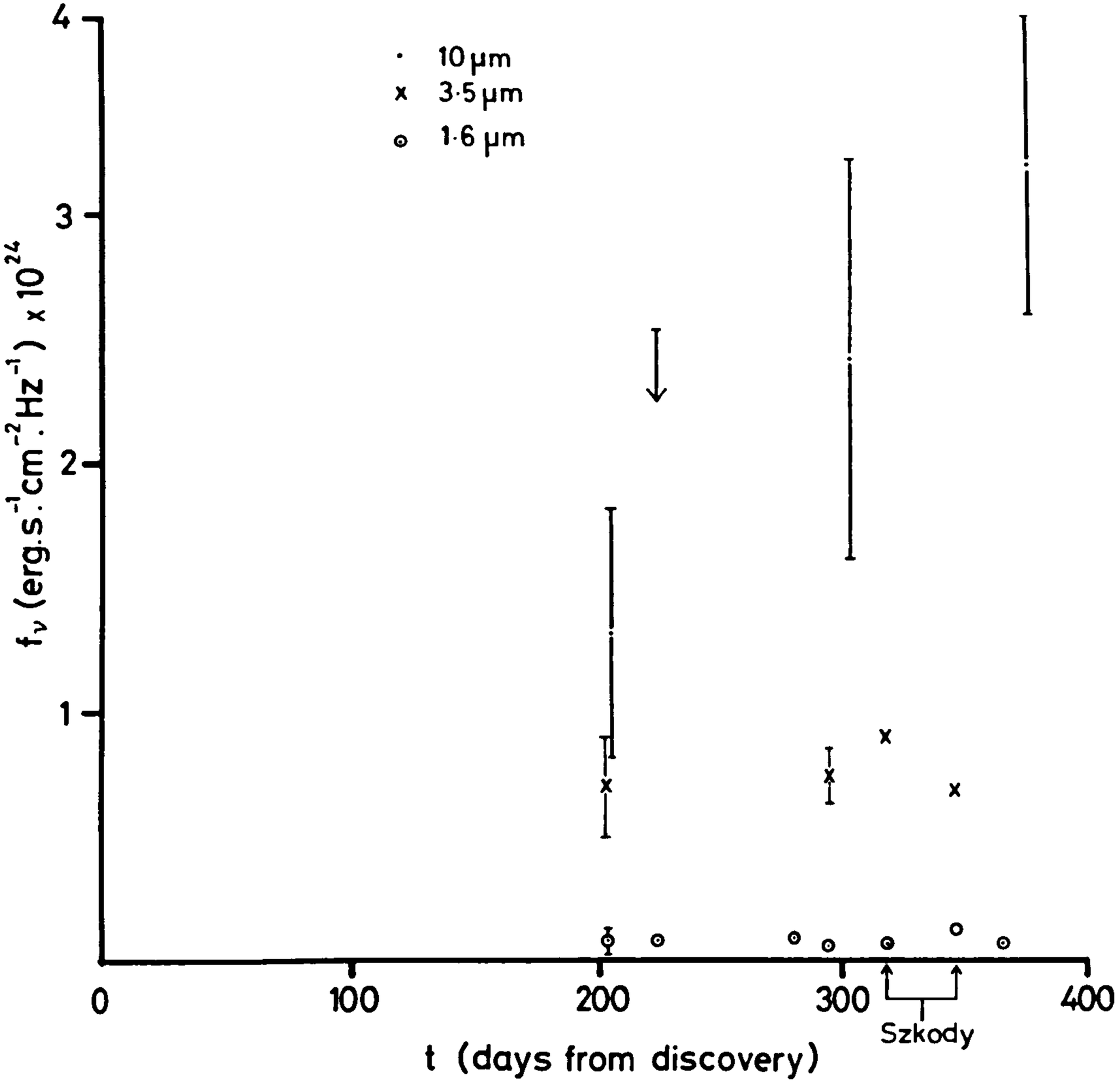
10 μm
3·5 μm
1·6 μm
f_ν (erg.s^{-1}.cm^{-2}.Hz^{-1}) x 10^{24}
4
3
2
1
0
100
200
300
400
Szkody
t (days from discovery)

of a small amount of dust by the nova. However Ferland and Shields (1978) have explained this excess as being due to [NeII] line emission in the nebular phase of the nova. The Szkody observations were not discussed.

Ultra-violet photometry of Nova Cygni 1975 by Wu and Kester (1977) 100 days after outburst revealed rapid periodic variations at short wavelengths. These were thought to have arisen in the hot spot of the nova remnant which would therefore be 'uncovered' at this stage. They concluded that from visual peak to day 100 the total luminosity had declined from $5 \times 10^5 L_\odot$ to $3 \times 10^4 L_\odot$ with the characteristic rise in observed black body temperature with time to $\sim 65000^\circ K$.

Recently Nova Cygni 1978 has shown an infra-red excess developing from about 25 days after outburst (Gehrz et al., 1978). The colour temperature of the excess emission changed from $\sim$ 1400 K to $\sim$ 1000 K between days 25 and 45 whilst the total infra-red flux increased by a factor of at least 10 (Joseph, 1979).

Prior to the 'dust emission' epoch observations in the infra-red by Phillips et al. (1979) had shown that there was little evidence for an excess at 5 μm as previously observed in Novae Vulpeculae 1976 and Serpentis 1970. There was however a marked depression at 3.5 μm suggesting a broad absorption feature due possibly to (ice) grains or molecular band absorption. The apparently rapid development of this feature indicates that it is of circumstellar rather than interstellar origin.

2.2.5 Summary

The infra-red observations of Novae Serpentis 1970, Aquilae 1975 and Vulpeculae 1976 are qualitatively similar. Several points are of particular note in this connection:-

(i) Both Novae Vulpeculae 1976 and Serpentis 1970 showed an early infra-red excess at around 5μmwhich faded at least 20

days before the larger rise in infra-red emission began.

(ii) All three novae showed a lag between observed maximum visual light and the onset of rapid infra-red increase.

(iii) The initial rise in infra-red luminosity was approximately linear with time for all 3 novae.

(iv) Novae Vulpeculae 1976 and Serpentis 1970 showed an increase in their infra-red luminosity at around 60 days which approximately coincided with the transition phase of the visual light curve.

(v) In the case of Nova Serpentis 1970 the infra-red luminosity picked up as the peak of the ultra-violet emission spectrum shifted to around 2000 Å.

(vi) In all three novae the black body temperature appeared to start somewhere above 1000°K and subsequently fell towards approximately 800°K.

(vii) The infra-red curves of Nova Vulpeculae 1976 showed that the decay after peak emission at each infra-red wavelength was approximately exponential.

2.3.1 Recurrent Novae

It has been proposed that all novae are recurrent in nature and that classical novae only appear to be 'one-off' events due to the length of time between outbursts (see e.g. Bath and Shaviv, 1978; Ford, 1978).

Recurrent novae are usually thought of as being the short period counterparts of classical novae although there are other differences in spectral characteristics, binary components etc. as well. The time between outbursts for a recurrent nova is of the order of decades rather than the estimated 10^4 years or more for many classical novae (e.g. Ford, 1978).

The visual amplitude of outburst of a recurrent nova usually lies in the range of 4 to 9 magnitudes (slightly less than that of a classical nova) although the bolometric luminosity in the pre-nova stage is generally accepted to be greater than for classical novae. The peak bolometric luminosity of recurrent and classical novae is thus comparable.

Recurrent novae are known to exist as binary pairs containing a hot, dense star as the primary and a cooler, much more extended star as the secondary. It appears however that whereas the secondary in recurrent novae is a late type giant the secondary in classical novae is usually thought to be a low mass, late-type main-sequence star (see e.g. Bath and Shaviv, 1978).

Table (2.2) taken from Warner (1976) shows the dates of outburst for 6 recurrents together with visual magnitudes at maximum and minimum. The last column, headed t_2 is the time in days for the object to decline in V by 2 magnitudes from peak. VY Aqur, TCrB, RS Oph and U Sco are objects with very rapid decline rates whereas T Pyx and V1017 Sgr are rather slow.

Table (2.3) taken from Faulkner (1974), shows the comparison between classical, recurrent and the much shorter period dwarf novae. Recurrent novae are obviously similar to classical novae in terms of mass ejection.

We now proceed to consider the recurrent nova RS Oph in some detail. This object has been widely studied during and between outbursts and it is suspected to already possess an extensive circumstellar shell.

2.3.2 RS Oph

Table (2.2) details the 4 outbursts of this nova observed over the last 80 years. Of these, those of 1958 and 1967 have been particularly well observed.

Table 2.2

Recurrent Novae (taken from Warner, 1976)

	Outburst dates	m_v (peak)	m_v (min)	Δm_v	t_2
VY Aqr	1907	8.0	16.6*	8.6	6
	1962	9.0		7.6	5
TCrB	1866	2.0	10.5	8.5	5
	1946	2.0		8.5	5
RS Oph	1898	4.3	12.3	8.0	4
	1933	4.3		8.0	4
	1958	5.0		7.3	6
	1967	4.9		7.4	7
T Pyx	1890	7.9	14.5	6.6	100
	1902	7.3		7.2	100
	1920	6.6		7.9	100
	1944	7.1		7.4	100
	1966	7.7		6.8	80
V1017 Sgr	1901	10.8	14.4	3.6	200
	1919	7.2		7.2	90
	1973	10.2		4.2	200
U Sco	1863	9.1	>17.6*	>8.5	2
	1906	8.8		>8.8	2
	1936	8.8		>8.8	1

* m_{pg} (min)

Table 2.3

Energy Requirements of Nova Models (taken from Faulkner, 1974)

	Classical Novae	Recurrent Novae	Dwarf Novae
Outburst Range (mag.)	$\sim$ 10 - 12	$\sim$ 6 - 8	$\sim$ 2 - 5
Outburst Energy, E(ergs)	$> 10^{45}$	$\sim 10^{43} - 10^{45}$	$\sim 10^{38} - 10^{39}$
Time Interval, T(years)	(300 - 1000??) (great uncertainty)	25 - 50	$\sim$ 0.05 - 1
Mass Ejected, M_{ej} (grams)	$\sim 10^{28} - 10^{29}$	$\sim 10^{28}$	?
M_{ej}/T ($M_\odot$ yr^{-1})	??	$\sim 10^{-7}$	$\sim 10^{-9}$?? (one example)
$E_.(0.007\ c^2T)$ ($M_\odot$ yr^{-1})	??	$\sim 10^{-10}$	$\sim 10^{-12} - 10^{-11}$
M^*_{burnt}/M_{ej} (nuclear explanation)	??	$\sim 10^{-3}$	?

*$M_{burnt} = E/(0.007\ c^2)$, the amount of hydrogen burnt on the nuclear explanation to produce the outburst energy, E.

Pottasch (1967) gave a detailed interpretation of the spectral development of the nova. From considerations of the observed magnitude and the implied absolute magnitude using equation (2.1) he concluded that the distance of the object is 5800 pc. This value is an upper limit as no account of reddening appears to have been made in the calculation. According to Svolopoulos (1966) $E_{B-V} \simeq + 0.82$. Assuming $A_V \simeq 3E_{B-V}$, we arrive at a dereddened distance of approximately 1800 pc.

From the study of spectra of the 1958 outburst Pottasch deduced that the ejecta were decelerated appreciably by pre-existing circumstellar matter. The presence of this matter was also indicated by the apparent increase of momentum of the expanding envelope which Pottasch ascribes to the 'sweeping up' of the pre-existing matter by the ejected shell. Further evidence for the existence of this shell is given by apparently stationary emission and absorption lines superimposed on the nova spectrum. From these and other considerations Pottasch deduced that RS Oph has an extensive circumstellar shell ($\simeq 0.7\ M_\odot$) with heavier elements overabundant.

Svolopoulos (1966) studied the 1958 outburst in the U, V, B, G, R and I bands between 1 and 10 days after visual maximum (see Figure (2.10)). These observations led Svolopoulos to conclude that RS Oph is heavily reddened. However the object lies well out of the galactic plane ($l^{II} = 19^o.8$, $b^{II} = + 10^o.38$) and it is difficult to explain this in terms of interstellar absorption. The greater part of the absorption would therefore seem to be circumstellar.

Figure (2.10) shows that fluxes shortward of 5000 Å decrease whilst those longward of 5000 Å appear to increase with time. Note also that the U-B index decreases (i.e. the object becomes bluer at those wavelengths) during the same period.

Svolopoulos (1966) concluded that RS Oph is surrounded by a

Figure (2.10) 6 colour photometry of the 1958 outburst of RS Oph on JD's 2436000 + 399.84 (·), 402.8 (0) and 406.78 (x). Ordinates are in relative magnitudes, the abscissae in effective inverse wavelength (from Svolopoulos, 1966).

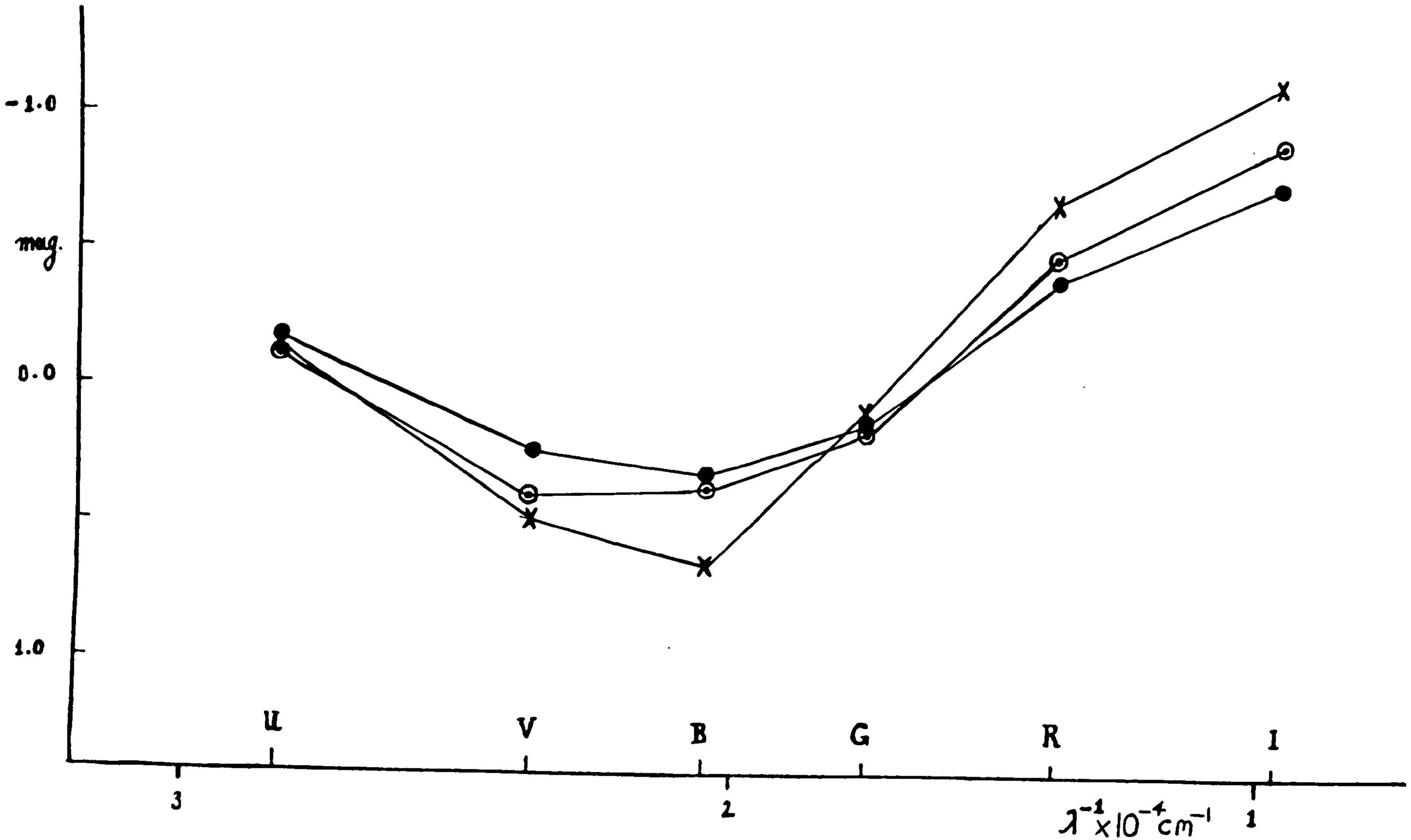
-1.0
mag.
0.0
1.0
U
V
B
G
R
I
3
2
1
$\lambda^{-1} \times 10^{-4} cm^{-1}$

circumstellar shell which existed prior to the outburst and is the result either of mass lost in previous outbursts or by continuous ejection from the central object between them.

Observations made during the 1967 outburst tend to confirm the conclusions reached after the 1958 outburst. Wallerstein (1968) again observed the almost stationary absorption and emission lines seen both during and between outbursts. He also speculated that they could be due to absorption and emission in a pre-existing circumstellar envelope.

Feast and Glass (1974) carried out photometry in the JHK and L bands. The J-H, H-K diagram drawn from their data suggests that the object is heavily reddened with $A_V \approx 5.5$ ($\pm \sim 1$).

Szkody (1977) made infra-red measurements of RS Oph between outbursts. She concluded that this object closely resembles symbiotic stars (the spectra of which appear to be a composite of a hot and a cool component) with a high degree of reddening. It is uncertain whether the infra-red emission she detected arises in the cool component or the circumstellar shell. Observation during outburst at infra-red wavelengths would clarify the matter.

2.4.1 Conclusion

In this chapter we have described the observational evidence for variability in thermal sources which arises possibly because of changes in the high frequency flux output of a centrally positioned object. The emphasis on novae has been deliberate as we shall apply principles developed in the following chapter to specific classical novae already described above.

CHAPTER 3

Review of Theoretical Background

3.1.1 Introduction

The evidence for the existence of small ($\lesssim$ 1 μm) dust grains in astrophysical environments is very strong (see e.g. Wickramasinghe, 1967; Burbidge & Stein, 1970 and references therein). Much work has been put into determining the properties of these grains on the microscopic and macroscopic scales.

This chapter commences with a discussion of the basic concepts used in the determination of grain properties. It then proceeds to discuss the origins of grains, their growth and possible destruction. Section (3.3) discusses the heating of grains by ultra-violet radiation both in the case when the grain is isolated and when it is embedded within an assembly of similar grains. Also considered in this chapter are the effects on grain heating and on subsequent emitted spectra of fluctuations in the primary high frequency source.

Although the geometry of the emitting region has in the past been studied by various authors (for example, Couderc, 1939; Morrison & Sartori, 1969 etc.) their results have not been applied to thermal emission from dust grains as far as we are aware. The work that has been carried out is described in section (3.4).

Section (3.5) deals with the theoretical interpretations of some of the characteristics of classical novae which have been described in the previous chapter. The final section then describes how certain parameters of nova dust shells have been derived in the past.

3.2.1 Scattering, Absorption and Extinction by Dust Grains

When radiation encounters a material object it may undergo scattering and/or absorption. This leads to a diminution of the incident radiation in particular directions (i.e. extinction). The exact nature of the subsequent changes in the radiation field about the object are dependent upon the frequency of the incident radiation; the grain size and geometry and the grain's intrinsic properties (these being dependent upon its composition). It is therefore clear that the exact treatment of this situation will be fairly complex. Here we restrict ourselves to a discussion of the theory of light scattering and absorption from small, spherical, homogeneous grains.

The problem of solving Maxwell's equations for a beam of radiation of intensity I_λ incident on a spherical surface was successfully tackled initially by Mie (1908). A detailed account of the solution was given by van de Hulst (1957). For the purposes of this work it will only be necessary for us to consider the more general results and their asymptotic forms.

If we define the effective cross section for absorption by the grain as C_{abs} and that for scattering as C_{sca} then

$$C_{ext} = C_{sca} + C_{abs}$$

Here $C_{ext} = Q_{ext}\ \pi a^2$ where Q_{ext} is the efficiency factor for extinction and a is the grain radius; similar relationships hold for scattering and absorption. Thus

$$Q_{ext} = Q_{sca} + Q_{abs} \qquad (3.1)$$

In the case where the wavelength, λ, of the incident radiation is much greater than the particle radius, the rigorous treatment of the Mie formulae as outlined by van de Hulst (1957) reduces the solutions to

$$Q_{ext} \cong -4.\left(\frac{2\pi a}{\lambda}\right). \text{Im}\left\{\frac{m^2 - 1}{m^2 + 2}\right\} \qquad (3.2a)$$

$$Q_{sca} \cong \frac{8}{3}.\left(\frac{2\pi a}{\lambda}\right)^4. \text{Re}\left\{\frac{m^2 - 1}{m^2 + 2}\right\}^2 \qquad (3.2b)$$

for conducting spheres and

$$Q_{ext} \cong Q_{sca} \cong \frac{8}{3}.\left(\frac{2\pi a}{\lambda}\right)^4. \text{Re}\left\{\frac{m^2 - 1}{m^2 + 2}\right\}^2 \qquad (3.2c)$$

for non-conducting dielectic particles (i.e. no absorption). In equations (3.2), m is the refractive index which contains an imaginary term for conductors (i.e. m = n - ik) and is wholly real for non-conductors (Im and Re indicate the taking of imaginery and real parts respectively).

The incident radiation carries with it momentum in the direction of propagation of the beam. Thus the beam exerts a force on the grain, P_r, where

$$P_r = \frac{I}{c}\ \pi a^2 Q_{pr} \ . \qquad (3.3)$$

Q_{pr}, the efficiency factor for radiation pressure, is given by

$$Q_{pr} = Q_{ext} - Q_{sca}\ \overline{\cos \phi}$$

where $\overline{\cos \phi}$ is the fraction of the incident intensity scattered into the forward direction (ϕ being the angle between the forward direction and any scattering direction). For isotropic scattering therefore $\overline{\cos \phi} = 0$ and if all the incident radiation continues to travel in the forward direction after scattering, $\overline{\cos \phi} = 1$.

If radiation of initial intensity $I_\lambda(0)$ passes through a uniform medium containing N_g grains per unit volume then in distance D the emergent intensity I_λ will be given by:-

$$I_\lambda = I_\lambda(0)\ e^{-\delta\lambda} \qquad (3.4)$$

where $\delta_\lambda = N_g \pi a^2 Q_{ext}(\lambda) D$ is referred to as the optical depth at wavelength λ.

For a star, the flux, $f_\lambda d\lambda$ between wavelengths λ and $\lambda + d\lambda$ observed above the Earth's atmosphere results from integration of the intensity I_λ over the solid angle, Ω, subtended by the star. The extinction in magnitudes A_λ is thus given by

$$A_\lambda = -2.5 \log \frac{f_\lambda}{f_\lambda(0)} = 1.086\ N_g \pi a^2 Q_{ext}(\lambda) D$$

where $f_\lambda(0)$ is the flux that would be observed in the absence of extinction. We can see that if Q_{ext} is wavelength dependent then so also is A_λ.

The first evidence indicating the presence of solid particles permeating the interstellar medium came with the advent of UBV photometry. Stebbins et al. (1939) made UBV measurements of 1332B type stars and concluded that A_λ varies approximately as λ^{-1} in the UBV range. Table (3.1) gives the wavelength dependence that would be expected for free electrons, atoms (or molecules), small non-conductors and relatively large solid particles. None of these gives the λ^{-1} dependence discovered by Stebbins et al. (1939).

With the introduction of wider range photometry, including the infra-red and ultra-violet regions of the spectrum, a more complex extinction curve emerged. Figure (3.1) taken from Greenberg (1978) shows schematically in curve (1) the average extinction curve derived from observation of a great number of objects. This curve is made up of 3 recognisably distinct portions. These are labelled (2) to (4) in the figure.

It can be seen that in the UBV bands the extinction follows the roughly λ^{-1} dependence already mentioned. This part of the curve is thought to be due to relatively large particles with a $\sim$ 0.1 μm (curve

Table 3.1

Wavelength dependence of Extinction for Possible interstellar medium components
(UBV wavelengths).

Type of Particle	Extinction Law
Free electrons	λ^0 (Thomson Scattering)
Atoms (or molecules)	λ^{-4} (Rayleigh Scattering)
Non-conductors. Small c.f. wavelength	λ^{-4} (Rayleigh Scattering)
Solid particles. Large c.f. wavelength	λ^0 (Geometrical Scattering)

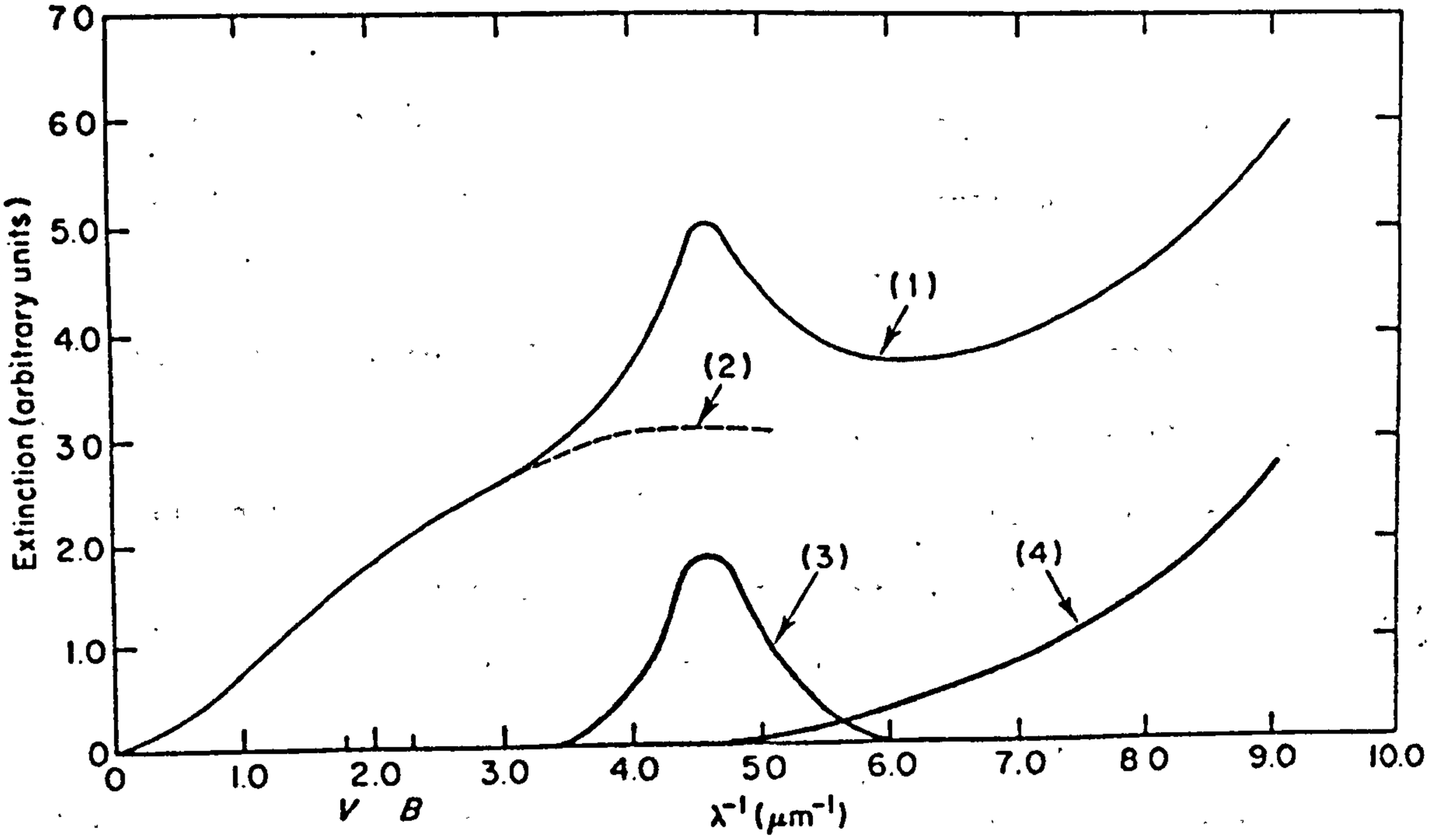

Figure (3.1) Schematic extinction curve as given by Greenberg (1978). The mean extinction curve (1) is arbitrarily divided into portions to which the major contributions are made by classically-sized particles (2) and very small particles (3) and (4).

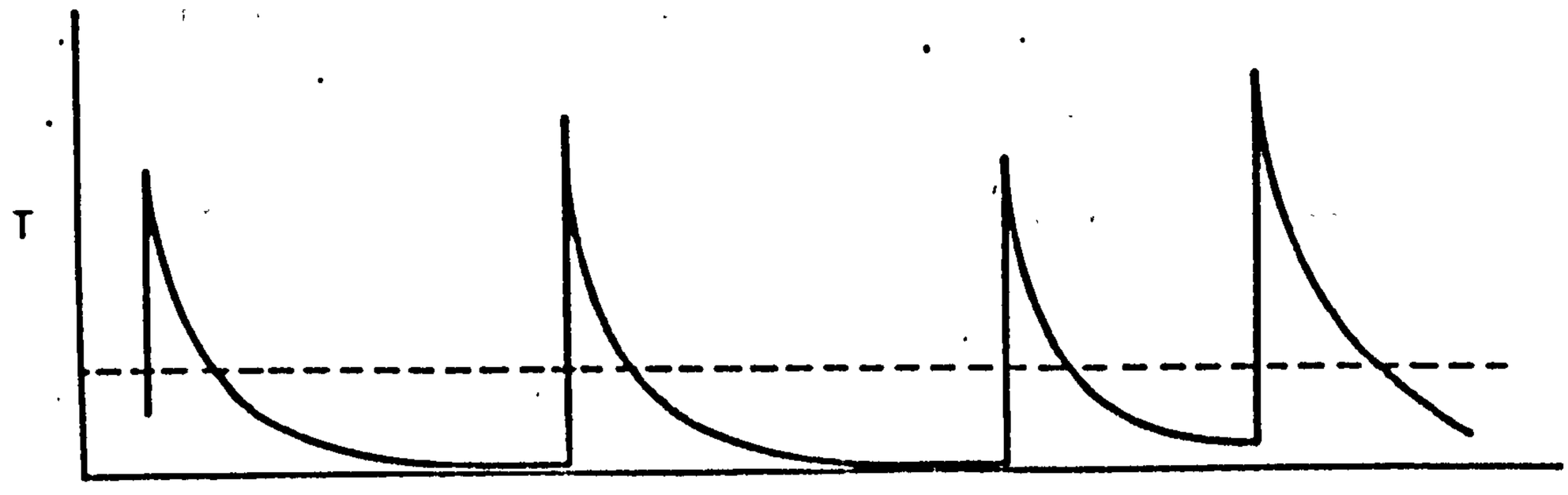

Figure (3.2) Schematic representation of the fluctuation of grain temperature due to single photon heating of small grains. The mean grain temperature is denoted by the horizontal dashed line (after Greenberg, 1976).

(2)). The well known feature at ∿ 2200Å is generally ascribed to absorption by small grains ($a \lesssim 0.02$ μm) which contribute little to the visual extinction. Various grain compositions have been suggested to give rise to this feature, for example graphite (Gilra, 1971) and silicate (Huffman & Stapp, 1973). According to Greenberg (1978) the rise in extinction shortward of $\lambda^{-1} \sim 6$ μm^{-1} is probably due to even smaller grains ($a \sim 0.008$ μm). The total extinction is therefore due to the mixing of these various-sized grains.

The extinction curve is of course the result of both absorption by the grains and scattering from them. There is now little doubt that the 2200Å 'bump' is largely an absorption feature (see for example Nandy et al., 1978). That is, the grains have on the whole a low albedo at this wavelength (albedo ≡ Q_{sca}/Q_{ext}). It appears however that in the far ultra-violet the albedo of the grains increases and their absorptivity drops even though the extinction curve rises steeply (see Witt, 1973). This is a rather contentious point at present however.

3.2.2 Formation, Growth and Destruction of Grains

The earliest theories of the origin of the solid particles responsible for the extinction in the UBV waveband involved the condensation of iron or ice grains within interstellar clouds (see for example Lindblad, 1935). It was felt that ice particularly could explain the high reflectivities of certain reflection nebulae.

Hoyle and Wickramasinghe (1962) proposed that graphite grains with

$$m^2 = 2 - 2i\ (1.2 \times 10^{15})\lambda/c$$

could well account for the extinction between $\lambda^{-1} \cong 0.6$ μm^{-1} and $\lambda^{-1} \cong 3$ μm^{-1}. They considered their work to be valid for particle sizes up to $a \sim 8 \times 10^{-6}$ cm for this wavelength range. This is of course

still within the present accepted range of grain size responsible for extinction in this waveband.

Because graphite surfaces have a low accommodation coefficient with carbon atoms it was difficult to visualise how any substantial grain formation could occur in interstellar space except in the densest clouds. Hoyle and Wickramasinghe therefore proposed that graphite 'flakes' could form in the outer layers of cool ($2000^{o} < T_{*} < 2700^{o}$) carbon stars (class N). In these stars the overabundance of carbon over oxygen means that there should be a surplus of carbon atoms available to form carbon molecules, but which would normally react to form CO. Condensation of the graphite grains then occurs when the effective temperature of the photosphere drops towards 2000^{o}K during pulsation. (Details of the nucleation process may be found in Wickramasinghe, 1967).

The rate of crystal growth of a spherical particle radius a was given by Wickramasinghe (1967) as

$$\frac{da}{dt} = \alpha_c \frac{p_c}{s}\left(\frac{m_c}{2\pi kT}\right)^{\frac{1}{2}} \qquad (3.5)$$

where p_c is the partial pressure of free carbon; α_c is the sticking coefficient; m_c is the mass of a carbon atom;T is the gas temperature and s is the bulk density of graphite. The basic process for the formation of platelets is similar except that the grain thickness is always roughly the same as the dimensions of the condensation nucleus ($\sim 5 \times 10^{-7}$ cm) and growth is essentially 2-dimensional. Donn et al. (1968) determined the rate of growth of a graphite platelet of initial radius a_o from the equation

$$a = 2a_o \exp\left(\frac{J\Omega_c t}{w}\right) - a_o$$

where $J = p_c (2\alpha_c m_c kT)^{-\frac{1}{2}}$ is the impinging molecular flux; Ω_c is the atomic volume of carbon ($\sim 10^{-23}$ cm^3); w is the plate thickness (assumed constant)

and t is the time measured from initial nucleation. Tabulation of $p_c(T)$ can be found in Wickramasinghe (1967).

Obviously, as the grains grow they will be subject to radiation pressure tending to push them out into space. The magnitude of this force at the stellar surface is approximately given by

$$P_r \cong \pi a^2 Q_{ext} \frac{\sigma_s T_*}{c} \tag{3.5}$$

where σ_s is Stefan's constant and T_* is the effective temperature of the stellar photosphere. Strictly we should use the efficiency factor for radiation pressure Q_{pr} here, but for metals and semiconductors $Q_{sca} \simeq 0$. We can see from equation (3.2a) that Q_{ext} is both wavelength and size dependent. Wickramasinghe (1967) assumed the value of $Q_{ext} \simeq 0.3$ for a mean particle size $a \simeq 5 \times 10^{-6}$ cm at $\lambda \simeq 1.2$ μm as appropriate for N-type stars. (Note that on the large scale, for a random distribution of plate orientations we may use the spherical particle Mie theory to determine gross optical properties.)

There are of course the competing forces of gravitational attraction, G, and drag due to motion through the stellar atmosphere, D_r. For the situation under consideration $P_r >> G$ and the terminal grain velocity is determined by drag where

$$D_r = 6\pi a \eta u \tag{3.7a}$$

where u is the relative grain-gas velocity,

$$\eta \cong \tfrac{1}{2} a\, m_H N_H \left(\frac{kT}{\pi m_H} \right)^{\frac{1}{2}}$$

m_H is the atomic mass of hydrogen and N_H the hydrogen number density. Again this is for spherical grains but for platelets Wickramasinghe considered that the force will be approximately the same.

If the relative grain-gas velocity is far greater than the thermal velocity of gas atoms and molecules then the drag force can be approximated by (Wickramasinghe, 1972)

$$D_r \simeq \pi a^2 N_H m_H u^2 \qquad (3.7b)$$

Once $D_r \simeq P_r$ acceleration ceases and u remains constant. As the grain moves out the gas density N_H decreases exponentially as will the drag force, D_r. Computation of the timescales involved in this process by Hoyle and Wickramasinghe (1962) showed that escape is possible for Carbon stars with a pulsational period $\sim$ 100 days. Before reaching interstellar space a grain must satisfy another condition however.

Having escaped from the stellar atmosphere no further appreciable growth takes place. The radiation field of the star will then be the only major process in changing the grain size. This is achieved by means of evaporation from the grain surface. The rate of decrease of radius due to evaporation is given by

$$\frac{da}{dt} \simeq - \frac{p_{sat}(T)}{s}\left(\frac{m_c}{2\pi kT}\right)^{\frac{1}{2}} \qquad (3.8)$$

where $p_{sat}(T)$ is the saturated vapour pressure of carbon over an infinite flat surface. Strictly an exponential term should also appear in equation (3.8) but its value is around unity for all but the smallest of grains (see Lefèvre, 1979). The sticking coefficient, α_c, is taken as unity here.

As $p_{sat}(T)$ falls steeply with temperature the grain needs only to move a short distance ($\sim$ 2 stellar radii) from the star to decrease å to a negligible figure. Calculations of ejection rate and initial radius by Hoyle and Wickramasinghe (1962) have shown that a grain of radius $a \sim 5 \times 10^{-6}$ cm will survive pretty well intact on the outward journey attaining a velocity of escape of $\gtrsim$ 1000 kms^{-1}. Interaction with the interstellar medium will effectively stop the grain in $\sim$ 3 pc for $N_H \simeq 10\ cm^{-3}$ and $\sim$ 300 pc for $N_H \simeq 0.1\ cm^{-3}$ (Wickramasinghe, 1972).

Gilman (1972, 1973) has shown that circumstellar gas drag will effectively reduce the initial ejection velocity of grains to a terminal velocity, $u_T < 100\ kms^{-1}$ for stars such as αOrionis. This object is

considered to have a circumstellar envelope at the bottom end of the density scale for observed cool stars. Other stars of the same type would therefore have a lower value of u_T.

More recent work has shown that grains may well form in the atmospheres of much more common M-type stars (e.g. Salpeter, 1974). These grains would be composed of silicates, iron or, more controversially, silicon carbide.

There is a great deal of observational evidence for the existence of dust grains more particularly near cool giant stars (see e.g. Salpeter, 1977 and references therein). In the case of silicates (and possibly silicon carbide) the evidence is not only in the form of an infra-red excess but also a characteristic absorption feature at around 10 μm which is also apparent in the interstellar extinction curve.

It has been suggested however that in some cases interstellar and circumstellar grains may be widely different in their properties (see e.g. Forrest et al., 1975). If this is so then exposure to the interstellar environment over long periods of time must have a modifying effect on the grains.

3.3.1 Grain Temperature

The temperature of an individual dust grain is obviously dependent on the equilibrium relationship between heating by short wavelength radiation and the subsequent re-radiation of energy at longer wavelengths. This balance between incident and re-radiated energy is expressed for spherical grains by

$$\frac{\pi a^2}{4\pi r^2} \int_0^\infty L(\nu)\, Q_{abs}\,(\nu, a)\, d\nu = 4\pi a^2 \int_0^\infty \pi B(\nu, T_g)\, Q_{abs}\,(\nu, a)\, d\nu \qquad (3.9)$$

In this equation r is the primary source-grain distance; $L(\nu)\, d\nu$ is the energy flux from the primary source between frequencies ν and $\nu + d\nu$

and $B(\nu, T_g)$ is the Planck function defined by the grain temperature T_g and the frequency of re-radiation, ν. In order to solve equation (3.9) for T_g we may follow the assumptions made by Rees *et al.* (1969).

Firstly Q_{abs} (ν, a) is assumed constant in the ultra-violet region where most of the flux in high temperature sources emerges. Thus we have

$$\int_0^\infty L(\nu)\ Q_{abs}\ (\nu, a)\ d\nu \cong L\ Q^*_{abs}\ (a) \qquad (3.10)$$

where L is the bolometric luminosity of the primary source and Q^*_{abs} (a) is the absorption coefficient of small graphite grains in the ultra-violet spectral region (from now on all variables carrying a super-scripted asterisk, *, refer to the ultra-violet values of those variables).

Rees *et al.* further assumed that for small graphite particles the absorption efficiency in the infra-red Q_{abs}, is proportional to ν^2. This can be derived by considering the limit $(2\pi a/\lambda) << 1$ in the Mie theory for ideal spherical metallic or dielectric grains (Wickramasinghe, 1967):-

$$Q_{abs} \simeq (12\pi a/c\sigma)\ .\ \nu^2 \qquad (3.11)$$

where σ is the conductivity of the grain material. They ignored any grain size dependence however. For grains of other compositions, or having impurities, $Q_{abs} \propto \nu^\alpha$ is a more general form of solution. With these approximations incorporated in equation (3.9) grain temperature T_g then takes the form

$$T_g^{\alpha+4} = \frac{C_0 e^{-\delta *}}{r^2}$$

where C_0 is a constant for a given source.

Rees *et al.* (1969) concluded that the infra-red emission observed in many Seyfert galaxies is consistent with thermal radiation from dust grains. They further concluded that the variability observed in the infra-red is due to variable heating. By assuming that the limit on

variability is set by the light travel time across the shell being less than the period of variation of the central object they derived a minimum timescale of variability t_{min} where

$$t_{min} \propto \lambda^{2.5}$$

and at a given wavelength

$$t_{min} \propto L^{\frac{1}{2}}$$

so that a less luminous central source can give rise to more rapid variation of the infra-red flux from the dust shell.

The question has arisen however of how correct it is to assume that small grains heated by ultra-violet photons can be ascribed a steady-state temperature. Greenberg (1976) has found that for grains of radius $a \lesssim 0.005$ μm absorption by single ultra-violet photons will heat the grains as shown schematically in figure (3.2); larger grains will however approximate more nearly to the steady state temperature.

In the same paper Greenberg found that the time for diffusion of the incident photon's energy across the grain, t_{diff}, $\sim 2a/v_s$ where v_s is the speed of sound in the grain material. For graphite grains with $a \sim 10^{-5}$ cm, $t_{diff} \sim 10^{-10}$s and is therefore negligible (see Chapter 4).

Burbidge and Stein (1970) considered the cooling time, t_{cool}, of a grain to be a measure of its reaction time to changes in the incident high frequency radiation field. If U is the internal energy of the grain and $\dot{U}$ the rate of energy loss by re-radiation for a black body, then

$$t_{cool} \sim \frac{U}{\dot{U}} \simeq \frac{U}{4\pi a^2 \sigma_s T_g^4}$$

where the energy content

$$U \simeq \frac{3}{2} kT_g \ (N_0/A) \ (4/3\pi a^3 \ s)$$

k is Boltzman's constant, N_0 is Avogadro's number and A is the atomic

weight of a grain atom. Thus

$$t_{cool} \simeq \frac{kN_0 s\ a}{2\sigma_s\ T_g{}^3 A} \qquad (3.12a)$$

i.e.

$$t_{cool} \propto a/T_g{}^3 \qquad (3.12b)$$

For 0.1 μm graphite (or silicate) grains therefore, $t_{cool} \sim 10^{-3}$ sec at $\sim 1000^{\circ}K$.

3.3.2 Radiation Transfer within Dust Clouds

In the case of a spherically symmetric dust shell surrounding a source of high frequency radiation, such as is shown in figure (3.3), taken from Rowan-Robinson (1974) , the observed surface brightness at a point on the surface is found by integrating the equation of radiation transfer along a line of sight.

If the cloud contains grains whose number density is radially dependent (N(r)) and whose presence gives rise to an extinction of radiation passing through the volume elements containing them, the solution of the transfer equation will be of the form

$$\sum_{\nu}(\theta_2) = \int_0^{2R \cos\theta_2} B(\nu, T_g(r)).\exp -\left\{ \int_0^q N(r)\ \pi a^2\ Q_{ext}\ (\nu, a)\ dq' \right\}.$$

$$N(r)\ \pi a^2\ Q_{abs}\ (\nu, a)\ dq. \qquad (3.13a)$$

In equation (3.13a) q is as defined in figure (3.3) and r is a function of q.

The observed flux from the cloud, f_{ν}, is defined as

$$f_{\nu} = \int_{\Omega} \Sigma_{\nu}(\theta_2)\ d\Omega \qquad (3.13b)$$

The observed flux in this case is then given by

$$f_{\nu} = \frac{2\pi R^2}{D^2} \int_0^{\pi/2} \Sigma_{\nu}(\theta_2)\ \sin\theta_2\ \cos\theta_2\ d\theta_2 \qquad (3.13c)$$

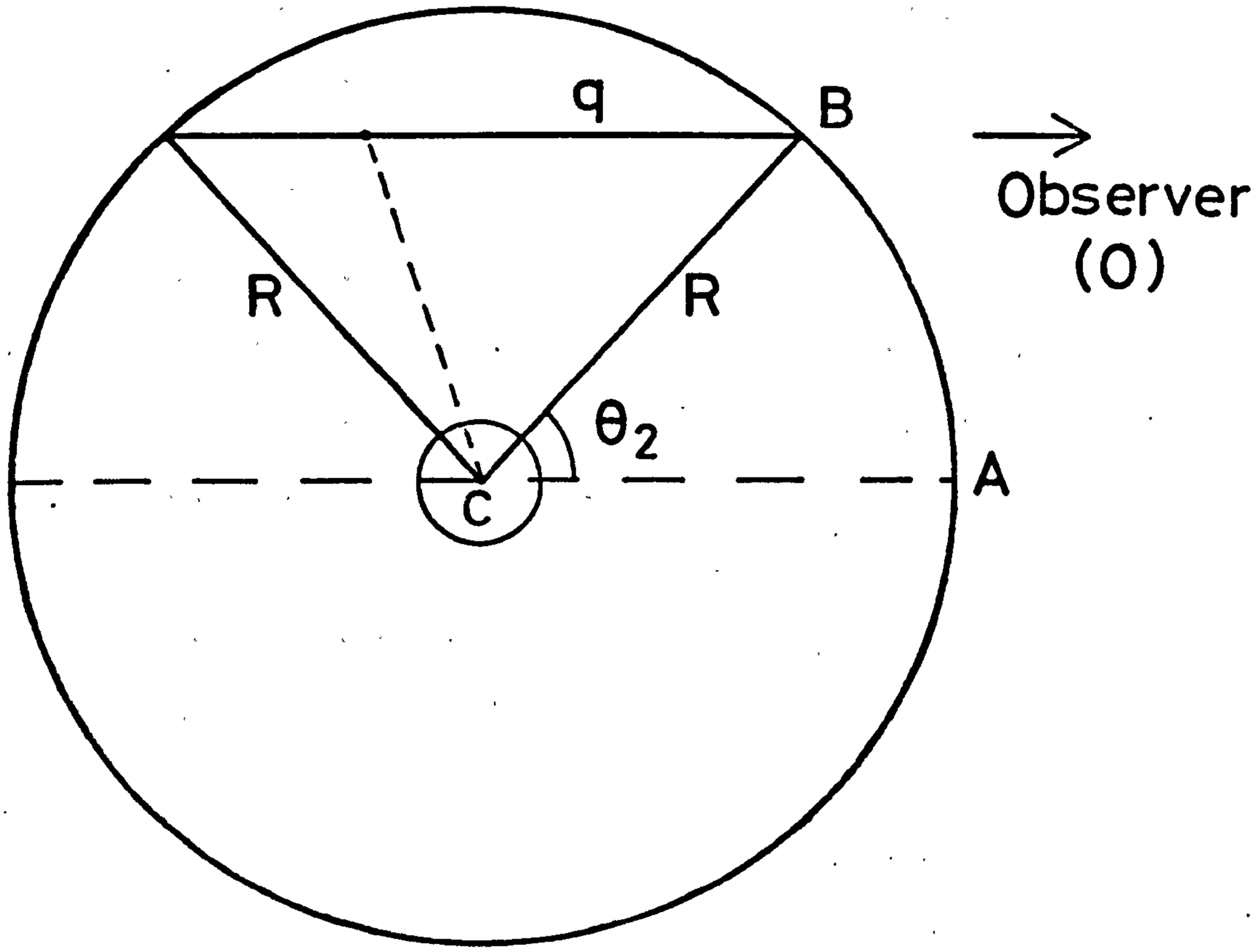

Figure (3,3) The geometry of a central source at C surrounded by a spherical shell of dust grains radius R. (after Rowan-Robinson, 1974). See text for further clarification.

Equation (3.13c) was solved by Larson (1969) and a modified solution was used by Rowan-Robinson (1974) to investigate infra-red emission from the Orion nebula. This latter work resulted in Rowan-Robinson ascribing the emission to very large (a $\lesssim 0.01$ cm) grains.

3.4.1 The Geometry of Variable Sources

Observations of Nova Persei 1901 revealed an expansion in the luminous 'halo' about the nova which appeared to be greater than the speed of light in vacuo (Stratton, 1928). Couderc (1939) suggested that the observed expansion was not that of material ejected by the nova but was in fact due to reflection from material which might have arisen from previous outbursts surrounding, or near, the nova. The geometry of the situation alone would then lead to super-light expansion being observed.

One case considered by Couderc and taken here as a general illustration from which some of the geometrical considerations of later chapters arise is that of a 'slab' of matter lying between the nova and the observer (see figure 3.4).

In figure (3.4), if the origin of time is taken to be the instant when a distant observer at O first sees the nova then the reflection (or re-emission) from matter at M or P is observed at time t later. At time t reflection from Q will also be observed. It can be seen that if NM = ct then NQ = ct/2 for both reflections to be seen at the same observer time.

Further, we can see that $NM + z = a = \sqrt{x^2 + z^2}$ where x and z are the coordinates of V in figure (3.4).

i.e.
$$z = \frac{x^2}{2ct} - \frac{ct}{2} \qquad (3.14)$$

which is the equation of a parabola with semi latus rectum ct and with the nova at the focus.

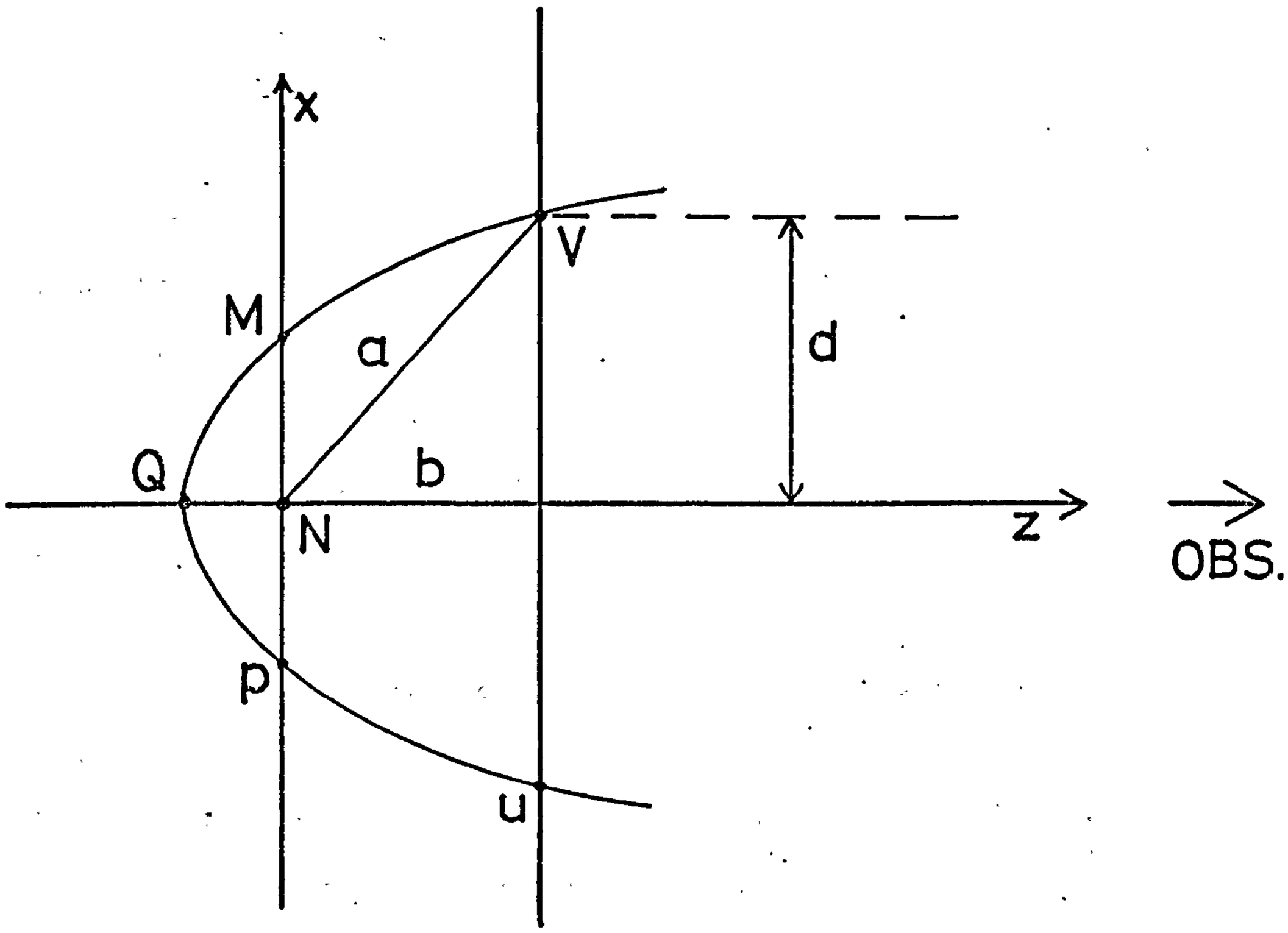

Figure (3.4) The geometry of a source of high frequency radiation at N with a 'slab' of material lying between it and the observer (after Couderc, 1939). The significance of points U, P, Q, M, V and distances a, b, d is given in the text.

If the plane containing the points VU is at right angles to the z-axis then the reflection (or emission) will appear to originate in a circle of radius d where $d = (2ctb + c^2t^2)^{\frac{1}{2}}$. The velocity of expansion of this circle is therefore given by

$$v_d = (cb + c^2t)(2bct + c^2t^2)^{-\frac{1}{2}} \qquad (3.15)$$

The velocity $v_d \geq c$ for all $b,t \geq 0$. This general model was used reasonably successfully by Couderc (1930) to explain the observations of Nova Persei 1901.

Morrison and Sartori (1969) utilised the ideas given by Couderc to explain the observed changes in the spectra and light curves of type I and II supernovae. They imagined the supernova to be at the centre of a volume of gas surrounding the original star. The explosion of the supernova was then considered to provide what is effectively a δ-function pulse of ultra-violet photons which excite the atoms and molecules of the surrounding gas. Because of the nature of the situation, the effects which are then observed at a distance persist for a long period of time relative to the length of the original pulse. The effect is therefore labelled 'optical reverberation' by the authors.

There are of course other astrophysical situations in which the 'optical reverberation' mechanism might well apply. These include compact extragalactic radio sources in which there appears to be a faster than light separation of source components if the red-shifts observed are cosmological (see e.g. Blandford, et al., 1977).

3.4.2 Phase and Amplitude Relationships for Fluctuating Sources

Terrell (1967) considered the situation in which a surface which is fluctuating sinusoidally and in phase as seen by a centrally placed observer is observed externally at a large distance.

In the source reference frame the intensity of radiation at any

point is given by:-

$$I = \bar{I} + I_f \sin \omega t \tag{3.16a}$$

where

$$\bar{I} \geq I_f \geq 0 \tag{3.16b}$$

If the observer is now at O external to the surface at a very large distance the fluctuation at point A (see figure 3.3) will follow that in equation (3.16a), but at point B the fluctuation will appear to be shifted in phase, i.e.

$$I = \bar{I} + I_f \sin(\omega t - \Delta t) \tag{3.16c}$$

where $\Delta t = R(1 - \cos\theta_2)/c$.

For a sphere opaque to its own radiation we find the total observed luminosity by integrating over the surface, i.e.

$$L = \int_0^{\pi/2} \left[\bar{I} + I_f \sin(\omega(t - \frac{R}{c}(1 - \cos\theta_2))\right] 2\pi R^2 \sin\theta_2 \cos\theta_2 \, d\theta_2$$

$$\equiv \pi R^2 \left[\bar{I} + I_f F(\chi) \sin(\omega t - \Phi)\right] \tag{3.17}$$

where $\chi = \omega R/c$ and Φ is the phase difference between centrally and externally observed fluxes. $F(\chi)$ is therefore the fraction of the true fluctuation observable at a distance. Terrell found that

$$F(\chi) = \frac{2}{\chi^2}(2 + \chi^2 - 2\cos\chi - 2\chi \sin\chi)^{\frac{1}{2}} \tag{3.18a}$$

$$\tan \Phi = (\chi - \sin\chi)/(1 - \cos\chi) \tag{3.18b}$$

For large values of χ, $F(\chi) \simeq 2/\chi$ and $\Phi \simeq \pi/2$. Thus we may set a limit on source radius, R, by using these results.

From equations (3.16b) and (3.17) the fractional change in luminosity, ΔL, can be seen to be limited by

$$\Delta L/\bar{L} \leq 2F(\chi) \tag{3.19}$$

Therefore if we substitute the asymptotic form of $F(\chi)$ in (3.19) we have the result

$$R \leq \frac{2cP}{\pi} \frac{\bar{L}}{\Delta L} \tag{3.20}$$

where P is the period of fluctuation.

Since $|dL/dt| < \pi \ \Delta\bar{L}/P$ for sinusoidal fluctuations we have

$$R \lesssim 2c\bar{L}\left(\left|\frac{dL}{dt}\right| \right)^{-1} \qquad (3.21)$$

Equation (3.21) applies for non-sinusoidal fluctuations as well (Terrell, 1967).

3.5.1 Classical Novae - Theoretical Background

Chapter 2 has already outlined the main observational data on classical novae. This section seeks to describe the current theories employed to explain some of the nova phenomena.

It has been known for some time that most (if not all) classical novae belong to semi-detached binary systems (Kraft, 1963) which have as their components a relatively cool main sequence star and a compact hotter star. For at least some of the lifetime of the binary system the cool component loses mass, through the inner Lagrangian point of the pair, to the primary hotter star. At some point in this process enough mass has been deposited on the surface of the primary for the temperature of the material to reach ignition point. Because the resultant material is degenerate, temperature is not very sensitive to pressure changes. Thus energy generation is not limited by the subsequent expansion of the surface material until degeneracy is lifted. The result is a thermonuclear runaway which produces a large amount of energy in a relatively short space of time. This is thought to be why a classical nova shows the characteristic steep rise in luminosity at the onset of activity and why certain elements appear to be overabundant with respect to solar values (see Sparks et al., 1977 and references therein).

As soon as the thermonuclear runaway starts, the surface layers of accreted matter are blown off and reach velocities far greater than that required for escape from the system. At maximum light a typical nova

will show a continuum which approximates to a black body at $\sim 7000^{o}K$ arising in the ejecta. The dimensions of the ejected shell giving rise to emission at this stage are $\sim 10^{13}$ cm compared with the binary separation of $\sim 10^{11}$ cm. The central system is thus hidden from view by an optically thick wind (see Bath, 1978a and references therein). The typical ejection velocity of the shell is $\lesssim 1000$ kms^{-1}.

It appears that the mass outflow is driven by the central object and that the outflow rate decreases with time. The results of this mass loss rate decrease are that, at short wavelengths, the photospheric radius appears to decrease as the optical depth decreases; also as more short wavelength radiation penetrates the shell the temperature of the nova appears to increase. This temperature increase is accompanied by a progressive photoionization of atoms and ions with increasing ionization potentials and an associated fall in the strength of the optical continuum (Bath, 1978b). The effective temperature for the photosphere when in radiative equilibrium, T_*, is given for post maximum times by (Bath & Shaviv, 1976)

$$T_* = \left(\frac{L}{4\pi\sigma_s} \right)^{\frac{1}{4}} \left(\frac{8\pi v}{3\kappa\dot{M}} \right)^{\frac{1}{2}} \qquad (3.22a)$$

where v is the ejection velocity and $\dot{M}$ the mass loss rate. κ, the opacity, is itself temperature dependent and equation (3.22a) must strictly be solved iteratively (Bath, 1978b). However one can see from equation (3.22a) that for a constant luminosity and velocity of ejection the effective temperature will increase only as the mass loss rate decreases. Figure (3.5) taken from Bath (1978b) shows how this mass loss rate change will affect the flux observed through a B filter. A fall in loss rate beyond $\sim 10^{22}$ gs^{-1} produces a much more rapid decline in the B magnitude.

The increase in the effective photospheric temperature can be related to the decline in magnitudes Δm of the observed flux from peak

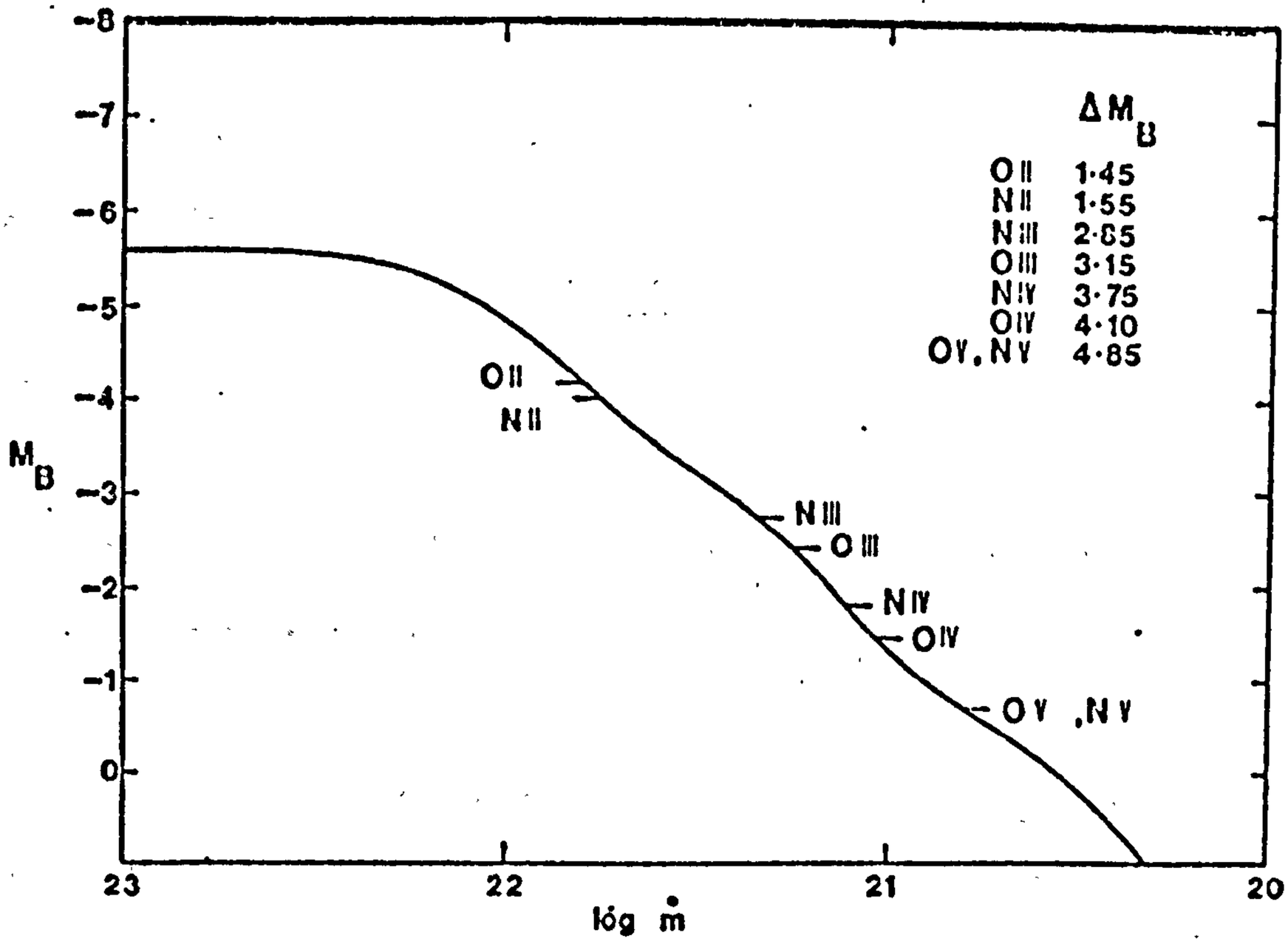

Figure (3.5) The variation of the absolute B magnitude with nova mass loss rate $\dot{m}$ for a source with a constant luminosity of 1.05×10^{37} erg s^{-1} (from Bath, 1978b). A constant outflow velocity of $10^3 kms^{-1}$ has been assumed. The stages at which various emission lines of oxygen and nitrogen might be expected to appear as a result of photoionization are also indicated.

by the relation (Bath & Shaviv, 1976)

$$\Delta m \sim -2.5 \log \left[\frac{0.05134}{T_*^3} \left[\frac{hc}{k\lambda_c} \right]^3 \right] \qquad (3.22b)$$

where λ_c is the assumed cut-off wavelength of the blue filter ($\sim$ 3500 Å). This relationship is only valid for cases where λ_c lies on the Rayleigh-Jeans tail of the Planck spectrum (i.e. $T_* \gtrsim 4 \times 10^4$K); the exact relationship is derived by integration of the full form of the Planck function.

The transition stage observed in many novae as a rapid decline in UBV magnitudes may be associated with the point in the mass ejection process where the ejecta become optically thin and the innermost photosphere of the binary system itself is uncovered (e.g. Warner, 1976 p. 123). The rapid rise in temperature therefore expected at transition is well known (see McLaughlin, 1960, p. 633).

Bosma (1975) has shown, by consideration of the state of ionisation of the shell, that the secondary maximum after transition probably arises as a result of a reionization of the ejecta by Lyman-α photons able to penetrate to the outermost reaches. He provides a complete semi quantitative explanation of the transition stage of Nova DQ Her 1934 in this way.

By the time the nebular stage of the nova is reached (see Chapter 2) the emission line profiles indicate that the ejecta are not isotropically distributed about the nova (Hutchings, 1972). The most likely form of the ejecta at this stage consists of polar blobs and a disc in the plane of the binary orbit. Figure (3.6), adapted from Boyarchuk and Gershberg (1977) shows the configuration of ejecta associated with Nova Cygni 1975.

It is now widely accepted that novae are generally recurrent phenomena with classical novae perhaps being rather long period versions of the known recurrent novae (see e.g. Ford, 1978). Thus they may

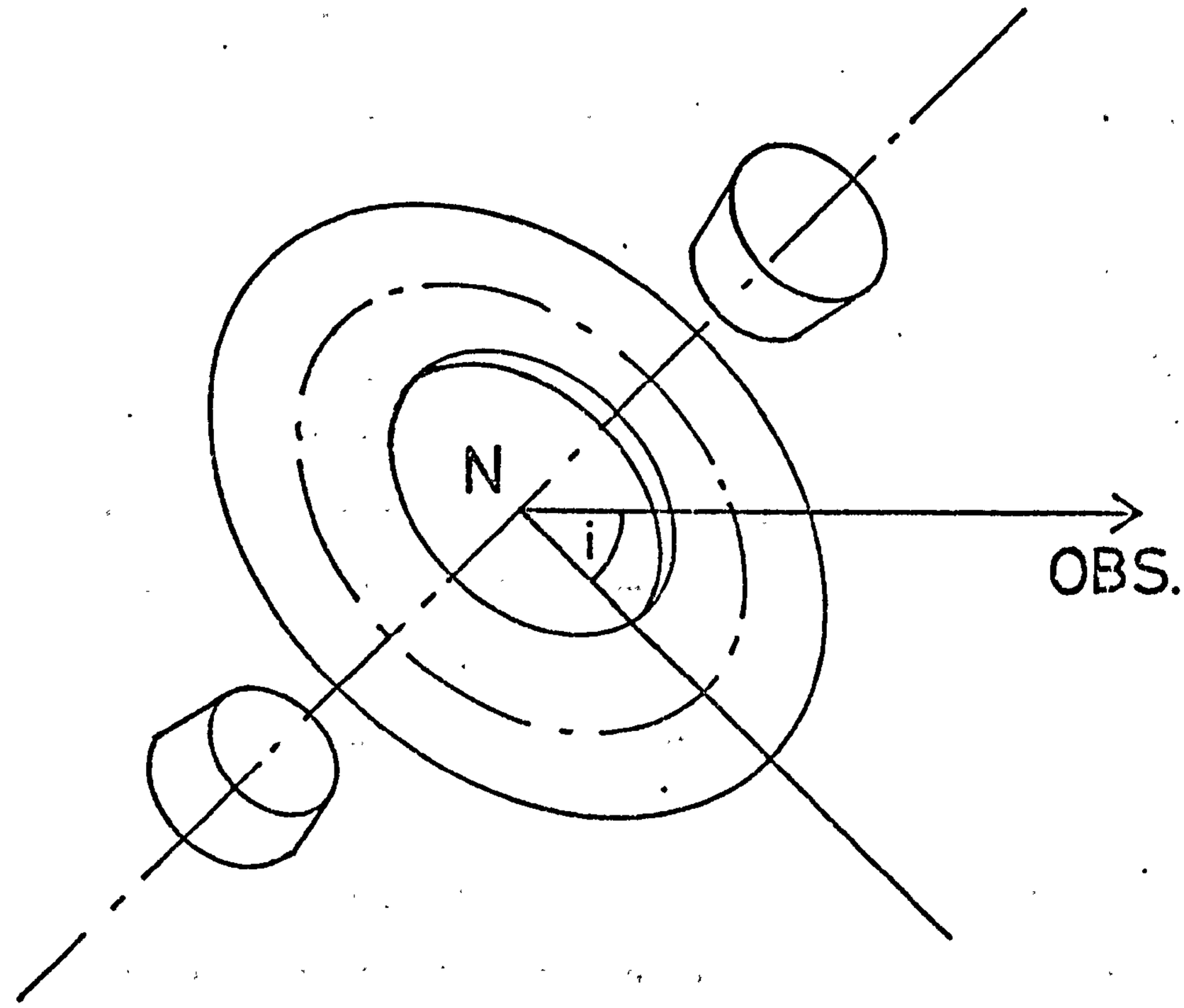

Figure (3.6) The polar blob - equatorial ring model of the ejecta of Nova Cygni 1975. (after Boyarchuk and Gershberg, 1977). In this case the inclination to the line of sight of the ring $i \sim 60^{o}$. The nova binary itself is at N.

provide a good deal of the interstellar mass density in the form of gas or condensed grains (see e.g. Clayton & Wickramasinghe, 1976).

3.5.2. Classical Novae - Grain Formation

The almost classic observations of Nova Serpentis 1970 in the infra-red (Geisel et al., 1970; Hyland & Neugebauer, 1970) showed that around the time of transition in the visual light curve of the nova, the infra-red flux increased by almost two orders of magnitude. The resulting spectra were characteristically thermal and resembled those of a cooling black body with temperature $\sim 900^{o}K$. Subsequent observations of other novae have shown that this behaviour is apparently common in moderate speed objects (see Chapter 2). From calculations of black body emission Geisel et al. derived a grain mass at $\sim$ 100 days after discovery of the order of 10^{-6} $M_{\odot}$ as being responsible for the infra-red flux.

Clayton and Hoyle (1976) assumed that grain formation within the ejecta of the current outburst gives rise to the development of an infra-red excess. The basis of their argument was that the overabundance of carbon in nova ejecta leads to a rapid condensation of graphite grains.

The site of formation of grains was taken to be the fast moving shell responsible for the observed diffuse-enhanced spectrum ($v \sim 2000$ kms^{-1}). The total mass of this shell was taken to be $\sim 3 \times 10^{-4}$ $M_{\odot}$ and the luminosity of the central star was assumed to decrease from $\sim 10^{5} L_{\odot}$ to $\sim 2 \times 10^{4}$ $L_{\odot}$ in the first 50 days.

Carbon grains were assumed to form initially at distance $r = r_o$ from the central star. With a condensation temperature of $\sim 2000^{o}K$ and $L \sim 10^{5}$ $L_{\odot}$, $r_o \sim 1.8 \times 10^{14}$ cm. At $v \sim 2000$ kms^{-1} this is reached after $\sim$ 11 days. If complete condensation occurred at $r = r_o$ the optical depth would be so great to the infra-red flux that it would be trapped within the shell and raise the grain temperatures again so that they would evaporate. However as r increases beyond r_o the optical

depth can increase beyond unity without evaporation provided $\delta(r_o/r)^2$ remains constant (δ is the optical depth to infra-red radiation). If the luminosity of the central star decreases as well, then δ can increase even more rapidly than $(r/r_o)^2$. The optical luminosity then falls as $e^{-\delta}$ according to the authors.

Figure (3.7), taken from Clayton and Hoyle (1976) shows that the growth of grains is thought to be associated with the decrease in visual light around the time of transition. The infra-red energy is stored by the optically thick shell as the visual curve drops. If growth ceases at $r = r_c$ the opacity will then decrease as $r_c^4/r_o^2r^2$ and the visual light curve will increase again. The visual attenuation is thus governed by

$$\left.\begin{array}{l} \exp\left\{-\left[\frac{r}{r_o}\right]^2\right\}, \; r_o < r < r_c \\ \exp\left\{-\frac{r_c^4}{r_o^2 r^2}\right\}, \; r_c < r \end{array}\right\} \qquad (3.23)$$

and the minimum of the transition will occur at $r = r_1$. Calculations relevant to Nova Serpentis 1970 showed that if $r_0/v \sim 19$ days, $r_1/v \sim 48$ days (i.e. grain growth complete at $t \sim 48$ days).

If we refer to figure (3.7) we can see that as the opacity drops, the infra-red radiation that was trapped is now released as the visual curve also rises. Clayton and Hoyle also expect the grain temperatures to drop rapidly, as observed by Geisel et al. (1970).

From the model the grain size at $r = r_1$ appears to have been large ($\sim$ 5 μm) and the total grain mass $\sim 10^{-5}$ $M_\odot$. This large mass of grains, if typical of novae, is thought to contribute a significant amount of anomalous isotope enriched grains to the interstellar environment.

The basic concept of grain formation on short timescales in novae has been developed further by Clayton and Wickramasinghe (1976). Again the parameters and results of the model were compared with Nova Serpentis

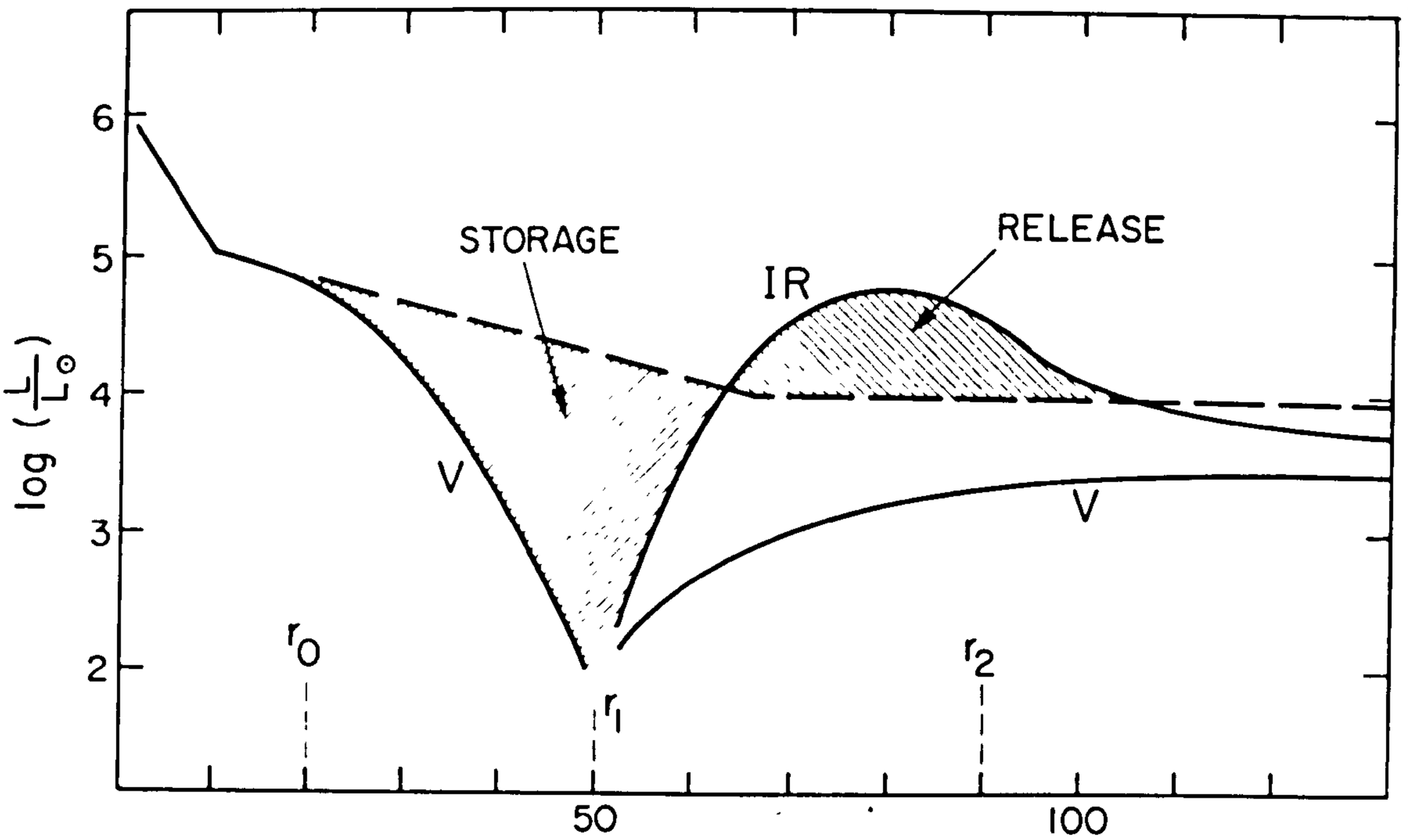

Figure (3.7) Schematic representation of the effects of rapid grain growth on the visual light curve of a nova (from Clayton and Hoyle, 1976). Note the storage and release mechanism associated with transition.

1970.

Clayton and Wickramasinghe assumed that the bulk of the ejected mass is in the form of carbon and that once the temperature appropriate for small ($a = a_0 \simeq 3 \times 10^{-7}$ cm) grains falls below the condensation temperature of graphite, grain growth will begin. For carbon densities of 10^7 cm$^{-3} \lesssim N_c \lesssim 3 \times 10^9$ cm^{-3} the condensation temperature T_c will be $1900^oK \lesssim T_c \lesssim 2100^oK$, i.e. $T_c \simeq 2000^oK$.

The point in the ejection at which this occurs ($r = r_0$, $t = t_0$) is determined by the luminosity of the central object and the optical properties of the grains. For small particles ($a < 10^{-4}$cm) the Planck mean of the absorption efficiency $\bar{Q}_{abs} << 1$ (Gilman, 1974) and is approximated by

$$\bar{Q}_{abs}\ (a, T_g) \simeq 3.22a \left[\frac{T_g}{10}\right]^{1.65} \tag{3.24}$$

for graphite (Clayton & Wickramasinghe, 1976).

If T_{rad} is the temperature of a perfect black body at distance r from the central object, then the grain temperature, T_g, is given by

$$T_g = (T_*^{1.65}\ T_{rad}^{4})^{1/5.65} \tag{3.25}$$

where T_* is the central star temperature, hence $T_g > T_{rad}$. Thus for $T_g = T_c = 2000^oK$, $T_{rad} = 1030^oK$ and r_0 is given by

$$r_0 \simeq 7.73 \times 10^{14} \left[\frac{L}{5 \times 10^4 L_\odot}\right]^{\frac{1}{2}} \cdot \left[\frac{T*}{10000^oK}\right]^{0.825} \text{ cm} \tag{3.26a}$$

which gives the time of condensation, t_0, as

$$t_0 \simeq 89.47 \left[\frac{L}{5x10^4 L_\odot}\right] \cdot \left[\frac{v}{10^8 cms^{-1}}\right]^{-1} \cdot \left[\frac{T_*}{10000^oK}\right]^{0.825} \text{ days} \tag{3.26b}$$

Clayton and Wickramasinghe (1976) assumed that grain nucleation occurs instantaneously at $t = t_0$ and that after that no new grains are formed. The total grain number, N_{TOTAL}, thus remains constant and

the grain radius at time t will be given by

$$a = a_0 + 0.8A' (N_c)_0 t_0 \left\{1 - \left[\frac{t}{t_0}\right]^{-5/4}\right\} \qquad (3.27a)$$

where $A' = 5.05 \times 10^{-20} \left[\frac{T*}{10^4}\right]^{-0.206}$ $cm^4 s^{-1}$ and $(N_c)_0$ is the carbon atom number density at time $t = t_0$.

Taking the maximum eventual size of the grains, $a_\infty \simeq 0.8A' (N_c)_0 t_0$,

$$a_\infty \simeq 1.571 \times 10^{-6} \left[\frac{t_0}{45 \text{ days}}\right] \left[\frac{(N_c)_0}{10^7 cm^{-3}}\right] \left[\frac{T*}{10^4 {}^oK}\right]^{-0.206} \text{ cm} \qquad (3.27b)$$

The initial growth of the grains will be rapid (see equation 3.27a) and will decrease as the shell expands resulting in a drop in N_c.

As grains increase in radius the temperature given by equation (3.25) ceases to be valid. Clayton and Wickramasinghe (1976) then calculated T_g using energy balance equations similar to those outlined earlier in this chapter except of course that both a and r are time dependent here. During rapid grain growth the temperature falls quickly due to an increase in radiating efficiency. When growth effectively ceases, there is a change in the slope of the temperature curve and the temperature then falls more slowly due to expansion alone. The authors found that the curve of the temperature against time graph for $a_\infty \sim 2 \times 10^{-4}$ cm most resembles the observed temperature behaviour of Nova Serpentis 1970 if $t_0 \simeq 45$ days. These large grains will emit radiation whose spectrum will closely resemble a black body at temperature T_g. The situation is complicated if the condensed shell is opaque to infra-red, as discussed by Clayton and Hoyle (1976) however. The infra-red luminosity, L_{1R}, is thus given by equation (3.28) where F_{abs} is the radiation absorbed by a dust grain:-

$$L_{1R} = \min \left[N_{TOTAL} F_{abs}, L\right] \qquad (3.28)$$

The resulting infra-red curves for $T_* = 10000^oK$ and $T_* = 15000^oK$ are shown in figure (3.8). For an optically thin nebula the maximum

Figure (3.8a) The development of the infra-red luminosity, L_{IR}, of a nova on the rapid grain growth model (from Clayton and Wickramasinghe, 1976). The central source effective temperature $T_* = 10000^{o}K$.

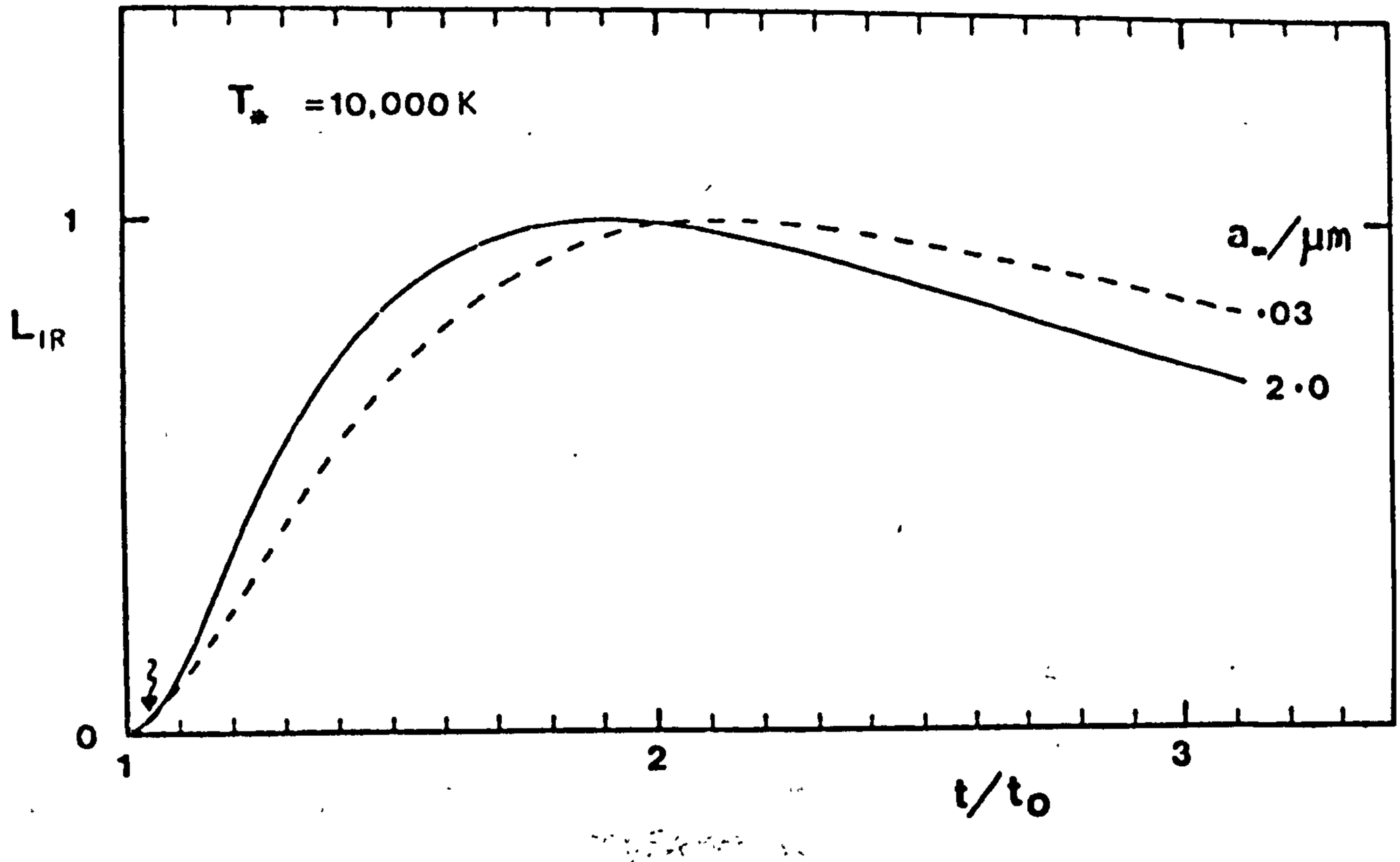

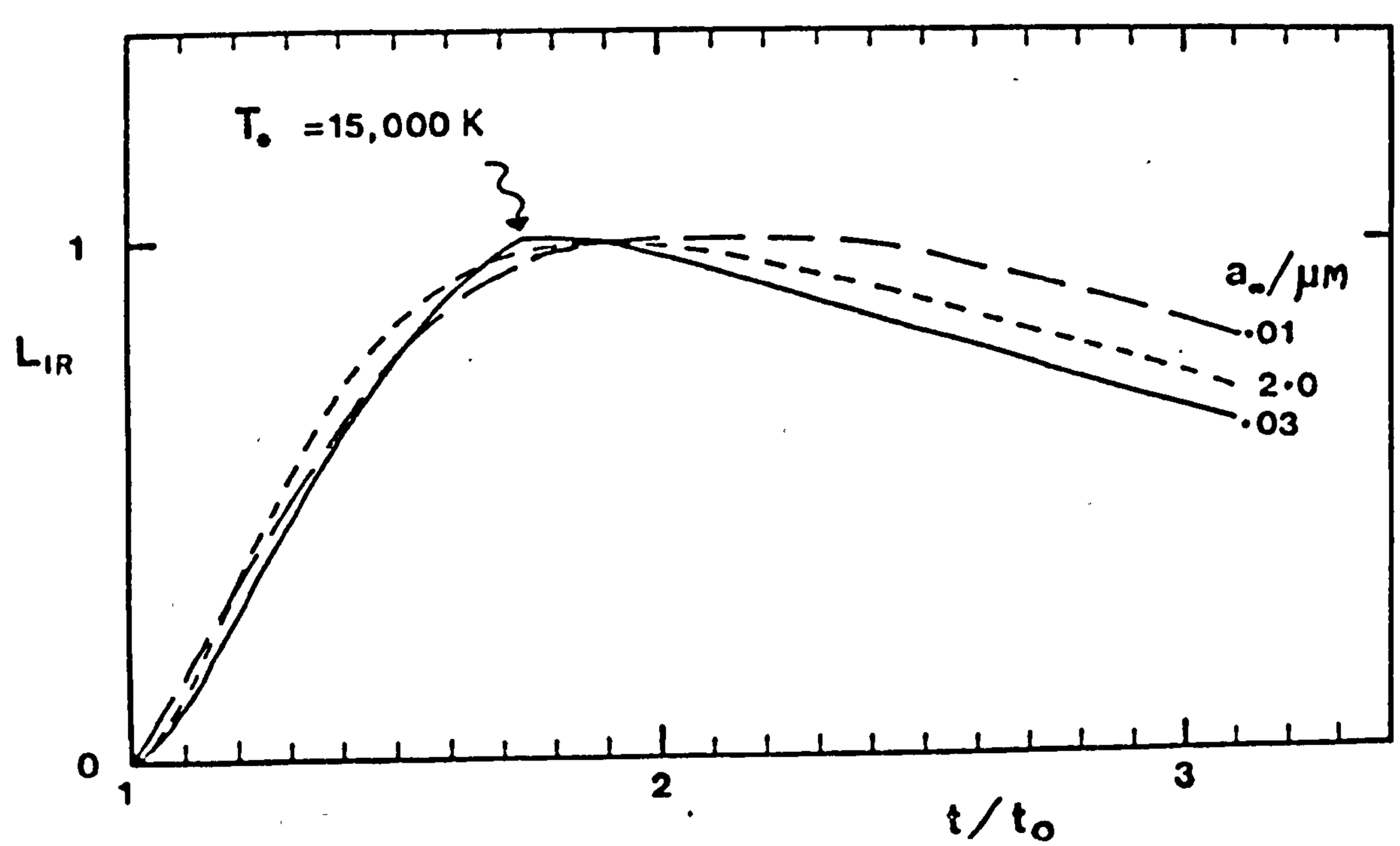

Figure (3.8b) As (3.8a) except $T_* = 15000^{o}K$. Note change of slope for 0.03 μm grains.

infra-red emission occurs at a time $t_{max} \simeq 2.33\ t_0$. The flux then falls slowly as t^{-2}. The arrowed discontinuity in the slope of the 0.03 μm curve of figure (3.8b) is due to the cessation of increase in the absorption efficiency of the grains ($\left[\bar{Q}_{abs}\right]_{max} = 1$). Clayton and Wickramasinghe note that this slope change appears in the light curves of Nova Serpentis 1970 at approximately t = 70 days.

After studying the effects of making the shell of grains optically thick, Clayton and Wickramasinghe (1976) considered how the parameters in the equations noted here can be chosen to give a qualitatively correct model for Nova Serpentis 1970. They set $t_0 = 45$ days which with $L \simeq 5 \times 10^5\ L_\odot$ and $T_* = 10^{4o}K$ gives $v \simeq 2 \times 10^8\ cms^{-1}$. For $L \simeq 1.9 \times 10^4\ L_\odot$ ($T_* = 10^{4o}K$), $v \simeq 1.226 \times 10^8\ cms^{-1}$. If $T_g < 900^oK$ after 90 days then $a_\infty \cong 2 \times 10^{-4}$ cm. The time of predicted peak in the infra-red then closely matches that observed. The atomic carbon number density at t = 0, $(N_c)_0$, = $1.27 \times 10^9\ cm^{-3}$ for $T_* = 10^{4o}K$ and $1.17 \times 10^9\ cm^{-3}$ for $T_* = 1.5 \times 10^{4o}K$.

The weak early infra-red excess at $\lambda \simeq$ 5 μm was ascribed to the stretching of molecular carbon bonds. These carbon molecules were thought to subsequently act as nucleation centres for grain growth. (Note - Ferland et al., 1979, have subsequently shown that excesses at this wavelength in both Nova Vulpeculae 1976 and Nova Serpentis 1970 are likely to be due to CO formation within the nova ejecta.)

Finally the authors concluded that $\sim 3 \times 10^{-5}\ M_\odot$ of grains were formed which would, if typical of novae, provide a substantial part of the interstellar grain density.

Yamamoto and Nishida (1977) carried out detailed calculations based on the assumption that the abundance of elements in nova ejecta is similar to the solar abundance. If this is in fact the case then the C/O abundance ratio is less than unity (as it is even with the heavy element enhancement of the theoretical models of Starrfield et al.,

1974). Thus it is considered that carbon atoms will almost all be depleted preferentially into CO molecules and therefore cannot condense to form graphite grains (see also Ferland et al., 1979). Yamamoto and Nishida then proceeded to consider the formation of grains from other elements.

Assuming spherically symmetric expansion of an ejecta envelope with uniform gas temperature, T, and atom number density, N(T), the radius of the ejected shell, $R_{gas}(T)$ and N(T) can be found for a particular T from equations (3.29a) and (3.29b),

$$R_{gas}(T) = 4.3 \times 10^{14} \left[\frac{1100K}{T}\right]^{2} \left[\frac{L}{5 \times 10^{4} L_{\odot}}\right]^{\frac{1}{2}} \text{ cm} \qquad (3.29a)$$

$$N(T) = 3.5 \times 10^{9} \left[\frac{T}{1100K}\right]^{6} \left[\frac{\Delta M}{3\times10^{-4} M_{\odot}}\right] \left[\frac{0.3}{G}\right] \left[\frac{5\times10^{4} L_{\odot}}{L}\right]^{3/2} \text{ cm}^{-2} \qquad (3.29b)$$

where L is the nova luminosity; ΔM is the total mass lost through ejection and G is a geometrical factor of the shell.

Consideration of condensation temperatures of Al_2O_3, Mg_2SiO_4, $MgSiO_3$, SiO_2 and Fe showed that they condense out in this order. However Al is about an order of magnitude less abundant than Si; Al_2O_3 grains were thus ignored. Magnesium silicate in the form of fosterite (Mg_2SiO_4) or enstatite ($MgSiO_3$) is thought to be a likely first condensate.

Having investigated the nucleation process in non-steady-state conditions Yamamoto and Nishida proceed to derive the maximum grain size, a_{max}, produced once the available condensate is exhausted. This is given by

$$a_{max} = 87 \frac{c_0}{5 \times 10^{5} \text{ cm}^{-3}} \frac{(R_{gas})_0}{3_v} / 10^{6} \text{ sec} \left[\frac{T_0}{1100^{o}K}\right]^{\frac{1}{2}} A^{o} \qquad (3.29c)$$

where c_0 is the monomer concentration at the time of onset of condensation,

t_0. $(R_{gas})_0$ and T_0 are the ejected shell radius and gas temperature respectively.

The main conclusions of the study were:-

(1) The major constraint on whether a nova is a grain producer or not is the ejected mass. For solar abundance and $v \simeq 1000$ kms^{-1}, $\Delta M > 10^{-4}$ $M_\odot$ for condensation to occur.

(2) Grains will grow from condensation to a_{max} in about 10 days.

(3) The grains that are formed will have a fairly flat grain size distribution from a few Å to several hundred Å. However the maximum size of grains will only be hundreds of Angstroms unlike the grains of Clayton and Hoyle (1976) and Clayton and Wickramasinghe (1976) which are much larger ($\gtrsim 10^{-4}$ cm).

(4) A 10 μm feature would be expected in novae corresponding to silicate absorption.

(5) Graphite grains will only form if C/O is far greater than unity. According to Yamamoto and Nishida there is little direct evidence that this is so.

Gallagher (1977) based his grain formation model of novae with infra-red excesses on the assumption that Nova Serpentis 1970 was typical of all dust forming novae. Like Clayton and Hoyle (1976), he contended that the transition region provides evidence of substantial formation of dust grains which cause obscuration of the pseudophotosphere beneath. The major difference between novae which form dust and those that do not was concluded to be the luminosity of the central system.

Assuming that the condensation temperature for all novae T_c is the same ($\sim 1300^{\circ}$K) as seemingly observed in Nova Serpentis 1970 (Geisel et al., 1970) Gallagher derived the following relationship between the time taken for dust to form, t_0, and the luminosity of a presumed constant luminosity phase, L_{CL}

$$t_0 = \left[\frac{320}{v}\right] \sqrt{L_{CL}/L_\odot} \text{ days} \qquad (3.30a)$$

(velocity v in kms^{-1}). Therefore assuming all novae form the same type of grains the time of expected grain formation for individual novae can be determined.

It was proposed however that if most of the ejecta are ionised then grain formation will be inhibited. The time taken for all the ejecta to ionise is given by

$$t_i = 2.2 \times 10^6 /_v (L_{CL}/L_\odot)^{1/3} \text{ days} \qquad (3.30b)$$

For grains to form therefore $t_i > t_0$, i.e. $L_{CL} < 4 \times 10^4 L_\odot$. Thus fast and very fast novae would not form grains on this model.

Gallagher noted that the expected dust formation in Nova Delphini 1967 at 45 days did not occur. This he put down to the low mass loss rate perhaps decreasing the density of condensates below levels where appreciable condensation might occur.

3.6.1 Theoretically derived dust shell parameters

It has proved very difficult to derive dust shell parameters from observation. However Malakpour (1977) concluded from studies of Balmer decrements in novae that substantial amounts of grains exist around the pre-nova prior to outburst. He accounted for the change in observed Balmer decrement by assuming that the ejecta encounter these grains causing them to grow. The radius, R, of the envelope giving rise to these observations lies in the range 5×10^{14}cm < R < 5×10^{15}cm. The dust particles themselves have a radius of $\sim 10^{-5}$ cm and the properties of interstellar dust. The evidence for a pre-existing dust shell was found to be particularly strong for Nova Delphini 1967 (Malakpour, 1973). He proposed that condensation of grains generally occurs slowly at large distances from the nova. As the radiation pressure from the previous outburst decreases these grains

fall toward the system but cannot approach closer than $\sim 3 \times 10^{15}$ cm because of radiation pressure from the quiescent nova system.

The lack of substantial infra-red emission from Nova Cygni 1975 was seen as indicating a lack of circumstellar matter prior to the outburst. Evidence for this view is the lack of thermal X-rays which according to Brecher et al. (1977) are due to collisional heating of the pre-existing circumstellar envelope by the ejecta.

The problem of deriving the actual dimensions of the dust shell has been tackled by Ney and Hatfield (1978), amongst others, by the use of black body considerations. Basically, if the grains are taken to be black bodies forming a spherical shell that is opaque to its own radiation the flux, f_λ, observed will be given by

$$f_\lambda = \frac{2hc^2}{\lambda^5} \frac{1}{e^{hc/\lambda kT} - 1} \frac{\pi \theta_{BB}^2}{4} . \qquad (3.31a)$$

Wein's law gives $\lambda_{max} T \cong 0.29$ cm^{o}K and if this is substituted into equation (3.31a) then the angular diameter in seconds of arc can be found from the expression

$$\theta_{BB}'' \simeq 2 \times 10^{11} (\lambda F_\lambda)_{max}^{\frac{1}{2}} T_{BB}^{-2} \qquad (3.31b)$$

where θ_{BB}'' is the 'black body angular diameter' in seconds of arc and T_{BB} is the black body temperature of the shell.

The mass of grains in the shell can be estimated from consideration of total infra-red luminosity and total grain number, N_{TOTAL}, i.e.

$$L_{IR} = 4\pi a^3 \sigma_s T_g^4 N_{TOTAL} \bar{Q}_{abs} \qquad (3.32a)$$

if T_g is constant throughout the shell (Vrba et al., 1977).

Substituting for $\bar{Q}_{abs}$ from equation (3.24) into equation (3.32) we have

$$M_g = \frac{4.62 \; s \; L_{IR}}{\sigma_s \; T_g^{5.65}} \qquad (3.32b)$$

Obviously this derived grain mass is liable to be only an approximation if the shell is extensive and T_g is thus radially dependent. For the nova models of Chapter 5 for example the total grain mass calculated by this method is somewhat less than we require.

3.7.1 Conclusion

As we have seen in this chapter, previous authors have dealt thoroughly with grain properties and the possible origins of both interstellar and circumstellar grains. They have also carried out detailed studies of the mechanisms behind variable sources such as novae. It appears however that the variability of thermal radiation resulting from changes in a source of ultra-violet radiation has not been treated as rigorously as it might have been. We therefore proceed to investigate such situations in more detail in the following chapters.

CHAPTER 4

Extension of Theoretical Background

4.1.1 Introduction

In this chapter the basic theory of infra-red emission from dust surrounding variable cosmic sources of higher frequency radiation is explored beyond the scope of previous work as described in chapter 3 by including light travel time arguments. At the end of this chapter the theory is applied more specifically and very general results are briefly discussed for nova and Seyfert-like models. It is left until chapter 5 before observations of individual astrophysical objects are compared in detail with theoretical models.

4.2.1 Grain Temperature

The temperature of an isolated spherical grain exposed to irradiation by ultra-violet photons is derived from the energy balance considered previously in equation (3.8). Following Rees et al. (1969) we assume that the absorption efficiency has a power law dependence on frequency in the infra-red and that Q^*_{abs} is effectively constant.

However equation (3.10) reveals that Q_{abs} is dependent on grain radius, a, and the conductivity of the grain material, σ. Greenberg (1968) has found that σ is in fact temperature dependent. We may therefore express the absorption efficiency, Q_{abs}, in the form:-

$$Q_{abs}(\nu, a, T_g) = Q_0' \, a \left(\frac{T_g}{T_0}\right)^{\rho} \left(\frac{\nu}{\nu_0}\right)^{\alpha} \qquad (4.1)$$

where Q_0', T_0, ρ and ν_0 are constants. Reference to experimental data (Goldsmith et al., 1961) reveals that ρ appears to vary between different graphite types but a value of $\rho \simeq -0.5$ would not be unreasonable for naturally occurring graphite.

Incorporating equations (3.9) and (4.1) in equation (3.8) and rearranging we find:-

$$\frac{LQ^*_{abs}}{16\pi r^2} = \int_0^{\alpha} \left(\frac{2h\,\nu^{3+\alpha}}{c^2}\right) \frac{Q_0'' \, T_g^{\rho} \, a}{\exp\left(\frac{h\nu}{kT_g}\right) - 1} \, . \, d\nu \qquad (4.2)$$

where $Q_0'' = Q_0' \, \nu_0^{-\alpha} \, T_0^{-\rho}$. Using the substitution $x = h\nu/kT_g$ in equation (4.2) and referring to the standard solution in Gradshteyn and Ryzhik (1965, p. 325) the grain temperature is given by

$$T_g^{\alpha+4+\rho} \left(\frac{L}{4\pi r^2}\right)\left(\frac{c^2}{2h}\right)\left(\frac{Q^*_{abs}}{Q_0'' \, a}\right)\left(\frac{h}{k}\right)^{\alpha+4} \left\{4\Gamma(\alpha+4) \; \zeta(\alpha+4)\right\}^{-1} \qquad (4.3)$$

where Γ and ζ are the gamma and Reimann zeta functions respectively.

(We may note that if $\rho = 0$ is assumed and α is adjusted to compensate, then no significant error in T_g will result.)

This expression for the temperature of individual grains can now be compared with the findings of previous workers. Using results similar to Gilman's (1974) for the computed Planck mean absorption efficiencies for small graphite grains, $\bar{Q}_{abs}$, Clayton and Wickramasinghe (1976) derived the following temperature relationship:-

$$T_g \propto \left|\frac{L}{r^2}\right|^{1/5.65} \qquad (4.4)$$

From equation (4.3) it can be seen that if we were to use the value of α for small pure graphite grains (i.e. $\alpha = 2$) together with Goldsmith et al's (1961) data ($\rho \simeq -0.5$) we would have an index of $1/5.5$ compared with Clayton and Wickramasinghe's value of $1/5.65$.

It is well known that for perfect black body radiators the wavelength of peak emission, λ_{max}, is related to the temperature of the black body, T, by Wein's Law, i.e.:-

$$\lambda_{max}\, T = 0.29 \text{ cm}^{\circ}\text{K}$$

Obviously, if the grains are not perfect black bodies then Wein's Law cannot be accurately used to determine the wavelength of peak emission for a given grain temperature, T_g. Assuming that $Q_{abs} \propto \nu^{\alpha}$ λ_{max} is defined by an expression of the form:-

$$e^{-z} + \frac{z}{5+\alpha} = 1 \qquad (4.5)$$

where $z = hc/(\lambda_{max}\, k\, T_g)$.

From equation (4.5) it can be seen that as α increases from the black body value of $\alpha = 0$ the peak emission in wavelength units shifts to shorter wavelengths even though the grain temperature remains constant. Thus for example, instead of the maximum emission being

at a wavelength of $\sim$ 3μm for a black body grain of T_g = 1000°K it will lie at $\sim$ 2μm for a grain with α = 2.

4.2.2 Grain Temperatures within Dust Shells

The temperature of a grain embedded within a cloud of similar grains is obviously different from that described in the previous section where it is assumed to be in isolation (equation 4.3).

At this stage it will be assumed that the cloud contains identical grains which are also assumed to be spherical as in section (4.2.1). This is of course a very much idealised case as a real cloud is likely to contain grains of several different compositions and geometries and because of grain growth, sputtering and evaporation there is also likely to be a distribution of grain sizes across the cloud.

If we consult figure (4.1) where the large-scale geometry of the situation is displayed we can see that the grains are distributed within a spherical shell such that their distance from the central source at C is given by r, where $R_1 \leqslant r \leqslant R$.

The lower bound on grain position (the evacuated cavity, radius R_1) could be due to grain evaporation by radiation from the central source; sputtering of the lattice atoms of the grains by incident protons ejected from the central source; radiation pressure on the grains effectively 'sweeping' them out or any combination of the three.

Assuming that the grain number density N is radially dependent, continuous, isotropic and power-law in form then we can express it as

$$\left.\begin{aligned} N(r) &= N_1 \left(\frac{R_1}{r}\right)^{\beta}, \quad R_1 \leqslant r \leqslant R \\ N(r) &= 0 \qquad \text{otherwise} \end{aligned}\right\} \quad (4.6)$$

where N_1 is the number density at the inner radius R_1. Thus a value of β = 2 here would perhaps stem from continuous grain outflow whereas a value of β = 0 denotes a uniform grain number density.

From equation (4.6) we can now find the mass of grains contained

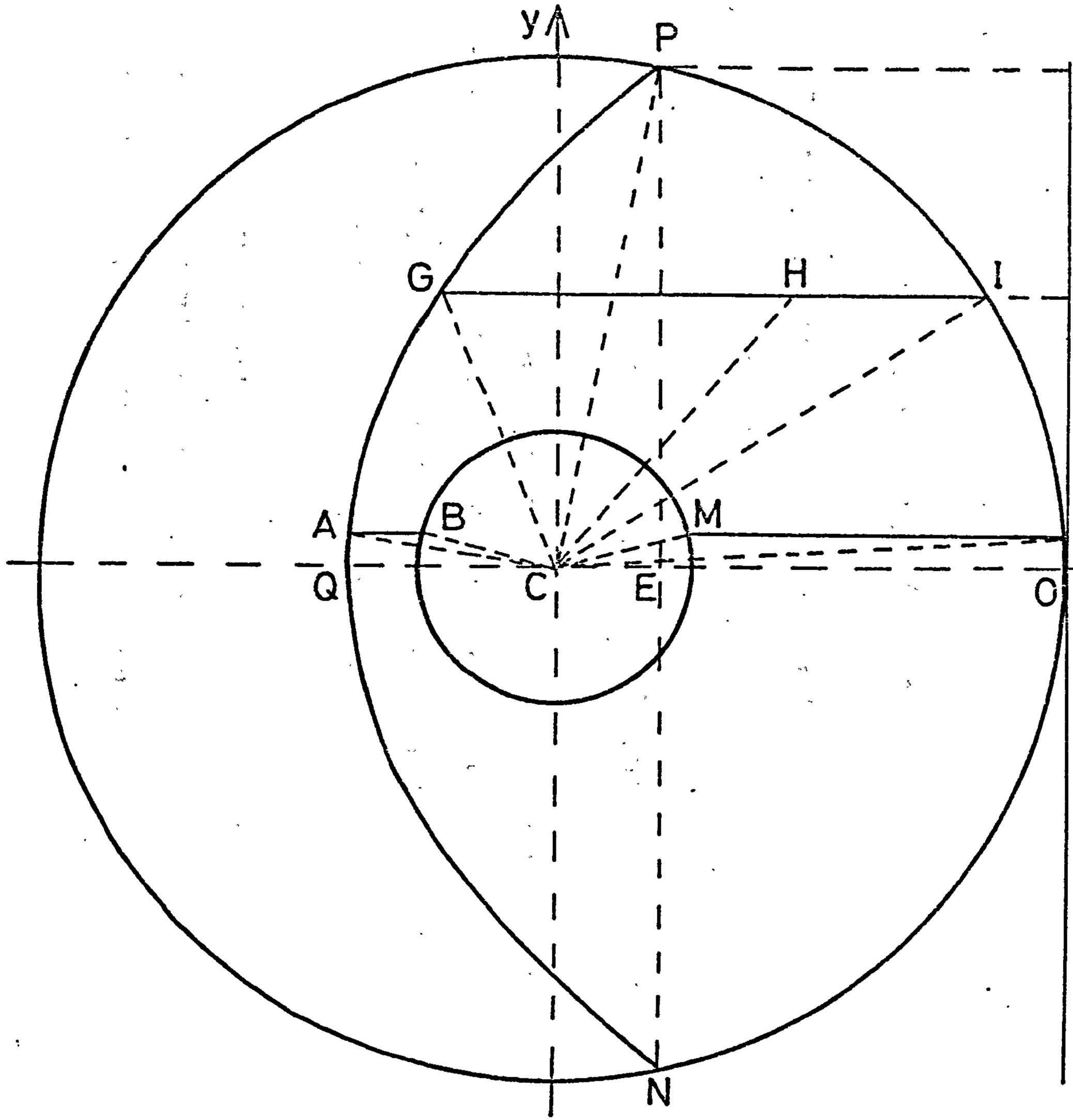

Figure (4.1) The large scale geometry of the situation in which a variable source at C is surrounded by a shell of dust grains outer radius R(= CO, CI, CP, CL), cavity radius R_1(= CM, CB). Radius vector from C to H or any other point within shell = r. Distances along OD are referred to as displacements, r'. $\widehat{OCP} = \theta_0$; $\widehat{OCI} = \theta_2$; $\widehat{OCH} = \theta$; $\widehat{OCG} = \theta_1$. The significance of lines GI, PD, AB, ML, CE, CQ and $\widehat{OCL}$, $\widehat{OCM}$, $\widehat{OCB}$, $\widehat{OCA}$ etc. explained in text.

in the shell from the expression:-

$$M_g = \frac{4}{3}\pi a^3 \, s \int_{R_1}^{R} N(r) \, . \, 4\pi r^2 . dr$$

Substituting for N(r) from equation (4.6) we have

$$M_g = \frac{16}{3} \pi^2 a^3 \, s \, N_1 R_1^{\beta} \int_{R_1}^{R} r^{(2-\beta)} . dr \qquad (4.7)$$

A grain at a distance r from the central source is shielded to some degree by grains lying interior to it in the radial direction. In the case of conducting spheres where the radiation is both scattered and absorbed the optical depth at frequency ν (δ_ν) contains the extinction coefficient Q_{ext}. Thus, if the heating effect of scattered radiation is ignored we have

$$\delta^*_{ext} = \pi a^2 \, Q^*_{ext} \int_{R_1}^{r} N(r') \, dr' \qquad (4.8)$$

Substituting equation (4.6) into equation (4.8) the optical depth can be found for any given value of β.

i.e.
$$\delta^*_{ext} = \pi a^2 \, Q^*_{ext} \, N_1 R_1^{\beta} \int_{R_1}^{r} r'^{-\beta} \, . dr' \qquad (4.9)$$

A complication arises however because the extinction is so far assumed to be due to absorption and scattering. However the scattered radiation need not necessarily be lost to the system (i.e. it can go towards heating other grains). Thus the extinction will effectively be decreased.

If the asymmetry factor for scattering is $g(\phi)$ (where ϕ is the angle between incident and scattered radiation) then in the lowest order approximation δ^*_{ext} should be replaced by (Greenberg, 1979)

$$\delta^*_{ext} \rightarrow \delta^*_{ext} - \delta^*_{scatt} \int_0^{\pi/2} g(\phi) \sin\phi \, d\phi$$

In what follows we make the assumption that the scattering is isotropic (i.e. $g(\phi) = g = 1$) and therefore the optical depth δ^* we consider is given by

$$\delta^* = \delta^*_{ext} - \delta^*_{scatt} \qquad \text{i.e. } \delta^* = \delta^*_{abs}$$

Therefore within the cloud it is more accurate to use the expression

$$I_\nu d\nu = (I_\nu)_0 \exp\left\{- \pi a^2 Q^*_{abs} N_1 R_1{}^\beta \int_{R_1}^{r} r'^{-\beta} \, dr'\right\} d\nu \quad (4.10)$$

for the intensity of radiation between frequencies ν and $\nu + d\nu$ impinging upon a given grain.

We can now include the extinction in our temperature expression given previously in equation (4.3):-

$$T_g{}^{\alpha+4} \simeq \left(\frac{L}{4\pi r^2}\right)\left(\frac{c^2}{2h}\right)\left(\frac{Q^*_{abs}}{Q_0 \pi a}\right)\left(\frac{h}{k}\right)^{\alpha+4} \left\{4\Gamma(\alpha+4)\ \zeta(\alpha+4)\right\}^{-1} .$$

$$. \exp\left\{-\pi a^2 Q^*_{abs} N_1 r_1{}^\beta \int_{R_1}^{r} r'^{-\beta} . \, dr'\right\} \quad (4.11)$$

where α in the exponent of temperature includes the conductivity term ρ as outlined above.

Figure (4.2) shows the distribution of grain temperatures about a constant source of ultra-violet radiation.

If $L\, e^{-\delta^*}$ is the total ultra-violet flux which reaches grains at the outer edge of the cloud, then $L(1 - e^{-\delta^*})$ is the total infra-red flux produced interior to it. Assuming the cloud is optically thin to infra-red radiation and that Q^*_{abs} and Q_{abs} are roughly constant over the wavelength ranges of interest with $Q^*_{abs} \gtrsim 10\, Q_{abs}$ as in the case of many

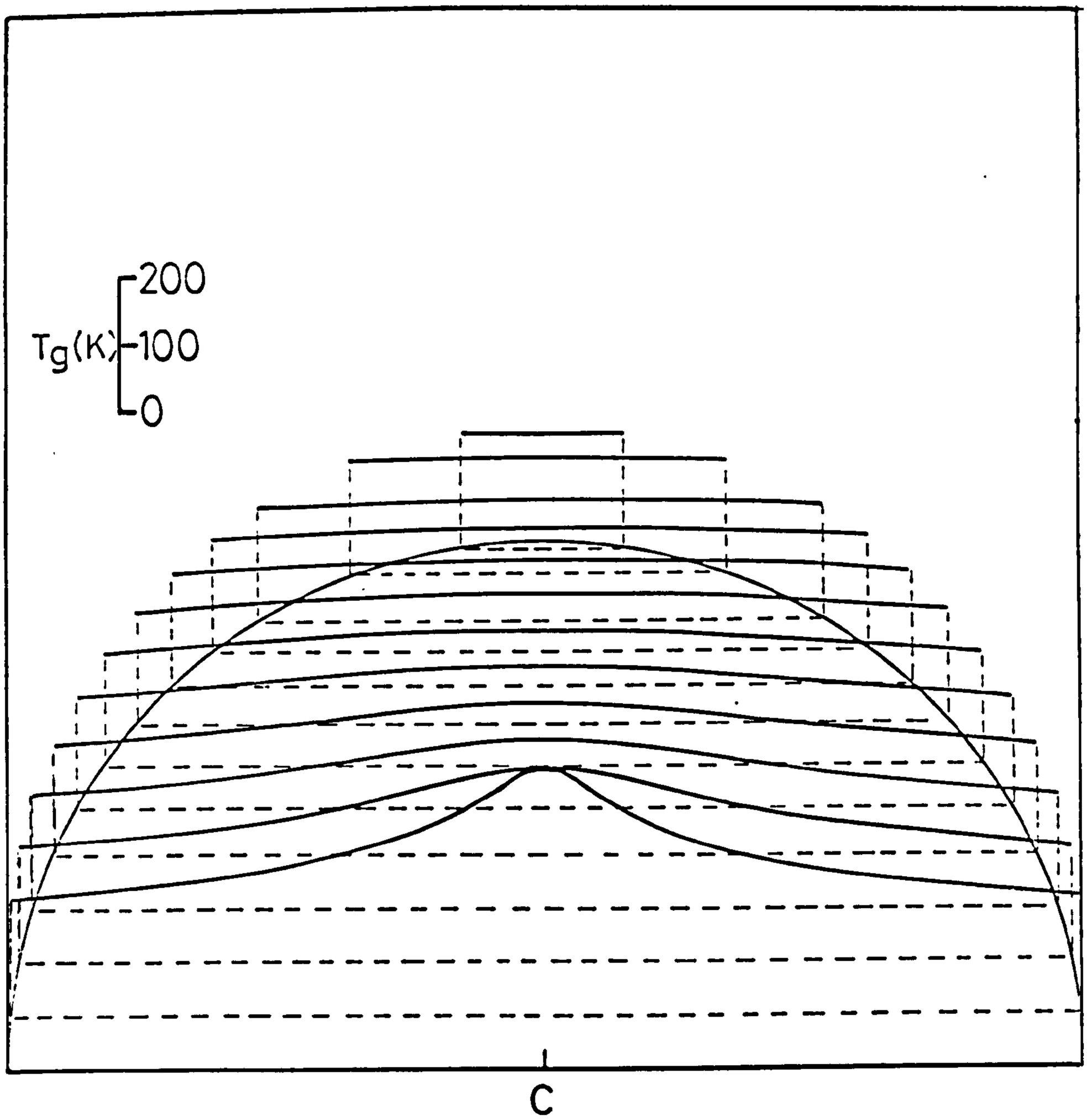

Figure (4.2) Distribution of grain temperatures within a spherical dust shell about a non-variable source at C of high frequency radiation with $L = 5 \times 10^{38}$ $ergs^{-1}$; shell parameters $R = 100\ R_1 = 5 \times 10^{17}$cm, $Mg = 3.3 \times 10^{-6} M_\odot$, $\beta = 2$ containing dust grains with $\alpha = 2$, $a = 10^{-5}$cm. Each solid curve gives the observed temperature along the corresponding line of sight (broken line) in the dust shell. Temperature scale is as indicated.

conductors, then for the two fields to contribute equally to grain heating

$$e^{-\delta^*} Q^*_{abs} = (1 - e^{-\delta^*}) Q_{abs}$$

$$\text{i.e. } e^{-\delta^*} \lesssim \frac{1}{11}$$

Thus $\delta^* \lesssim 2.4$ for the ultra-violet radiation field to dominate the heating of the grain. At first sight it may appear surprising that as more ultra-violet radiation is absorbed the effect of the infra-red field increases. It must be stressed that the above relationship applies to grains which, because of ultra-violet absorption interior to them in the cloud, may receive little high frequency radiation themselves.

However, unless the grain distribution is such that grains are concentrated toward the outer edge of the shell ($\beta < 0$) then the outer-most grains will contribute comparatively little to the infra-red flux in any case and therefore the ultra-violet optical depth could be increased beyond the above limit without infra-red heating becoming important overall.

4.2.3 The Timescales of Reaction of Grain Temperature to Incident Radiation

In this subsection we consider the effective timescales of reaction of grain temperature to changes in the incident radiation field.

The reaction time will obviously have great bearing on the validity of subsequent theory in which it is implicitly assumed to be negligible in comparison to the fluctuation timescales of certain sources.

The most important parameters are a) the time taken for radiation incident on one face of a grain to diffuse through the grain so that all parts can be ascribed the same temperature at any given instant and b) the cooling time of the grain, t_{cool}, which is taken to be the time

for a grain to reach equilibrium after a change in the incident radiation field.

We saw in Chapter 3 that for 0.1 μm grains Greenberg (1976) calculated that the diffusion time of absorbed energy through the grain is $\sim 10^{-10}$s. For smaller grainsthis would of course be even less and is in any case negligible.

The grain cooling time has been estimated by Burbidge and Stein (1970) (see Chapter 3). Their estimate is based on the ratio of the internal grain energy, U, to the rate of energy loss by radiation, $\dot{U}$. Using classical thermodynamics and assuming that the grains are perfect black body radiators their expression gives a cooling time, t_{cool}, ~ 1 s for 0.1 μm graphite or silicate grains at $T_g \sim 100\ ^oK$.

We note however that real grains are unlikely to behave as black bodies and that at low temperatures the classical form of the specific heat will not be valid.

If we consider the right hand side of equation (3.9) above we have

$$\dot{U} = 4\pi a^2 \int_0^\infty \left(\frac{2\pi h\ \nu^{3+\alpha}}{c^2}\right) \frac{(Q''_0\ T_g{}^\rho\ a)}{(e^{h\nu/kT_g} - 1)} \cdot d\nu$$

i.e.
$$\dot{U} = \frac{8\pi^2 h}{c^2}\ Q''_0\ a^3\ T_g{}^{\alpha+4+\rho} \left[\frac{k}{h}\right]^{\alpha+4} \Gamma(\alpha+4)\ \zeta(\alpha+4) \qquad (4.12)$$

The internal energy of the grain is proportional to the specific heat at constant volume, c_v, and as $T_g \to 0$,

$$c_v \to \frac{12\pi^4\ R_c\ T_g{}^3}{5\ \Theta^3}$$

where R_c is the gas constant in erg $^oK^{-1}$ mole^{-1} and Θ is the Debye temperature. Thus

$$U \simeq \frac{4\pi a^3}{3} s \frac{12\pi^4 R_c T_g^4}{5 \Theta^3} \quad (4.13)$$

Combining equations (4.12) and (4.13) we have

$$t_{cool} \simeq \left|\frac{U}{\dot{U}}\right| \sim \frac{2}{5} \frac{s\pi^3 R_c c^2}{\Gamma(\alpha+4)\ \zeta(\alpha+4)\ h\ Q_0^{\pi}} \left[\frac{h}{k}\right]^{\alpha+4} \Theta^{-3} T_g^{-(\alpha+\rho)} \quad (4.14)$$

i.e. $$t_{cool}\ (T_g << \Theta) \propto \Theta^{-3} T_g^{-(\alpha+\rho)} \quad (4.15)$$

Therefore we can see from equation (4.15) that at very low temperatures the cooling time is independent of grain size as long as the grains are small and $Q_{abs} \propto \nu^{\alpha}$ is still valid.

If, for example, we have graphite grains at $100^{o}K$ ($\alpha = 2$ $\rho = 0$) then $t_{cool} \sim 300s$ assuming $\Theta \sim 1000^{o}K$ (We note that graphite does not have a unique Debye temperature but that this varies with direction through the lattice. However $\Theta \sim 1000^{o}K$ may not be unreasonable for any given direction - Greenberg, 1979).

As in subsequent models no grains have $T_g \lesssim 100^{o}K$ and the fluctuation times of the sources considered are >> 300s we assume that reaction to changes in the radiation field is effectively instantaneous.

4.3.1 Geometrical Considerations

In figure (4.1) the observer is considered to be very distant from the spherical shell of dust grains surrounding the primary source at C. The radiation from different parts of the source can then be considered to reach the observer along lines which are effectively parallel (PD, GF, AL).

Section (4.2.3) illustrated the fact that grains of the sizes and

compositions with which we are concerned will react to changes in the incident radiation virtually instantaneously (even if their temperature is below the Debye temperature of the grain material) for the types of primary sources we are to consider. The development of the re-emitting region can then be deduced in much the same way as in previous work (see e.g. Conderc, 1939 and section 3.4.1) for a central source that instantaneously starts to radiate.

If time is measured from the instant when the observer first sees the central object and if the observer is at a distance d (>> R) from O, the time t taken for the re-emission from point G to be seen will be:-

$$t = \frac{1}{c} \left| (CG + GF + d) - (CO + d) \right|$$

$$\text{i.e.} \quad t = \frac{1}{c} \left| r_1 - r_1 \cos \theta_1 \right| .$$

$$\text{Thus } r_1 = \frac{ct}{1 - \cos \theta_1} \qquad (4.16)$$

which is the equation of a paraboloid with semi-latus rectum ct having the primary source at the focus.

Strictly, if d is finite, then PD, CO etc. are not parallel and the paraboloid becomes an ellipsoid. However d is considered to be very large compared to the dimensions of the shell and equation (4.16) is therefore assumed to be strictly valid.

We may also note that equation (4.16) should contain an angular term for the transverse direction in three dimensions. However due to the symmetry about the QCO axis we may disregard this in the subsequent analysis.

In general terms the origin of time can be taken at any point on the light curve of the central object. The paraboloid of emission is then due to the propogation of this point on the curve through the shell

as seen by the observer a time t later.

In the case where the central object suddenly turns on, we can see that the infra-red emitting region in reality takes the form of an expanding paraboloid but appears to the observer as an expanding disc. Consulting figure (4.1) again we can derive the observed velocity of expansion of the disc at any instant using light travel time arguments.

Taking the origin of time to be when the observer sees a given fluctuation of the central object, then at a time t later re-emission will appear to arise along the parabola PQN of figure (4.1) as the path lengths from central source to observer via the re-emitting grains must be the same. i.e.

$$2CQ + CO = CP + PD$$

$$\text{and } CE = CO - EO$$

$$\text{where } CQ = ct/2,\ CP = CO = R.$$

Thus $PD = ct$

and therefore $y_p^2 = R^2 - (R - ct)^2$

where y_p is the y co-ordinate of the point P. Hence

$$v_d = \frac{dy_p}{dt} = \frac{d}{dt}\left[(2Rct - c^2t^2)^{\frac{1}{2}}\right] = (Rc - c^2t)(2Rct - c^2t^2)^{-\frac{1}{2}} \qquad (4.17)$$

where v_d is the apparent transverse velocity of expansion with respect to the central source.

In order to generalise the measurement of time it will be useful to use units independent of shell size. We therefore redefine time in terms of τ, where $\tau = ct/R$. Equation (4.17) becomes:-

$$v_d = \frac{c(1 - \tau)}{(2\tau - \tau^2)^{\frac{1}{2}}} \qquad (4.18)$$

Therefore the observed expansion and subsequent contraction will be at sub-light velocity with respect to the central source for a time

$$1 - {}^{1}/\sqrt{2} \leqslant \tau \leqslant 1 + {}^{1}/\sqrt{2}$$

and outside these limits the expansion will be super light. (Note - there is of course no real material motion involved so there is no violation of causality implied here.)

From equation (4.18) it can be seen that at time $\tau = 1$ the expansion ceases and contraction (if visible) will begin.

We now consider the more general case of a central source which varies over a period of time such that different points within the emission region are observed to experience a different phase of the central source variation.

At any given instant the observer will see a grain at H in figure (4.1) reacting to a central source fluctuation that occurred time Δt previously. Δt can be expressed as

$$\Delta t = \frac{r}{c} (1 - \cos \theta) \qquad (4.19)$$

from considerations similar to those above.

If for example the central source varies as $L(t) = L_0 f(t)$, equation (4.19) enables us to determine the central source luminosity the observer sees the grain receiving at any observer time t, i.e.

$$L(\theta, r, t) = L_0 f \left\{ t - \frac{r}{c} (1 - \cos \theta) \right\}$$

or in terms of our generalised time units

$$L(\theta, r, \tau) = L_0 f \left\{ \frac{R}{c} \left(\tau - \frac{r}{R} (1 - \cos \theta) \right) \right\} \qquad (4.20)$$

Equations (4.20) and (4.11) enable us to derive the temperature of any grain within the shell if we have observed the central source for a sufficient time (Δt) prior to the time t of observation. Thus the temperature of a grain within a circumstellar dust cloud where the central source is varying as $L(t) = L_0 f(t)$ is given by

$$T_g^{\alpha+4} = \left(\frac{L_0\, f\left[\frac{R}{c}\left(\tau - \frac{r}{R}\left(1 - \cos\theta\right)\right)\right]}{4\pi r^2}\right)\left(\frac{c^2}{2h}\right)\left(\frac{Q^*_{abs}}{Q_0}\right)\left(\frac{h}{k}\right)^{\alpha+4} \cdot$$

$$\cdot\left\{4\Gamma(\alpha + 4)\ \zeta(\alpha + 4)\right\}^{-1} \exp\ (-\delta^*) \qquad (4.21)$$

(Note - as discussed above the expressions used for grain temperature exclude the case where grains may be situated in a dense cloud such that the ultra-violet optical depth is large and the infra-red component of the radiation field is dominant in heating the grain).

To illustrate the effect of observing grain temperatures about a fluctuating source from a large distance external to the dust shell, figures (4.3a) to (4.3d) have been included. The parabolic distribution of maxima and minima is self evident in figure (4.3a) which shows the temperature variation about a sinusoidally varying central source. Notice how this effect 'bunches' the fluctuations toward the rear end of the shell. Figures (4.3b) to (4.3d) show the temperature variation about a source with a nova-like light curve.

i.e.

$$\left.\begin{aligned} L &= 0 \qquad & \tau < 0 \\ L &= L_0 e^{-\omega t} \qquad & \tau \geq 0 \end{aligned}\right\} \qquad (4.22)$$

Strictly this would seem to violate the condition that the fluctuation time is far greater than the time it takes for the grain to react (t_{cool}). However, if $t_{cool} \ll$ rise time at $t = 0 \ll \omega^{-1}$ then we are still justified in using these light curves for grain heating to a high degree of accuracy.

Before considering the derivation of the observed infra-red flux it is interesting to consider the way in which the emitting volume appears to change. This will of course be different for a centrally placed observer than for one at a large distance external to the shell.

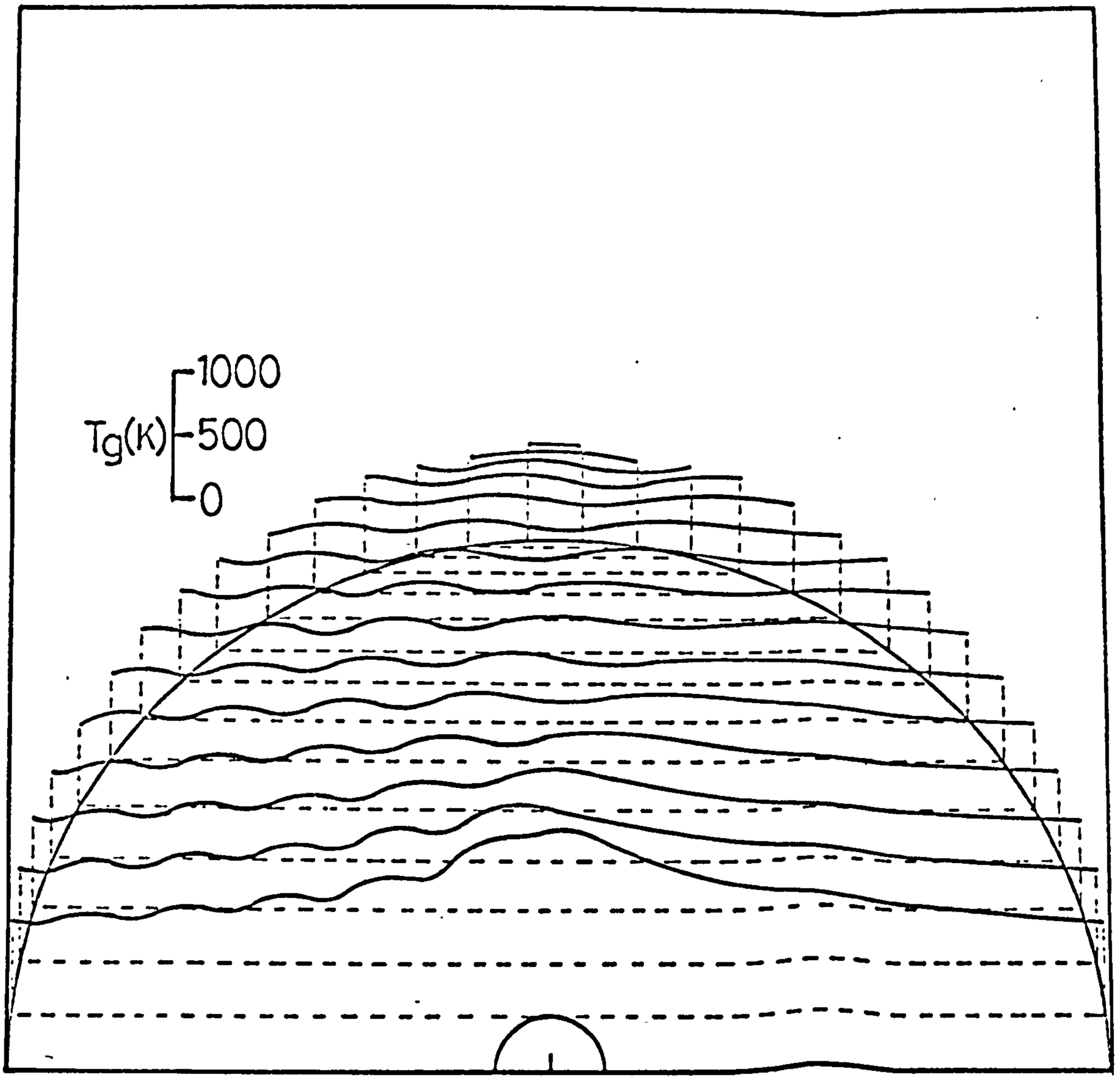

Figure (4.3a) Distribution of grain temperatures about a Seyfert-like central source as observed by a distant observer situated to the right of the figure. Parameters are as in figure (4.2) except $L = L_0 + L_1 \sin \omega t$ where $\omega = 10^{-6}\ s^{-1}$, $L_1 = 0.3\ L_0 = 3 \times 10^{43}$ $ergs^{-1}$, $R = 10R_1 = 5 \times 10^{18} cm$ and $Mg = 3 \times 10^{-4}\ M_\odot$.

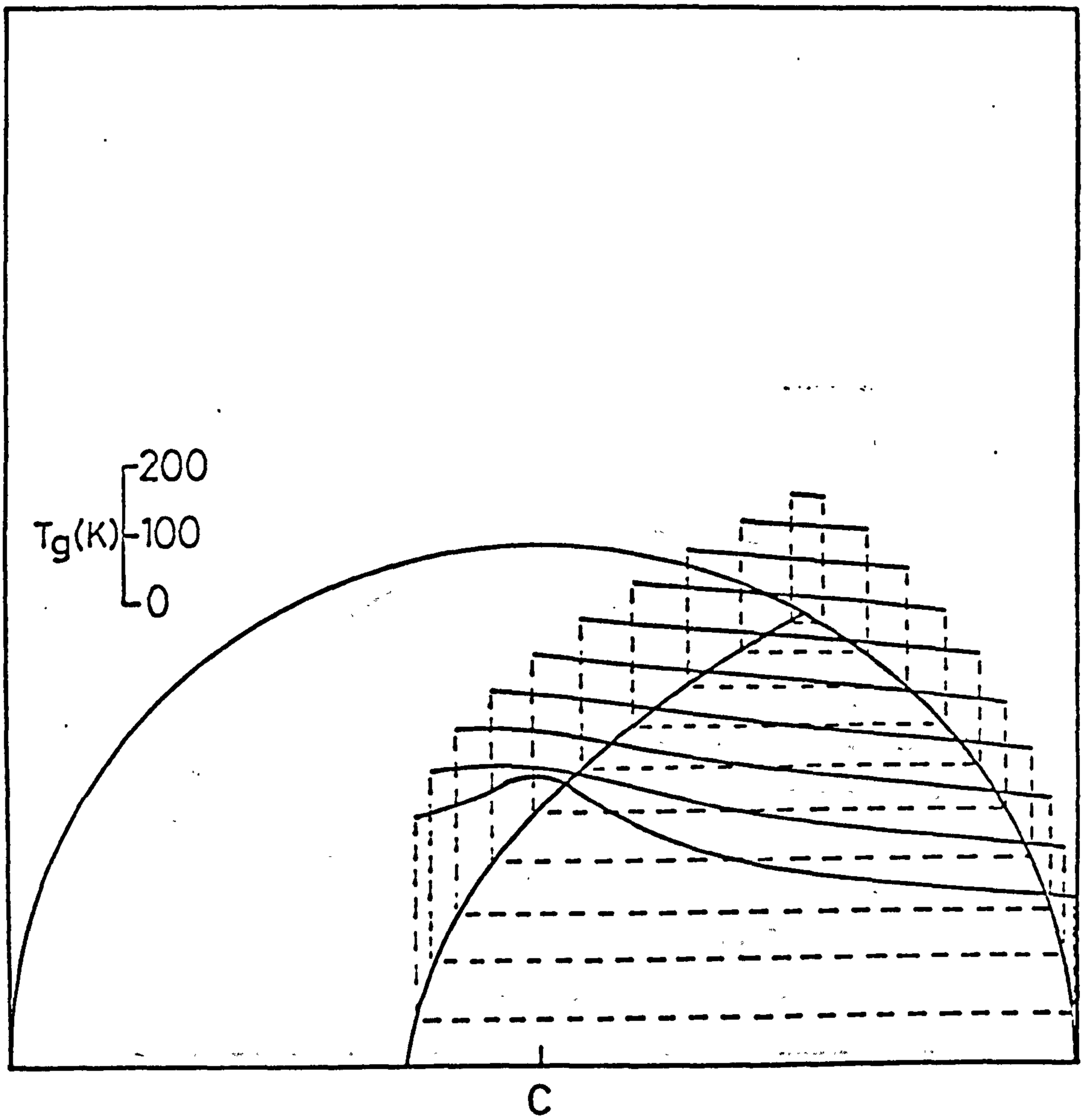

Figure (4.3b) Distribution of grain temperatures about a nova-like central source with a light curve as defined by equation (4.22) with $\omega = 10^{-6}$ s^{-1} at time $\tau = 0.5$. All other parameters as in figure (4.2).

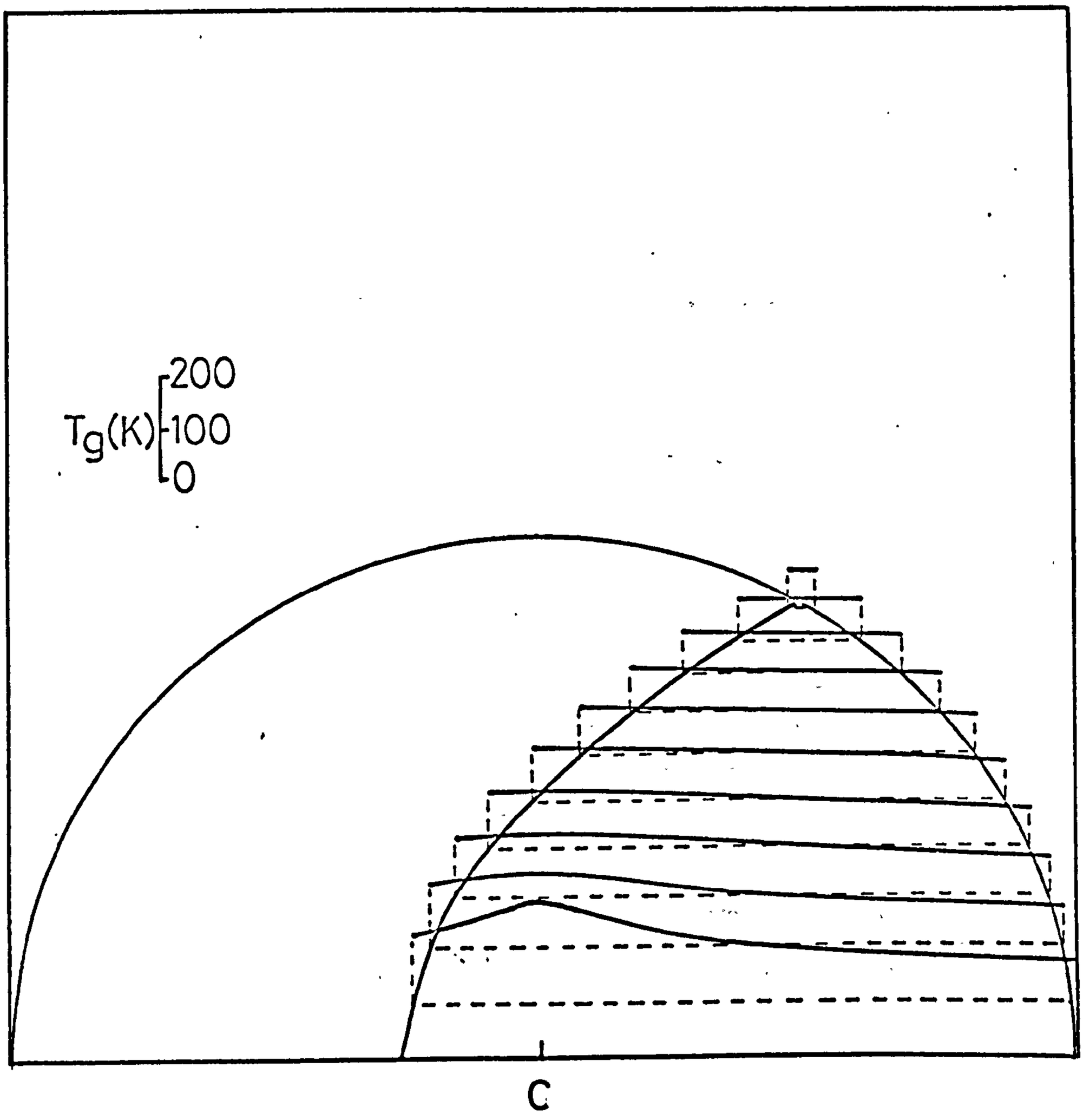

Figure (4.3c) Distribution of grain temperatures about a nova-like central source with all parameters as in figure (4.3b) except $\alpha = 1$.

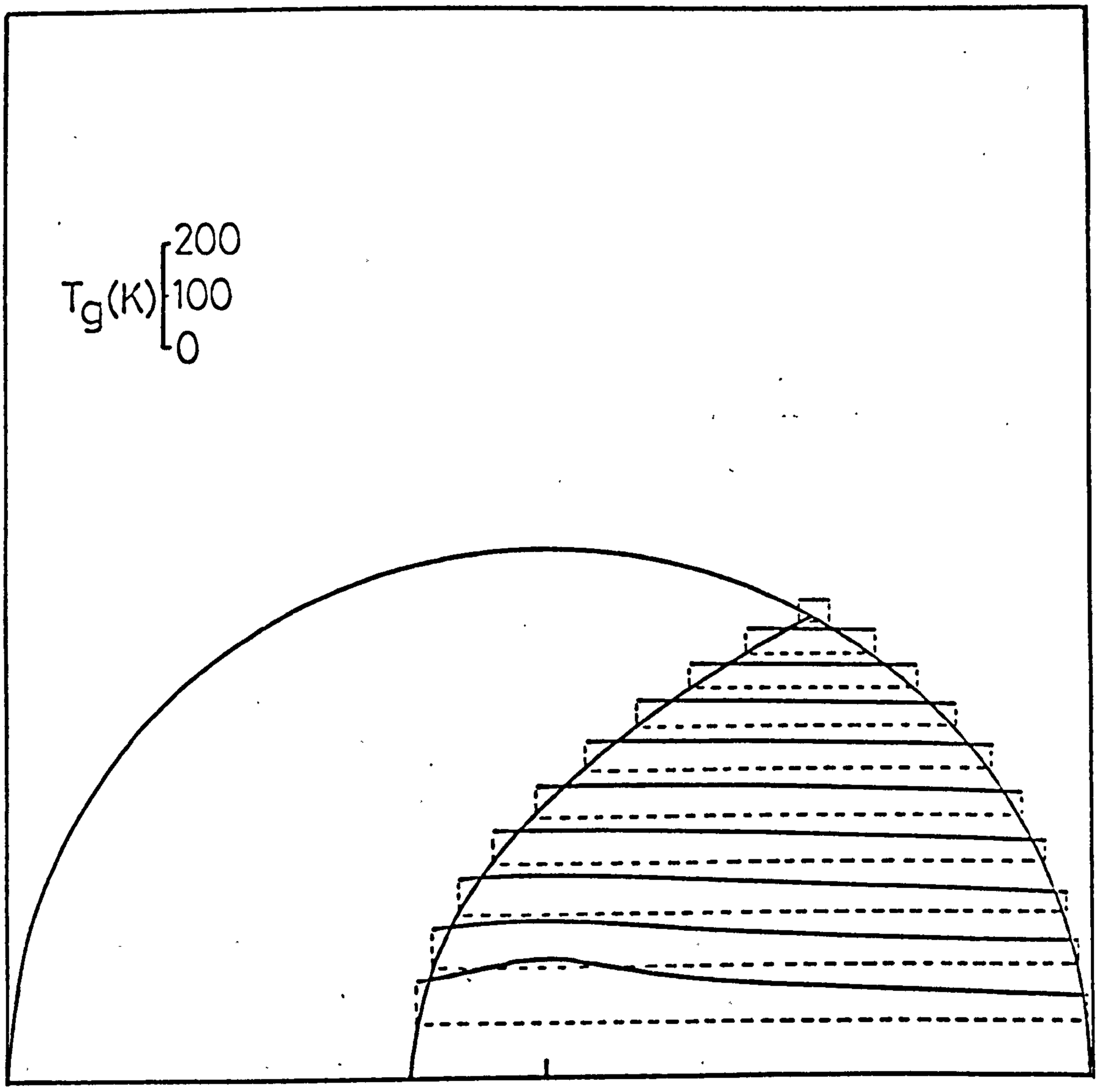

Figure (4.3d) Distribution of grain temperatures about a nova-like central source with all parameters as in figure (4.3b) except $\alpha = 0.5$.

Obviously, for a centrally placed observer the emitting volume will increase as $\left(\frac{ct}{2}\right)^3$ (i.e. Volume $\propto \tau^3$).

For an external observer at a large distance the situation is more complex. Figure (4.1) illustrates the 2 regions of integration which are the truncated spheroid enclosed by OPEN and the paraboloid enclosed by NEPQ. The volume V_s of the truncated spheroid is given by

$$V_s(t) = \pi \int_{R\cos\theta_0}^{R} y^2 \, . \, dx$$

and that of the paraboloid V_p, by

$$V_p(t) = \pi ct \int_{\frac{-ct}{2}}^{R\cos\theta_0} (ct + 2x) \, . \, dx$$

where by substituting in equation (4.16) we can see that $\cos\theta_0 = 1 - \tau$. Replacing t by its generalised form τ and solving we arrive at the expression for the externally observed emitting volume $V_{oe}(\tau)$:-

$$V_{oe}(\tau) = V_s(\tau) + V_p(\tau) = \pi R^3 \tau\left[1 - \frac{\tau^2}{12}\right] \qquad (4.23)$$

this is compared with the centrally observed emitting volume $V_{oc}(\tau)$ in figure (4.4) where

$$V_{oc}(\tau) = \frac{\pi}{6} R^3 \tau^3 \qquad (4.24)$$

Both equation (4.23) and equation (4.24) give a volume of $^4/_3 \pi R^3$ at $\tau = 2$ as this is the point in time when the shell is filled by the radiation of the central source (note - the origin of time for internal and external observers is not the same here. However it is with the

Figure (4.4) The variation of the emitting region volume with time. V_{Oe} is the upper curve, V_{Oc} the lower curve. The dust is distributed in a unit volume spherical shell about the ultra-violet source which has a step function light curve. The central cavity is assumed negligible.

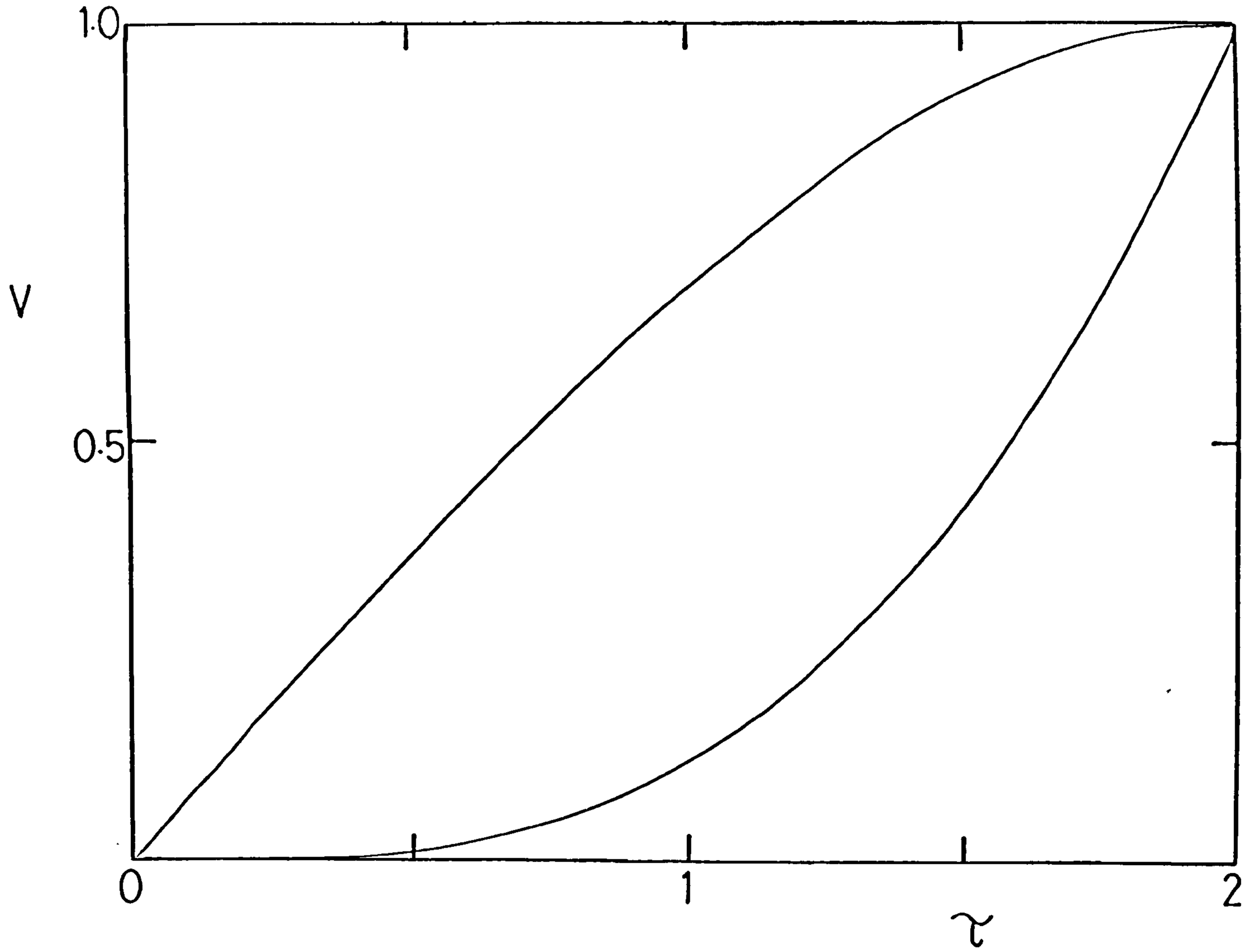
1·0
0·5
V
0
1
2
τ

qualitative difference in the evolution of the emitting volume that we are primarily concerned).

If we assume that the grains radiate as black bodies and that the distribution is uniform ($\beta = 0$) then, if the cloud is also optically thin, the infra-red flux should be approximately proportional to the emitting volume for a step function central source light curve. i.e.

$$L_{oe} \propto \tau(1 - \tau^2/12)$$

where L_{oe} is the externally observed infra-red flux. Thus

$$\frac{L_{oe}}{\dot{L}_{oe}} \simeq \frac{R}{c} \tau\left[\frac{1 - \tau^2/12}{1 - \tau^2/4}\right] .$$

For $\tau \ll 1$ therefore,

$$R \gg c\left(\frac{L_{oe}}{\dot{L}_{oe}}\right) \qquad (4.25)$$

which is to be expected at early times where the observed expansion velocity of the emission surface is super-luminal (c.f. Terrell, 1967 summarised in section 3.4.2).

4.4.1 The Equation of Transfer

We now consider the derivation of the observed infra-red flux from the dust shell for a step function central source light curve. This involves solving the equation of radiation transfer along lines of sight within the shell. Figure (4.1) shows one such integration line, IHG. This line is an example of those lines of sight with a transverse displacement, r', from the central source greater than R_1 ($r' = R \sin\theta_2$).

Grains exist along IHG with distance from I given by the variable q; distance IG is designated q_0. Angle θ_2 is determined by the transverse displacement of the line and θ_1 is a function of θ_2 and τ. (For lines with displacements $< R_1$ the extreme values of θ will of course be

different. We will consider this below.)

In order to determine the surface brightness Σ_ν from an element of area about the point I we integrate along IG for the reradiating grains lying along this line, i.e.

$$\Sigma_\nu(\theta_2) = \int_0^{q_0} B(\nu, T_g(q)).\ N(q).\ \pi a^2\ Q_{abs}\ \exp\left\{-\int_0^q N(q')\ \pi a^2\ Q_{abs}\ .\ dq'\right\}\ dq \qquad (4.26)$$

We can express dq in terms of dr and dθ :-

$$dq = d\theta\left(r^2 + \left(\frac{dr}{d\theta}\right)^2\right)^{\frac{1}{2}}$$

and as $r = \dfrac{R \sin\theta_2}{\sin\theta}$, $\dfrac{dr}{d\theta} = -R \sin\theta_2 \dfrac{\cos\theta}{\sin^2\theta}$,

$$\text{thus}\quad dq = \frac{R \sin\theta_2}{\sin^2\theta}\ .\ d\theta \qquad (4.27)$$

Substituting equations (4.6) and (4.27) into equation (4.26) we are left with

$$\Sigma_\nu\ (\theta_2) = \int_{\theta_2}^{\theta} B(\nu, T_g(r)).\ N_1 R_1^{\beta}\ [R \sin\theta_2\ ]^{1-\beta}\ (\sin\theta)^{\beta-2}\ \pi a^2.$$

$$.\ Q_{abs}.\ \exp\left\{-\int_{\theta_2}^{\theta} N_1 R_1^{\beta}\ [R \sin\theta_2\ ]^{1-\beta}\ (\sin\theta')^{\beta-2}\ \pi a^2\ Q_{abs}.\ d\theta'\right\}.$$

$d\theta$

where the central cavity may be accommodated by the conditions of equation (4.6) when appropriate.

Substituting for $B(\nu, T_g(r))$

$$\Sigma(\theta_2) = \frac{2h\nu^3}{c^2} N_1 R_1^{\beta} (R \sin\theta_2)^{1-\beta} \pi a^2 Q_{abs} \int_{\theta_2}^{\theta_1} (\sin\theta)^{\beta-2}$$

$$\left[\exp\left(\frac{h\nu}{k T_g(\theta)}\right) - 1 \right]^{-1} \exp\left\{ - N_1 R_1^{\beta} (R \sin\theta_2)^{1-\beta} \pi a^2 Q_{abs} \right.$$

$$\left. \int_{\theta_2}^{\theta} (\sin\theta')^{\beta-2} . \, d\theta' \right\} . \, d\theta \qquad (4.28)$$

where

$$T_g^{\alpha+4}(\theta) = \left(\frac{L(\theta, \theta_2, \tau) \sin^2\theta}{4\pi R^2 \sin^2\theta_2}\right)\left(\frac{c^2}{2h}\right)\left(\frac{Q^*_{abs}}{Q''_O a}\right)\left(\frac{h}{k}\right)^{\alpha+4} .$$

$$\left\{4\Gamma(\alpha + 4) \zeta(\alpha + 4)\right\}^{-1} . \exp\left\{ \pi a^2 Q^*_{abs} N_1 R_1^{\beta} (R \sin\theta_2)^{1-\beta} . \right.$$

$$\left. \int_{R_1}^{\frac{R\sin\theta_2}{\sin\theta}} (\sin\theta)^{\beta-2} \cos\theta . \, d\theta \right\}$$

and

$$L(\theta, \theta_2, \tau) = L_O \, f\left\{\frac{R}{c}\left(\tau - \frac{\sin\theta_2}{\sin\theta}\left(1 - \cos\theta\right)\right)\right\} .$$

. The flux density, f_ν, from an object subtending solid angle Ω and surface brightness Σ_ν is given by

$$f_\nu = \int_\Omega \Sigma_\nu \, d\Omega$$

Defining $\widehat{OCP} = \theta_0$, and with

$$f_\nu = \int \frac{2\pi\ r'\ dr'}{D^2}\ \Sigma_\nu(\theta_2)$$

then

$$f_\nu = \int_0^{\theta_0} \Sigma_\nu(\theta_2) . \frac{2\pi R^2}{D^2} . \sin\theta_2 \cos\theta_2 . d\theta_2 \qquad (4.29).$$

Equation (4.29) is true for $\tau < 1$. If $\tau \geq 1$, the upper integration limit, θ_0, is replaced by $\pi/2$.

Substitution in equation (4.29) from equation (4.28) gives the time dependent flux, $f_\nu(\tau)$ as

$$f_\nu(\tau) = A_1 \int_0^{\theta_0} (\sin\theta_2)^{2-\beta} \cos\theta_2 . d\theta_2 \int_{\theta_2}^{\theta_1} (\sin\theta)^{\beta-2} .$$

$$\left[\exp\left[B_1 \exp\left(C_1 \int_{R_1}^{\frac{r'}{\sin\theta}} (\sin\theta)^{\beta-2} \cos\theta\ .\ d\theta\right)\left[\frac{\sin\theta}{r'}\right]^{\frac{-2}{\alpha+4}} \right] - 1\right]^{-1} .$$

$$\exp\left\{- C_1 \frac{Q_{abs}}{Q^*_{abs}} \int_{\theta_2}^{\theta} (\sin\theta')^{\beta-2} . d\theta' \right\} . d\theta \qquad (4.30)$$

where

$$A_1 = \frac{4\pi R^{3-\beta}}{D^2}\ \frac{h\nu^3}{c^2}\ N_1 R_1^{\beta}\ \pi a^2\ Q_{abs} ,$$

$$B_1 = \nu \left[\frac{L(r, \theta, \tau)\ c^2\ Q^*_{abs}}{32\pi h\ Q_0''\ a\ \Gamma(\alpha+4)\ \zeta(\alpha+4)}\right]^{-1/\alpha+4}$$

and

$$C_1 = \frac{\pi a^2\ Q^*_{abs}\ N_1 R_1^{\beta}\ (R \sin\theta_2)^{1-\beta}}{\alpha + 4} .$$

With lines of integration for $r' < R_1$ crossing the central evacuated cavity the solution of equation (4.30) by analytical and numerical methods is somewhat complicated. However, we now proceed to consider the derivation of $f_\nu(\tau)$ from the shell (under certain limiting conditions) by analytical means.

4.4.2 Analytical Solution of the Equation of Transfer

In section (4.4.1) we derived the general form of the integrands for a spherical dust distribution. Before attempting to solve equation (4.30) analytically we must express θ_1 in terms of θ_2. It can be seen from figure (4.1) that

$$R \sin\theta_2 = ct \frac{\sin\theta_1}{1 - \cos\theta_1} \qquad (4.31)$$

thus

$$\theta_1 = \sin^{-1}\left[\frac{2\tau \sin\theta_2}{\tau^2 + \sin^2\theta_2}\right] \qquad (4.32)$$

where as before θ_1 is $\widehat{OCG}$ with G lying on the expanding parabola.

Figures (4.5a), (b) and (c) show the regions of integration in real space for the expanding parabola in a spherical shell. The three cases for the ratio $\psi = {}^{R1}/_{R}$ are required because, for example, in figure (4.5a) the parabola leaves the central cavity ($\tau = 2\psi$) before it reaches the limb of the shell ($\tau = 1$) whereas in figure (4.5c) it leaves the inner cavity after $\tau = 1$. Also in figure (4.5b) the parabola leaves the cavity ($\tau = 2\psi$) before the intersection of the parabola with the shell is at a vertical displacement less than $R_1(\tau = 1 + \sqrt{1 - \psi^2})$. Each separate figure in (4.5) shows the different regions of integration required to obtain the infra-red flux at any given time τ for any cavity to shell radius ratio ψ. Table (4.1) gives the limits on θ and θ_2 for figures (4.5a), A - E; from these,

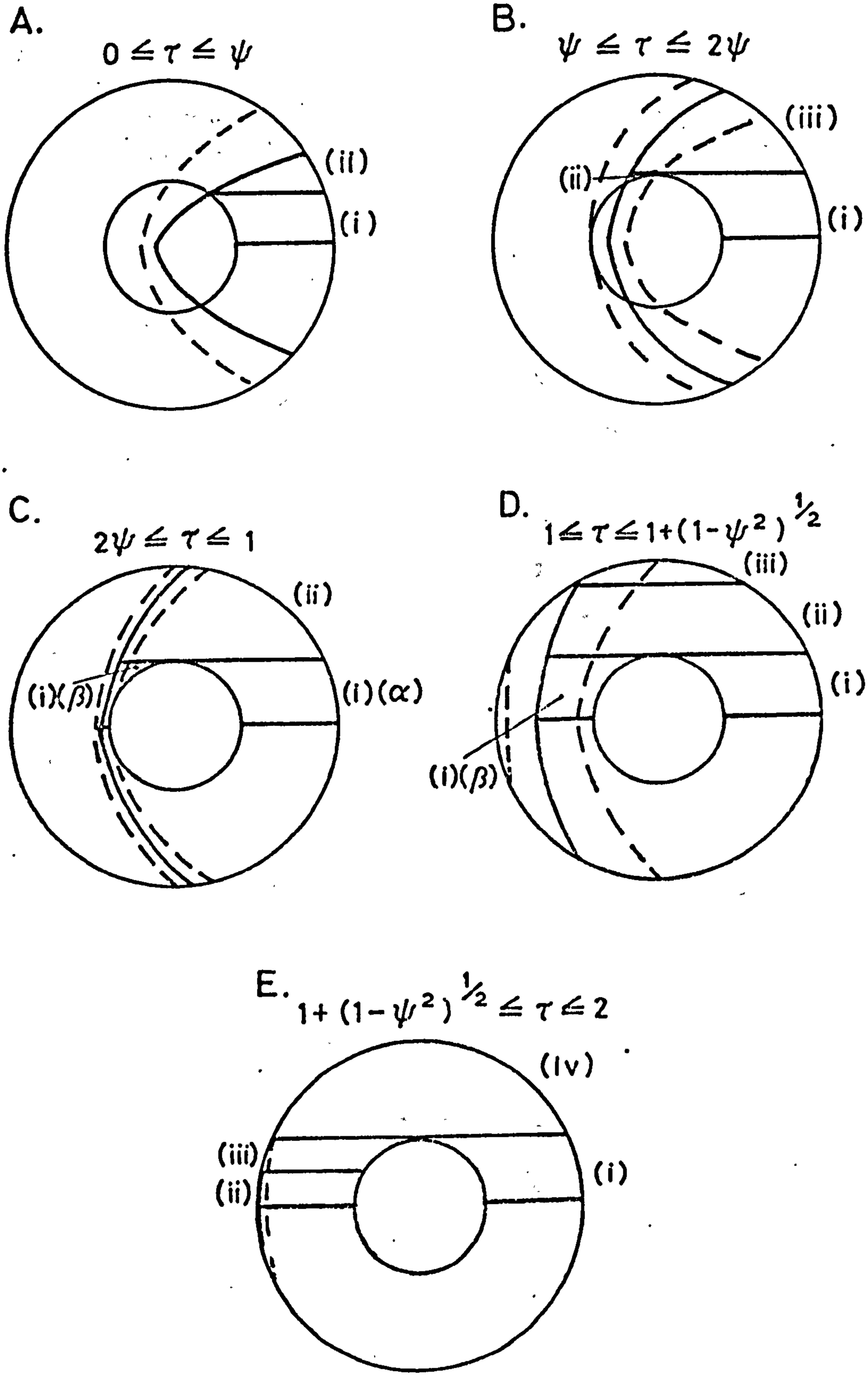

Figure (4.5a) The development of the emitting region of a distantly observed dust shell in section for $R_1 < R/2$. Broken lines give limits on the position of the emission parabola within the times, τ, given for each sub-figure A-E.

A.

$0 \leq \tau \leq \psi$

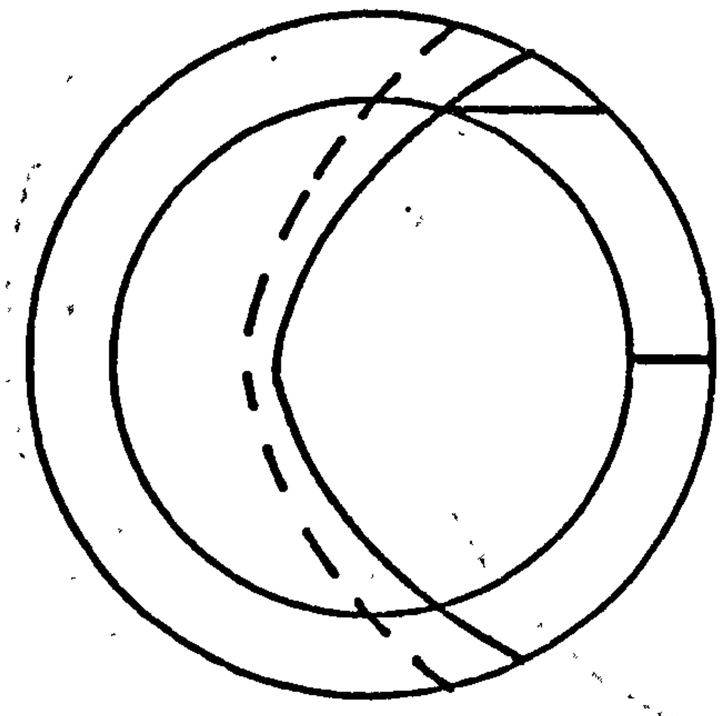

B.

$\psi \leq \tau \leq 1$

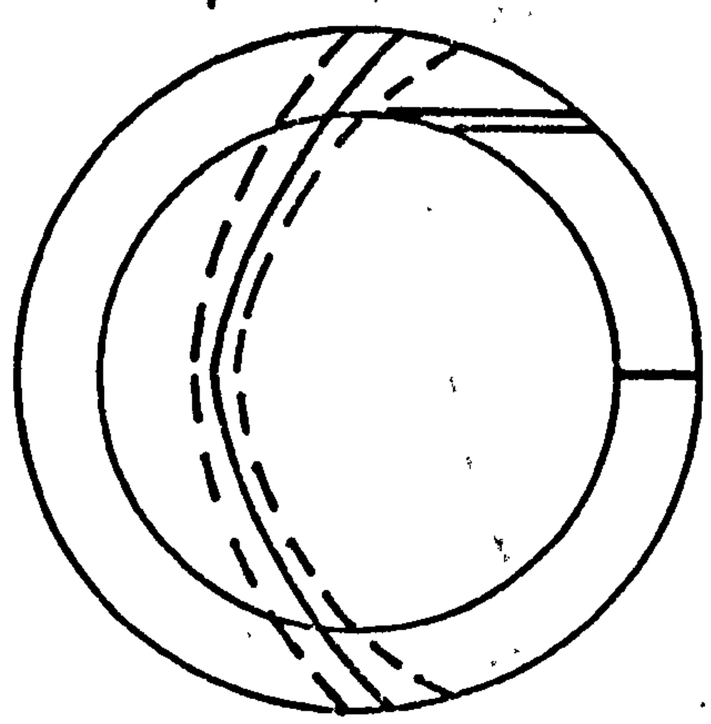

C.

$1 \leq \tau \leq 2\psi$

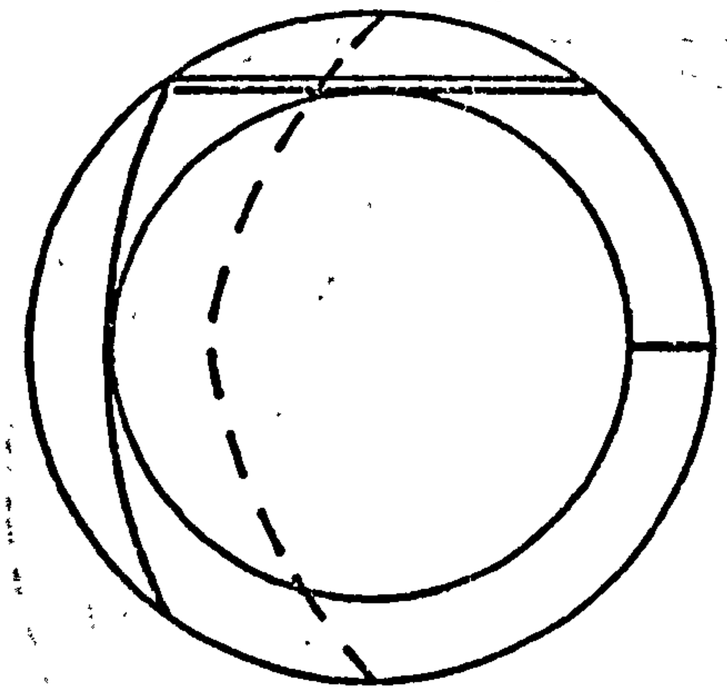

D.

$2\psi \leq \tau \leq 1+(1-\psi^2)^{\frac{1}{2}}$

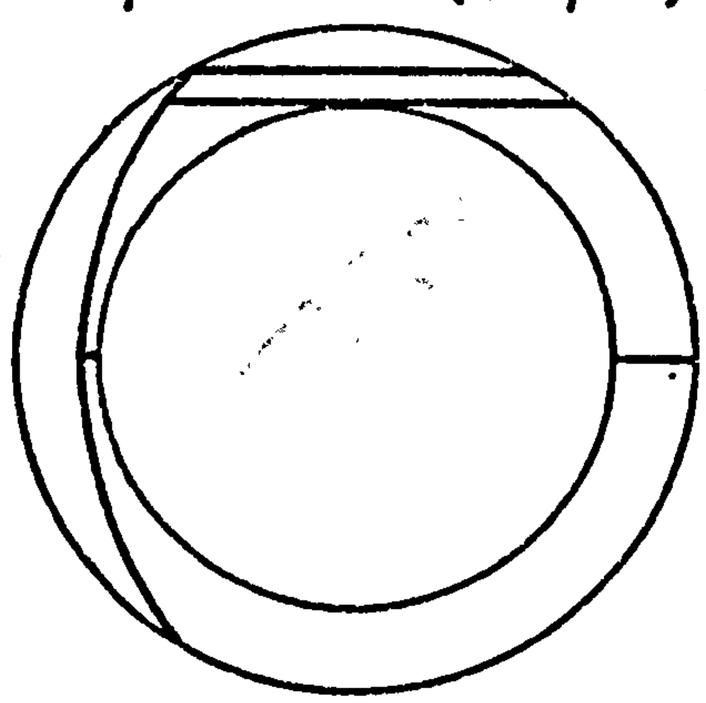

E.

$1+(1-\psi^2)^{\frac{1}{2}} \leq \tau \leq 2$

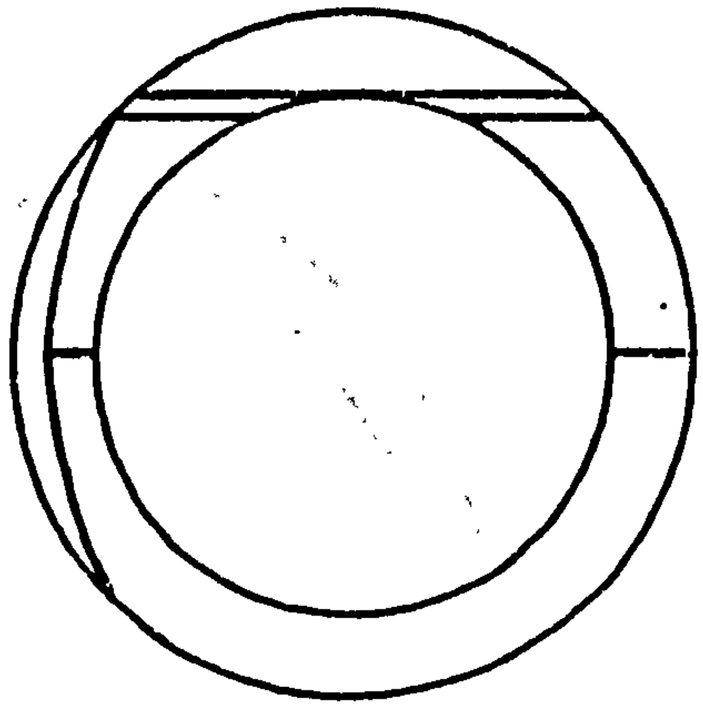

Figure (4.5b) As figure (4.5a) except $R/2 < R_1 < 4/5R$

A.

$0 \leq \tau \leq \psi$

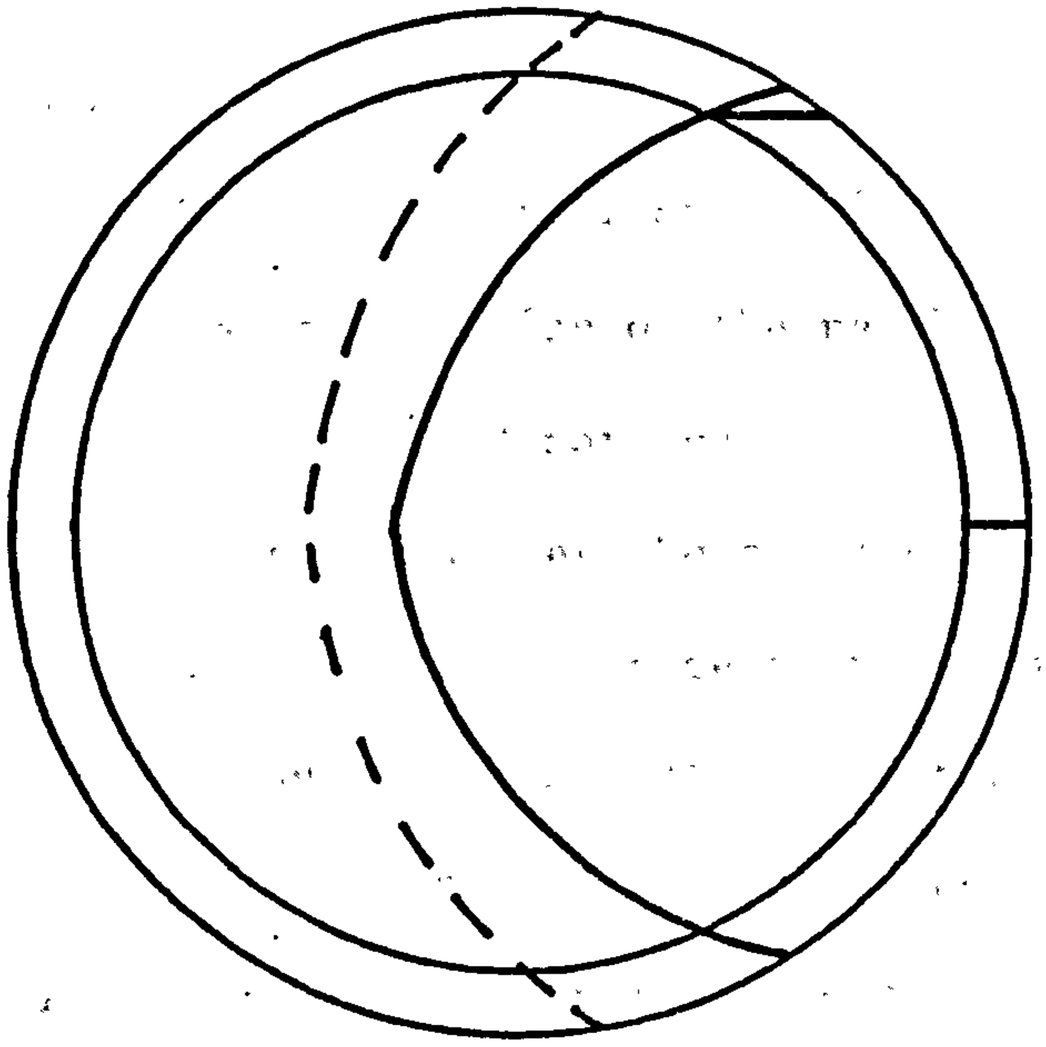

B.

$\psi \leq \tau \leq 1$

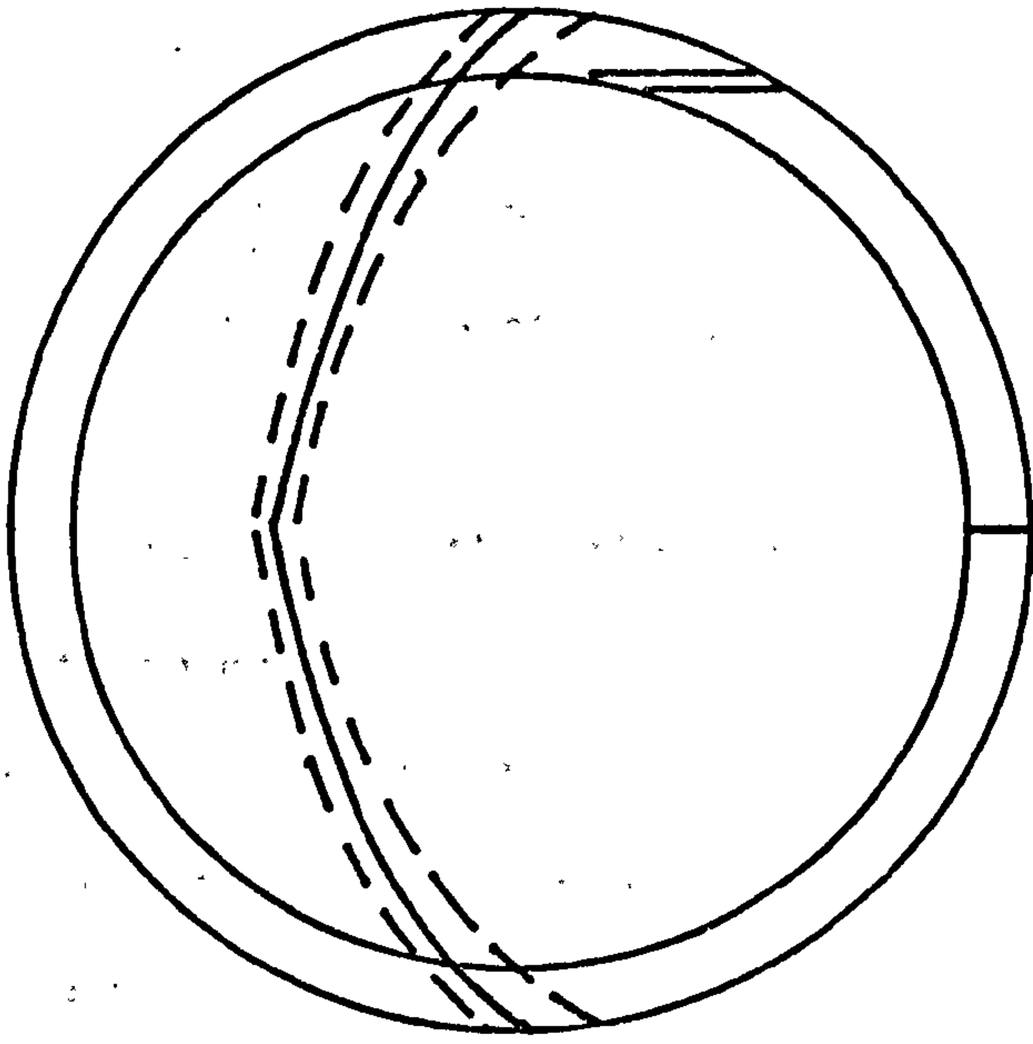

C.

$1 \leq \tau \leq 1+(1-\psi^2)^{1/2}$

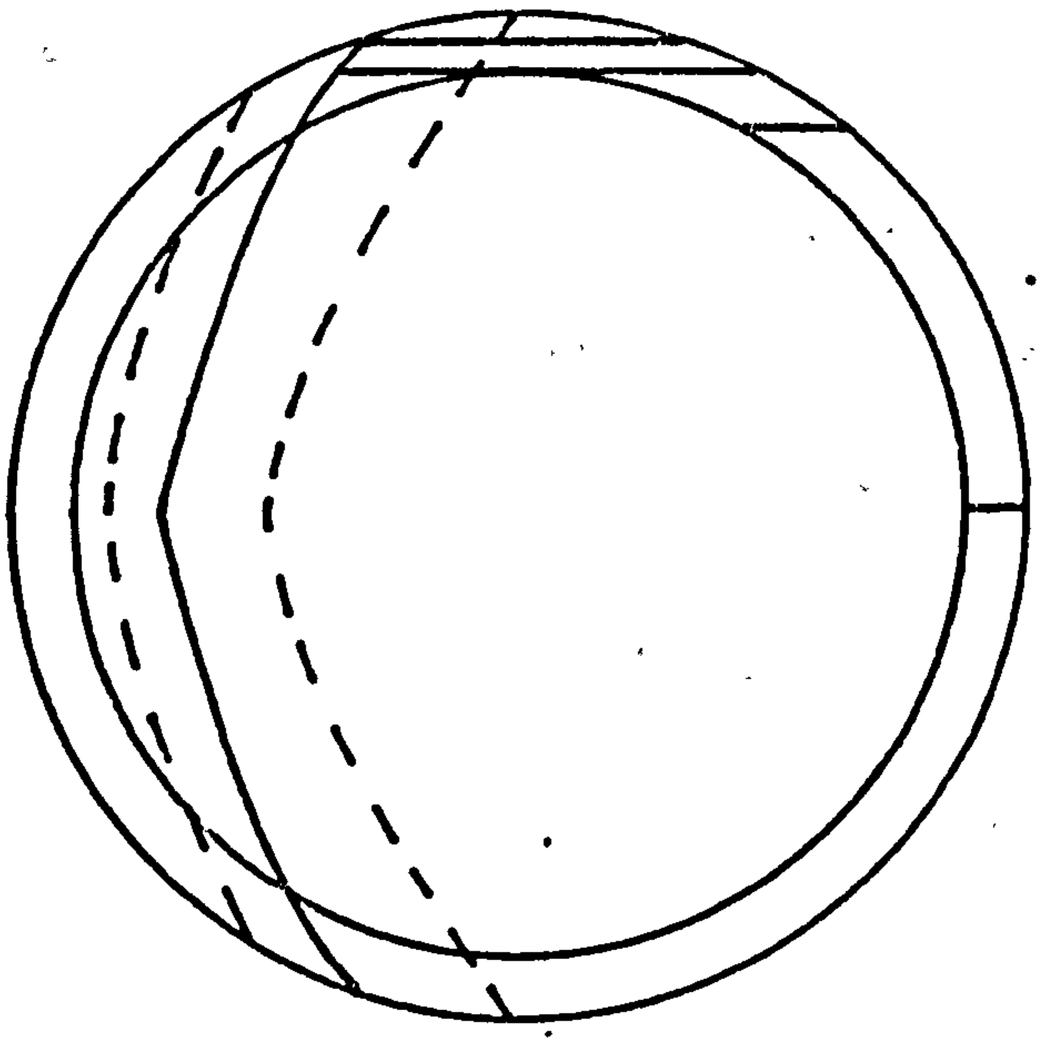

D.

$1+(1-\psi^2)^{1/2} \leq \tau \leq 2\psi$

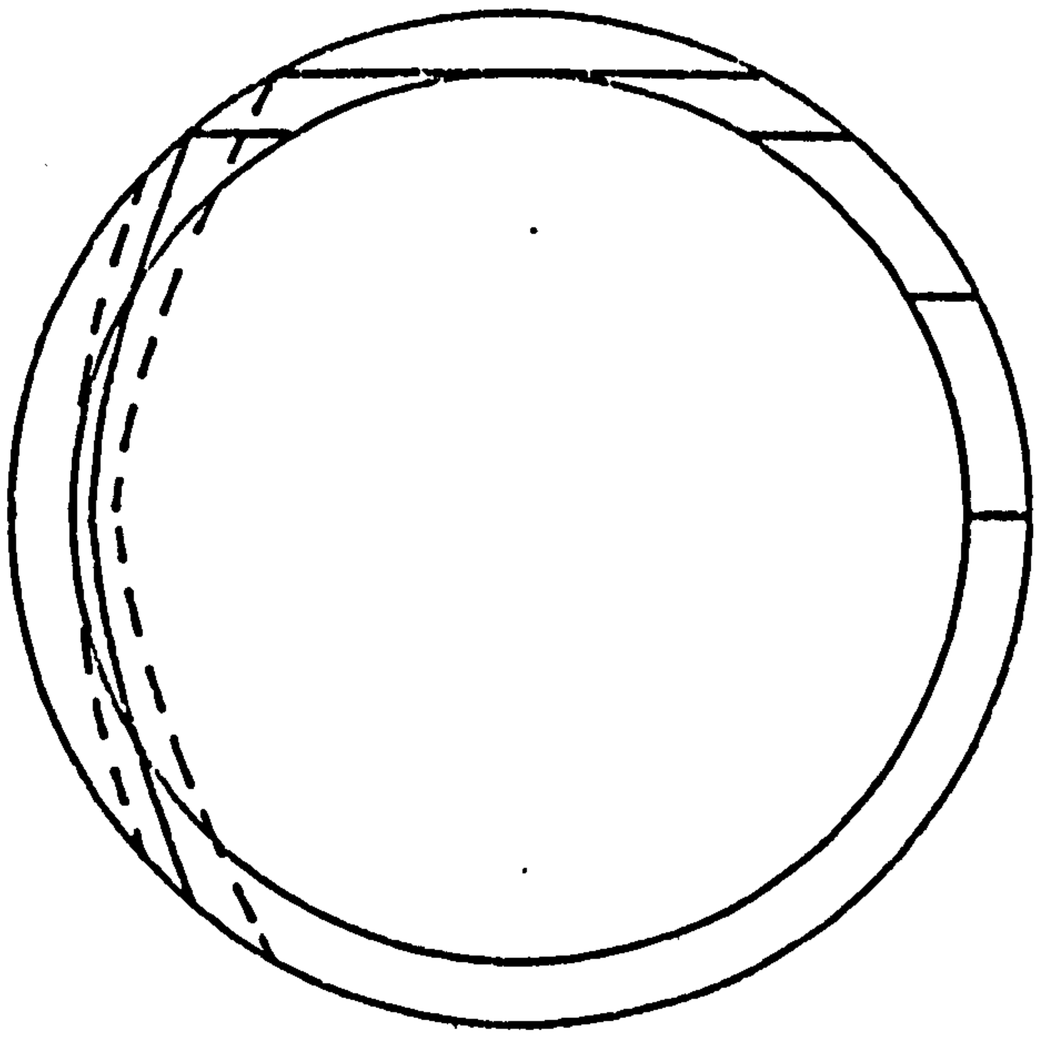

E.

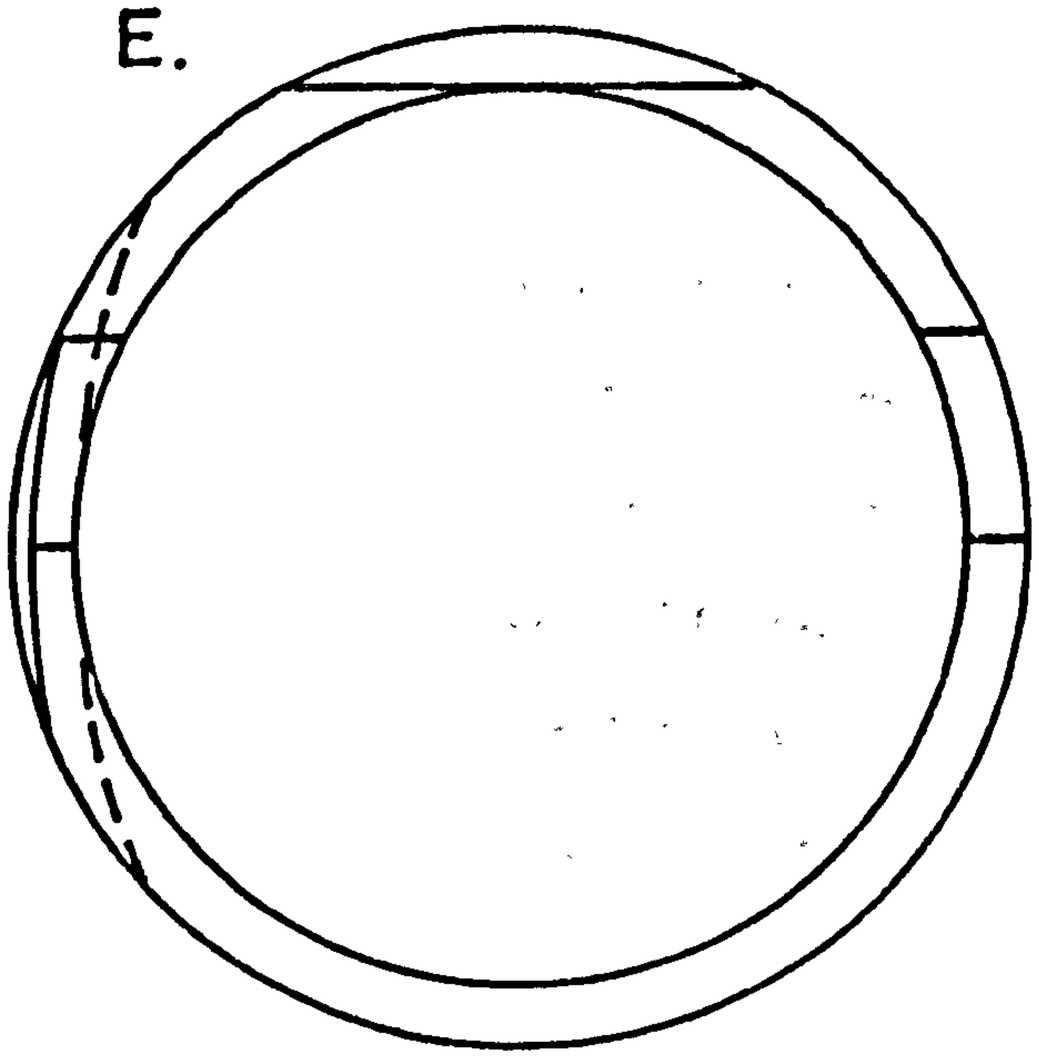

$2\psi \leq \tau \leq 2$

Figure (4.5c) As figure (4.5a) except $^4/_5R < R_1 < R$.

limits for figures (4.5b) and (c) follow.

The functions f_1 and g_1 in table (4.1) refer to the inner cavity and the intersection of the parabola and inner cavity respectively. These are defined more explicitly below:

We now consider the solution of equation (4.30) for the spherical shell. This requires certain assumptions to be made.

If we consider that the source is optically thin to both ultra-violet and infra-red radiation and that the central source has a step function light curve (i.e. equation (4.22) with $\omega = 0$) then the integrands simplify considerably. The basic equation now has the general form

$$f_\nu(\tau) = A_1 \int_{\theta_2=g(\tau)}^{\theta_2=g'(\tau)} (\sin\theta_2)^{2-\beta} \cos\theta_2 \cdot d\theta_2 \cdot$$

$$\int_{\theta_2=f(\theta_2,\tau)}^{\theta=f'(\theta_2,\tau)} \frac{(\sin\theta)^{\beta-2}}{\exp\left[H\left(\frac{\sin\theta_2}{\sin\theta}\right)^{2/\alpha+4}\right] - 1} \cdot d\theta \qquad (4.33)$$

where the generalised integration limits g and g' are functions of τ; the generalised integration limits f and f' are functions of τ and θ_2 and $H = B_1 r^{2/\alpha+4}$. The precise forms of these functions will depend on the relative values of ψ and τ.

Figures (4.6a) to (4.6e) show the regions of integration transformed to the (θ, θ_2) plane for the five time intervals of figure (4.5a). A larger cavity giving a larger value of ψ would of course reduce the area of integration as well as altering limits on θ and θ_2 with time

(see figure (4.5)).

If we define

$$f_1(\theta_2) = \sin^{-1}\left(\frac{\sin\theta_2}{\psi}\right),$$

and $g_1(\tau) = \sin^{-1}\left(\left[\tau(2\psi - \tau)\right]^{\frac{1}{2}}\right)$

then in figure (4.6a) for example

$$X \equiv \frac{f_\nu(\tau)}{A_1} = \int_{\theta_2=0}^{g_1(\tau)} (\sin\theta_2)^{2-\beta} \cos\theta_2 \cdot d\theta_2 \int_{\theta=\theta_2}^{f_1(\theta_2)} (\sin\theta)^{\beta-2} \cdot$$

$$\left[\exp\left[H\left(\frac{\sin\theta_2}{\sin\theta}\right)^{2/\alpha+4}\right] - 1\right]^{-1} \cdot d\theta +$$

$$\int_{\theta_2=g_1(\tau)}^{\theta_0} (\sin\theta_2)^{2-\beta} \cos\theta_2 \cdot d\theta_2 \int_{\theta=\theta_2}^{\theta_1} (\sin\theta)^{\beta-2} \cdot$$

$$\left[\exp\left[H\left(\frac{\sin\theta_2}{\sin\theta}\right)^{2/\alpha+4}\right] - 1\right]^{-1} \cdot d\theta \qquad (4.34)$$

By reversing the order of integration of equation (4.34) we re-define X as:-

$$X = \int_{\theta=0}^{\theta_0} (\sin\theta)^{\beta-2} \cdot d\theta \int_{\theta_2=f_1'(\theta)}^{\theta} \frac{(\sin\theta_2)^{2-\beta} \cos\theta_2 \cdot d\theta_2}{\exp\left[H\left(\frac{\sin\theta_2}{\sin\theta}\right)^{2/\alpha+4}\right]-1}$$

$$+ \int_{\theta=\theta_0}^{k'(\tau)} (\sin\theta)^{\beta-2} \cdot d\theta \int_{\theta_2=f_1'(\theta)}^{\theta_1'} \frac{(\sin\theta_2)^{2-\beta} \cos\theta_2 \cdot d\theta_2}{\exp\left[H\left(\frac{\sin\theta_2}{\sin\theta}\right)^{2/\alpha+4}\right]-1} \qquad (4.35)$$

where $f_1'(\theta) = \sin^{-1}\left[\psi \sin\theta\right]$, $\theta_1' = \sin^{-1}\left[\tau \sin\theta/(1-\cos\theta)\right]$

$$k'(\tau) = \sin^{-1}\left[2\tau(2\tau\psi - \tau^2)^{\frac{1}{2}}\right]$$

If we take the first term of equation (4.35) and call it X_1 (i.e. $X = X_1 + X_2$) then make the substitution

$$x = H\left(\frac{\sin\theta_2}{\sin\theta}\right)^{2/\alpha+4} ,$$

we arrive at the expression

$$X_1 = \left(\frac{\alpha+4}{2}\right) H^{-(\gamma+1)} \int_0^{\theta_0} \sin\theta \int_{H'}^{H} \frac{x \cdot x^{\gamma-1}}{e^x - 1} \cdot dx$$

where $H' = H\psi^{2/\alpha+4}$ and $\gamma = \left(\frac{\alpha+4}{2}\right)\left(3 - \beta\right) - 1.$

The integrand in x is in fact a standard form (Gradshteyn and Ryzhik, 1965, p. 1076) which reduces the above equation to the form

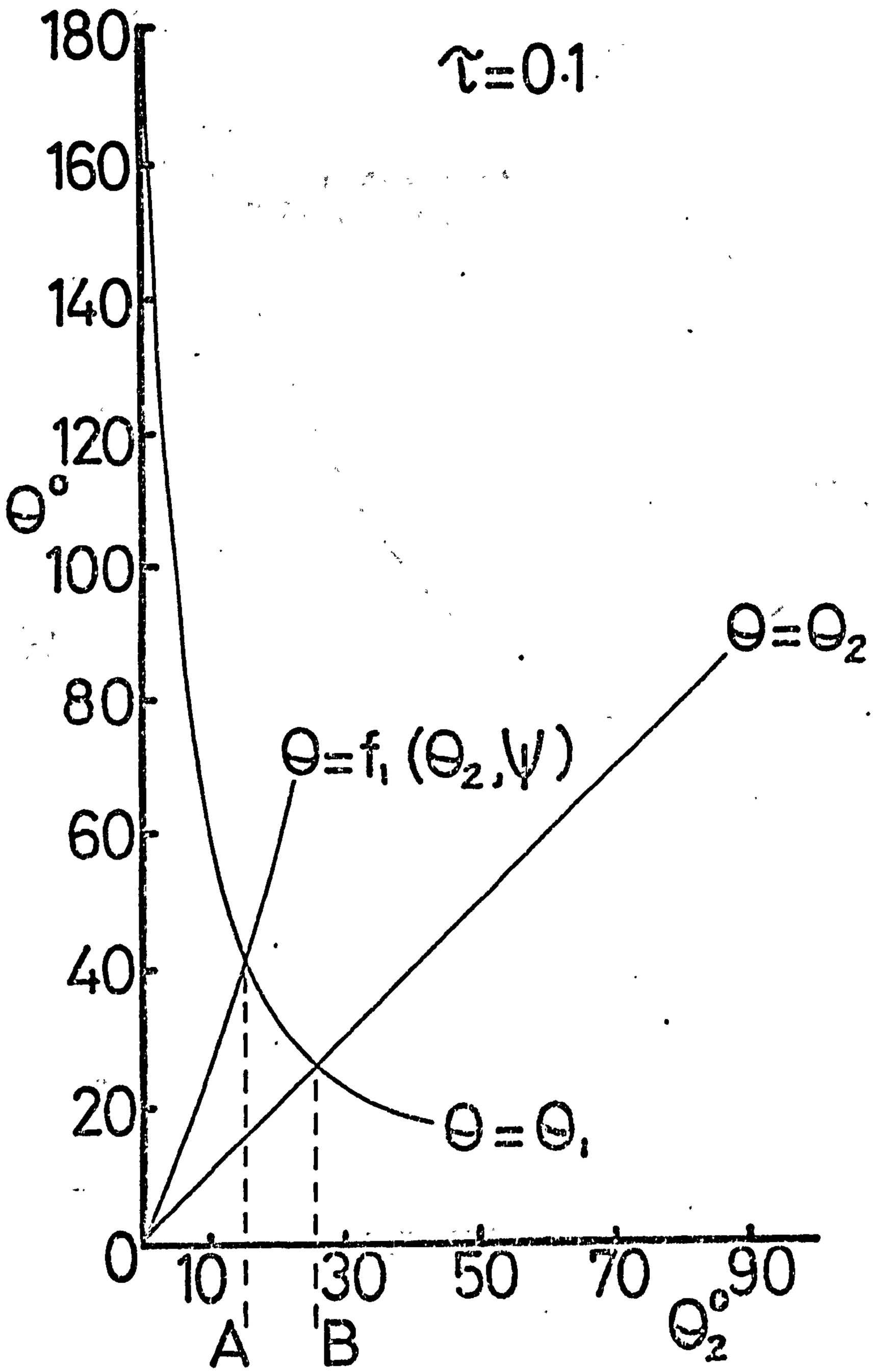

Figure (4.6a) The region of integration in the (θ, θ_2) plane corresponding to stage A of figure (4.5a). On the θ_2 axis at point A, $\theta_2 = g_1(\tau)$; at B, $\theta_2 = \theta_0$. The curves described by functions f_1, θ_1 and θ_2 relate to the cavity, parabola and outer shell respectively.

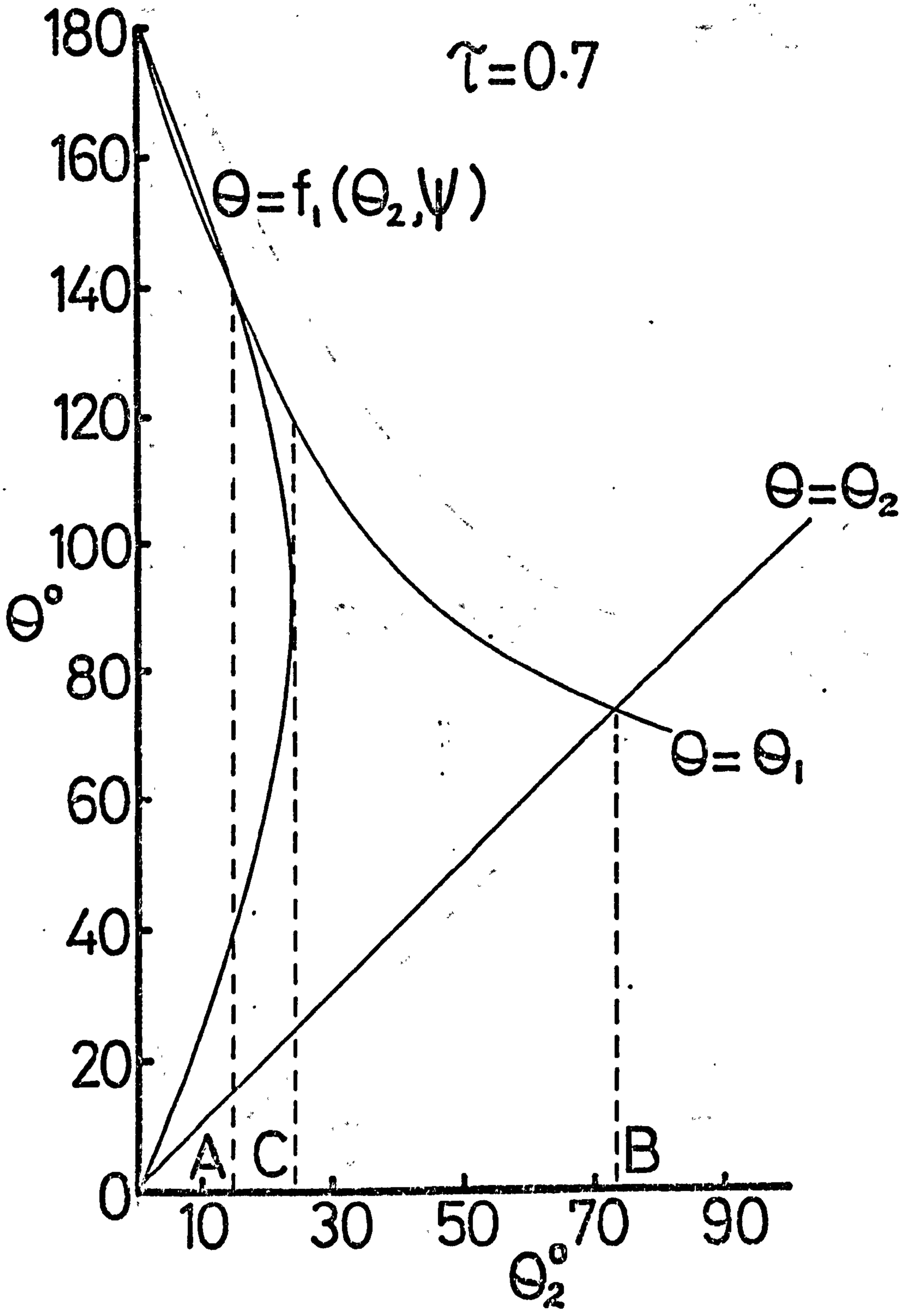

Figure (4.6b) As figure (4.6a) except that this relates to stage B of figure (4.5a). At point C, $\theta_2 = \sin^{-1}\psi$

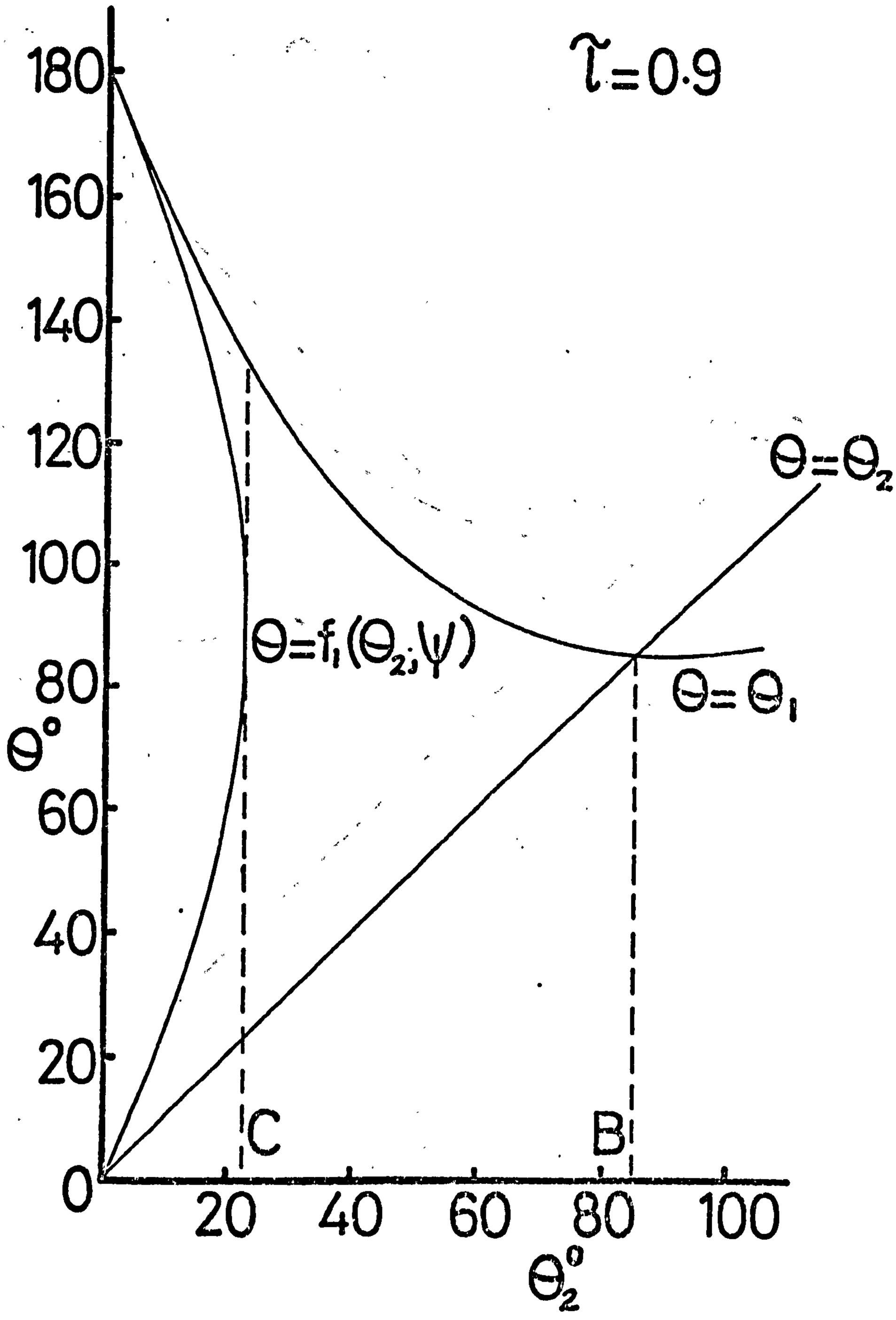

Figure (4.6c) As figure (4.6a) except that this relates to stage C of figure (4.5a).

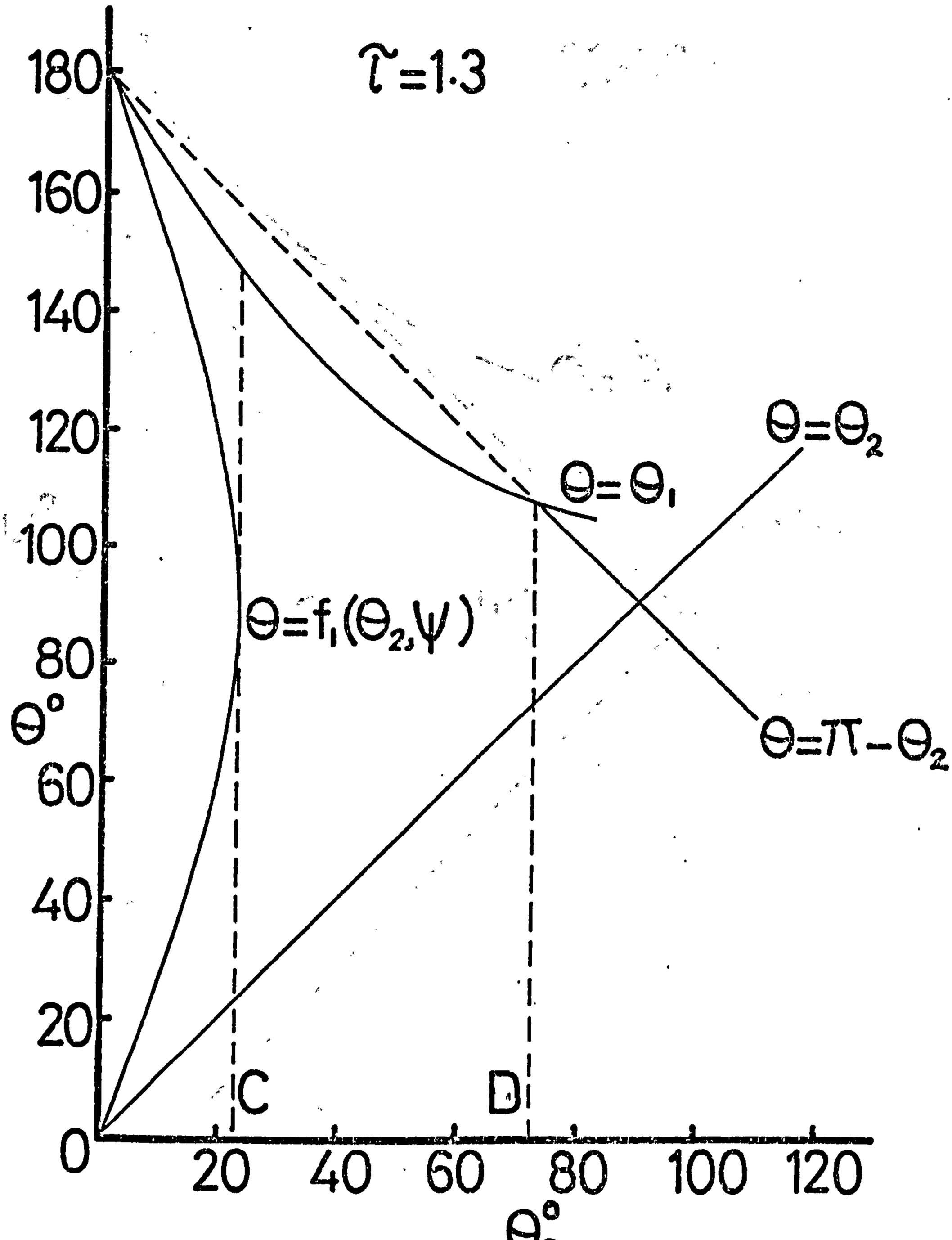

Figure (4.6d) As figure (4.6a) except that this relates to stage D of figure (4.5a). At point D, $\theta_2 = \pi - \theta_0$.

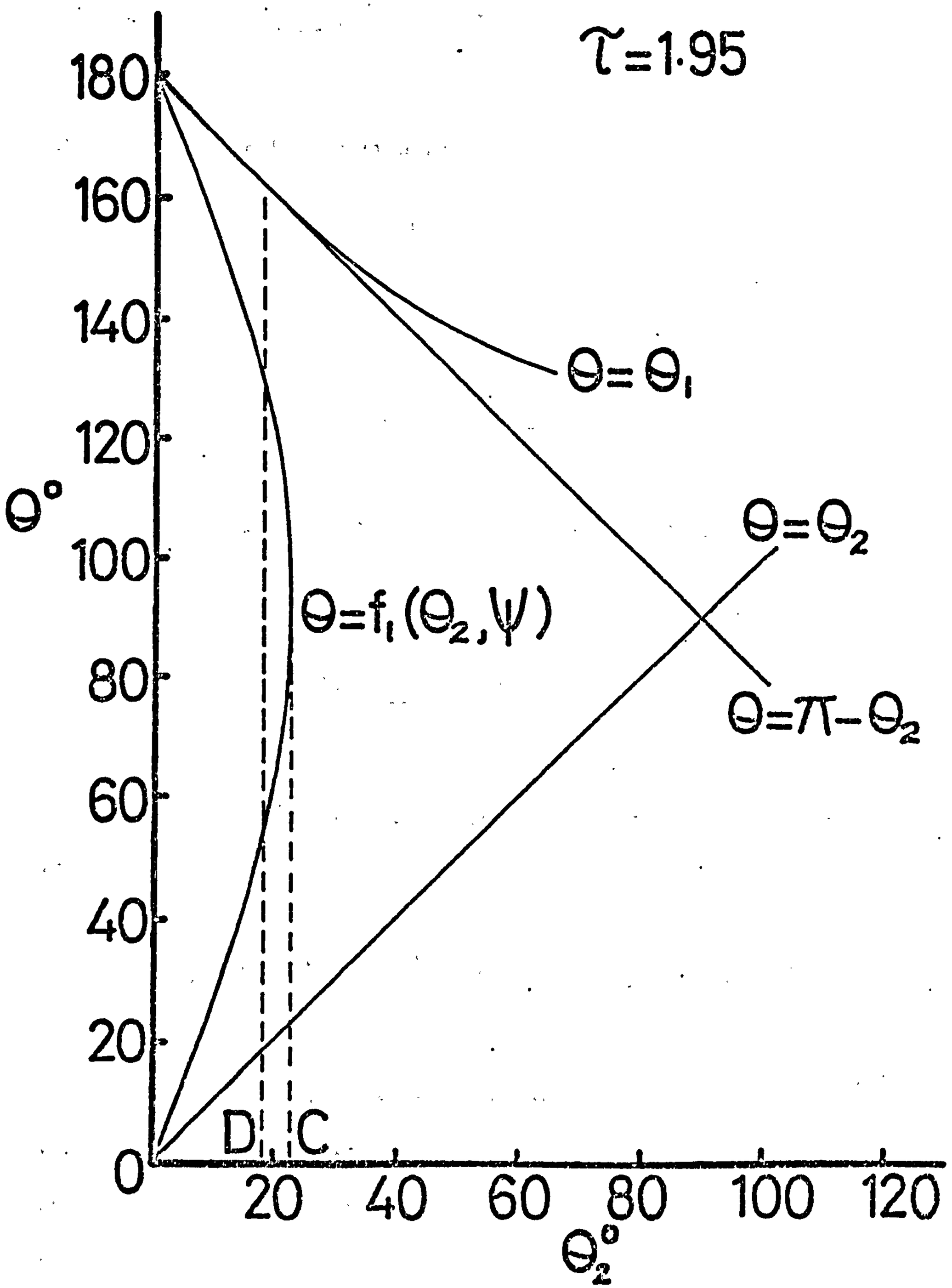

Figure (4.6e) As figure (4.6a) except that this relates to stage E of figure (4.5a).

$$X_1 = \left(\frac{\alpha+4}{2}\right) H^{-(\gamma+1)} \int_0^{\theta_0} \sin\theta \sum_{n=0}^{\infty} \frac{B_n}{n!} \frac{H^{n+\gamma}}{(n+\gamma)} \left[1 - \psi^{n'}\right] \cdot d\theta$$

where B_n are the Bernoulli numbers and

$$n' = \left(\frac{2}{\alpha+4}\right)(n+\gamma) \quad .$$

Thus

$$X_1 = \left(\frac{\alpha+4}{2}\right) \sum_{n=0}^{\infty} \frac{B_n}{n!} \frac{H^{n-1}}{(n+\gamma)} \tau\left[1 - \psi^{n'}\right] \qquad (4.36a)$$

Similarly for X_2, substituting in the exponential and integrating leaves us with

$$X_2 = \left(\frac{\alpha+4}{2}\right) \sum_{n=0}^{\infty} \frac{B_n}{n!} \frac{H^{n-1}}{(n+\gamma)} \tau\left[\psi^{n'-1}\left(\psi - \frac{n'}{n'-1}\right) - \frac{1}{n'-1}\right]. \qquad (4.36b)$$

Combining equations (4.36a) and (4.36b) and simplifying we arrive at the solution

$$f_\nu(\tau) = A_1\left(\frac{\alpha+4}{2}\right)\tau \sum_{n=0}^{\infty} \frac{B_n}{n!} \frac{H^{n-1}}{(n+\gamma)} \left(\frac{n'}{n'-1}\right)\left(1 - \psi^{(n'-1)}\right) \qquad (4.37a)$$

Surprisingly, when the integrations are performed for all cavity ratios where $\tau \leq 2\psi$ equation (4.37a) is obtained. From this equation we can see that the infra-red flux rises linearly with time ($\propto \tau$) for $\tau \leq 2\psi$ despite the complexity of the original conditions.

When we consider the integrations for $\tau > 2\psi$ the following result is found for all ψ, namely

$$f_\nu(\tau) = A_1 \frac{\alpha+4}{2} \tau \sum_{n=0}^{\infty} \frac{B_n}{n!} \frac{H^{n-1}}{n+\gamma} \left\{ \left[\frac{n'}{n'-1} \right] \left(1 - \frac{1}{n'} \left(\frac{\tau}{2} \right)^{n'-1} \right) - \frac{2}{\tau} \psi^{n'} \right\} \qquad (4.37b)$$

Obviously, when $\tau \geq 2$ the flux will take a constant value as the spherical shell is then filled with ultra-violet radiation from the central source, i.e.

$$f_\nu(\tau=2) = A_1(\alpha+4) \sum_{n=0}^{\infty} \frac{B_n}{n!} \frac{H^{n-1}}{(n+\gamma)} \left[1 - \psi^{n'} \right] \qquad (4.37c)$$

Apart from the approximations made earlier, these solutions also have other limitations. For example we can see that from the definition of n' and its rôle in the series, that if it ever equals zero or 1 the series must diverge. To avoid this we choose $\beta \lesssim 1$ in the summation. The Bernoulli series itself diverges for certain values of wavelength because the identity

$$\frac{x}{e^x - 1} = \sum_{n=0}^{\infty} \frac{B_n x^n}{n!}$$

is defined only for $|x| < 2\pi$ (Abramowitz & Stegun, 1972, p.804). Substituting for H we find that the limiting wavelength, λ_B, for convergence is given by:-

$$\lambda_B \simeq \frac{c}{2\pi} \left[\left(\frac{L}{4\pi R^2} \right) \left(\frac{c^2}{2h} \right) \left(\frac{Q^*_{abs}}{Q''_o \, a} \right) \left\{ 4\Gamma(\alpha+4) \; \psi(\alpha+4) \right\}^{-1} \right]^{-1/\alpha+4}$$

which is not, so far as we are aware, due to any physical cause such as taking the Rayleigh-Jeans limits of the Planck function.

According to equation (4.37a) the infra-red flux rises linearly with time at all wavelengths. This means that at early times the

re-radiated spectrum is time independent (therefore so is the 'black body' temperature, T_{BB}). Figures (4.7a) to (d) illustrate some of the effects that changing the values of variables will have.

(4.7a) for example clearly shows that there is little spectral change, particularly at times $\tau < 2\psi$. We may also note that in this case $f_\nu \propto \nu^{1.8}$ approximately at long wavelengths; the Rayleigh-Jeans approximation for a perfect black body gives $f_\nu \propto \nu^2$ in this region. A single temperature shell of realistic grain material would give $f_\nu \propto \nu^{2+\alpha}$ from what we saw previously in section(4.2.1). The resulting spectrum in figure (4.7a) is of course for a shell in which a range of temperatures are encountered. Thus although the flux from the hottest grains dominates, the cooler grains contribute more long wavelength radiation than is the case for a perfect black body or a realistic grain shell at a single temperature. The spectrum is therefore less steep at long wavelengths.

The steepening of the spectrum with increasing α is shown clearly in figure (4.7b) where different α values give different spectra - all other parameters remaining constant. The $\alpha = 0$ spectrum illustrates the fact that we do not see a black body spectrum in an optically thin, extended source, although we might arrive at a pseudo-black body spectrum by choosing α, β, R, R_1 and the optical depth appropriately.

Using the parameters of figure (4.7b) but varying β little change of spectral shape was found. This is due to the fact that in this case the shell is geometrically thin ($\psi \sim 1$) and thus the number of high temperature grains will be little affected.

Figure (4.7c) shows the light curves for different values of R_1, all else remaining constant. One can clearly see that as ψ increases so does the extent of the linear rise. The peak luminosity is however diminished as there are fewer emitting grains at high temperatures.

Figure (4.7d) illustrates the fact that the flux at any given

Figure (4.7a) Observed spectra from a dust shell with $R = 2.5 \times 10^{16}$ cm, $Mg = 2.2 \times 10^{-7} M_{\odot}$ and step function central source light curve ($L = 5 \times 10^{38}$ ergs^{-1}). Different values of τ are shown above each curve. The significance of λ_B in the analytical solution of the transfer equation as used here is explained in the text. $a = 10^{-5}$ cm, $\alpha = 2$, $\beta = 1$.

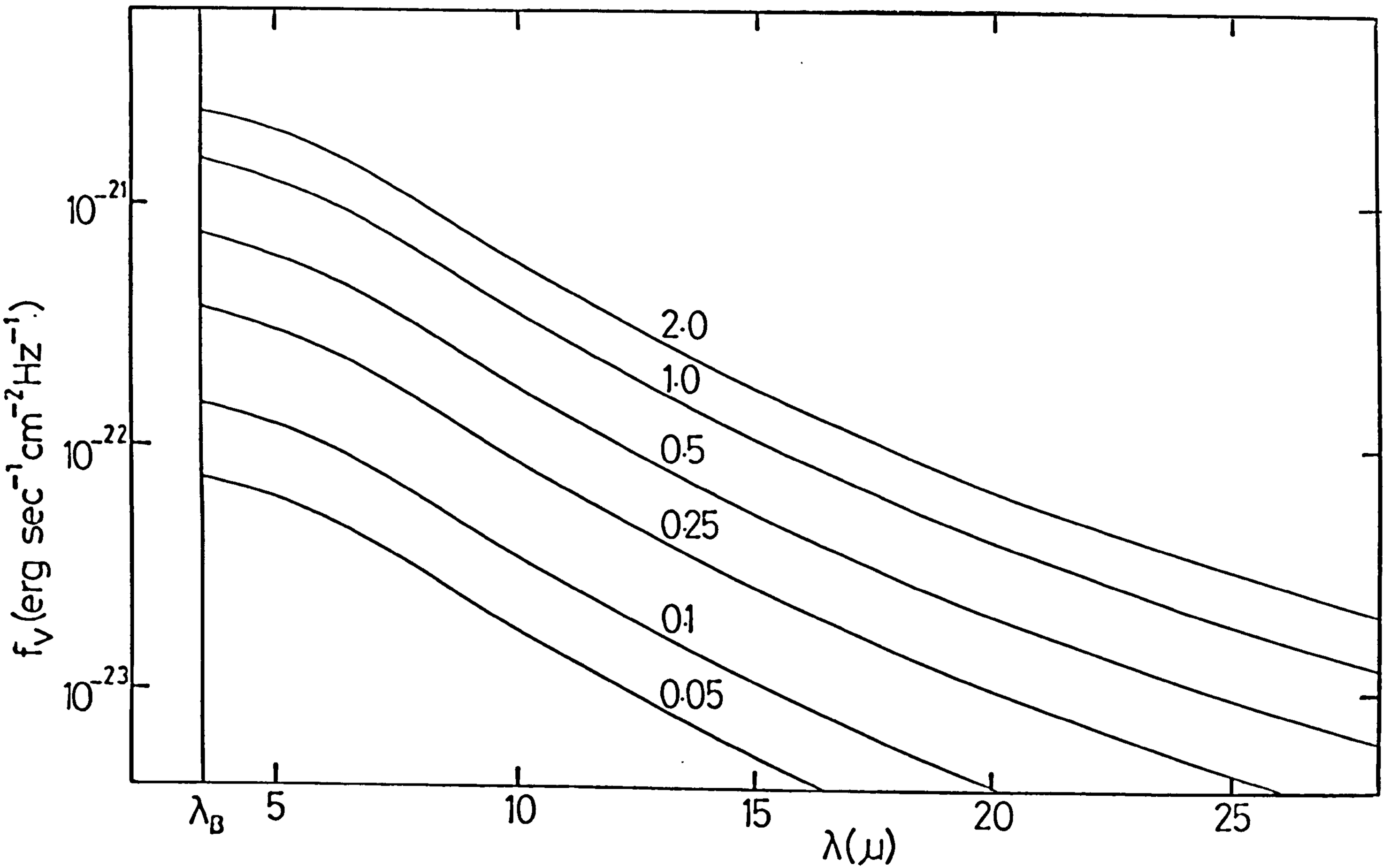
10^{-21}
10^{-22}
10^{-23}
f_ν(erg sec^{-1}cm^{-2}Hz^{-1})
2·0
1·0
0·5
0·25
0·1
0·05
λ_B
5
10
15
20
25
$\lambda(\mu)$

Figure (4.7b) Spectra at $\tau = 1$ for several values of α and β. All other parameters as in figure (4.7a). Curves are labelled in the form (α, β).

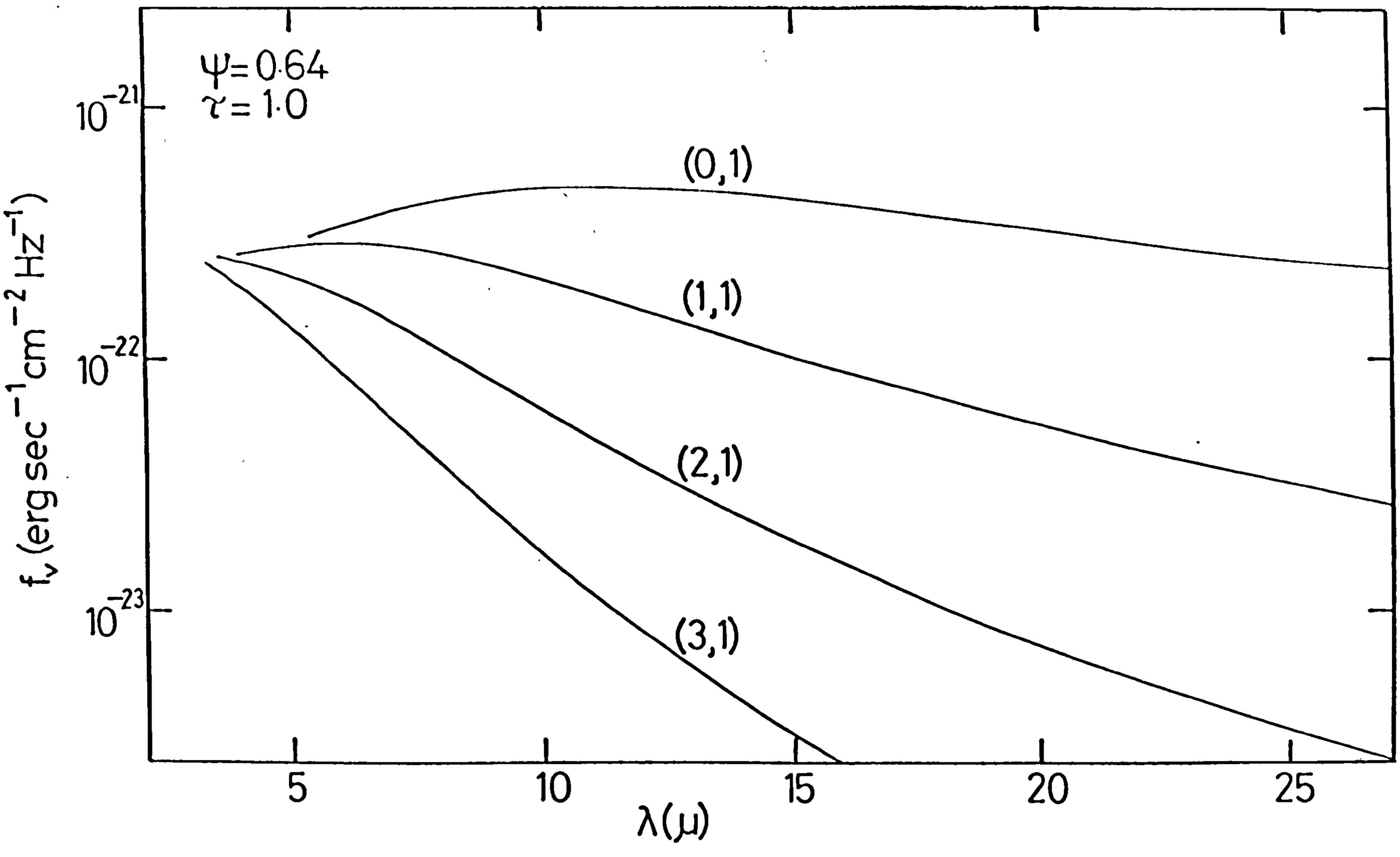
Ψ=0·64
τ=1·0
(0,1)
(1,1)
(2,1)
(3,1)
10^{-21}
10^{-22}
10^{-23}
f_ν (erg sec^{-1}cm^{-2}Hz^{-1})
5
10
15
20
25
λ(μ)

Figure (4.7c) Infra-red light curves at an observing wavelength $\lambda = 30\ \mu m$. Parameters of dust shell and central source are as in figure (4.7a) except ψ is varied. Its value is marked on each curve. The termination of linear rise is marked as a tick.

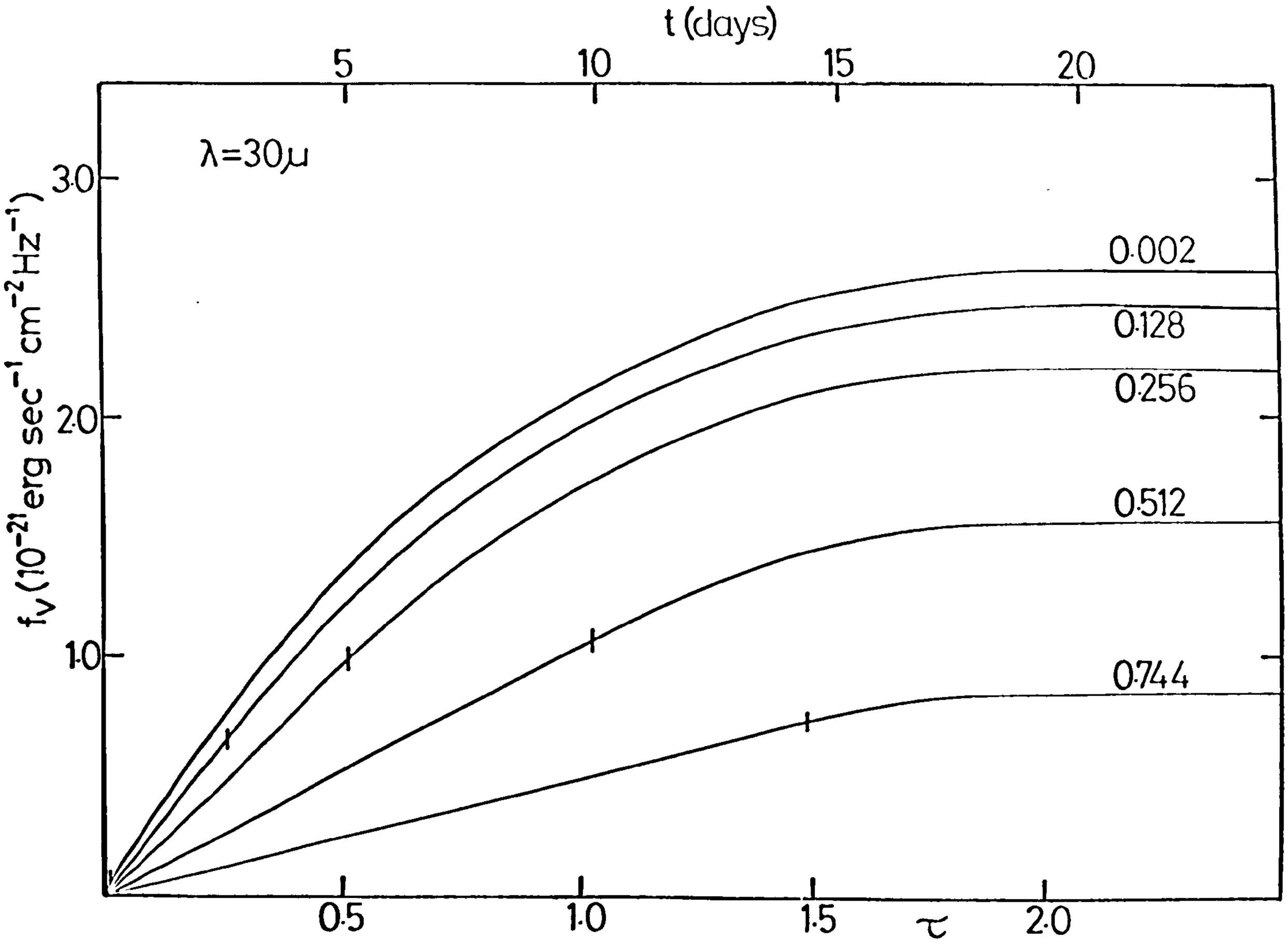
t (days)
5
10
15
20
λ=30μ
3·0
2·0
1·0
f_ν (10^{-21} erg sec^{-1} cm^{-2} Hz^{-1})
0·002
0·128
0·256
0·512
0·744
0·5
1·0
1·5
τ
2·0

Figure (4.7d) Infra-red light curves observed from a dust shell and central source with parameters as in figure (4.7a) except $\psi = 0.64$, $\lambda = 10$ μm for several values of α. Again curves are labelled in the form (α, β).

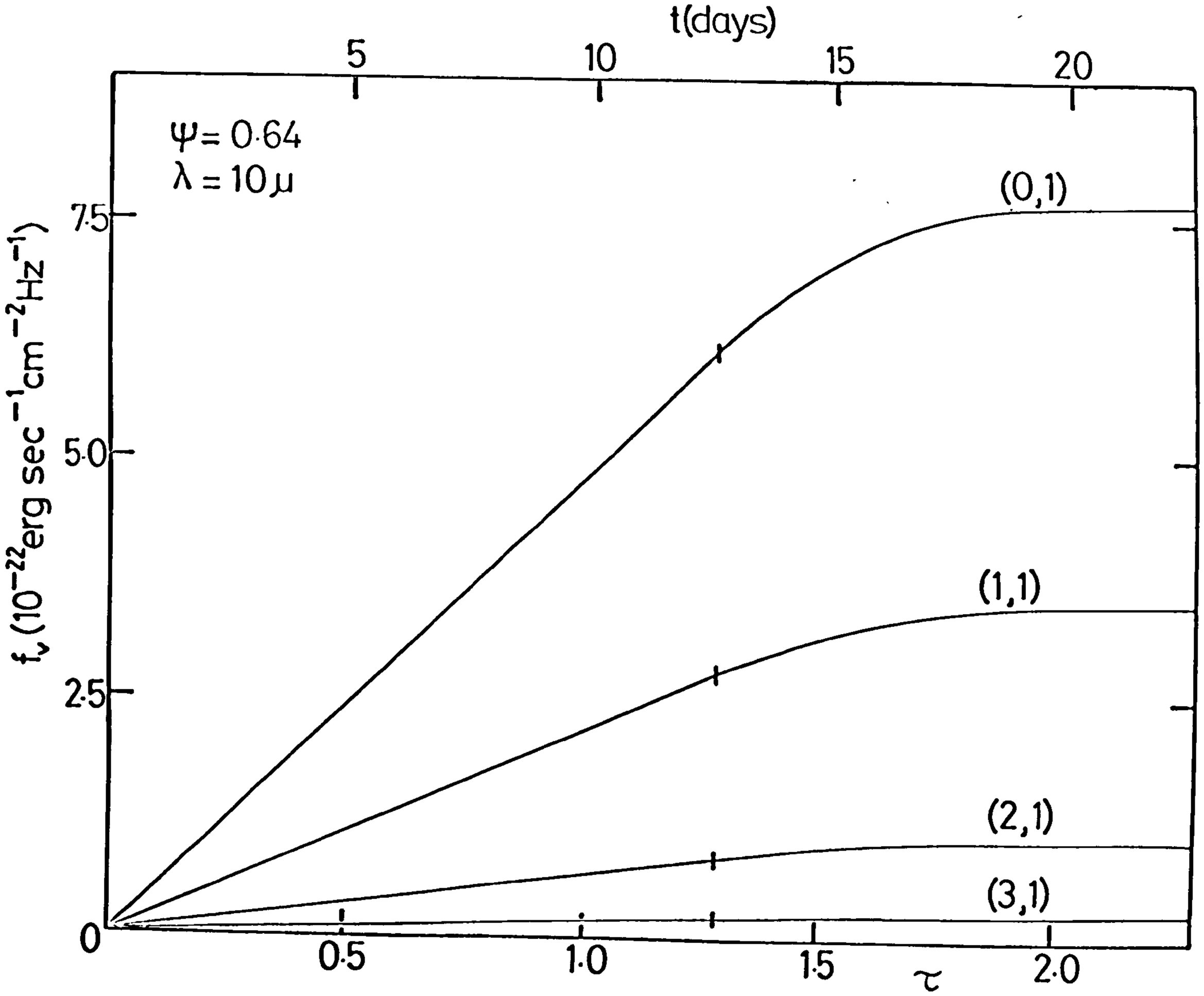
t(days)
5
10
15
20
ψ = 0·64
λ = 10 μ
(0,1)
(1,1)
(2,1)
(3,1)
7·5
5·0
2·5
0
0·5
1·0
1·5
2·0
τ
$f_\nu (10^{-22} \text{erg sec}^{-1} \text{cm}^{-2} \text{Hz}^{-1})$

instant for a particular wavelength can be increased by decreasing α (as we would expect from equation (4.3)).

We now proceed to consider general illustrative models of more realistic situations.

4.4.3 Numerical Solution of the Equation of Transfer - General Models

The computations for the infra-red fluxes derived in section (4.4.2) were basically straight forward and required only small amounts of computer time. Here however we deal with more realistic cases where the full form of equation (4.30) is used between limits detailed in figures (4.6a), (b) and (c) and table (4.1). This required a much longer programme which solved the equations numerically. Reference should be made therefore to Appendix A1 where a detailed description of the functioning of the programme is given.

Before the numerical integration method was used with more detailed and realistic models it was run alongside the analytical solution described in the previous section with a step function light curve; an optically thin dust shell and all the other conditions required by that analysis. This was carried out for a large number of values of τ, R, λ etc. The result was that, with 50 integration steps in θ_2 and 100 in θ, the two programmes did not differ by more than $\pm$ 1% which was considered satisfactory agreement. We now proceeded using the numerical integration method as a much more versatile tool having checked first for example that the infra-red flux now increased as the shell becomes slightly more opaque to ultra-violet radiation.

To explore the effects of a more realistic set of parameters the first model chosen was that of a typical nova with what were considered fairly reasonable dust shell parameters. Figure (4.8a) for example results from choosing the parameters

Table 4.1

Regions of Integration (see fig. (4.5a) and Appendix A1)

LIMITS ON θ_2	LIMITS ON TIME, τ				
	A. $0 < \tau \leq \psi$	B. $\psi < \tau \leq 2\psi$	C. $2\psi < \tau \leq 1$	D. $1 < \tau \leq 1+(1-\psi^2)^{\frac{1}{2}}$	E. $1+(1-\psi^2)^{\frac{1}{2}} < \tau \leq 2$
(i)	$0 < \theta_2 \leq g_1(\tau)$ $\theta_2 \leq \theta \leq f_1(\theta_2,\psi)$	$0 < \theta_2 \leq \sin^{-1}\psi$ $\theta_2 \leq \theta \leq f_1(\theta_2,\psi)$	(α) As B(i) (β) $0 < \theta_2 \leq \sin^{-1}\psi$ $\pi-f_1(\theta_2,\psi) \leq \theta \leq \theta_1$	(α) As B(i) (β) As C(i)(β)	As B(i)
(ii)	$g_1(\tau) \leq \theta_2 \leq \theta_0$ $\theta_2 \leq \theta \leq \theta_1$	$g_1(\tau) \leq \theta_2 \leq \sin^{-1}\psi$ $\pi-f_1(\theta_2,\psi) \leq \theta \leq \theta_1$	As B(iii)	$\sin^{-1}\psi \leq \theta_2 \leq \pi - \theta_0$ $\theta_2 \leq \theta \leq \theta_1$	$0 < \theta_2 \leq \pi - \theta_0$ $\pi-f_1(\theta_2,\psi) \leq \theta \leq \theta_1$
(iii)		$\sin^{-1}\psi \leq \theta_2 \leq \theta_0$ $\theta_2 \leq \theta \leq \theta_1$		$\pi-\theta_0 \leq \theta_2 \leq \pi/2$ $\theta_2 \leq \theta \leq \pi - \theta_2$	$\pi-\theta_0 \leq \theta_2 \leq \sin^{-1}\psi$ $\pi-f_1(\theta_2,\psi) \leq \theta \leq \pi - \theta_2$
(iv)					$\sin^{-1}\psi \leq \theta_2 \leq \pi/2$ $\theta_2 \leq \theta \leq \pi - \theta_2$

Figure (4.8a) Infra-red light curves observed by an observer at D = 1 kpc from a dust shell with parameters $R = 500R_1 = 5 \times 10^{17}$ cm, $Mg = 3.3 \times 10^{-6}$ $M_\odot$, $a = 10^{-5}$ cm, $\alpha = \beta = 2$, $Q^*_{abs} = 2$. The central source has a light curve of the form described by equation (4.22) with $\omega = 10^{-6}$ s^{-1}. The five infra-red wavelengths in μm are denoted by figures above curves. The locus of maximum flux is shown by a dashed curve.

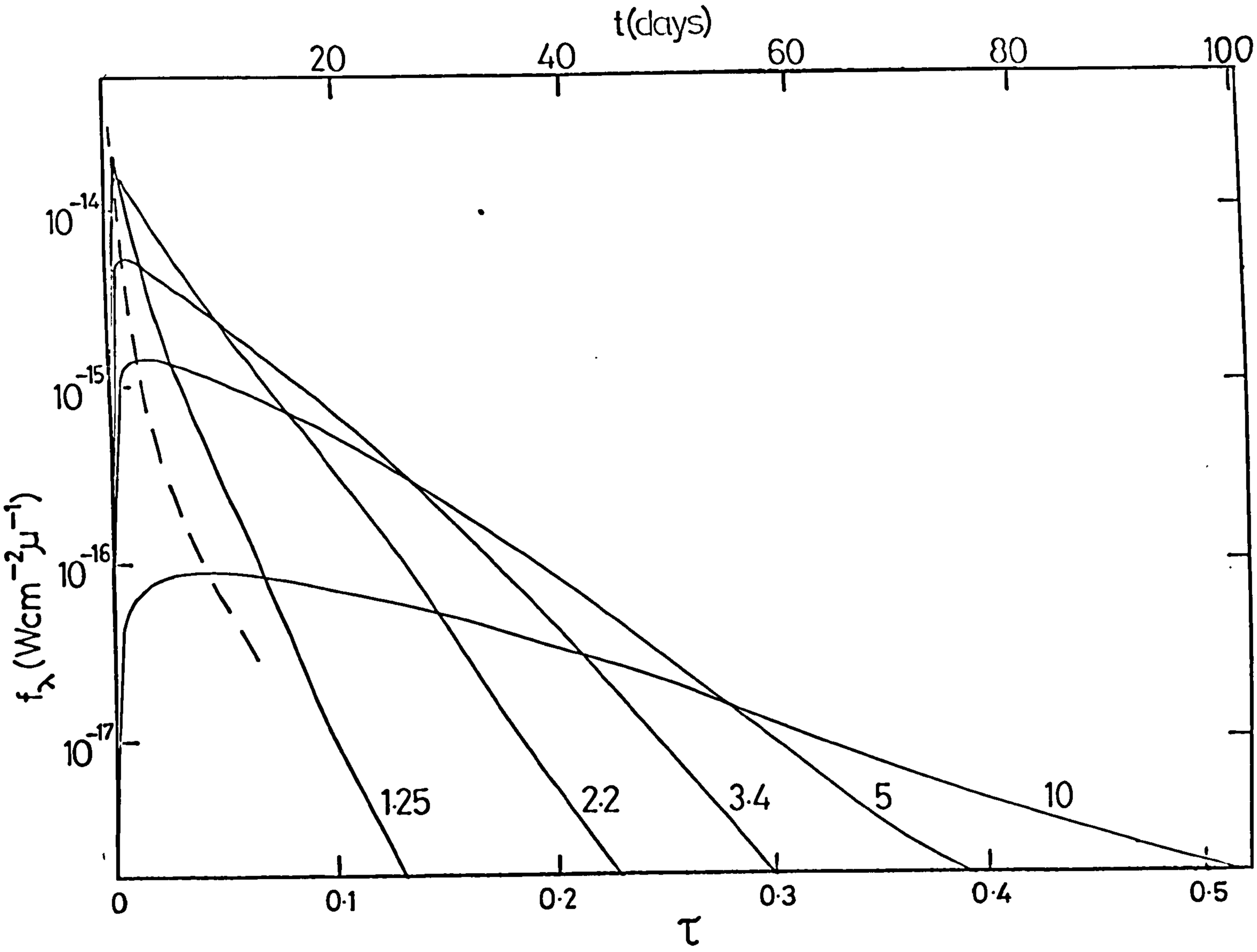
t(days)
20
40
60
80
100
10^{-14}
10^{-15}
10^{-16}
10^{-17}
f_λ (Wcm$^{-2}\mu^{-1}$)
1·25
2·2
3·4
5
10
0
0·1
0·2
0·3
0·4
0·5
τ

$R = 5 \times 10^{17}$cm $\qquad R_1 = 10^{15}$cm

$\alpha = \beta = 2$ $\qquad D = 1$ kpc

$a = 10^{-5}$cm $\qquad M_g = 3.3 \times 10^{-6} M_\odot$

$Q^*_{abs} = 2$

The light curve responsible for grain heating was given a peak bolometric luminosity of 5×10^{38} ergs/sec and an exponential decay with an e-folding time of approximately 10 days. This was taken from the visible light curve of a moderately slow nova. There is reason to suspect that this is in fact not the curve to be considered as responsible for grain heating but the true curve is probably somewhat similar (see Chapters 2, 3 and 5).

The grains are presumed to exist before the nova outburst, either due to condensation from mass lost in previous outbursts or from ejecta from the system between outbursts. As in the analytic solution we normalise the absorption efficiency such that $Q_{abs} = 0.135$ at $\nu = 1.36 \times 10^{14}$Hz for the 10^{-5}cm grains considered here. With these parameters and a dust mass of $3.3 \times 10^{-6} M_\odot$ the shell is optically thin both to ultra-violet and infra-red radiation.

Figure (4.8a) clearly shows that there is a rapid rise to maximum (this would be less rapid for a larger value of R_1 of course) and a much more gentle decline after the peak for all wavelengths. The position of the peak changes however and occurs later for longer wavelengths. We may also note that the decline from maximum is roughly exponential with a steeper decline for shorter wavelengths. This causes the light curves to cross so that one wavelength predominates at a given time. This in turn gives rise to a 'cooling' effect as is shown in figure (4.8c). The black body temperatures were derived from spectra such as those in figure (4.8b). This rapid fall in temperature towards a constant value is similar to the behaviour of the novae which have been studied in some detail in the infra-red and described in Chapter 2.

Figure (4.8b) Observed spectra at different values of τ (figures above curves). Parameters as in figure (4.8a).

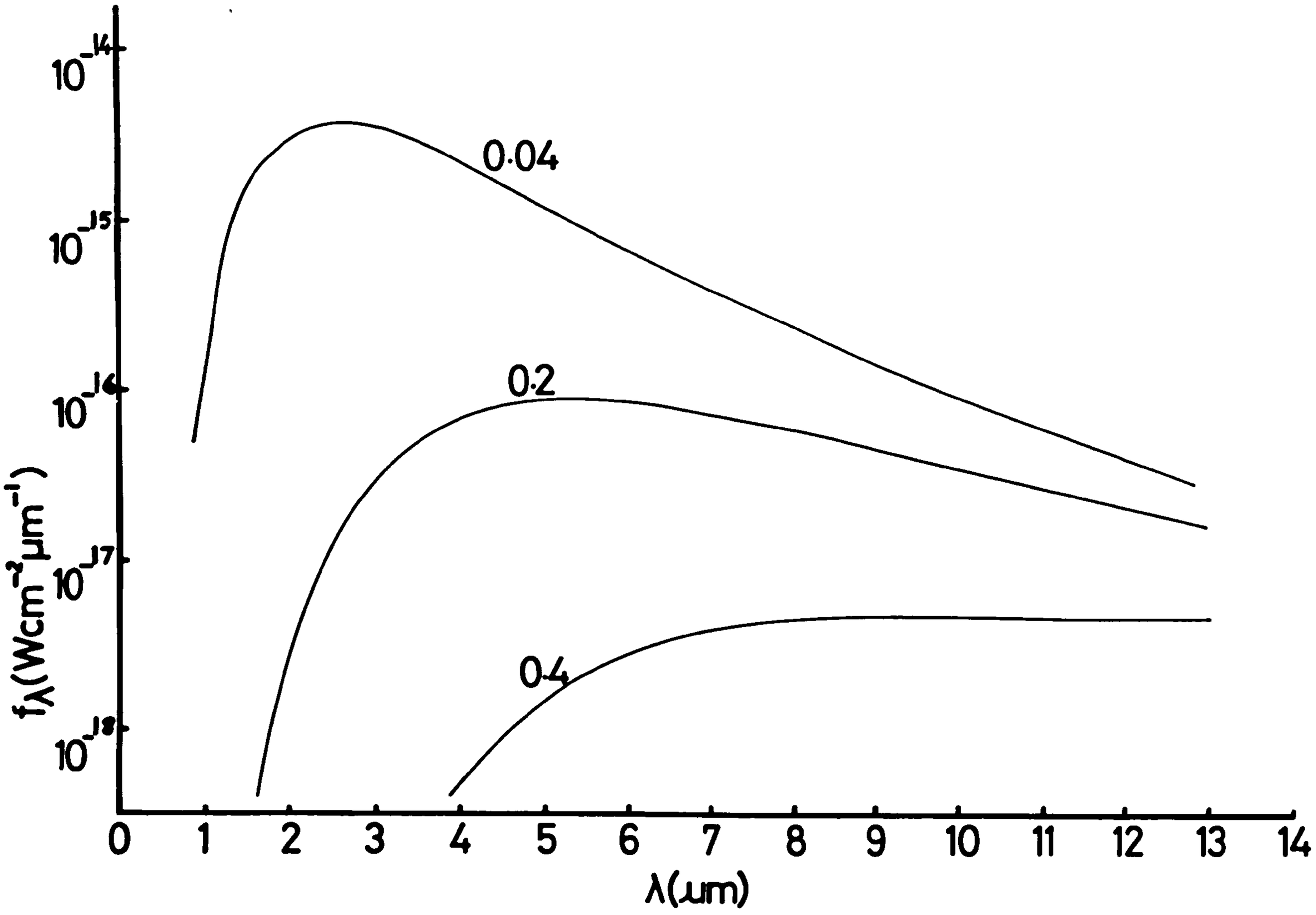
10^{-14}
10^{-15}
10^{-16}
10^{-17}
10^{-18}
$f_\lambda(Wcm^{-2}\mu m^{-1})$
0.04
0.2
0.4
0 1 2 3 4 5 6 7 8 9 10 11 12 13 14
$\lambda(\mu m)$

Figure (4.8c) Variation of the observed black body temperature, T_{BB}, with time for the dust shell and nova-like central source as described in figure (4.8a).

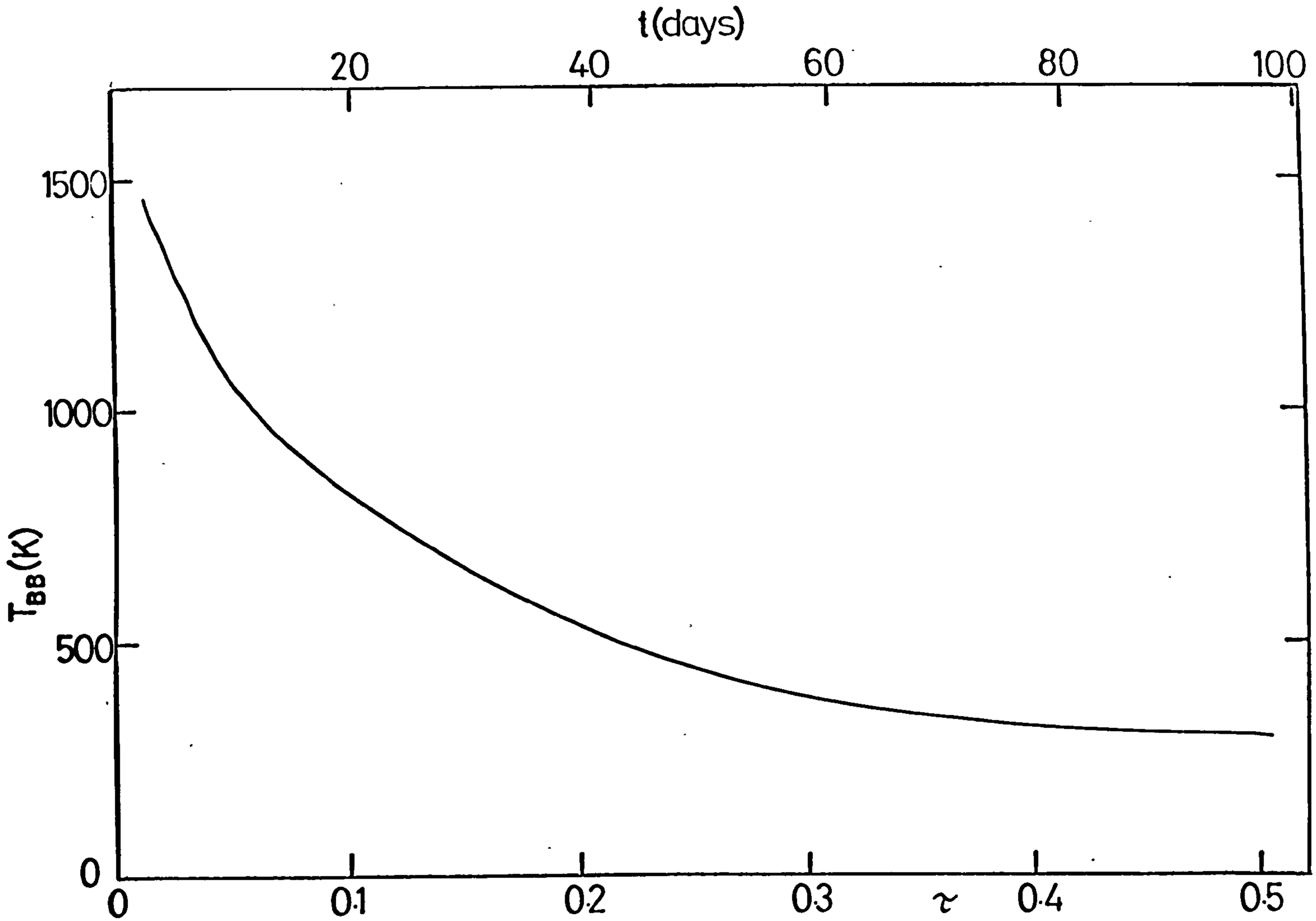
t(days)
20
40
60
80
100
1500
1000
500
0
T_{BB}(K)
0
0·1
0·2
0·3
τ
0·4
0·5

Figure (4.8d) shows the variation in the theoretically calculated black body and real angular diameters of the emitting region with time (θ_{BB} and θ respectively). It can be seen here that the real and theoretical values differ by a factor of $\gtrsim 2 \times 10^3$ and thus θ_{BB} is not a reliable indicator of source dimensions.

If figures (4.8a) (b), (c) and (d) are compared with the observations of Nova Vulpeculae 1976 (Ney & Hatfield, 1978) then the qualitative resemblance at times after the visible light has undergone 'transition' are quite striking. This in fact led us to apply our model more specifically to individual novae (see Chapter 5).

The effects of changing α and β are illustrated in figure (4.9) where the flux at 10 μm is plotted against time. It can clearly be seen that as α decreases so the peak flux increases. This behaviour was encountered in section (4.4.1). We may also note that the lower the value of α, the steeper the decline from peak and the earlier that peak occurs. This is because $T_g \propto r^{-2/\alpha+4}$ and therefore the smaller α is the greater the temperature gradient across the shell which concentrates the highest temperature grains into a smaller volume.

Decreasing β decreases the flux drastically because there are fewer high temperature grains ($N_1 R_1^{\beta}$ decreases) and the greater number of low temperature grains cannot compensate for this. However the fact that a lower value of β gives more grains at large distances (for a given grain mass, M_g) means that the peak emission occurs later and the light curves are somewhat shallower, particularly at long wavelengths.

We will now consider the variation of surface brightness with time across the disk as seen by a distant observer for the case of a nova-like central source.

4.4.4 The Variation of the Observed Surface Brightness

Figures (4.10a) and (4.10b) illustrate the temporal variation of

Figure (4.8d) Variation of the calculated black body angular diameter θ_{BB} (solid curve) and real angular diameter $\emptyset$ (broken curve) with time for the dust shell and nova-like central source with parameters as in figure (4.8a).

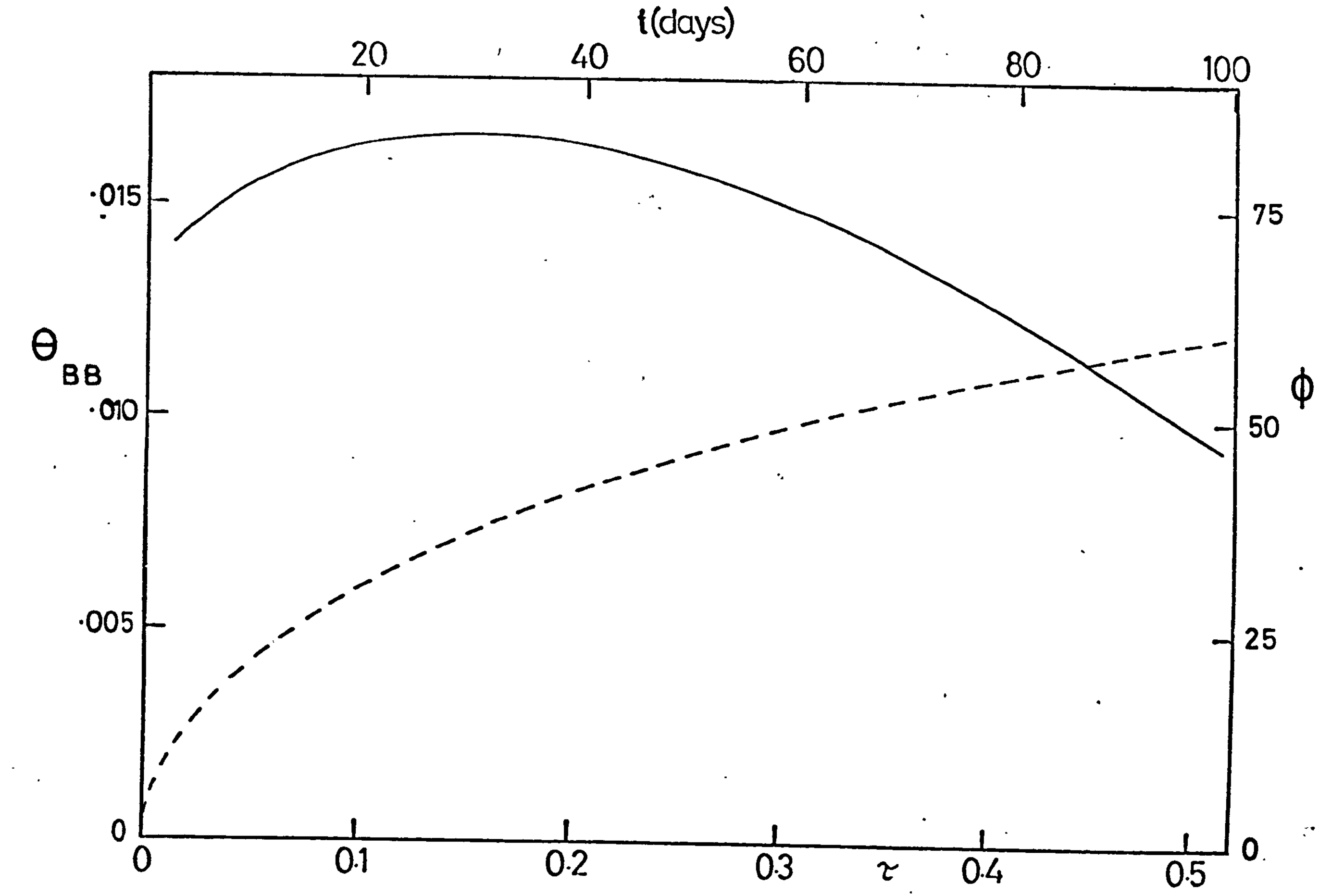
t(days)
20
40
60
80
100
·015
·010
·005
0
θ
BB
75
50
25
0
ϕ
0
0·1
0·2
0·3
τ
0·4
0·5

Figure (4.9) Infra-red light curves for the dust shell and nova-like central source as given in figure (4.8a) except λ = 10 μm and several values of α and β. Curves are labelled in the form (α, β).

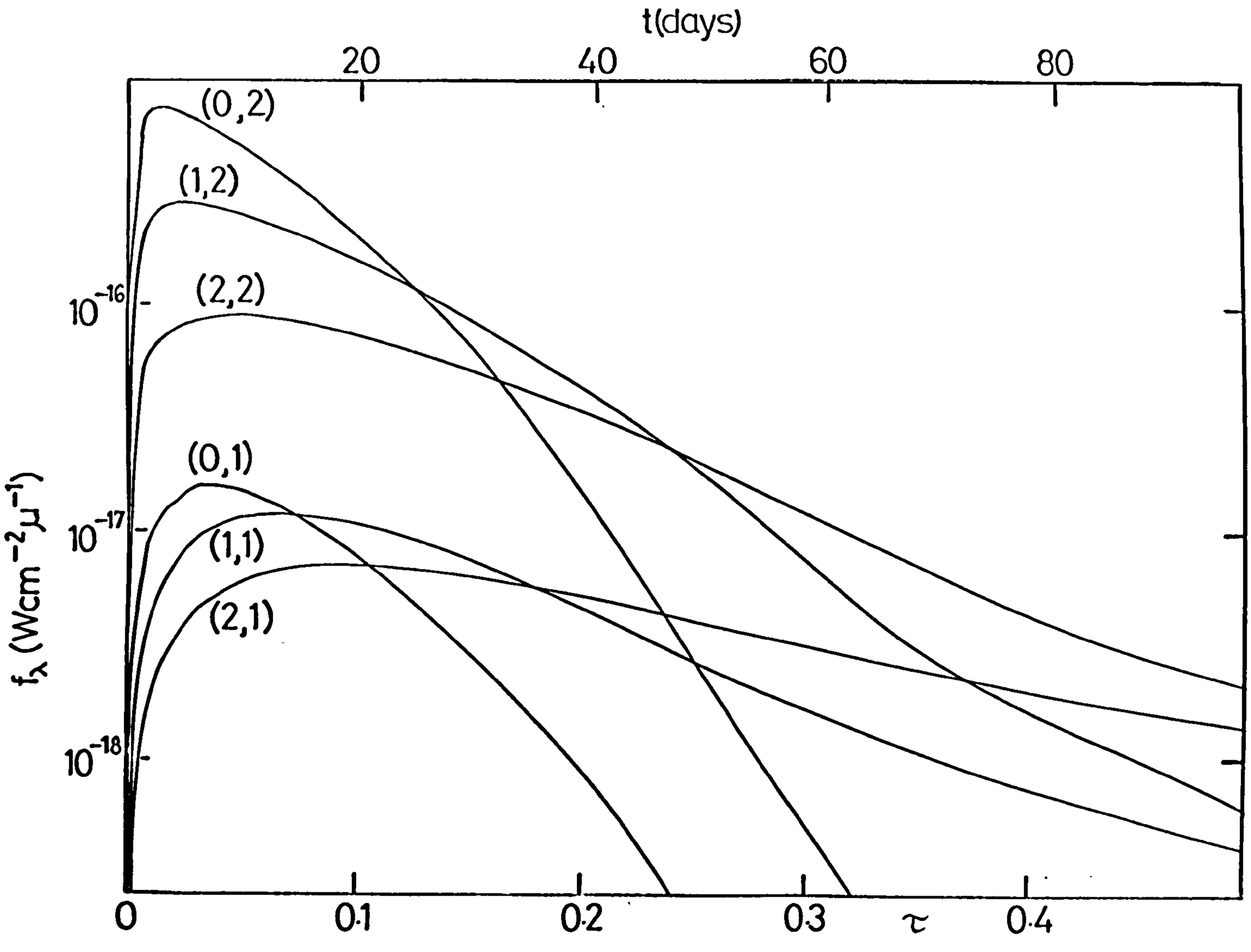
t(days)
20
40
60
80
(0,2)
(1,2)
(2,2)
(0,1)
(1,1)
(2,1)
10^{-16}
10^{-17}
10^{-18}
f_λ (Wcm$^{-2}\mu^{-1}$)
0
0·1
0·2
0·3
τ
0·4

surface brightness as observed by a distant observer across a diameter of the visible disc of grains. In both cases the observing wavelength is 5 μm and the dust shell and central source parameters are similar to those of the novae discussed in the following chapter.

If we consult figure (4.10a) where the grain density falls away as r^{-2} ($\beta = 2$) we can see that the surface brightness at time $\tau = 0.13$ peaks at a displacement from the centre $r' = 10^{16}$cm ($r' \equiv$ DISP in Appendix A1). At later times it peaks more sharply at $r' = R_1$. This is because the highest grain temperatures are to be found at early times ($\tau < \psi$) where the parabola of emission cuts the inner cavity. At later times the longest lines of sight through the source which contain high temperature grains lie at displacement R_1. A distant observer thus sees an expanding disc or ring (depending on the resolution of the object against the background; see below). The expansion continues until $\tau = \psi$ for the brightest part of the observed disc, then ceases.

The expansion of the brightest portion of the disc is related to R_1 rather than R for the reasons given above. Thus superlight effects would be most easily observed for a time $\tau_1 \lesssim 1 - {}^1/\sqrt{2}$ where $\tau_1 = ct/R_1$. This conclusion is slightly different from that reached in Bode and Evans (1979a) where it was not at that time appreciated that the surface brightness at the inner cavity would so far exceed that near the outer shell boundary.

The region of maximum surface brightness ceases expansion at $\tau_1 = 1$. Thus if the time t_c from outburst to cessation of expansion is known then R_1 can be found as $R_1 = ct_c$. Therefore, knowing the angular diameter of the source, the distance of the object (independent of interstellar extinction) could be found.

Figure (4.10b) shows the variation of surface brightness across the observed face of a similar dust shell but where the grain density is

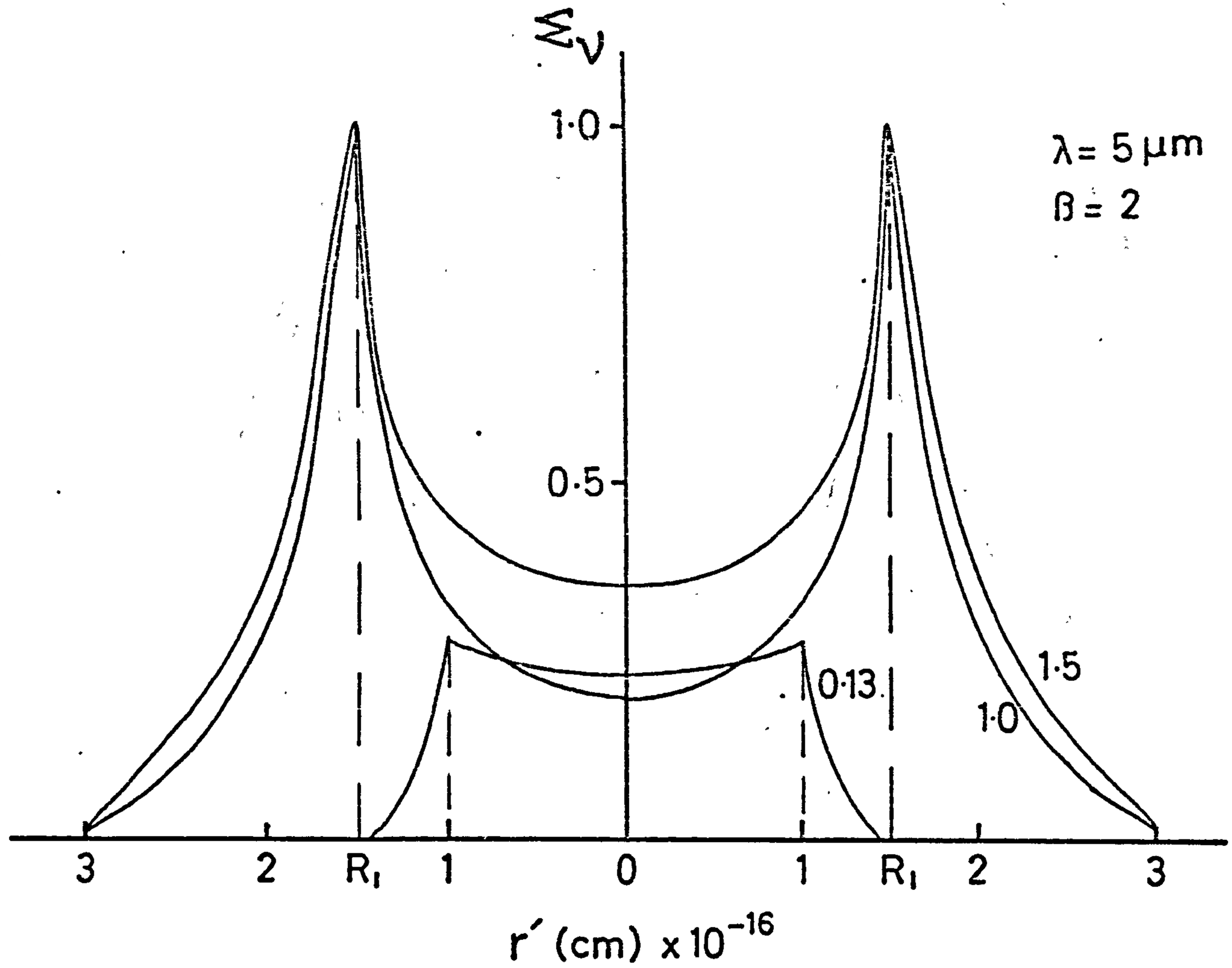

Figure (4.10a) Variation of the observed surface brightness at 5 μm across a diameter of a dust shell with R = $2R_1$ = 3 x 10^{16} cm, Mg = 3.3 x 10^{-6} $M_\odot$, a = 2 x 10^{-6} cm, α = 1, β = 2. The central source has a light curve described by equation (4.22) with L_o= 4 x 10^{38} $ergs^{-1}$, ω = 2 x $10^{-7}s^{-1}$. The surface brightness at 3 values of τ is shown (values by curves). Σ_ν is normalised to peak.

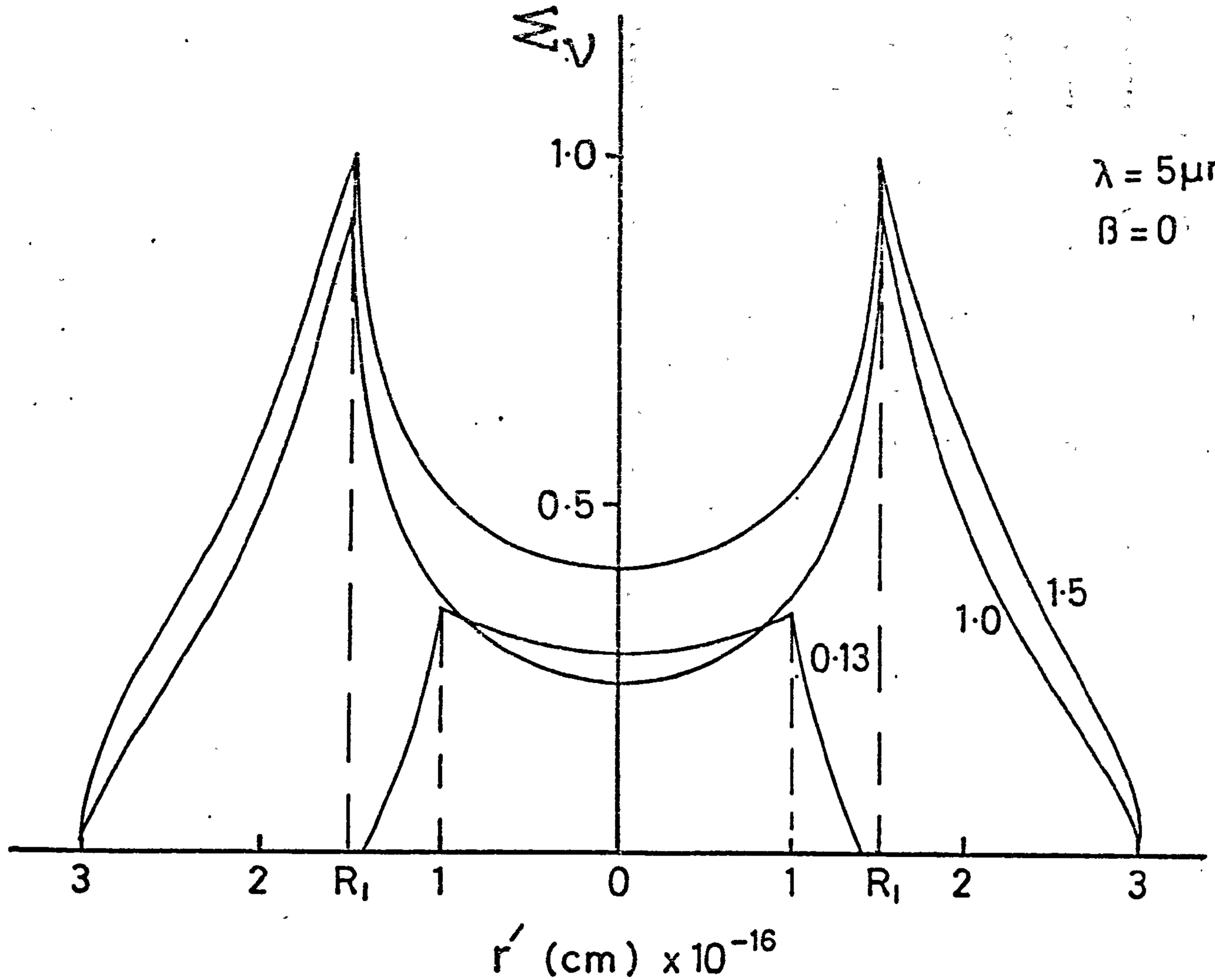

Figure (4.10b) Variation of the observed surface brightness at 5 μm across a dust shell with parameters as in figure (4.10a) except that β = 0 (Normalised to peak).

constant ($\beta = 0$). The behaviour is obviously similar to that for the $\beta = 2$ case particularly as far as the variation of the maximum surface brightness is concerned. We may also note that as in figure (4.10a) the surface brightness in the central region falls for $\tau < 2\psi$ then increases again as the parabola of emission leaves the central cavity.

As well as the flux from the source itself we would of course observe in any real situation that from any background there may be present. Any source observed through the dust shell will be seen to experience an extinction of its emitted flux dependent upon the displacement of the line of sight from the centre of the observed disc. Therefore for a background surface brightness $(\Sigma_{BG})_0$ the contribution to the dust shell surface brightness will be given by

$$\Sigma_{BG}(\theta_2) = (\Sigma_{BG})_0 \exp\left\{-\delta_{BG}(\theta_2)\right\}$$

where $\delta_{BG}(\theta_2)$ is the optical depth across the shell at displacement $R \sin\theta_2$. We therefore have

$$\delta_{BG}(\theta_2) = 2\pi a^2 N_1 R_1 Q_{abs} (R \sin\theta_2)^{1-\beta} \int_{\theta_2}^{f_1(\theta_2)} (\sin\theta)^{\beta-2} d\theta$$

$$(\theta_2 < \sin^{-1}\psi) \qquad (4.38a)$$

$$\delta_{BG}(\theta_2) = 2\pi a^2 N_1 R_1 Q_{abs} (R \sin\theta_2)^{1-\beta} \int_{\theta_2}^{\pi/2} (\sin\theta)^{\beta-2} d\theta$$

$$(\theta_2 \geq \sin^{-1}\psi) \qquad (4.38b)$$

If we plot optical depth against displacement r' then we can see from figure (4.11) that for the dust shell of figures (4.10a) and (4.10b) the extinction peaks at displacement R_1, with decreasing extinction between R_1 and the centre of the disc. This means that the surface brightness at R_1 will be less clearly defined against the infra-red background.

4.4.5 Sinusoidal Variability

So far in this work we have dealt with central sources whose light curves qualitatively resemble those of classical novae. We will now briefly investigate the effect on the resultant infra-red flux of placing a sinusoidally varying source of ultra-violet radiation at the centre of the dust shell.

The central source has a light curve of the form

$$L(t) = L_0 + L_1 \sin(\omega t) \qquad (4.39)$$

where $L_0 = 5 \times 10^{45}$ ergs^{-1}, $L_1 = 2 \times 10^{45}$ ergs^{-1}, $\omega = 10^{-7}$ s^{-1} here. Thus a dust shell with $R \simeq 1.89 \times 10^{18}$ cm has a radial light travel time equivalent to the period of the central source. These parameters are similar to those for certain Seyfert galaxies.

If we now consider figure (4.12a) where the relative amplitude of the flux is plotted against time we can see that varying the dimensions of the inner radius has an effect both on the amplitude and phase of the infra-red flux with respect to those of the central source. Apparently the larger the cavity the larger the observed phase difference between the ultra-violet and infra-red fluxes on the whole. The most unexpected feature at first sight is that the actual period of the variation is not at all affected by cavity size change and in fact is an 'echo' of the variation of the central source.

It is also interesting to note that the largest relative variation is for the largest cavity. In real terms however this is the smallest

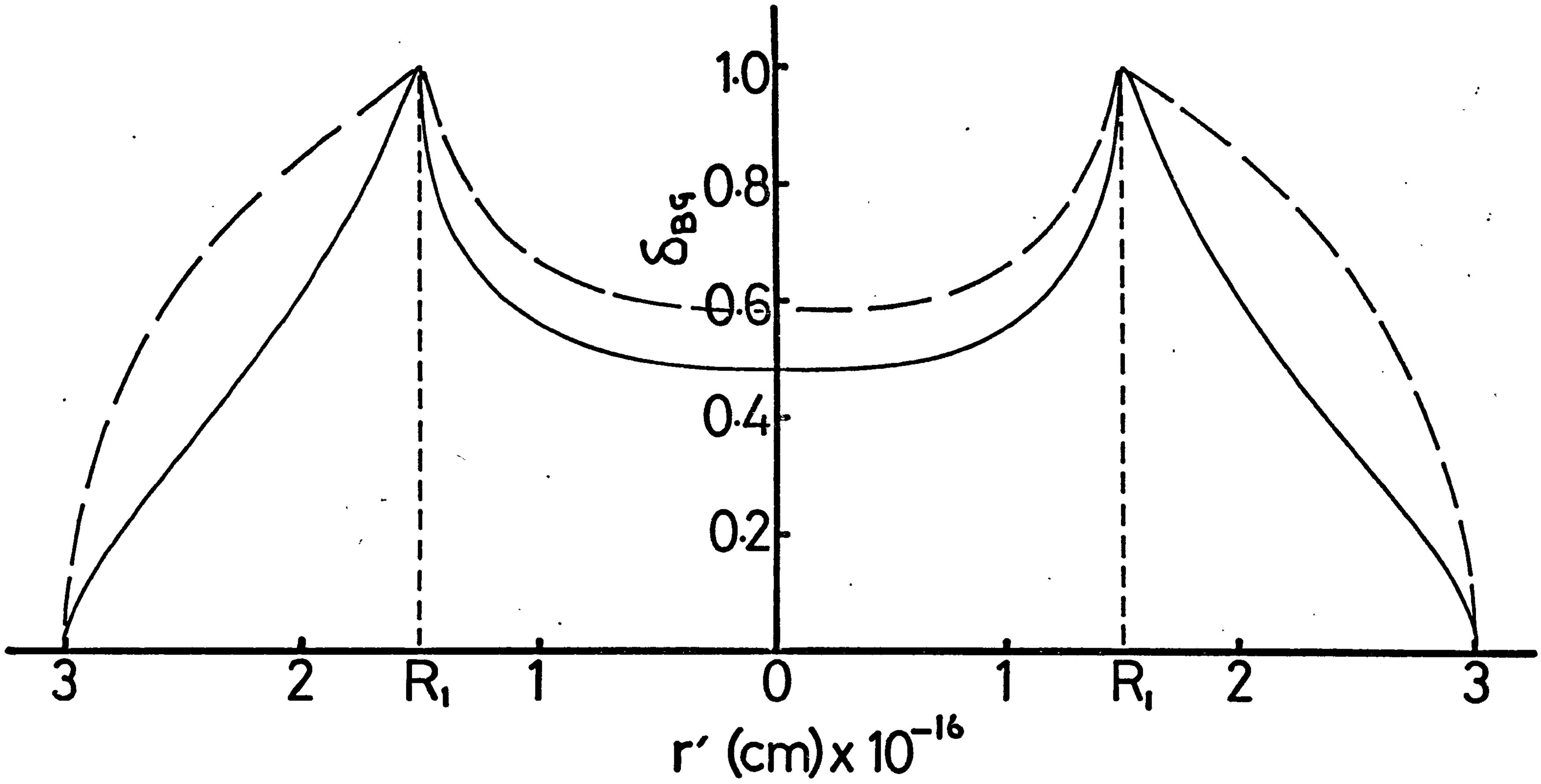

Figure (4.11) Normalised infra-red optical depth to background radiation δ_{BG} through a spherical dust shell with parameters as in figure (4.10a) except that $\beta = 0$ is shown (broken line) as well as $\beta = 2$ (solid line).

Figure (4.12a) Relative amplitude and phase of observed variation of flux at $\lambda = 5$ μm from a dust shell surrounding a sinusoidally varying central source with $L_0 = 5 \times 10^{45}$ ergs^{-1}, $L_1 = 2 \times 10^{45}$ ergs^{-1} and $\omega = 10^{-7}$ s^{-1}. Numbers at termination of light curves indicate the value of ψ ($R = 1.89 \times 10^{18}$ cm in each case). The shell is optically thin to ultra-violet radiation in all cases and is composed of 10^{-5} cm graphite grains ($\alpha = 1$, $\beta = 2$). Note the sinusoidal nature of the infra-red light curves and their phase difference from the central source light curve (C-S).

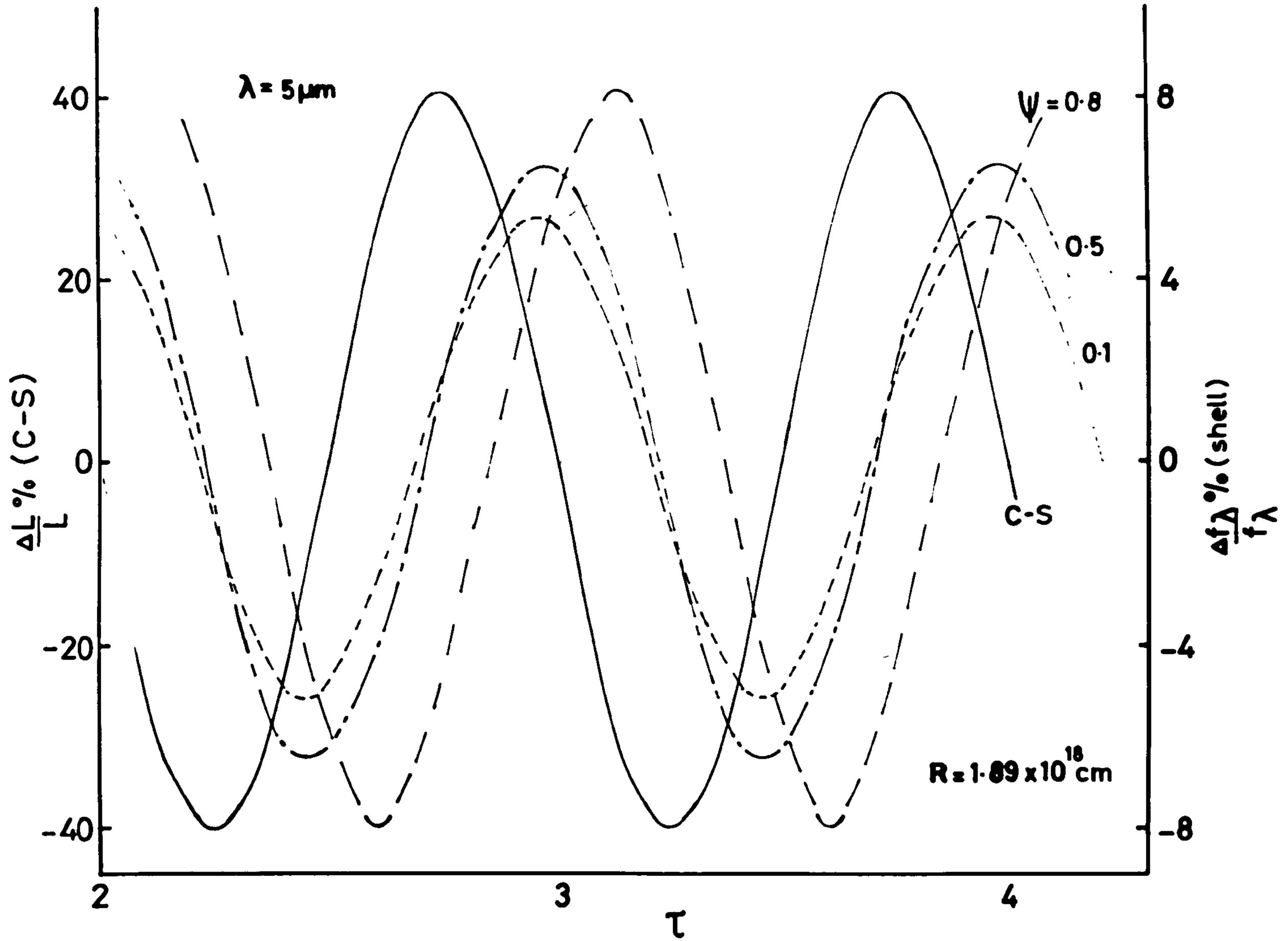
λ = 5μm
ψ = 0·8
0·5
0·1
C-S
R = 1·69 x 10^18 cm
40
20
0
-20
-40
8
4
0
-4
-8
2
3
4
τ
ΔL/L % (C-S)
Δf_λ/f_λ % (shell)

Figure (4.12b) As figure (4.12a) except shell dimensions are constant. Mg is varied to give three values of δ^* (marked at the termination of each curve).

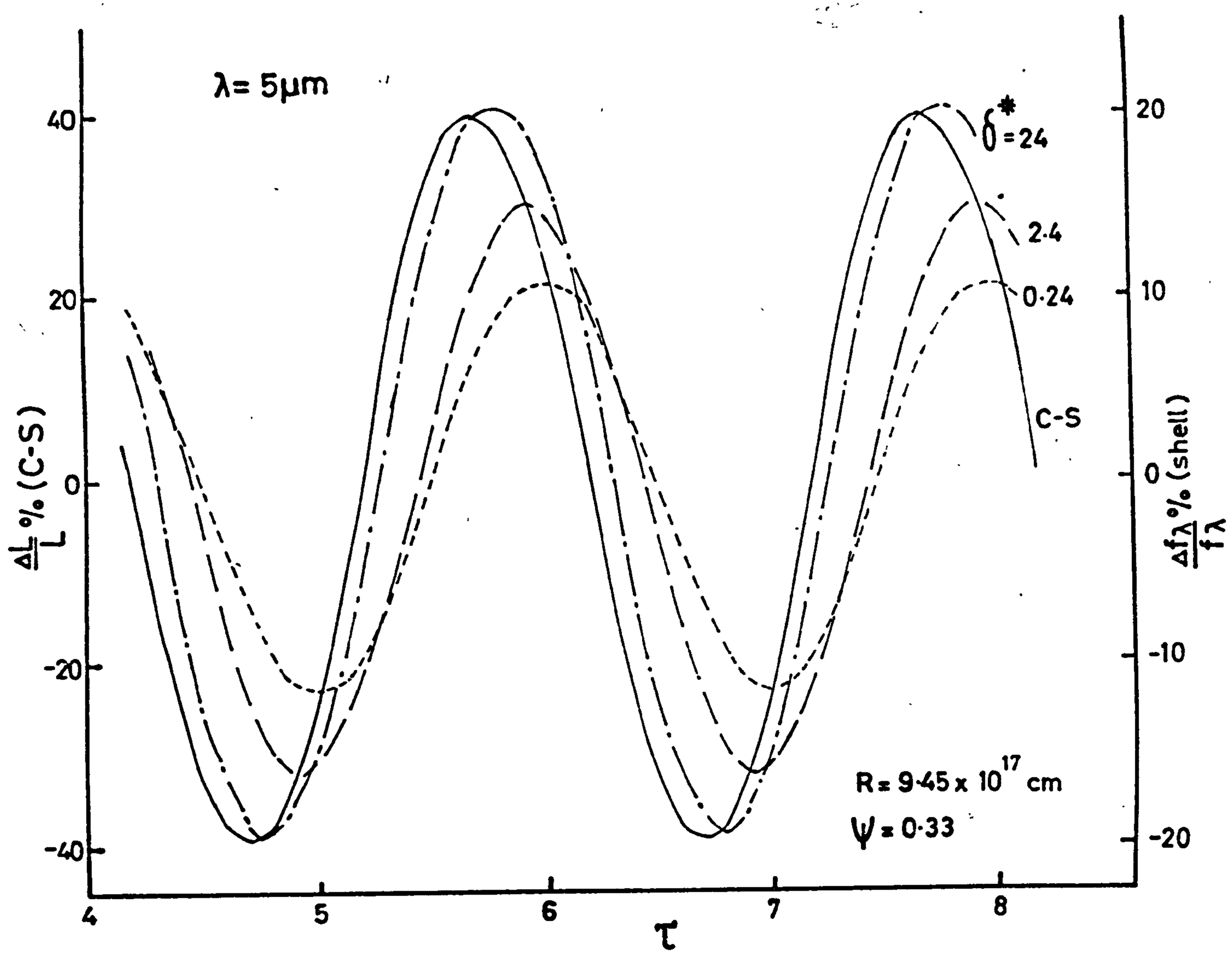
λ= 5μm
40
20
0
-20
-40
$\frac{\Delta L}{L}$ % (C-S)
4
5
6
7
8
τ
δ^*=24
2·4
0·24
C-S
20
10
0
-10
-20
$\frac{\Delta f_\lambda}{f\lambda}$ % (shell)
R= 9·45 x 10^{17} cm
Ψ= 0·33

Figure (4.12c) As figure (4.12b) except the shell is optically thin. The relative flux is plotted for observing wavelengths of 2.2, 5 and 10 μm as denoted at terminations of light curves.

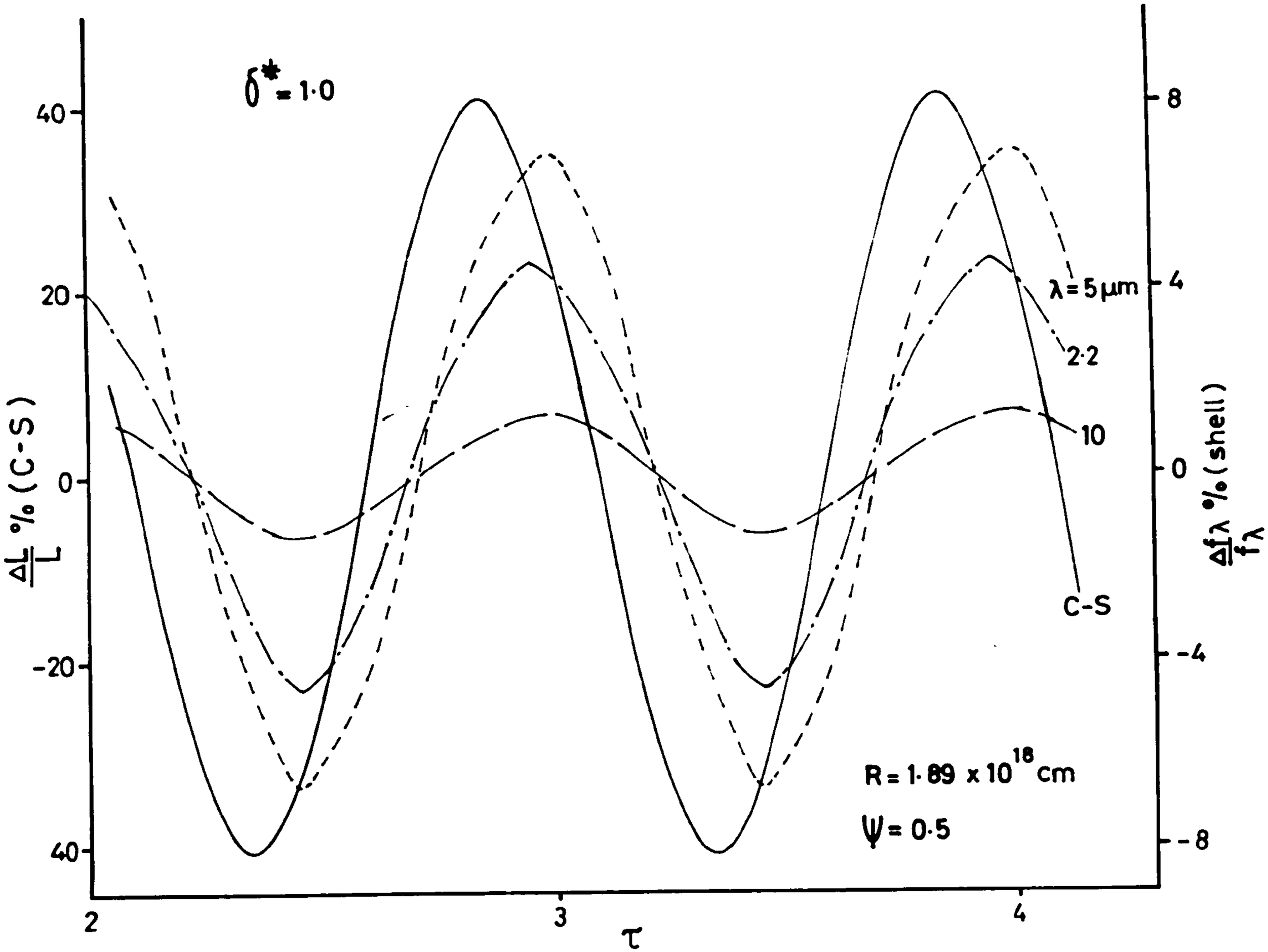
δ* = 1·0
40
20
0
-20
40
2
3
4
τ
ΔL/L % (C-S)
8
4
0
-4
-8
Δfλ/fλ % (shell)
λ = 5 μm
2·2
10
C-S
R = 1·89 x 10^18 cm
Ψ = 0·5

variation. Not surprisingly, from what has been seen before, alteration of R has little effect compared with alteration of R_1.

Figure (4.12b) details the variation of phase and relative amplitude with changing δ^* (all else constant). As the shell becomes progressively more opaque one can see that the phase difference becomes less and the relative amplitude increases. The former effect is probably due to the effective shell producing the bulk of the 5 μm flux decreasing in size whilst the latter is due to there being less mixing of emissions from grains at larger distances.

If we consider equation (4.3) we can see this illustrated as the bulk of the flux at wavelength λ will come from a region the dimensions of which are approximately given by

$$r_\lambda \sim \text{const.}\lambda^{(\alpha+4)/2}\ e^{-\delta^*/2} \qquad (4.40)$$

thus as δ^* increases, r_λ will decrease and so will the phase difference.

We now consider figure (4.12c) where relative flux is plotted against time for 2.2, 5 and 10 μm. Again it is at first sight surprising that the period of variation is not sensitive to shell size. The phase difference between the ultra-violet and infra-red flux curves is also similar for all three wavelengths. However the relative amplitude for the 5 and 2.2 μm curves is far greater than for the 10 μm. This is not unexpected as equation (4.40) suggests that larger wavelength contributions will come from regions more distant from the central source. This will tend to mix the fluctuations together so that the relative amplitude will diminish.

4.5.1 Conclusion

In this chapter previous theoretical work has been extended by the inclusion of finite light travel time considerations to the theory of

variable thermal infra-red sources. The application of the findings of the early sections of this chapter to actual cosmic sources has been qualitative thus far. However in the next chapter we will attempt to apply the results of this chapter to specific astrophysical objects.

CHAPTER 5

Models of the Infra-red Development of Specific Novae

5.1.1 Introduction

It had long been suspected that the visual light curve of novae was not representative of the development of emission at all wavelengths when observations were made of Nova Serpentis 1970 (see Chapters 2 and 3). This nova has since been called 'the Rosetta Stone of nova energetics' (Gallagher, 1977) as it was among the first to be observed in detail from radio to ultra-violet wavelengths. The ultra-violet observations confirmed earlier suspicions that novae increase in observed effective temperature as the visible flux declines.

The development of an increasing infra-red excess after $\sim$ day 45 was however unexpected (Geisel et al., 1970). This seems to be a common characteristic of moderate speed novae as it has also been observed in Novae Aquilae 1975, Vulpeculae 1976 and Cygni 1978 for example.

In all cases the late developing infra-red spectrum has resembled a fairly featureless black body emission with characteristic temperature $\lesssim 1300^{o}$K. This has led previous workers to associate it with thermal emission from dust grains (see for example Ney & Hatfield, 1978). The absence of any apparent emission features at $\lambda \sim$ 10 μm has tended to indicate that the grains are not silicates and most authors have considered them to be composed of graphite (Clayton & Wickramasinghe, 1976).

The question has arisen as to how these grains formed and how this formation process might account for the lag between optical and infra-red peak emission. Most authors have taken the view that grains form rapidly in the ejecta of the concurrent outburst and subsequently

cool as they grow and increase their distance from the central object (see section (3.5.2)). This mechanism has been seen as naturally accounting for the change of slope of the visual light curve (transition) which appears to coincide with the onset of infra-red rise. In this chapter we will examine the plausibility of rapid grain formation as the mechanism behind the infra-red emission of novae.

As we have already seen in chapter 4 certain characteristics of the infra-red light curves of novae arise simply by placing centrally a source with a light curve as defined in equation (4.22) in a spherically symmetric dust shell. The main difference between this simple model and the observed infra-red behaviour of novae is the lag between visual flux maximum and infra-red rise. We will show that for small graphite grains this follows quite naturally as the central source effective temperature increases. The correlation between infra-red rise and the onset of transition then results.

5.2.1 Rapid Grain Formation in Nova Ejecta - Introduction

In this section we will consider in some detail the rapid grain formation models of the infra-red evolution of novae. Reference should be made to section (3.5.2) where a summary of each of the papers considered is given.

5.2.2 Discussion of Clayton and Hoyle (1976)

The first detailed attempt to explain the correlation between visual and infra-red behaviour in Nova Serpentis 1970 made by Clayton and Hoyle (1976), utilised a storage and release of energy by a shell of grains initially optically thick and then becoming optically thin to the central object flux. This would not only explain why the visual luminosity drops but also why the peak infra-red luminosity was, according to Clayton and Hoyle, greater than the visual luminosity at that time.

Taking the latter point first, it appears that it is generally accepted now that the infra-red luminosity peak was actually less than the luminosity of the underlying object (e.g. Clayton & Wickramasinghe, 1976; Tylenda, 1978). Thus the shell of grains need not be very opaque (i.e. $\delta^* \lesssim 1$) and the storage and release mechanism is not required.

The steady decline in the visual light curve is now thought to be due to the shift in the peak continuum flux from the central object to shorter wavelengths (see section (3.5.1) and references therein). As we have seen in chapter 2 the ultra-violet observations of Gallagher and Code (1974) have supported this point of view. Indeed Clayton and Hoyle themselves state that unless the ultra-violet flux originates externally to the growing dust grains there can be no substantial dust formation prior to day 57. As we have seen in section (3.5.1) the shift in continuum flux to short wavelengths is generally thought to

be due to the gradual uncovering of the central object as the ejecta expand. The change of slope at transition is part of this process (see below).

The assumption of Clayton and Hoyle that the grains that formed in the ejecta were graphite is based on the fact that carbon may well be over-abundant in nova events (see for example, Starrfield et al., 1974) and that no silicate emission feature emerged in the 10 μm observations of the nova (Geisel et al., 1970).

The work of Starrfield et al. (1974) has however tended to indicate that although carbon is over abundant, so also is oxygen so that the abundance ratio C/O is less than unity. In that case most of the carbon would be taken up in CO molecules and therefore would not be free to form grains (Yamamoto & Nishida, 1977).

Evidence that CO did indeed form in large quantities during the outbursts of Nova Serpentis 1970 and Nova Vulpeculae 1976 before transition is deduced by Ferland et al. (1979) from the excess at early times (< 30 days from outburst) in the 5 μm flux. This early excess has been attributed by Clayton and Hoyle (1976) to thermal emission from very early forming grains. However, by using the principal spectrum velocity in their model the time of onset of grain growth would be around 33 days which is rather late to explain the early excess. It is now generally accepted that this apparently narrow emission at 5 μm is actually a line feature (Ney & Hatfield, 1978; Ferland et al., 1979).

5.2.3 Discussion of Clayton and Wickramasinghe (1976)

Clayton and Wickramasinghe (1976) have, as we have seen, developed the model of Clayton and Hoyle to accommodate the optically thin grain growth case. Like Clayton and Hoyle they assumed that graphite grains formed in the ejecta of Nova Serpentis 1970 from over-abundant carbon

atoms. For their model to fit the observations qualitatively they required that the ejecta consisted solely of carbon atoms so that the depletion of atoms into grains did not affect the number density of atoms at all (this is not crucial however). With an ejected mass of 3×10^{-4} $M_\odot$, 3×10^{-5} $M_\odot$ of 2×10^{-4} cm graphite grains were needed at day 100 from discovery. This rapidly growing shell of grains is then thought to cause the rapid decline of the transition stage which begins at $\sim$ 58 days from discovery in Nova Serpentis 1970.

If we suppose that the increasing grain size of Clayton and Wickramasinghe's model does indeed cause the steep drop in visual luminosity of the transition then the optical depth to visual light must maximise at around day 90 (i.e. at the transition minimum). Assuming a difference of $\sim$ 3.8 magnitudes during transition from an extrapolation of the pre-transition light curve gives the optical depth to visual light, δ_v, $\simeq$ 3.5. Thus the dust cloud would need to be optically thick even at these comparatively long wavelengths.

In order for the carbon gas density $(N_c)_0$ at day 45 to be $\sim 10^9$ cm^{-3} with $v_{ej} \sim 2000$ kms^{-1} and $M_{ej} \sim 3 \times 10^{-4}$ $M_\odot$, $\psi_0 \sim 0.99$ where ψ_0 is the value of ψ at $t = t_0$. This would mean that the bulk of the ejection occurred within one day of outburst if the ejected shell maintained constant thickness. If we assume more realistically that $\psi_0 \simeq 0.9$ (i.e. ejection lasted $\sim$ 5 days) then $(N_c)_0 \sim 10^8$ cm^{-3}. With this latter value of ψ_0 and assuming that the shell moves outward with constant velocity, retaining constant thickness, we can use equations (3.27a) and (4.8) to find the change in optical depth with time at UBV wavelengths as the grains grow and the shell expands.

With the total number of grains remaining constant on this model (Clayton & Wickramasinghe give $N_{TOTAL} = 7.3 \times 10^{38}$) we arrive at an expression for the change of optical depth with time, i.e.

$$\delta_\lambda(t) \simeq 0.61\left[\frac{a(t)}{10^{-6}\text{cm}}\right]^2 Q_{abs}\ (\lambda,\ a(t))\left[\frac{t}{1\ \text{day}}\right]^{-2} \qquad (5.1)$$

Using results from Mie theory computations (Evans, 1979) for the change of Q_{abs} with a at UBV wavelengths together with the values (Clayton & Wickramasinghe, 1976) $a_0 = 3 \times 10^{-7}$ cm and $a_\infty = 2 \times 10^{-4}$ cm in equation (3.27a) for the increase of grain size with time, figure (5.1) was drawn. From this figure it can be seen that the optical depth does indeed maximise at $\sim$ 90 days although the maximum optical depth is $\sim$ 1 only (this is little affected if a larger value of ψ_0 is taken).

During the period of grain growth the colour excesses, E_{B-V} and E_{U-B}, change with time as 1.086 $(\delta_B - \delta_V)$ and 1.086 $(\delta_U - \delta_B)$. On this model the nova would appear to redden slightly during the first day ($(E_{B-V})_{max} \sim + 0.04$, $(E_{U-B})_{max} \sim + 0.02$) but subsequently up to day 75 would appear bluer than the underlying photospheric temperature would suggest ($(E_{B-V})_{min} \sim - 0.05$, $(E_{U-B})_{min} \sim - 0.03$). Surprisingly therefore the growth of grains would, on this model, have a virtually undetectable effect on the nova colour during this time. The fact that little general reddening was seen by Hutchings and Fisher (1973) does not rule out the hypothesis that large grains ($\gtrsim 1.5 \times 10^{-5}$cm) formed relatively quickly. It does however tend to rule out smaller grains being present in sufficient numbers to cause the change of slope and give rise to the infra-red excess from $\sim$ 45 days. This is because small grains would cause a substantial increase in reddening at this time.

The work of Lefèvre (1979) on the formation of graphite and silicate grains in 'nova' and 'cool stellar' environments has however shown that to form the 2×10^{-4} cm graphite grains required by Clayton and Wickramasinghe's model $(N_c)_0 \gtrsim 10^{11}\text{cm}^{-3}$ is needed. This would require

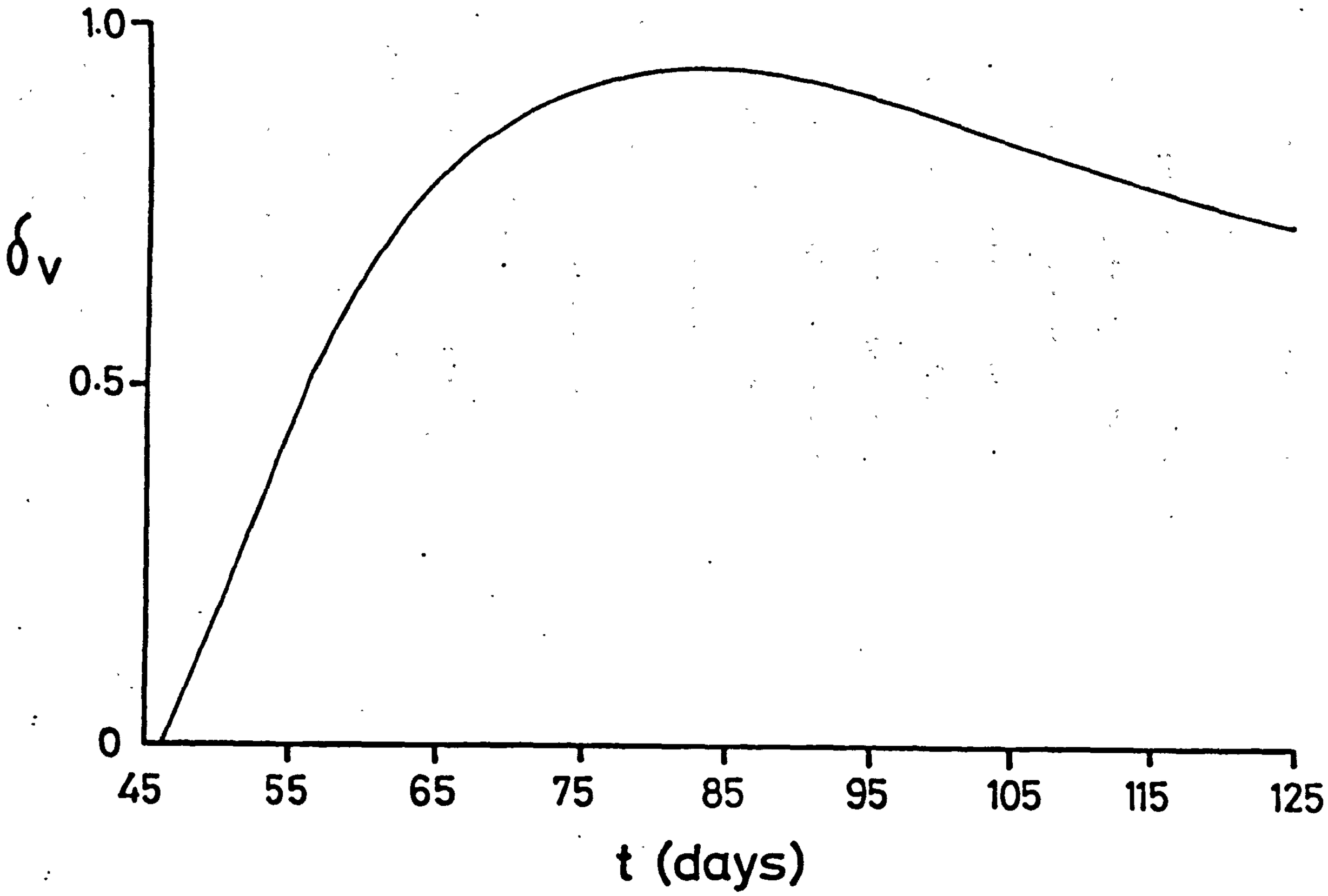

Figure (5.1) Change of optical depth at visual wavelengths, δ_v, with time from discovery for the Nova Serpentis 1970 rapid grain growth model of Clayton and Wickramasinghe (1976).

$1 - \psi_0 \lesssim 10^{-4}$ if $v_{ej} \simeq 2000$ kms^{-1}. In other words the total ejection would have occurred in $\lesssim 6\frac{1}{2}$ minutes. Lefèvre also concluded that even under ideal conditions with $\alpha_c = 1$ and no monomer depletion (or grain erosion by evaporation or sputtering) there will be effectively no grain growth for $(N_c)_0 \lesssim 3.10^8$ cm^{-3} even if v_{ej} is as low as 500 kms^{-1}. For graphite grains of $a_\infty \geq 1.5 \times 10^{-5}$ cm, $(N_c)_0 \gtrsim 10^{10}$ cm^{-3} and thus $1 - \psi_0 \lesssim 2 \times 10^{-3}$. It would therefore appear that the rapid formation of large graphite grains, even under ideal conditions, is somewhat difficult in nova ejecta (this point of view is also supported by Krelowski, 1978).

If, however, only small grains are formed then we have to explain why during transition the U-B index decreased indicating the object was actually becoming bluer (Borra & Andersen, 1970) and why there was little indication of grain growth (up to day 57) from the observations of Gallagher and Code (1974). The latter of course could be explained by assuming that large scale growth did not occur until the onset of transition which would also explain why the steep drop in visual flux occurs here (unfortunately Gallagher and Code's observations ceased before transition). We may also note that if small graphite grains are used in the model of Clayton and Wickramasinghe (1976) then the reasonably good fit to the temperature behaviour of the infra-red excess for large grains is lost.

Finally we must note that from the work of Bath and Shaviv (1976) and the observations of Gallagher and Code (1974) the continuum temperature of the nova, $T_* \gtrsim 14000^oK$ at 45 days and $\gtrsim 19000^oK$ at 57 days (see section (5.4.1)). Thus if we use the value $T_* = 15000^oK$ with $v_{ej} = v_p \simeq 700$ kms^{-1} in equation (3.26b) we find $t_0 \sim 180$ days by which time, according to both theory and observation, T_* will have in any case increased as well (see section (3.5.1) and references therein) making this value of t_0 an underestimate.

5.2.4 Discussion of Gallagher (1977)

Gallagher (1977) based his predictions of grain forming novae on the assumption that Nova Serpentis 1970 was typical of all grain forming novae. Thus the decision to choose $T_c = 1300^oK$ in his model was based on this assumption although he calculates $T_c \simeq 2000^oK$ (as do Clayton & Wickramasinghe, 1976). If we assume this latter value of T_c the onset of dust formation, t_o, is decreased considerably and even Nova Cygni 1975 would be expected to produce dust, as would other novae without transition slope breaks.

The main assumption of this paper is that the transition slope break marks the onset of large scale dust formation. However Gallagher himself points out that this is somewhat controversial. McLaughlin (1960) has for example pointed out that the deep transition minimum of DQ Herculis was not, as originally thought, due to the formation of an obscuring cloud of dust grains in front of the nova. A favoured explanation for transition is the point in the outburst where the central object is uncovered (see for example, Payne-Gaposchlin, 1957, p. 299; Warner, 1976, p. 123; Bath, 1979 etc.). Certainly the underlying continuum flux appears to shift its peak to much shorter wavelengths at this time (see e.g. Nariai, 1974) and the spectrum generally changes from stellar to nebular (McLaughlin, 1960, p. 609) with excitation increasing with time (see figure (3.5)). It is rather difficult to associate these transition phenomena with grain formation.

Gallagher notes that Geisel (1970) has correlated the emergence of FeII and [FeIII] emission lines with infra-red excesses, however this may be indicative of the product of the central source spectrum and the absorption efficiency profile at this particular part of the outburst (see section (5.4.1)). The fact that slow and moderate speed novae possess a notable FeII emission and fast novae do not may, according to McLaughlin (1960) p. 609, be just a contrast effect.

There are other details of the theory which bear further scrutiny. For example Gallagher himself notes that in Nova Serpentis 1970 during the epoch when nucleation centres would have to form, the material giving rise to the principal spectrum was overtaken by that giving the diffuse enhanced and Orion spectra. As we have seen in chapter 2 the velocity difference exceeded 1000 kms^{-1}. Gallagher notes that disruption of the large-scale nucleation process might result from these shocks.

He also makes the point that grain formation will of course be inhibited by ionisation. Yet it is at the transition stage that much of the ejecta become ionised. In other words just as grains are growing the material from which they would grow is becoming unavailable to them. The point t_0 in this work would therefore not only mark the point of instantaneous formation of nucleation centres as in Clayton and Wickramasinghe (1976) but in fact almost instantaneous grain growth before the shell became completely ionised at time t_i ($\simeq$ 130 days in Nova Serpentis 1970 using Gallagher's arguments and parameters).

Finally, if we examine his success with the prediction of which novae appear to have detectable infra-red excesses and/or a slope break we find that the fast nova EU Scuti has a slope break whereas it appears that Nova Cygni 1978 has none (Dunlop, 1979) and yet developed a large infra-red excess (Gehrz *et al.*, 1978). It is still uncertain whether the very fast nova Cygni 1975 developed a thermal infra-red excess (see Chapter 2). The slow nova HR Del (Nova Delphini 1967) has a predicted dust formation time of 45 days but the slope break did not occur until $\sim$ 350 days. As we have seen in chapter 2, Geisel *et al.* (1970) detected a small, $\sim 300^{o}K$, excess after 1150 days.

5.2.5 Discussion of Yamamoto and Nishida (1977)

Yamamoto and Nishida have, as we have seen in chapter 3, concluded that carbon atoms will preferentially be taken up by oxygen to form carbon monoxide, not graphite grains, if C/O < 1. The work of Ferland et al. (1979) on the 5 μm excesses of Novae Serpentis 1970 and Vulpeculae 1976 seems to support this. Their conclusion is also supported by the spectra of Nova Serpentis 1970 which do not indicate that carbon was the main constituent of the ejecta as would be required by Clayton and Hoyle (1976). Yamamoto and Nishida therefore considered silicate grain formation more likely.

This latter aspect of Yamamoto and Nishida's theory does not appear to fit the observations however. The growing grains are expected to reach maximum radius in ∿ 10 days. Thus if grain formation causes transition the transition minimum should occur < 10 days from slope break, which, in the case of Nova Serpentis 1970, it does not. The most conclusive observational evidence against the formation of silicate grains is the lack of any apparent spectral features at around 10-12 μm in Nova Serpentis 1970 or Nova Vulpeculae 1976 which are characteristic of this grain type.

Again Lefèvre found that high densities of SiO molecules are required for grains to form in a nova environment. However, unlike graphite grains he concluded that the required densities were so high as to always preclude any rapid formation in that situation.

5.3.1 Pre-existing grains - Introduction

If one is to conclude that large scale formation of grains in each nova outburst is not altogether a reasonable proposition the problem remains of providing sufficient grains from other processes to explain the undoubtedly thermal origin of the late developing infra-red excesses of certain novae. Obviously, if we say that grains are not

formed in large enough numbers in the concurrent outburst they must have existed prior to that outburst.

5.3.2 Observations Indicating Pre-existing Grains

Evidence for the pre-existence of circumnova material has come from several areas of study. Spectral scans of HR Del revealed the presence of narrow emission lines of ionised metals, SiII and hydrogen with initial half widths $\lesssim$ 30 kms^{-1} increasing to $\simeq$ 140 kms^{-1} during postmaximum; these lines would seem to arise from a pre-existing shell (Antipova, 1978). Similar narrow lines (HWHM $\simeq$ 30 kms^{-1}) with blue shifts of -95 kms^{-1} have been seen in absorption in Nova Cygni 1978 (Cassatella et al., 1979). The latter have been ascribed to MnII, FeII and MgI in a pre-existing circum-nova shell.

As we have seen in chapter 2 there is strong evidence that grains existed prior to outburst in Novae Delphini 1967 and Serpentis 1970 from the polarisation studies of Zellner (1971) and the Balmer decrement studies of Malakpour (1973 and 1977). Zellner detected little change in the polarisation during the time the infra-red excess developed and he concluded that the polarising grains were not responsible for the infra-red rise. Malakpour on the other hand suggested that these pre-existing grains were large nucleation centres ($a \lesssim 10^{-5}$ cm) on which condensation took place giving still larger grains and hence the infra-red excess. However Draine and Salpeter (1979) have found that the sputtering yield of hydrogen on graphite maximises when the hydrogen atomic velocity $\sim$ 1 kms^{-1} and remains high thereafter. Thus the relatively dense fast-moving ejecta might be expected to destroy rather than enlarge more or less stationary grains at $\sim 5 \times 10^{14}$ cm.

5.3.3 Possible Grain Origins

Assuming that it is unlikely that classical novae are 'accidentally' embedded within inter-stellar dust clouds of relatively high density we are left with several other alternatives for their origin.

Malakpour (1978) has speculated that the grains he detected prior to infra-red rise may have formed in the ejecta of the last outburst over a long inter-outburst period. If novae are recurrent phenomena (Ford, 1978) then the amount of circum-nova grains would perhaps increase as the system gets older. Malakpour has found that the inter-outburst timescale of 10^3 to 10^7 years is, in the latter case, great enough to form 10^{-5} cm graphite grains from the ejecta. It is suggested that these grains will not approach closer than $\sim 3 \times 10^{15}$ cm to the quiescent system (Malakpour, 1978).

In the formation of the nova system some of the original material may have been left over at great distances from the central object. From this material grains could have slowly condensed. Objects where this is apparently the case do exist. Harvey et al. (1979) have found that there are several emission line stars, which are relatively young objects, possessing substantial far infra-red excesses. These excesses are thought to be due to extensive clouds of dust with cloud diameters $\gtrsim$ 40 arc sec surrounding the central objects. The best fit to the observed fluxes arose by assuming a grain density profile with $\beta = 1$ (which is a value which will be relevant later). It is perhaps questionable however whether novae are relatively young.

Direct observational evidence exists that cataclysmic binary stars lose mass (e.g. Robinson, 1973). This is thought to be due to instabilities in accretion increasing the accretion disc radius beyond that of the Roche lobe. In the case of the dwarf nova Z Cam the mass lost between outbursts is calculated to be $\sim$ 90% of that which actually reaches the white dwarf surface (i.e. $\gtrsim 2.4 \times 10^{-9}$ $M_\odot$ yr^{-1} -

Robinson, 1973).

Antipova (1978) ascribes the narrow emission lines and deceleration of ejecta in Nova Delphini 1967 to a shell of material lost by the cool component of the nova system during the quiescent stage. As it is well known that grains do form in the ejected circumstellar gas of numerous systems (see for example Salpeter, 1974) it is not unreasonable to suppose that this may be the case in a nova between outbursts. Indeed Coullin-Souffrin (1978) has shown that in several novae the CNO elemental abundances decrease with time in the post nova stage. Some of this depletion might perhaps be due to grain condensation.

Grains may also form within the atmosphere of the cool component and be ejected into circumstellar space by radiation pressure as they grow. This process depends on the atmospheric gas temperature being low enough at some point for condensation to proceed; the availability of condensates and a high enough ratio of stellar luminosity to mass for escape to occur. The cool component, although possibly capable of forming grains within its atmosphere, would (following Salpeter, 1974) have difficulty ejecting them due to its relatively low luminosity ($\lesssim L_{\odot}$).

5.3.4. Trapping of Outflowing Grains

If grains form in the concurrent outburst as described by Clayton and Wickramasinghe (1976) then we expect them to be affected by 3 main forces:-

i) Radiation Pressure, P_r

ii) Gravitation, G

iii) Gas Drag, D_r.

If the radiation pressure function, PFN $\equiv \bar{Q}_{pr} L$ (where L is the nova luminosity and $\bar{Q}_{pr}$ is the Planck mean of the efficiency factor for radiation pressure) peaks at the time the grains are formed (at

which time L is at a maximum) then this must decay in some way over the inter-outburst period. It is usually thought that classical novae at the quiescent stage have $L \sim L_\theta$ (defining $(PFN)_1$ for $\bar{Q}_{pr} \sim 1$). Indeed Gallagher and Holm (1973) failed to detect Nova Serpentis 1970 at $\lambda < 4250\text{Å}$ 1.6 years after it was observed as a very bright ultraviolet source (Gallagher & Code, 1974).

It will be shown in the following section that for small (10^{-6} cm) graphite grains the radiation pressure function will be similar to the 'heating function' HFN in its qualitative behaviour. If this is so then the exponential decay of HFN derived below may also apply to PFN. In the absence of contrary evidence we will assume this to be the case. Thus the radiation pressure force on a grain will be described by equation (5.2a) below where $(PFN)_0$ is the radiation pressure function at $t = t_0$ (taken to be equivalent to L at this time), i.e.

$$P_r = \frac{a^2}{4r^2c} \left[(PFN)_0 \exp(-\omega t) + (PFN)_1\right] \qquad (5.2a)$$

Gravitational force between the grain and nova system is of course given by

$$G = \frac{4}{3} \frac{\pi a^3 s M_* \gamma_G}{r^2} \qquad (5.2b)$$

and gas drag (for the relative gas-grain velocity $\dot{r} >>$ thermal velocity of gas atoms) by

$$D_r \simeq \pi a^2 N_H M_H \dot{r}^2 \qquad (5.2c)$$

if the circum-nova gas is assumed to be predominantly hydrogen (Wickramasinghe, 1972). If, as is most likely, the gas originates from the central object then the gas density will be radially dependent, i.e. $N_H = N_H(r)$.

For particles moving through what would undoubtedly be at least a

partially ionised gas there would also be drag induced by Coulombic interactions of grain and ions (Draine & Salpeter, 1979). We will however ignore this together with sputtering of grains and interaction of grains with the current ejecta.

The equation of grain motion is then given by

$$\frac{4}{3}\pi a^3 s\,\ddot{r} = P_r - G - D_r \qquad (5.3)$$

The initial conditions derived for grain formation by Clayton and Wickramasinghe (1976) are assumed (i.e. $\dot{r} \simeq 1000$ kms^{-1}, $r = r_1 \cong 5 \times 10^{14}$ cm at $t = 0$) and $\omega = 1.39 \times 10^{-7}$ s^{-1} ($(PFN)_0 = 3 \times 10^{38}$ ergs^{-1}, $(PFN)_1 = 4 \times 10^{33}$ ergs^{-1}). This choice of ω stems from the decay rate of the heating function (defined in the next section) as applied to Nova Serpentis 1970.

Antipova (1978) found that the law of conservation of momentum if applied to the deceleration of ejecta in Nova Delphini 1967 implied a gas density of $\sim (0.5 - 1.0) \times 10^6$ cm^{-3}. This is an order of magnitude less than the densities found in the gas shells of Symbiotic stars but it gives an indication of the gas number density $(N_H)_1$ that might be found at the initial radius r_1. The gas number density is then assumed to fall as r^{-2} (i.e. corresponding to constant gas outflow) although the gas itself is assumed static with respect to the outflowing grains.

Equation (5.3) was solved numerically using the NAG library routine D02AJF for various values of $(N_H)_1$ and a (though a was assumed constant for each case as grain growth was considered to be complete).

From these results figure (5.2) was drawn for various combinations of grain radius a and gas density at r_1, $(N_H)_1$. It was found that for $(N_H)_1 = 10^4$ cm^{-3} even grains with $a \sim 10^{-6}$ cm would escape the system with terminal velocities ~ 500 kms^{-1}. However it can be seen from the figure that if $(N_H)_1 = 10^5$ cm^{-3} grains with $a \sim 10^{-6}$ cm

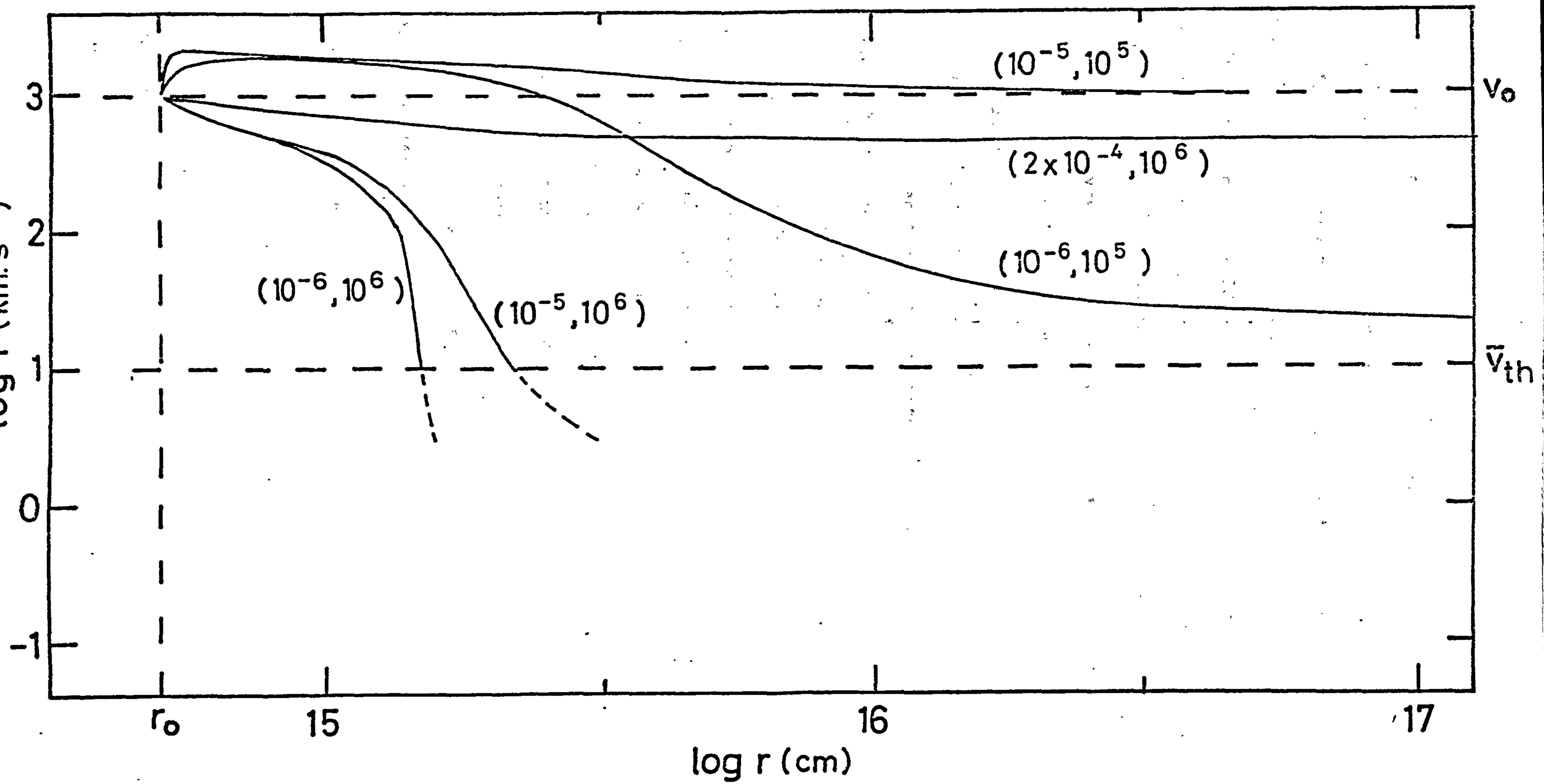

Figure (5.2) Grain outflow from a nova with $L = L_1 + L_0 \exp(-\omega t)$ where $L_1 = 4 \times 10^{33}$ ergs^{-1}, $L_0 = 3 \times 10^{38}$ ergs^{-1}. The initial grain velocity and formation distance are given by the lines v_0 and r_0 respectively. Combinations of grain size a(cm) and inner gas density $(NH)_1$(cm^{-3}) are denoted above each curve in the form $(a, (NH)_1)$.

reach a terminal velocity $\sim$ 20 kms^{-1} after $\sim$ 1000 yrs. Again for a $\sim 10^{-5}$ cm and above the grains escape rapidly.

If the gas density at r_1 is assumed to be 10^6 cm^{-3} then although 2×10^{-4} cm grains still have a high velocity after $\sim$ 1000 years (> 400 kms^{-1}) both $a = 10^{-5}$ and $a = 10^{-6}$ cm grains are quickly reduced to velocities less than the mean thermal velocity of the gas very rapidly. For 10^{-5} cm grains this occurs in 1.2 yrs and for 10^{-6} cm grains in 2.2 yrs. Of course at these low velocities equation (5.2c) will not be strictly valid but qualitatively the results are expected to be similar.

If the gas density were 10^5 cm^{-3} at $r_1 = 5 \times 10^{14}$ cm with $\dot{r} = 10$ kms^{-1} then the mass loss rate at the surface of the cool component, $\dot{M}_{gas}$, $\sim 10^{-7} - 10^{-6}$ $M_\odot$ yr^{-1} if $v_{gas} \sim 10 - 100$ kms^{-1}. This rate of mass loss is rather higher than Reimers (1975) deduced for a star similar to that generally accepted as a nova secondary. However it may not be unreasonable for a nova system where not only is a large amount of mass lost at outburst but also possibly from the accretion disc between outbursts as well.

Of course the circum-nova gas shell will neither be uniform or completely continuous. However the above results suggest that ambient gas can trap grains formed at outburst and will also act as a selector of grain size allowing progressively smaller grains to escape as lower gas densities are assumed.

5.4.1 The Heating Function

If grains do exist around the nova before outburst in sufficient quantity to give rise to the late developing infra-red flux then it is at first sight surprising that they do not emit most strongly at the time of visual maximum. However as we have seen in chapters 2 and 3 the visible light curve is a misleading indicator of what is truly

happening to the bolometric luminosity of the nova.

In figure (2.4) the observational results of Gallagher and Code (1974) clearly show that the continuum flux of Nova Serpentis 1970 gradually shifted to shorter wavelengths with time whilst the bolometric luminosity remained constant. If a dust grain were of a size and composition such that its absorption efficiency peaks in the ultra-violet then its peak temperature would occur when the product of the luminosity of the central object, $L(\nu)$, and the absorption efficiency, $Q_{abs}(\nu, a)$, integrated over all frequencies, maximised. What we are thus concerned with is the temporal behaviour of what we will henceforth call the 'heating function', HFN. We will define this by the expression

$$HFN = \int_0^\infty L(\nu)\ Q_{abs}(\nu, a)\ d\nu \qquad (5.4)$$

For a moderate speed nova the bolometric luminosity is now generally taken to be constant. Therefore to compensate for the increase in the effective temperature of the pseudo-photosphere, T_*, the photospheric radius, r_*, must decrease as T_*^{-2}. From the work of Bath and Shaviv (1976) T_* is related to the drop in visual magnitudes from visual maximum Δm, i.e. from solution of the expression

$$\Delta m = -2.5 \log \left\{ 1 - \frac{\int_0^{\lambda c} B(\lambda, T_*) d\lambda}{\int_0^{\infty} B(\lambda, T_*) d\lambda} \right\} \qquad (5.5)$$

For the later stages of novae T_* is large enough for the emission through the filter (whose cut-off wavelength is taken to be λ_c) to be in the Rayleigh-Jeans tail of the Planck spectrum, thus equation (3.22b) was derived by Bath and Shaviv (1976). However for $\lambda_c = 5000\text{Å}$ (V-filter) at temperatures below $T_* \sim 10000^\circ K$ the full form of the Planck function was used in the solution of equation (5.5).

Following Bath and Shaviv (1976) the bolometric luminosity of the

central source was taken to be the Eddington luminosity of a one solar mass object.

The change in Δm with time for Nova Serpentis 1970 was taken from the smoothed data of Grygar et al. (1971). This led to derived values of T_* which agreed reasonably well with the observations of Gallagher and Code (1974) over the first 57 days of the outburst. The steepening of the light curve at transition obviously led to an increased rate of temperature rise at this time.

In order for the heating function to peak at late times the absorption efficiency must peak at ultra-violet wavelengths. Thus if graphite grains are assumed to be present in the nova envelope they must be small ($\lesssim 2 \times 10^{-6}$ cm) for absorption to predominate at $\lambda \lesssim 2500$Å. Figure (5.3) shows the variation of absorption efficiency with wavelength for 10^{-6} cm graphite spheres calculated from values of n and k supplied by Isobe (1971) (Evans, 1979). The well known 2200Å peak is accompanied by another higher peak at $\sim$ 800Å. (Note - no allowance is made for the temperature dependence of the conductivity as was outlined in chapter 4.)

This order of grain size has been utilised in fits of the inter-stellar extinction by many authors (see for example, Greenberg, 1978). It is seen by some as the core type upon which mantles of ice might grow (c.f. figure (3.1)).

Evidence exists that infra-red emission arising from grains with absorption peaking in the ultra-violet does occur. For example Pottasch et al. (1977) found that the optical thickness of dust in some planetary nebulae at visible and near ultra-violet regions is very small and cannot account for the large infra-red flux emitted. The central stars of these planetary nebulae are usually luminous O-B types and recent studies have shown some to be binary in nature (Livio et al., 1979). Antipova (1978) has rather interestingly

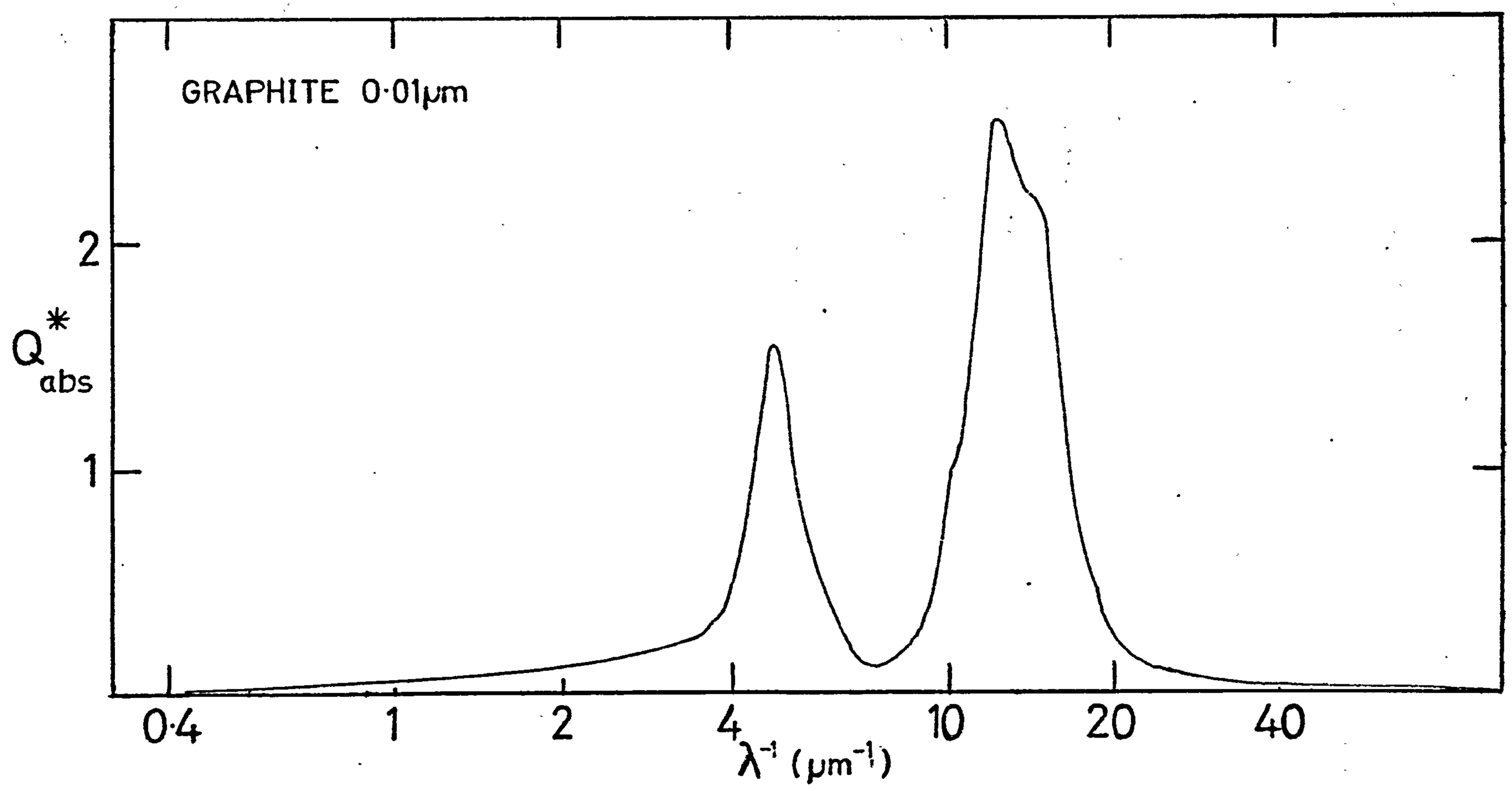

Figure (5.3) The variation of absorption efficiency Q_{abs} with inverse wavelength λ^{-1} for 10^{-6} graphite spheres. (from Evans 1979).

concluded that the slow Nova Delphini 1967 is quite possibly forming what will eventually appear as a planetary nebula due to its large mass loss rate.

Assuming that 10^{-6} cm spherical graphite grains were present in Nova Serpentis 1970 and that the effective temperature of the pseudo-photosphere was described by solution of equation (5.5) then the heating function's temporal behaviour was determined. Initially $Q_{abs}(\nu, a)$ was fitted using three Lorentzians for $a = 10^{-6}$ cm and convoluted with the luminosity function. However it was found more efficient to use results at small intervals of frequency from the Mie theory programme results and to perform numerical integration of the product of $L(\nu)$ and $Q_{abs}(\nu, a)$ (Evans, 1979). The resulting temporal behaviour of the heating function for Nova Serpentis 1970 is shown in figure (5.4) with the V curve superimposed.

There are several features worthy of note in this curve. For example the function is very small initially relative to the peak. However there is a gradual climb toward $\sim$ day 58 when there is a slope break in the V curve and transition commences. Because of the steep rise in temperature of the central object at this time (see for example Nariai (1974) for verification) the heating function undergoes a sudden and rapid rise. (The real rate of rise must be greater as the drop in continuum flux is compensated to some extent by a rise in emission line flux (Bosma, 1975) during transition.) The function peaks at $\sim$ 75 days with a decline rate equivalent to putting $\omega = 1.39 \times 10^{-7}$ s^{-1} in equation (4.22) (dotted line in the figure illustrates this decay rate). As with the rise to peak, the value of ω may be affected by the emission line contribution to the visual flux at transition. However the actual value of ω will be close to this figure.

We can now see why the transition can coincide with significant infra-red emission despite the fact that no new grains may be formed.

Figure (5.4) The visual light curve (V) and heating function (HFN) (for 10^{-6} cm graphite grains) for Nova Serpentis 1970. Dashed line illustrates a decay rate of $\omega = 1.39 \times 10^{-7}\ s^{-1}$. Date of discovery denoted by vertical broken line.

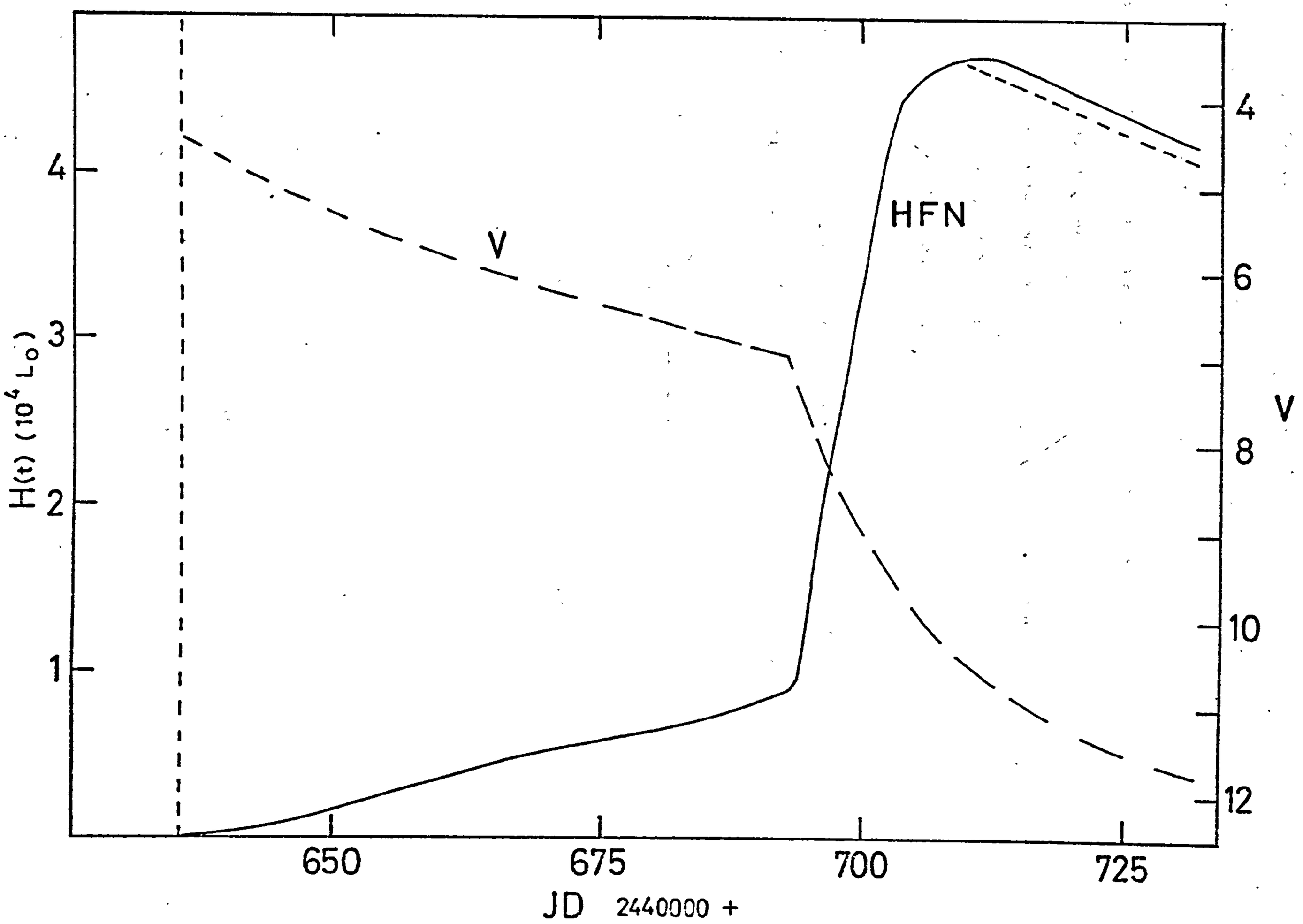
HFN
V
H(t) (10^4 $L_\odot$)
4
3
2
1
4
6
8
10
12
V
650
675
700
725
JD 2440000 +

The rise in the heating function from day 58 to day 75 is nearly an order of magnitude. Of course small spherical graphite grains may not be the only alternative as far as ultra-violet absorption goes but in the present work we will confine ourselves to this type.

It was stated in chapter 3 that for isotropic scattering $Q_{pr} \simeq Q_{ext}$. Thus the radiation pressure function PFN for 10^{-6} cm graphite grains was found by replacing Q_{abs} by Q_{ext} in the above analysis. The resulting curve was extremely similar to the heating function except that it peaked at $\sim$ 2HFN. From this the qualitative behaviour of the function PFN for the grain outflow programmes of the previous section was derived.

Finally we may note that if both sides of equation (5.4) are divided by the bolometric luminosity of the central object then we have

$$\frac{HFN}{L} = \frac{\int_0^\infty Q_{abs}(\nu, a)\ B(\nu, T_*)\ d\nu}{\int_0^\infty B(\nu, T_*)\ d\nu} \equiv \bar{Q}(a, T_*) \qquad (5.6)$$

In other words the heating function is proportional to the Planck mean of the absorption efficiency at temperature T_* (Gilman, 1974) where the constant of proportionality is the bolometric luminosity of the nova (assumed to be constant with time). Thus figure (5.4) maps the change of the Planck mean with time for 10^{-6} cm graphite grains surrounding Nova Serpentis 1970.

5.5.1 Models of Specific Novae - Introduction

In order to accurately compare theoretical models of Novae Serpentis 1970, Aquilae 1975 and Vulpeculae 1976 with observation the observational results had to be accurately reduced from magnitudes given in the literature to flux units.

In the case of Nova Serpentis 1970 the original results of Geisel *et al.* (1970) were found to be unavailable (Low, 1978). Thus the

results as plotted in Geisel et al. were read off using a digitiser and stored on paper tape; a library routine then output them as fluxes. Comparing the digitised results with the published observations of Hyland and Neugebauer (1970) which appear in the figures of Geisel et al. it was found that the digitised results were accurate to within $\sim \pm$ 2%.

The magnitude data of Vrba et al. (1977) were reduced from the standard zero magnitude fluxes as given by Allen (1973) as verified by Vrba (1978).

For Nova Vulpeculae 1976 the zero magnitude fluxes were found in Strecher and Ney (1974) although the effective filter wavelengths varied slightly from those given by Ney and Hatfield (1978). Here, as in the other 2 novae, the observed and theoretically derived fluxes at each wavelength were compared directly in the programme for the nova to determine how good the model fit was to the data (see appendix A1).

The models for each nova are relatively simple. For example no account is taken of any grain size distribution that might be expected due to gradual growth of grains in the circum-nova material or grain destruction by evaporation or sputtering. The dust cloud is also assumed to be spherical and centred on the nova. The heating function is approximated by a step function in Nova Aquilae 1975 and as defined by equation (4.22) in Novae Serpentis 1970 and Vulpeculae 1976.

The onset of rise of the heating function is taken to be the transition slope break in the visual light curve. As the continuum flux falls line emission increases and therefore the transition slope is less steep than continuum flux decline alone would suggest. The heating function peak would therefore occur sooner than estimated in the previous section. Thus the coincidence of the heating function peak and transition slope break would be more marked and the approximation of equation (4.22) more valid. In the case of Nova Aquilae 1975 the heating function peak was assumed to have occurred on the 9th day from

discovery for reasons outlined below.

The general fitting procedure was as follows. Firstly the time from discovery to the transition slope break, Δt_u, was determined as marking the onset of rise of the heating function. With a fixed value of the heating function peak and the maximum observed grain temperature, R_1 could roughly be determined. Then from the time of maximum flux at the longest observed infra-red wavelength the minimum value of R was found. For Nova Serpentis 1970 approximately 100 programmes were run with different values of α and β and slightly different values of R, R_1, ω and $(HFN)_0$ before the fit given below was obtained. This excludes the final adjustment of D to place the object within accepted distance limits and of M_g to give the final model fit.

5.5.2 Nova Serpentis 1970

The dust grains in Nova Serpentis 1970 are assumed to be graphite spheres of radius 10^{-6} cm. From Mie theory (Evans, 1979) the absorption efficiency, Q_{abs}, was determined at long wavelengths and plotted for different grain sizes in figure (5.5). The corresponding value of α was thus fitted by eye and found to be $\simeq 1.61$.

From figure (5.4) it can be seen that the peak of the heating function is $\simeq 1.8 \times 10^{38}$ ergs^{-1}. Nova Serpentis was modelled using $(HFN)_{peak} = 1.5 \times 10^{38}$ ergs^{-1}. The decay rate from peak was fitted using $\omega = 1.39 \times 10^{-7}$ s^{-1} as in the heating function ($\Delta t_u = 57.5$ days). The free parameters of the model were essentially β, R, R_1, M_g and D, the latter two being more for final adjustment than detailed fitting.

Figures (5.6a) and (5.6b) show the light curves and spectra obtained from a model with $\beta = 0$, $R = 10R_1 = 5 \times 10^{16}$ cm, $M_g = 6 \times 10^{-6} M_\odot$ and D = 0.98 kpc. The dust shell inner radius is comparable with that derived by Malakpour (1978) for closest grain approach during the quiescent stage (though our grains are rather smaller) and the outer

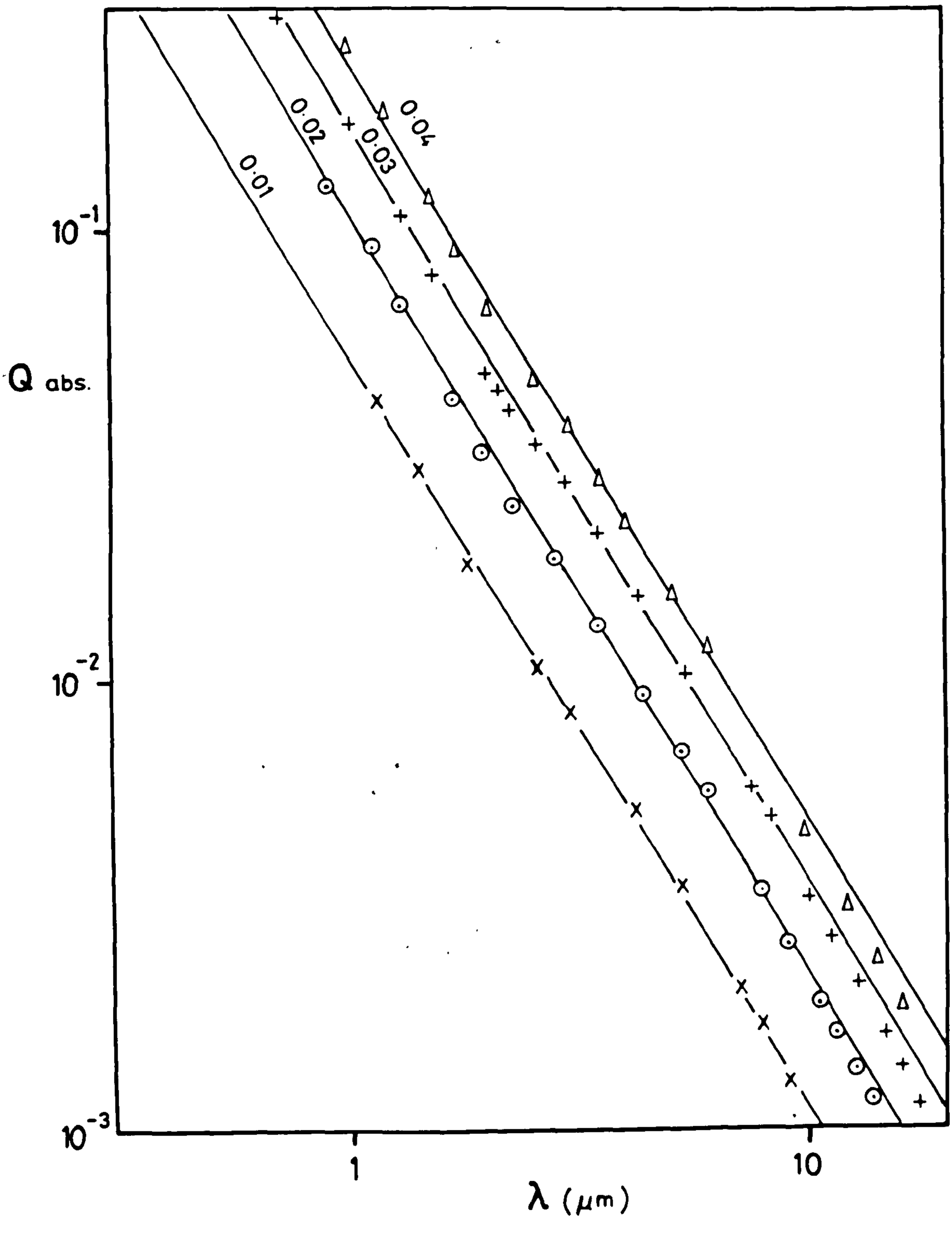

Figure (5.5) The long wavelength behaviour of Q_{abs} for four grain sizes (labels above graph lines are a in μm). Data from Mie theory calculations are fitted by lines with $\alpha = 1.61$.

Figure (5.6a) Comparison of the light curves of Nova Serpentis 1970 obtained by Geisel et al. (1970) with the theoretical model fit (solid lines) where $\beta = 0$, $R = 10R_1 = 5 \times 10^{16}$ cm, $Mg = 6 \times 10^{-6} M_\odot$, $D = 0.98$ kpc, $\Delta t_u = 57.5$ days, $(HFN)_0 = 1.5 \times 10^{38}$ ergs^{-1}, $\omega = 1.39 \times 10^{-7}$ s^{-1}, $a = 10^{-6}$ cm and $\alpha = 1.61$. Numbers at bottom right of each curve refer to observational wavelength in microns. The vertical dashed line is at $t = \Delta t_u$ (transition).

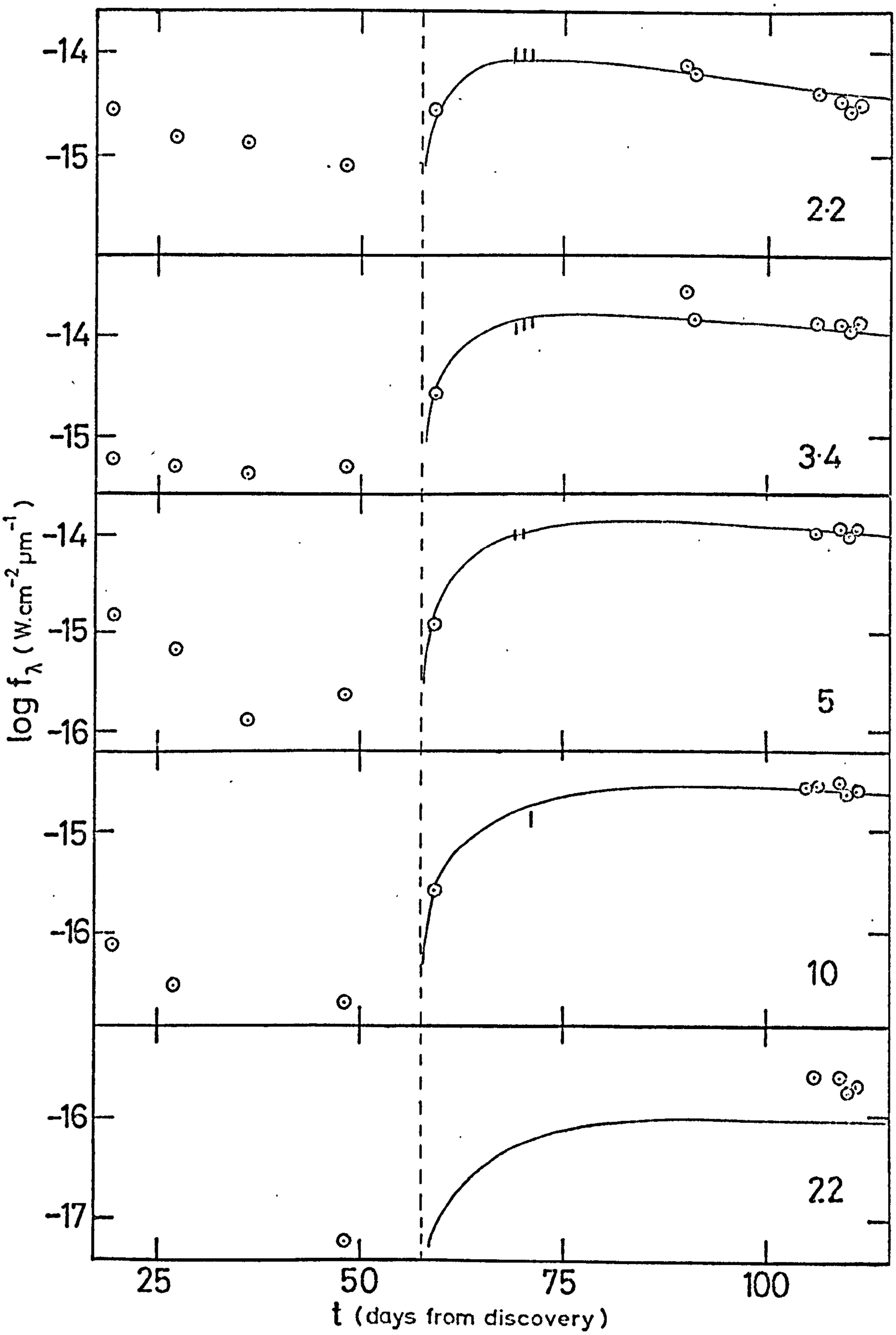
-14
-15
2·2
-14
-15
3·4
-14
-15
5
-16
-15
10
-16
-16
-17
22
25
50
75
100
log f_ν (W.cm^{-2} μm^{-1})
t (days from discovery)

Figure (5.6b) Comparison of the spectra of Nova Serpentis 1970 obtained by Geisel et al. (1970) with those of the theoretical model fit as in figure (5.6a) (solid lines). Numbers at top right of each section refer to the time in days from discovery. Days 69, 70, 71 are the observations of Hyland and Neugebauer (1970).

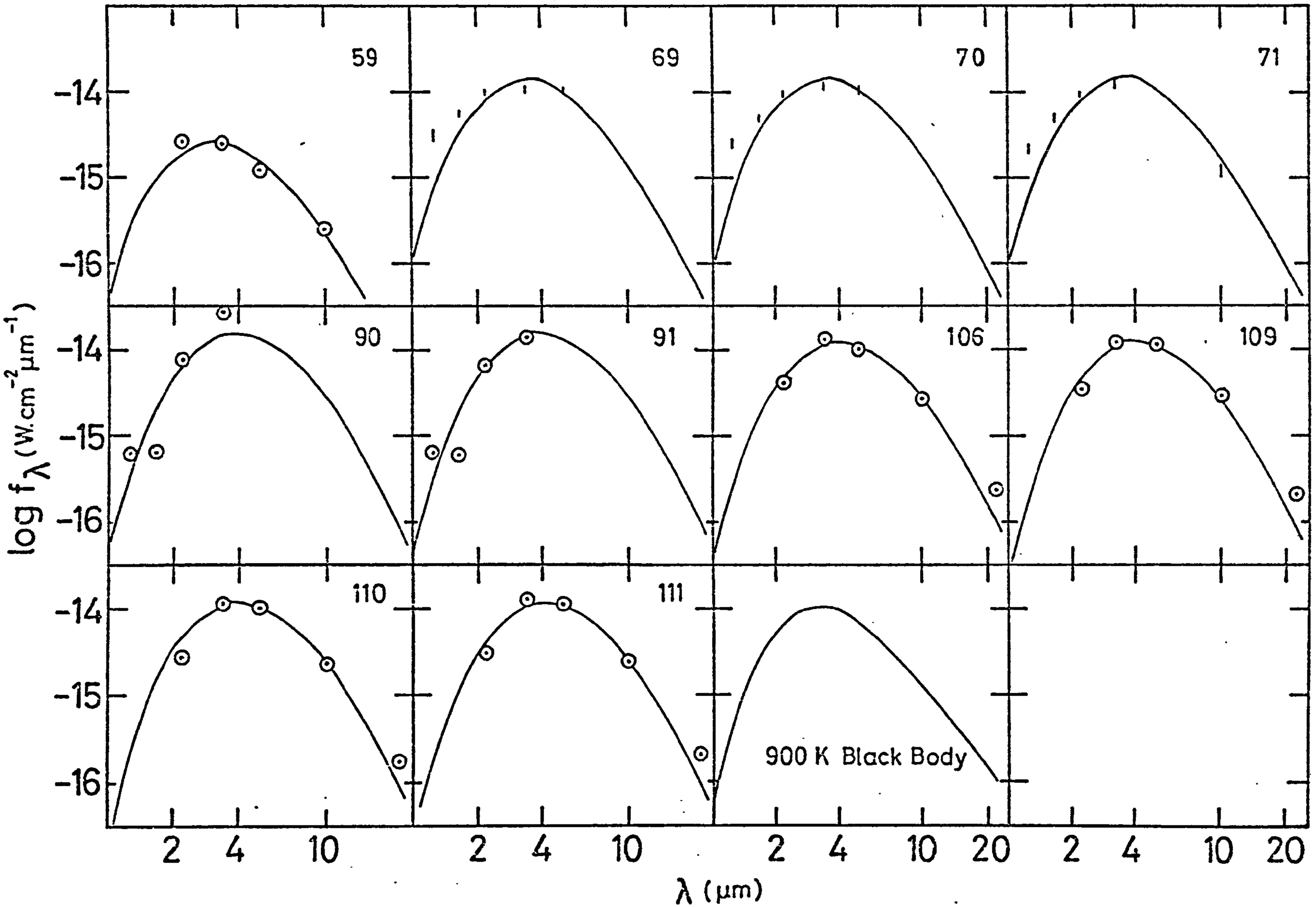
59
69
70
71
90
91
106
109
110
111
-14
-15
-16
log f_λ (W.cm^{-2}μm^{-1})
900 K Black Body
2
4
10
20
λ (μm)

Figure (5.6c) Comparison of the colour temperatures T_{K-N} derived from observations of Nova Serpentis 1970 by Geisel et al. (1970) with those from the theoretical model fit as given in figure (5.6a) (solid line).

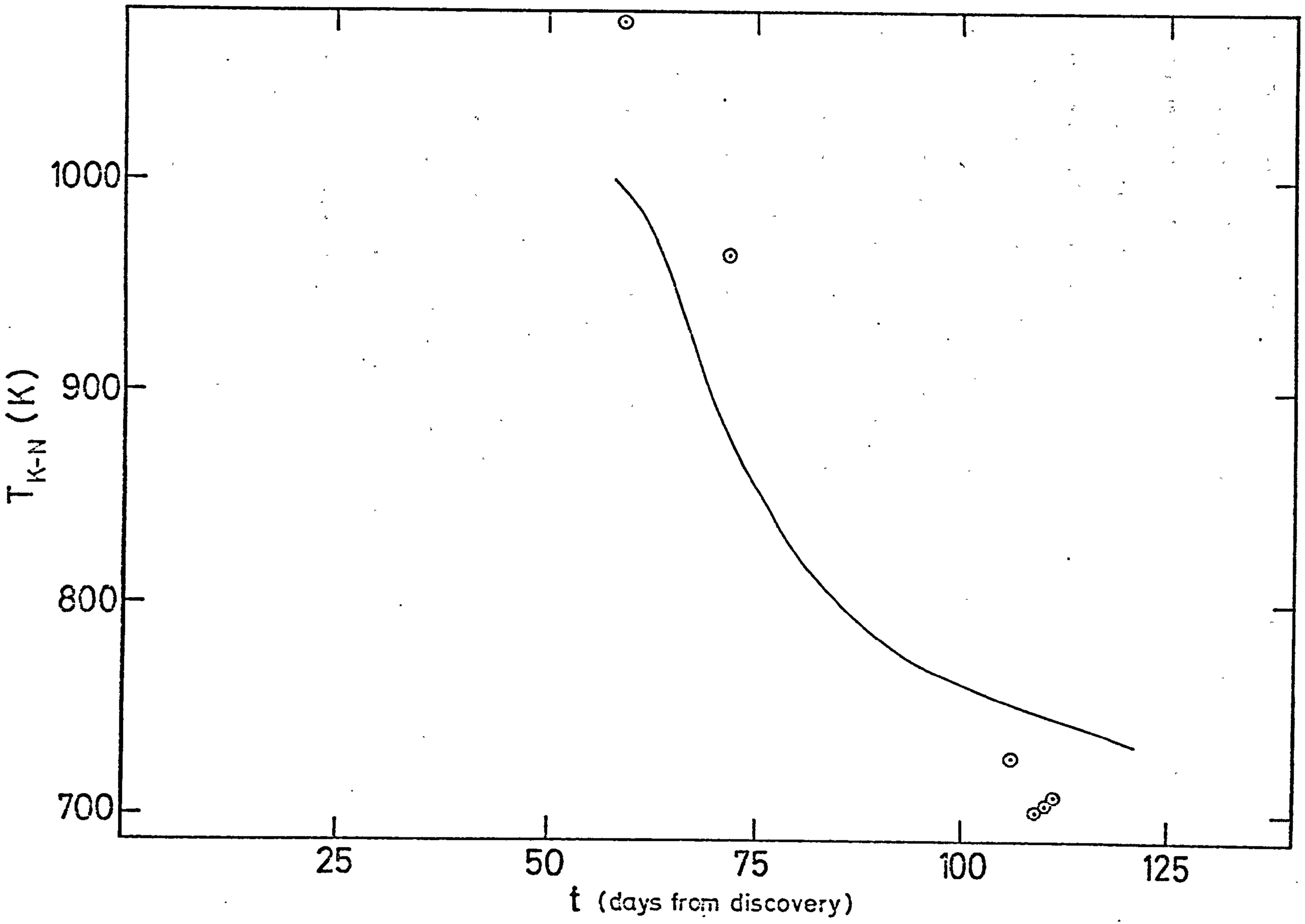
1000
900
800
700
T_{K-N} (K)
25
50
75
100
125
t (days from discovery)

radius is similar to the distance 10^{-6} cm grains formed in previous ejecta might have attained in $\sim$ 1000 yrs ($(N_H)_0 = 10^5$ cm^{-3}).

The value of $\beta < 2$ follows if grains outflowing from the central object are slowed by circum-nova gas, or if they have formed from material left over in the nascency of the system (c.f. Harvey et al., 1979) though the latter must be considered the less likely. The grain mass is perhaps not unreasonable as previous workers have assumed values from 10^{-6} $M_\odot$ (Geisel et al., 1970) to 3×10^{-5} $M_\odot$ (Clayton & Wickramasinghe, 1976). The object distance of 980 pc falls within the range usually quoted of 550 pc (Borra & Andersen, 1971) to 1.2 kpc (Hyland & Neugebauer, 1970) although slight adjustment of grain mass could be used to change this without affecting the results appreciably.

The dust shell at this distance would have an angular diameter of $\simeq$ 7 arc sec. Although the beam size of the particular telescopic arrangement used is unknown to the present author it is expected from the beam size quoted in earlier work by Kleinmann and Low (1967) of $\sim$ 20 arc sec that the shell could be within the beam by a comfortable margin.

If we now proceed to compare the theoretical and observed results we can see that except for the 22 μm light curve the majority of points at $t > 57.5$ days are fitted by the theoretical curves. The poor fit of the 22 μm points could be due to incorrect data reduction or observational errors (note that Geisel et al., unlike Hyland & Neugebauer, do not include indications of error in their results). The rise in observed flux prior to transition may be due to the initial rise in heating function as shown in figure (5.4).

Figure (5.6c) shows the computed T_{K-N} colour temperatures from theoretical and observational results. A point worthy of note is that whilst the colour temperature falls from $\sim$ 1000°K to $\sim$ 800°K the infrared flux is still rising in both the theoretical and observational

results. This, from our point of view, is due to the increase in emission of lower temperature grains with time as the parabola traverses the shell. If the T_{K-L} colour temperature were plotted on this graph the results would not agree with those of T_{K-N}. This indicates that in neither the case of the observed nor theoretical results could a black body (such as the 900°K one shown in figure (5.6b)) be fitted to the spectrum.

5.5.3 Nova Aquilae 1975

The main problem with Nova Aquilae 1975 is that discovery and peak visual flux do not appear to have coincided. Spectrally the nova was known to be in its early nebular stage 43 days from discovery (see section 2.2.3). Figure (2.6) shows that the early observations of the nova by Wild (1975) if correct indicate that a slope break may have occurred around the time of the initial observations by Vrba *et al.* (1977). The U-B and B-V behaviour also shown in figure (2.6) is extremely similar to that of Nova Serpentis 1970 at the onset of transition. According to Vrba *et al.* there also existed a large ultraviolet (3500Å) excess at the time of their observations, consistent with this indeed being the transition which, as in Nova Serpentis 1970, would thus produce a sudden rise in the heating function for small graphite spheres.

If indeed the observations of Vrba *et al.* (1977) caught the nova at transition then the use of $t_{3,v}$ in equation (2.1) would be incorrect as this applies to the immediate post-maximum phase only. Indeed the use of this erroneously small value of $t_{3,v}$ would lead to a much smaller value of M_v and thus the object distance would be too large. This might resolve the paradox revealed by van Genderen and Uiterwaal (1979) concerning the nova's distance.

Assuming that transition occurred 9 days from discovery a step

heating function with $(HFN)_0 = 2 \times 10^{38}$ ergs^{-1} was used in our model. Other parameters were the same as those for Nova Serpentis 1970 except that $M_g = 10^{-7}\ M_\odot$, D = 2.15 kpc and $\beta = 1$. Again both M_g and D were essentially free parameters even when the final model was decided upon. However an increase in D giving a necessary $\sim M_g^2$ increase to retain the observed flux levels would eventually affect the model's spectral fits as the optical depth grew. Thus it would be more convenient to decrease rather than increase the distance and retain the spectral fits.

The higher value of β may seem rather arbitrary. However if dust grains are 'trapped' by gas drag β should increase if the amount of circum-nova gas were decreased (i.e. terminal velocities increase) and as this happens more grains might be expected to escape the system between outbursts. Thus the higher value of β together with a lower total mass of trapped grains, as found in Nova Aquilae, should be expected on this model.

With $R = 10R_1 = 5 \times 10^{16}$ cm again, but with D = 2.15 kpc the dust cloud angular diameter is $\sim$ 3 arc sec. Thus the quoted beam size of the telescopic arrangement ($\sim$ 30 arc sec, Vrba et al., 1977) would easily have contained the source.

If we now examine the observational and theoretical results contained in figures (5.7a) to (5.7c) we can see that the light curves and spectra fit reasonably well except at the earliest times (day 10) when the observed flux, particularly at 1.6 and 2.2 μm, is too high. This is in part due to the 'contamination' of the shorter wavelengths by the relatively strong flux of the central object at this time. However it must also be remembered that a true heating function would have finite rise time and thus the true origin of HFN would be somewhat before day 9 with grains in the shell being heated and emitting before this.

Figure (5.7c) shows that, with the exception of the observation at

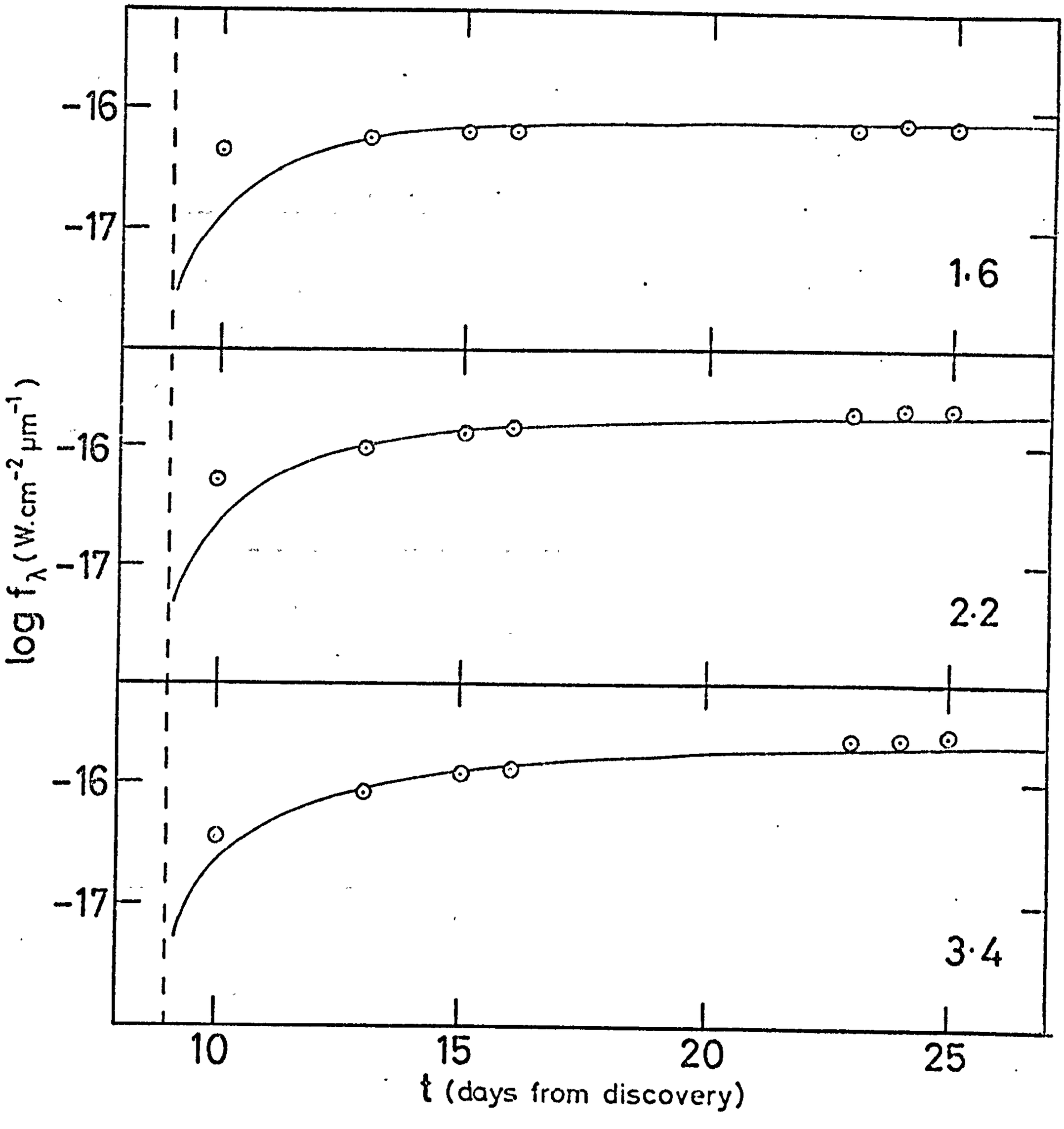

Figure (5.7a) Comparison of the light curves of Nova Aquilae 1975 as observed by Vrba et al. (1977) with the theoretical model fit (solid lines) where the model parameters are as for Nova Serpentis 1970 except $\beta = 1$, $Mg = 10^{-7}\ M_\odot$, $D = 2.15$ kpc, $\Delta t_u = 9$ days and the heating curve is step function in form with $(HFN)_o = 2 \times 10^{38}$ ergs^{-1}. The vertical dashed line is at $t = \Delta t_u$. (see figure 5.6a).

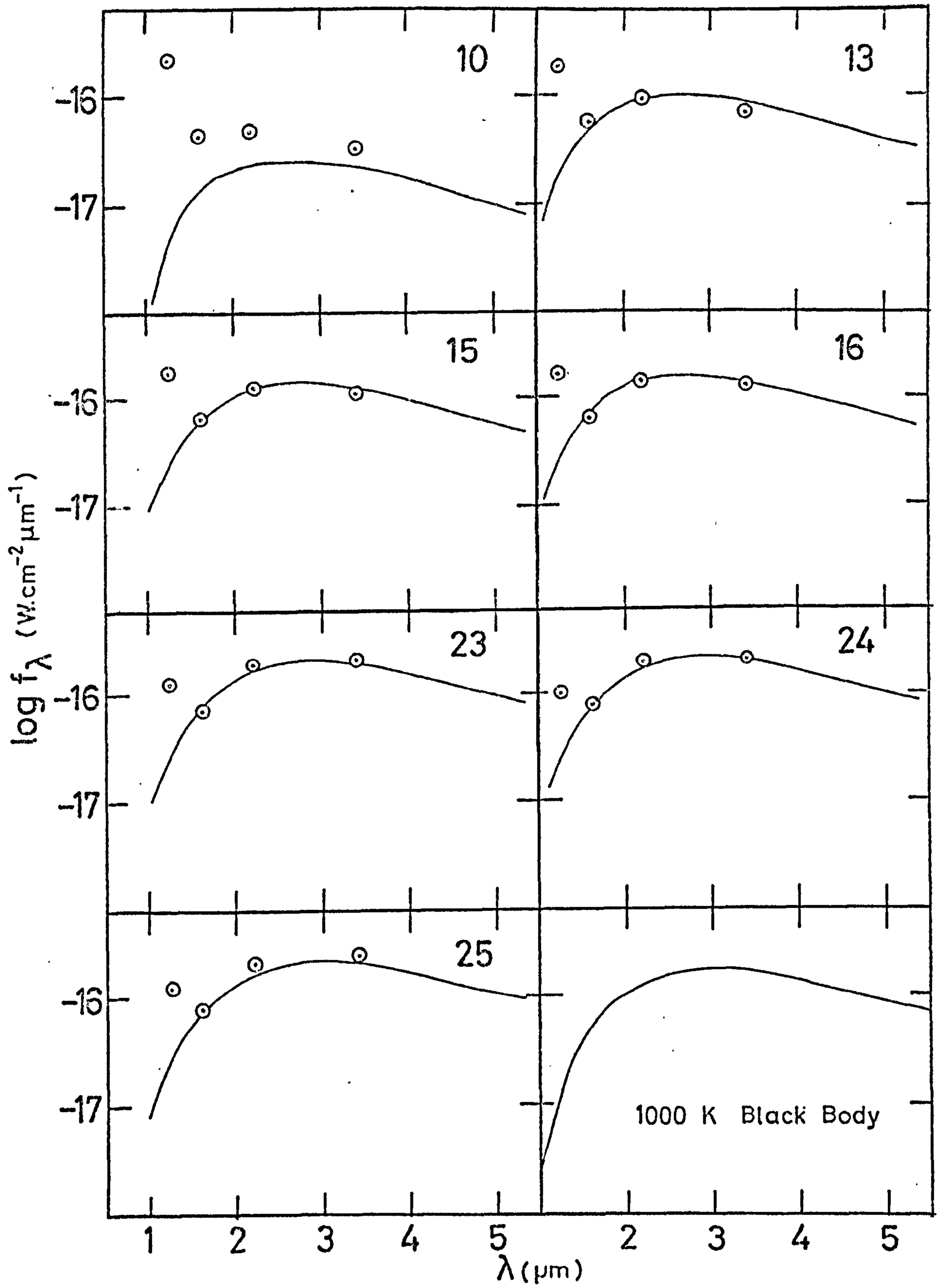

Figure (5.7b) Comparison of the spectra of Nova Aquilae 1975 obtained by Vrba et al. (1977) with those of the theoretical model fit as in figure (5.7a) (solid lines).

Figure (5.7c) Comparison of the colour temperatures T_{K-L} derived from observations of Nova Aquilae 1975 by Vrba et al. (1977) with those from the theoretical model fit as given in figure (5.7a) (solid line).

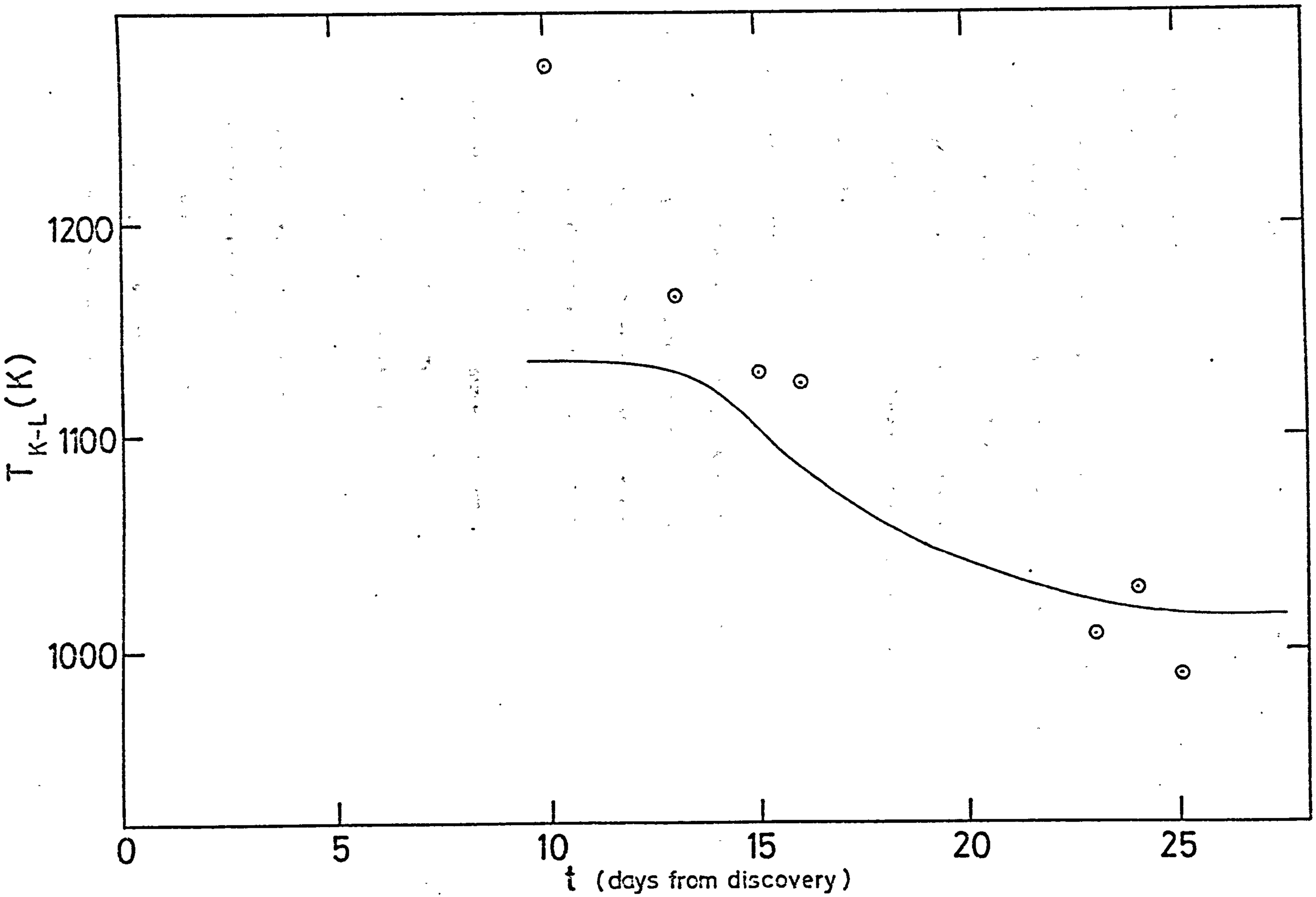
1200
1100
1000
T_{K-L} (K)
0
5
10
15
20
25
t (days from discovery)

day 10, the observed temperatures T_{K-L} and the theoretically derived values agree reasonably well, Again the total flux rises substantially whilst the temperature drops due to the increasing number of outlying, lower temperature grains.

In this model we have assumed an optically thin shell and a step function light curve. Thus the analysis of section (4.4,1) applies. Therefore the flux would be expected to rise linearly with time for all $\tau \leqslant 2\psi$ (see equation (4.37a)). This means that the infra-red flux rise should be linear from day 9 to $\sim$ day 13 with a declining rate of increase to a maximum at $\sim$ day 49. The integrated infra-red flux results of Vrba et al. (1977) shown in their paper indicate that this may well have been so.

5.5.4 Nova Vulpeculae 1976

Unlike Nova Serpentis 1970 and Nova Aquilae 1975, Nova Vulpeculae 1976 does not appear to have been extensively observed at short wavelengths (i.e. U, B or ultra-violet) during and after transition. However from the decrease in visual flux with time and the obvious transition slope break at $\sim$ 65 days a heating function similar to that of Nova Serpentis 1970 may be assumed for small graphite grains. For the purposes of the theoretical model a light curve described by equation (4.22) was again utilised with Δt_u = 63.5 days, $\omega = 2.2 \times 10^{-7}$ s^{-1} and $(HFN)_0 = 2 \times 10^{38}$ $ergs^{-1}$.

For consistency with previous models the dust grains were assumed to be graphite spheres of radius 10^{-6} cm ($\alpha = 1.61$). It was found that slightly better fits to the data arose for $\alpha = 1.0$ and a marginally lower value of ω. However it was considered that a consistent value of α between the three models in this chapter was at this stage desirable.

The shell parameters used in the model fit illustrated in figures

(5.8a-c) are $R = 4R_1 = 2 \times 10^{16}$cm, $\beta = 0$ and $M_g = 10^{-6}\ M_\odot$. Again the value of $\beta < 2$ is consistent with a 'piling-up' of grains at large distances from the nova. The total grain mass is intermediate between that found for Nova Serpentis 1970 ($M_g = 6 \times 10^{-6}\ M_\odot$) and Nova Aquilae 1975 ($M_g = 10^{-7}\ M_\odot$) as was expected from the relative infra-red luminosities. The dust shell inner radius is the same as in the previous two models but the outer radius is somewhat less. From black-body angular diameter considerations Ney and Hatfield (1978) determined the dust shell diameter to be $\sim 5 \times 10^{14}$ cm on day 70 for an assumed distance of 1.5 kpc. As we have seen in chapter 4 however the black body angular diameter of an optically thin source such as the dust shell of Nova Vulpeculae 1976 will be an underestimate of its true dimension.

The distance of the nova used in the model is 980 pc. This is rather less than that found by Ney and Hatfield (1978) of 1.5 kpc but is not unreasonable considering the uncertainties of their model. In any case adjustment of D and M_g in our model without changing the fits to the data would again be fairly straightforward. The angular diameter of the shell at this distance would be $\sim$ 3 arc sec, presumably contained wholly in the beam of the telescope.

If we now compare the theoretical and observational results as shown in figures (5.8a-c) we can see that the fits are not as good as for the previous two novae. The light curves of figure (5.8a) show the exponential decay at $t \gtrsim 80$ days for all wavelengths remarked on by Ney and Hatfield (1978) but the theoretical curves are too steep at short wavelengths and too shallow at long wavelengths. This behaviour leads to the too rapid 'cooling' of the system as shown in figure (5.8c) of the T_{K-N} colour temperature and indicated in the sample spectra of figure (5.8b).

The temperature behaviour of the infra-red excess of the nova is difficult to explain from either rapid condensation or pre-existing

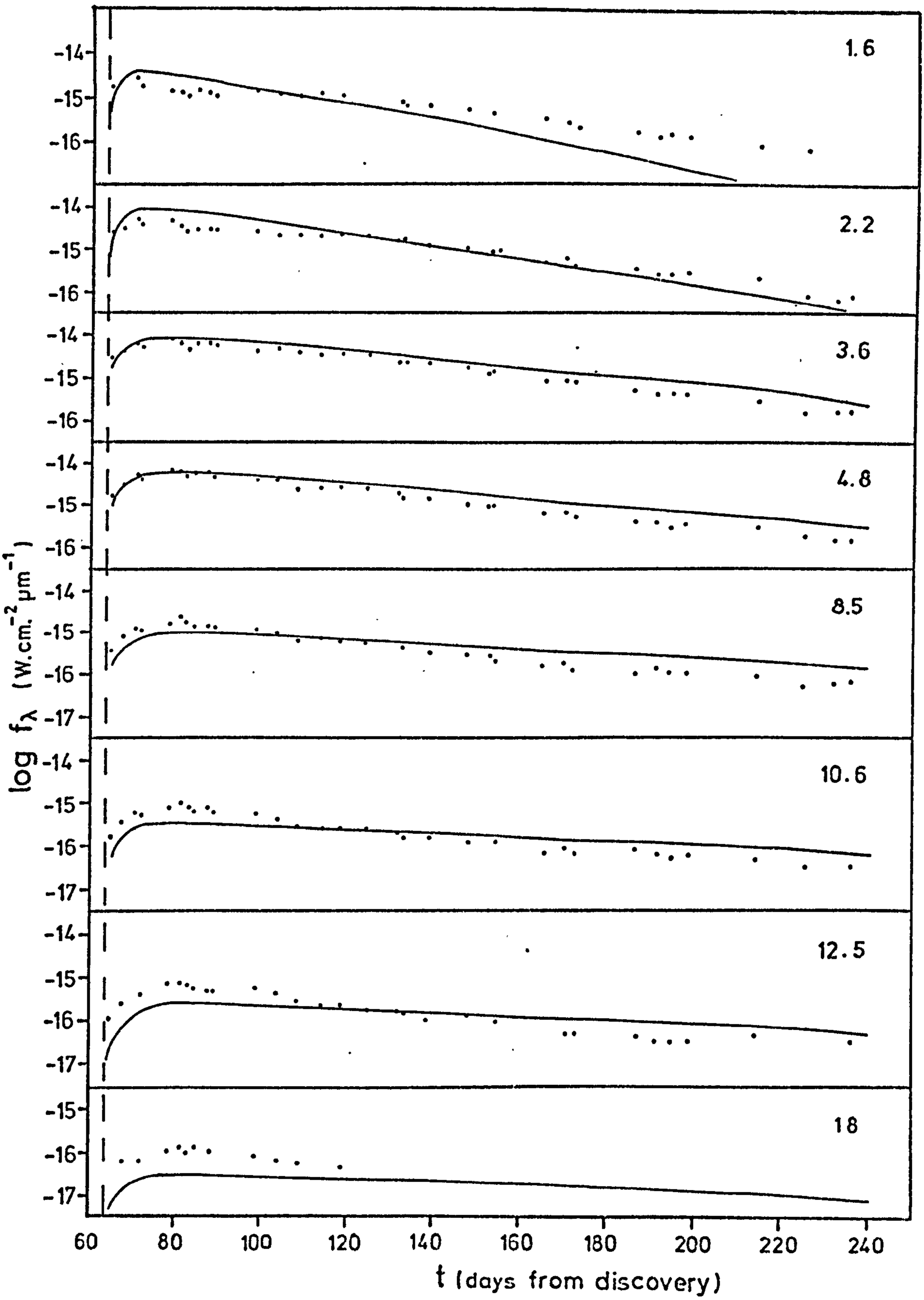

Figure (5.8a) Comparison of the light curves of Nova Vulpeculae 1976 obtained by Ney and Hatfield (1978) with the theoretical model fit (solid lines) where $\beta = 0$, $R = 4R_1 = 2 \times 10^{16}$ cm, $Mg = 10^{-6} M_\odot$, $D = 0.98$ kpc, $\Delta t_u = 63.5$ days, $(HFN)_0 = 2 \times 10^{38}$ ergs^{-1}, $\omega = 2.2 \times 10^{-7}$ s^{-1}, $a = 10^{-6}$ cm and $\alpha = 1.61$. The vertical dashed line is at $t = \Delta t_u$ (see figure 5.6a).

Figure (5.8b) Comparison of the spectra of Nova Vulpeculae 1976 obtained by Ney and Hatfield (1978) with those of the theoretical model fit as in figure (5.8a) (solid lines).

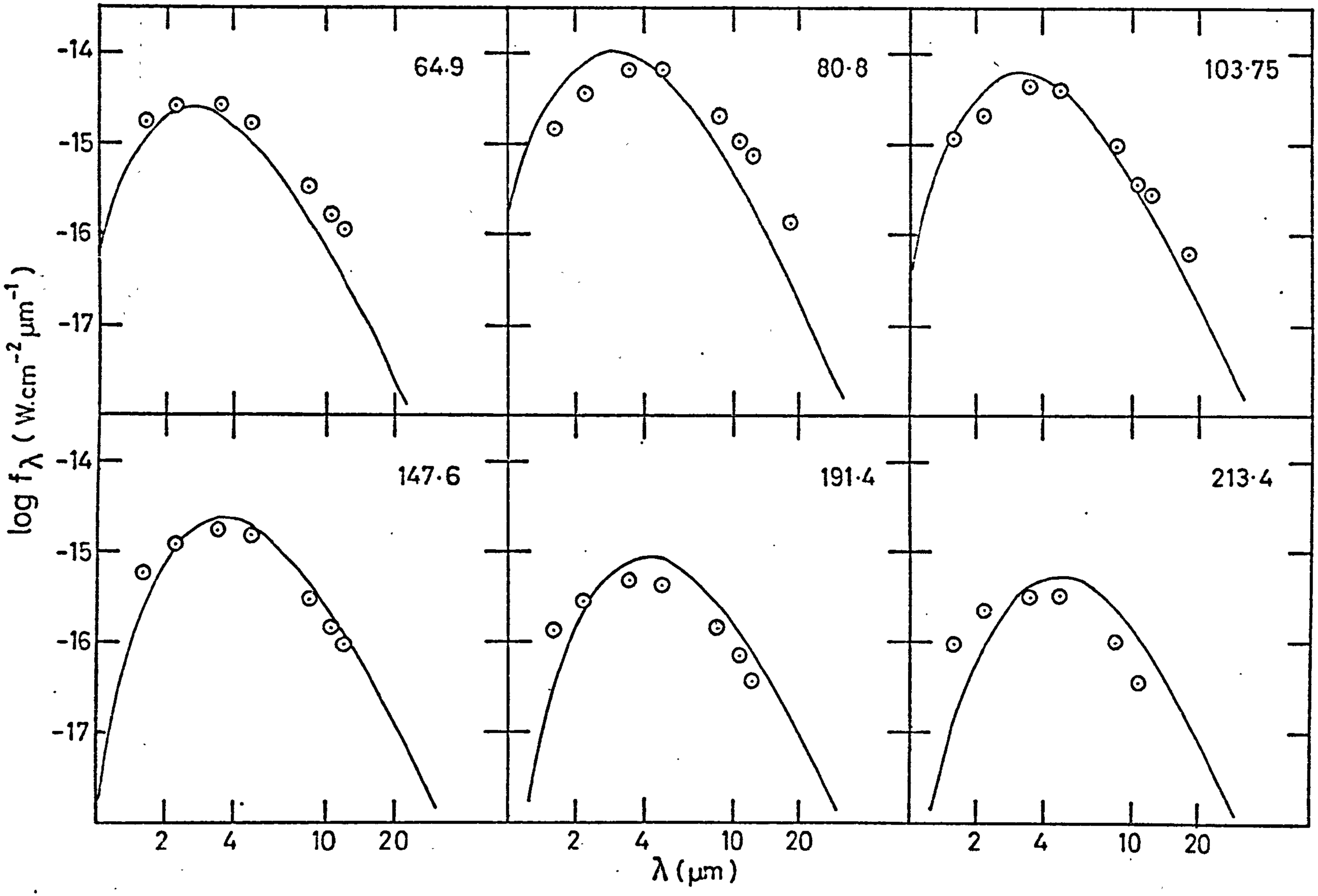
64·9
80·8
103·75
147·6
191·4
213·4
-14
-15
-16
-17
log f_λ (W.cm^{-2} μm^{-1})
2
4
10
20
λ (μm)

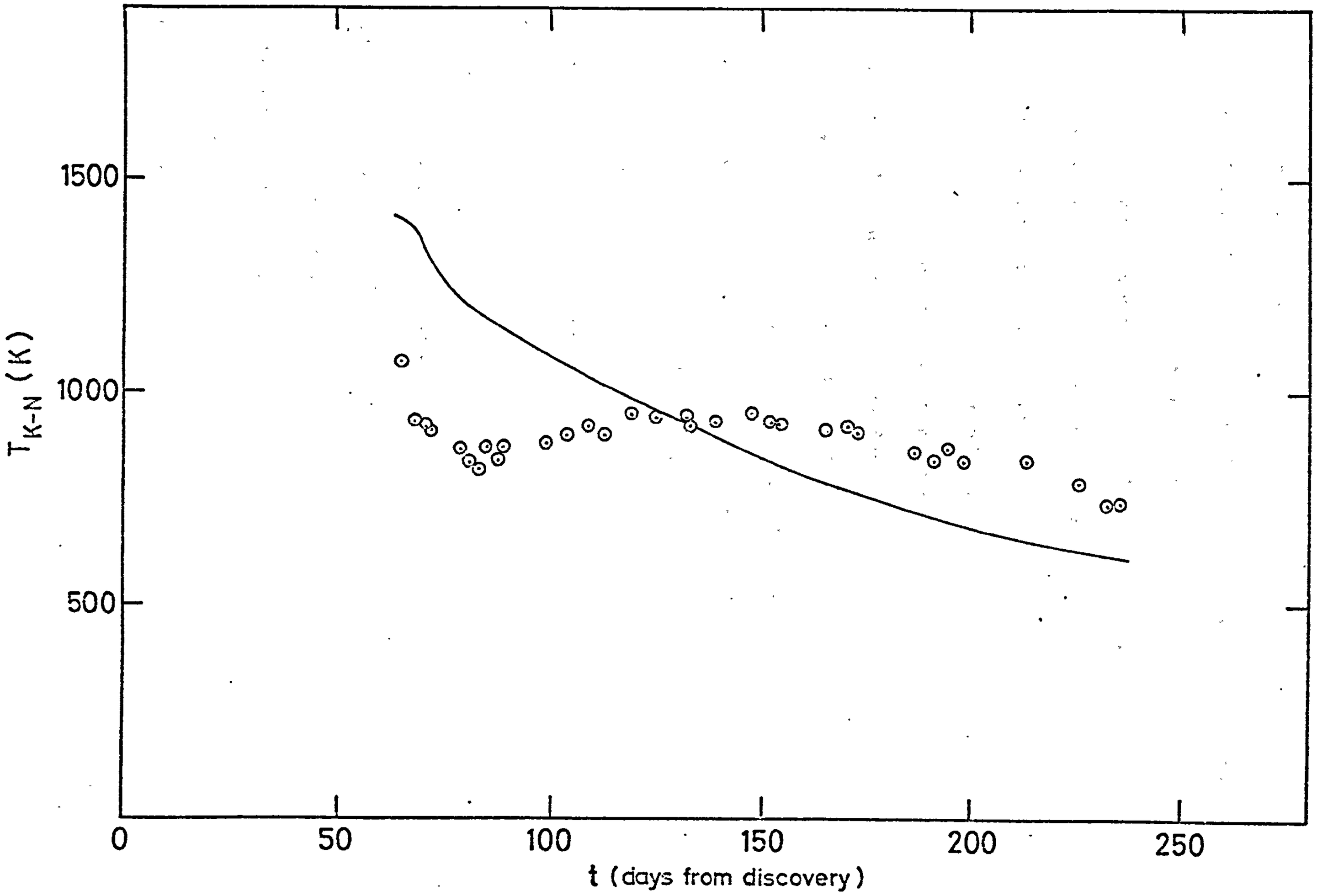

Figure (5.8c) Comparison of the colour temperatures T_{K-N} derived from observations of Nova Vulpeculae 1976 by Ney and Hatfield (1978) with those from the theoretical model fit as given in figure (5.8a) (solid line).

grain standpoints. Ney and Hatfield have ascribed the nearly isothermal nature of the shell to continuing formation of grains at $\sim 900^{o}K$ in the nova wind. As the formation rate drops so therefore would the infra-red flux. The main difficulty with this theory is that the grains which have already formed would still be emitting and as they continued to move out and (possibly) grow they would contribute more flux at progressively longer wavelengths. This would therefore tend to broaden the thermal spectrum of the nova with time. Sato et al. (1978) confirmed the observed time dependence of the black body temperature but found no evidence of spectral broadening.

From the point of view of the pre-existing grain model the almost isothermal behaviour of the nova dust shell is perhaps due to evaporation of grains. As the grains decrease in size so their temperature will increase (equation 4.3). However as the grains nearer to the nova completely evaporate so the cloud will become more transparent and hence the total flux will decay. Eventually the central object flux must begin to decline and at late times (possibly not covered by the observations) some re-condensation of grains might be expected. The qualitative effects of evaporation are explored more fully in chapter 7.

The differences in behaviour between Novae Serpentis 1970 and Aquilae 1975 and Nova Vulpeculae 1976 indicate that the initial conditions of grain type, size and distribution may well have been different. In the case of Nova Vulpeculae 1976 the initial parameters of the dust shell may have perhaps resulted in the evaporation of grains being important. This in turn led to its behaviour being rather different from the other two novae studied.

5.6.1 Discussion and Predictions

If our assumption that pre-existing grains give rise to the observed infra-red development of novae is correct then there should be several ways in which it could be verified.

With a pre-existing dust shell similar to those above, observations should show that considerable emission only occurs when the effective temperature of the central object is high and the dust shell is sufficiently opaque at short wavelengths. Thus infra-red emission will be relatively low if

(i) There is little pre-existing circum-nova dust

(ii) The nova does not reach a sufficiently high temperature at high luminosity ($\sim 60{,}000^{o}K$ at the peak of the heating function for graphite spheres with $a = 10^{-6}$ cm).

A nova such as Nova Cygni 1975 in which thermal X-rays from any pre-existing circum-nova shell of gas were expected but not detected (Brecher et al., 1975) probably did not have appreciable circum-nova dust either. Indeed Malakpour (1978) believes that this may have been the object's first outburst. Thus although the nova was highly luminous and reached $\sim 65000^{o}K$ by day 100 from outburst (Wu & Kester, 1977) there was little pre-existing dust to give rise to any appreciable infra-red flux. The rise at 10 μm could be due to line emission (Ferland & Shields, 1978) and the 3.4 μm excess detected by Szkody (1977) to the cool component of the system. An alternative qualitative explanation is given in the next chapter.

A slow nova such as Nova Delphini 1967, although it may have a substantial dust shell, may not at any time reach high enough luminosity at high temperature to give a particularly high value of the heating function. Indeed Tylenda (1978) noted that the ultra-violet luminosity of this nova during the infra-red emission stage was almost two orders

of magnitude lower than for Nova Serpentis 1970. The grain temperatures appear to have been lower as well (Geisel et al., 1970) indicating a lower value of the heating function.

Moderate speed novae such as Serpentis 1970 and Vulpeculae 1976 thus probably fulfil both conditions of high temperature during high luminosity and substantial pre-existing dust shells.

The existence of a dust shell before transition might be evidenced by an excess at long infra-red wavelengths which rapidly grows and shifts to shorter wavelengths at transition. Between outbursts a nova is thought to consist of an O-B type system with approximately solar luminosity (Payne-Gaposchkin, 1957). This would give rise to the infra-red emission between outbursts shown in figure (5.9) for the dust shell deduced above for Nova Serpentis 1970. Those of Novae Aquilae 1975 and Vulpeculae 1976 would probably be undetectable.

The presence of a static shell of small graphite grains during outburst could be determined by observation of the 2200Å region of the nova spectrum. For growing grains (whilst small) the relative depth of the absorption feature here should increase. Of course static circumstellar grain absorption would not change though it might be difficult to distinguish this from interstellar absorption. Observations using the IUE satellite at this wavelength have been suggested by Wright (1979).

In the case of the recurrent nova RS Oph the presence of an interuption dust shell has been indicated by a near infra-red excess (Feast & Glass, 1974). This excess would be expected to increase at outburst but not as much as in classical novae as recurrents are thought to be more luminous (particularly at short wavelengths) between outbursts and their rise to maximum is not as great (Bath & Shaviv, 1978).

We saw in the previous chapter that the surface brightness at the intercept of the emission parabola with the inner cavity was the highest

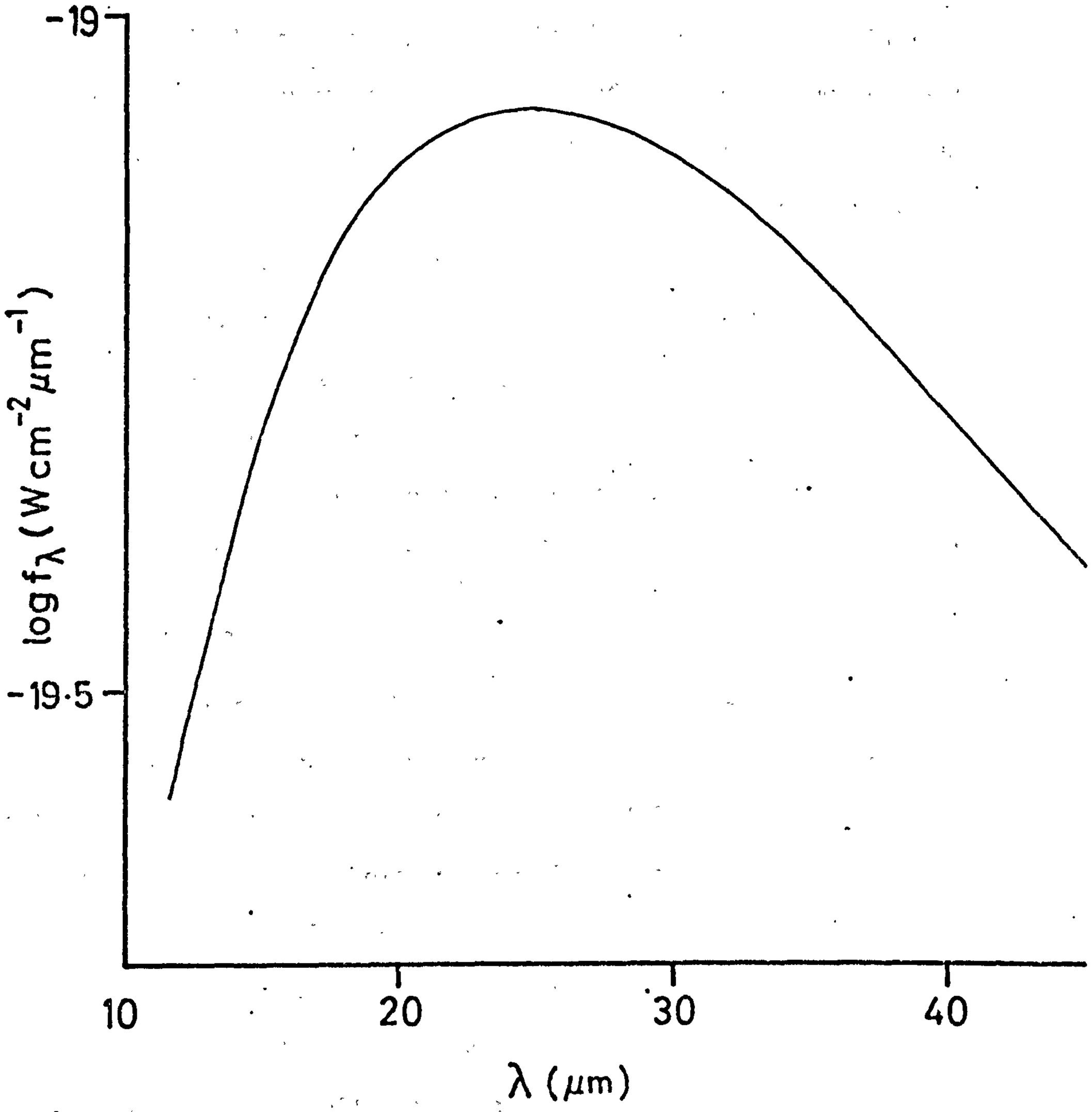

Figure (5.9) Nova Serpentis 1970 quiescent stage infra-red spectrum for the assumed dust shell parameters of figure (5.6a) but with $L = L_\odot$, $\bar{Q}_{abs} = 1$ at this time.

until $\tau_1 = 1$. After this the maximum stays at a displacement of R_1 from the nova. As explained in section (4.4.4) timing of the expansion of the brightest region of the observed disc gives R_1 and a measure of the maximum angular diameter of the source thus gives D.

If the dust distribution were spherically distributed about the nova then the transverse velocity of expansion of the emitting disc should vary with time as given by equation (4.18). Superlight effects would then have lasted $\sim$ 1 to 2 days in Nova Serpentis 1970.

Finally by studying the spectra and light curves of the central object and dust shell it may be possible to deduce the form of the heating function and hence the variation of $\bar{Q}_{abs}$ with temperature. Thus the grain size and type might be derived especially if R_1 is known.

5.7.1 Conclusion

We have shown in this chapter that the pre-existing dust grain model of novae can help to bring together many nova phenomena. The model fits to the observational data on Nova Serpentis 1970 and Aquilae 1975 are felt to be quite good. However those for Nova Vulpeculae 1976 are not as accurate. Obviously the simplicity of the model in not considering different grain types, non-spherical dust shells and grain destruction mechanisms could explain the inadequacies of the models. We now proceed to consider briefly an alternative geometrical situation.

Chapter 6

Infra-red Emission from an Inclined Disc of Dust Grains

6.1.1 Introduction

In chapter 4 we developed the theoretical background to the situation in which a variable high frequency source is surrounded by a spherical shell of dust grains. Application of this model to novae produced reasonable fits to the data if the grains were assumed to be predominantly heated by the short wavelength flux of the central source.

In this chapter the central object is assumed to be surrounded by a thin disc of identical dust grains which is inclined to the observer's line of sight. In section (6.2.1) we examine the general geometry of the situation then proceed in section (6.3) to derive the observed infra-red flux from this type of source. Finally section (6.4) attempts to apply the results of the previous sections to Nova Cygni 1975.

6.2.1 Geometry of the Inclined Disc

In section (3.4.1) the basic theory of 'optical reverberation', as described originally by Couderc (1939) was outlined. If instead of a continuous 'slab' of material placed some distance from the central source of radiation we consider a disc of dust grains with a central evacuated cavity surrounding a centrally positioned source then the geometrical situation is as shown in figure (6.1). Obviously a distant observer will not observe a disc of grains but an ellipse the eccentricity of which depends upon the inclination i of the disc to his line of sight.

If at time t = 0 a δ function pulse of high frequency radiation is emitted from the central source at N, then re-emission of infra-red radiation from the dust grains will occur only where the paraboloid of revolution, semi-latus rectum ct, cuts the disc. (We may note however that strictly a δ-function pulse would violate the condition that grain cooling time be less than the fluctuation time of the central object. However it is used here for illustrative purposes only.) It can be appreciated from figure (6.1) that whilst the expanding paraboloid of emission lies within the inner cavity, radius R_1, there will be no re-emission and for a δ-function pulse re-emission will cease once the paraboloid has left the disc. We will consider these effects later with particular reference to Nova Cygni 1975.

Figure (6.2) shows the situation in cross-section. The plane containing the disc is defined by

$$z = x \cot i \qquad (6.1)$$

where (x, y, z) define a Cartesian co-ordinate system with z lying along the observer's line of sight. Also it can easily be shown that

$$ct + z = a = \sqrt{x^2 + z^2}$$

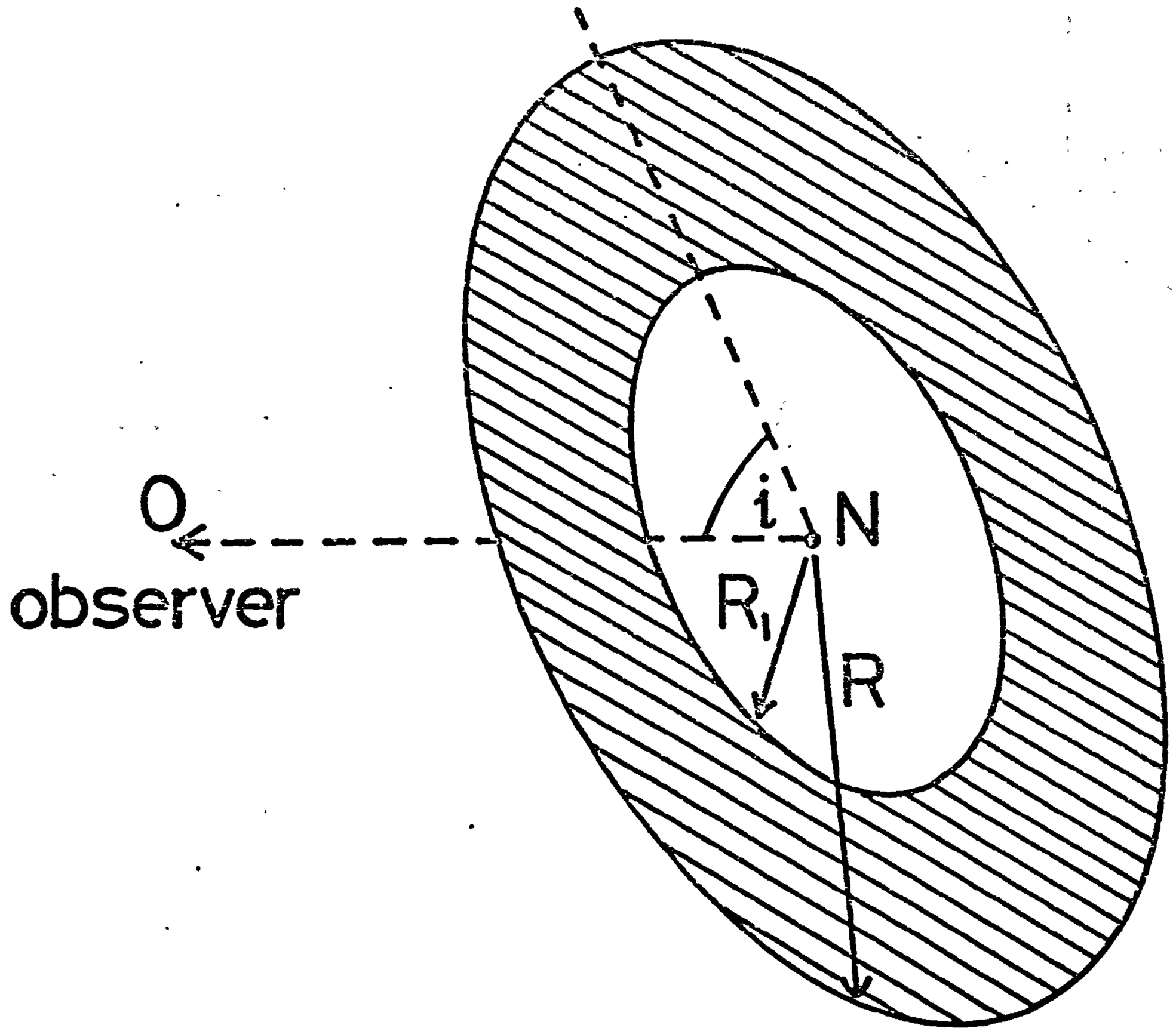

Figure (6.1) The general geometrical situation in which an inclined disc of dust grains outer radius R and cavity radius R_1 surrounds a variable source of high frequency radiation at N. The angle of inclination of the plane of the disc to the observer's line of sight is given by i.

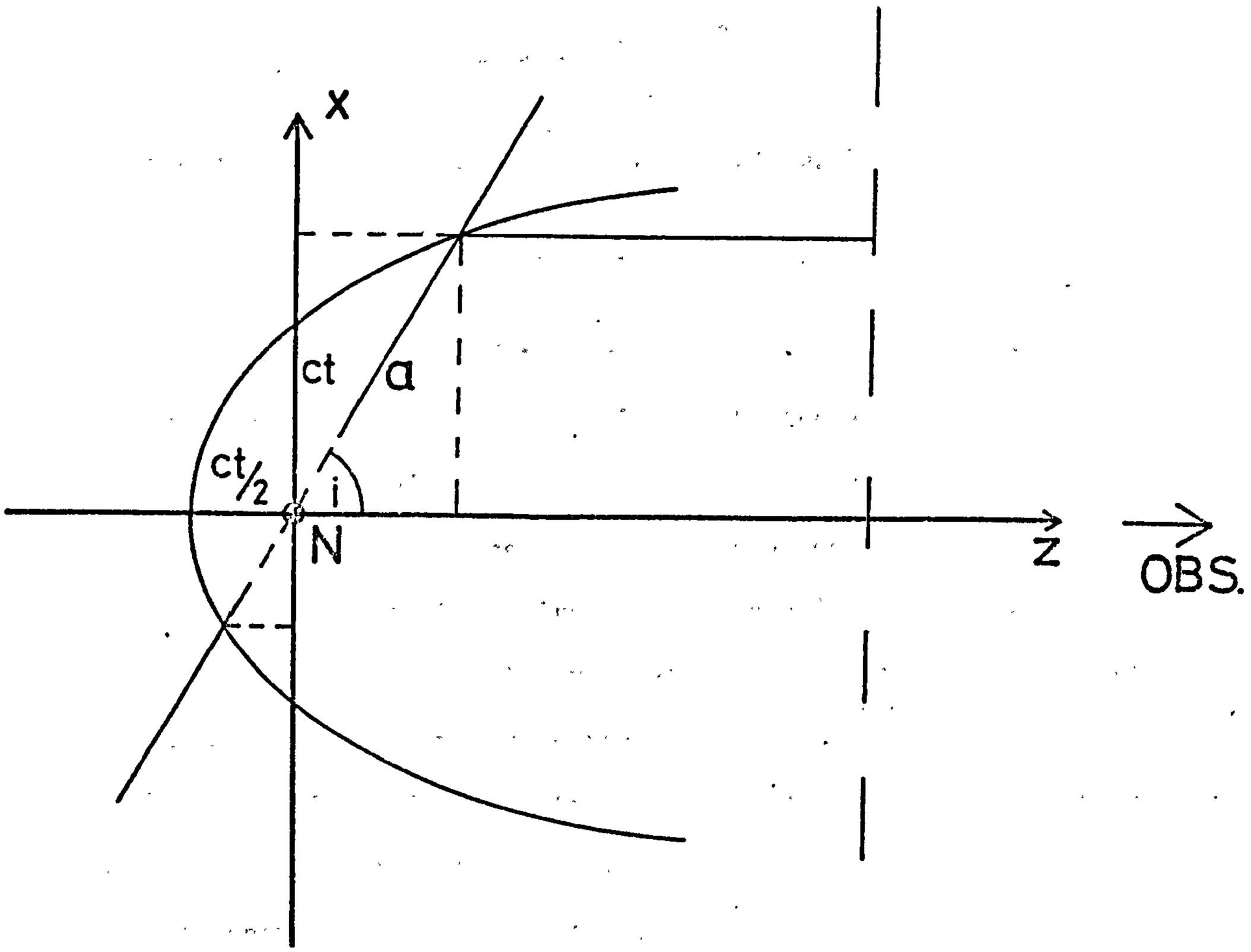

Figure (6.2) Cross-sectional view of the disc with the parabola of emission as seen by a distant observer shown. The central source is at N. The significance of the variables a, x, z, c and t is explained in the text.

which leads, in 3-dimensions, to the expression

$$\frac{ct}{2} + z = \frac{x^2 + y^2}{2ct} \tag{6.2}$$

Eliminating z between equations (6.1) and (6.2) we have

$$x^2 + y^2 = c^2t^2 + 2ct \cot i.x \tag{6.3}$$

Equation (6.3) is that of the projection of the edge of the emitting region bounded by the paraboloid onto the xy plane as seen by a distant observer. This is of course the equation of a circle with radius r_c = ct cosec i displaced from N by an amount d = ct cot i. The expansion velocity v_r of this 'circle of emission' is thus constant and $v_r > c$ for all $i < \pi/2$. The rate at which the centre of the circle of emission moves away from the central source will also be superlight for $i < \pi/4$. At $i = \pi/2$ the centres of the disc and circle of emission will of course lie at N at all times.

If the central cavity radius is R_1 and that of the outer radius is R then the disc projections at these limits onto the xy plane are concentric ellipses with equations

$$\text{Inner} \quad x^2 \operatorname{cosec}^2 i + y^2 = R_1^2 \tag{6.4a}$$

$$\text{Outer} \quad x^2 \operatorname{cosec}^2 i + y^2 = R^2 \tag{6.4b}$$

The general equation for the projection of a point on the disc radial distance r from the central source is given by

$$r = (x^2 \operatorname{cosec}^2 i + y^2)^{\frac{1}{2}}. \tag{6.5}$$

Whilst the circle of emission lies within the ellipse of (6.4a) there will be no observed infra-red re-emission. Thus the time from observation of the pulse from the central object until re-emission begins, Δt_0, is given by

$$\Delta t_0 = \frac{R_1}{C} \left\{1 - \cos i\right\} \tag{6.6}$$

6.3.1 The Development of the Infra-red Flux Observed by a Distant Observer with i = 90°

We now consider the development of the infra-red flux from the disc as viewed by a distant observer. In order to solve the equation of transfer analytically we choose to investigate the special case of a very thin disc (both optically and geometrically) inclined at 90° to the observer's line of sight. In addition the heating function is assumed to be a step function (c.f. equation (4.22) with $\omega = 0$).

The surface brightness of the disc is given by

$$\Sigma_\nu = B(\nu, T_g(r))\ N(r)\ \pi a^2\ Q_{abs}\ \Delta z$$

where Δz is the disc thickness and we assume that $N(r) = N_1\left(\frac{R_1}{r}\right)^\beta$. From equation (4.7) $T_g(r) = K_0'\ r^{-2/\alpha+4}$, where K_0' is a constant in this case.

The observed flux from the disc $f_\nu(t)$ is again given by

$$f_\nu(t) = \int_\Omega \Sigma_\nu\ d\Omega$$

where Ω is the solid angle defined by the disc at the observer distance, i.e.

$$f_\nu(t) = C_0' \int_{R_1}^{r_c} \frac{r^{1-\beta}}{\exp\left[\frac{h\nu}{kK_0}\ r^{2/\alpha+4}\right] - 1}\ .\ dr \qquad (6.7)$$

where for $i = 90°$, $r_c = ct$. C_0' is a constant given by

$$C_0' = \left(\frac{2\pi}{D^2}\right).\left(\frac{2h\nu^3}{c^2}\right) Q_{abs}\ N_1 R_1{}^\beta\ \pi a^2\ \Delta z$$

Using the substitution $\omega = \frac{h\nu}{kK_0'}\ r^{2/\alpha+4}$ equation (6.7) integrates reasonably easily to give

$$f_\nu(t) = \frac{\alpha+4}{2} C_0 \sum_{n=0}^{\infty} \frac{B_n}{n!} \left(\frac{h\nu}{kK_0'}\right)^{n-1} \frac{R^{\frac{2(n+\gamma')}{\alpha+4}}}{n+\gamma'} \left\{ \tau^{\frac{2(n+\gamma')}{\alpha+4}} - \psi^{\frac{2(n+\gamma')}{\alpha+4}} \right\} \quad (6.8)$$

where α, B_n, τ and ψ have their former meanings and $\gamma' = \gamma - \frac{\alpha+4}{2}$.

Again it is fairly obvious from equation (6.8) that there is no observed infra-red flux from the disc until a time $\tau > \psi$ for $i = 90^o$.

The solution given by equation (6.8) was not used to plot extensive spectra and light curves as there is a short wavelength cut-off in the convergence of the Bernoulli series (see section (4.4.2)). The prime importance of this solution is to serve as a check on numerically derived results described subsequently.

6.3.2 Numerical Solution and More General Cases

In section (6.3.1) we described the analytical solution of the transfer equation in a very special case. Here we proceed to solve the equation of transfer using numerical methods. These have enabled us to derive the observed infra-red flux from a disc at any value of disc inclination, for any wavelength and for a wider range of central source light curves, L(t), which are assumed to correspond to the grain heating function (see Chapter 5). We shall still assume that the disc is thin, both optically and geometrically, and that the grains are initially of a uniform size which does not alter with time.

The numerical integrations were performed using a simple Simpson's rule method. In this case however the double integration was performed over y and then x.

If we define the observed flux as in previous sections, then in Cartesian coordinates

$$f_\nu(t) = \int_\Omega \Sigma_\nu \, d\Omega = \frac{1}{D^2} \int_x \int_y \Sigma_\nu \, dy \, dx. \qquad (6.9)$$

i.e.

$$f_\nu(t) = C_1' \int_x \int_y \frac{(x^2 \operatorname{cosec}^2 i + y^2)^{-\beta/2}}{\exp\left[\frac{h\nu}{kK_0} (x^2 \operatorname{cosec}^2 i + y^2)^{1/\alpha+4}\right] - 1} \, dy \, dx$$

where $C_1' = C_0' \operatorname{cosec} i/2\pi$.

Figures (6.3a) and (6.3b) show the development of the emission region with time for all cases. In case (a) the emission circle leaves the top of the outer ellipse before leaving the inner cavity ellipse altogether. In case (b) the emission circle leaves the inner ellipse before cutting the outer one. The limiting condition will thus depend not only on the relative size of the cavity but also the disc inclination, i.e.

$$\psi_{LIMIT} = \frac{1 - \cos i}{1 + \cos i} .$$

The limits on x and y in each case were found for each region of the emission area (see figures (6.3a) and (6.3b)). For example the points at which the emission circle cuts the disc projections are given for x by:-

$$\text{Inner} \quad x_i(\tau) = R_1(1-\tau_1) \tan i, \quad y_i(x(\tau)) = (R_1^2 - x_i^2 \operatorname{cosec}^2 i)^{\frac{1}{2}}$$

$$\text{Outer} \quad x_0(\tau) = R(1-\tau) \tan i, \quad y_0(x(\tau)) = (R^2 - x_0^2 \operatorname{cosec}^2 i)^{\frac{1}{2}}$$

(Note that due to the symmetry of the situation about the x axis, integration was performed over the 1st and 4th quadrants and then the resultant flux doubled.)

Therefore in figure (6.3a) (ii), for example, the integration takes

(i)

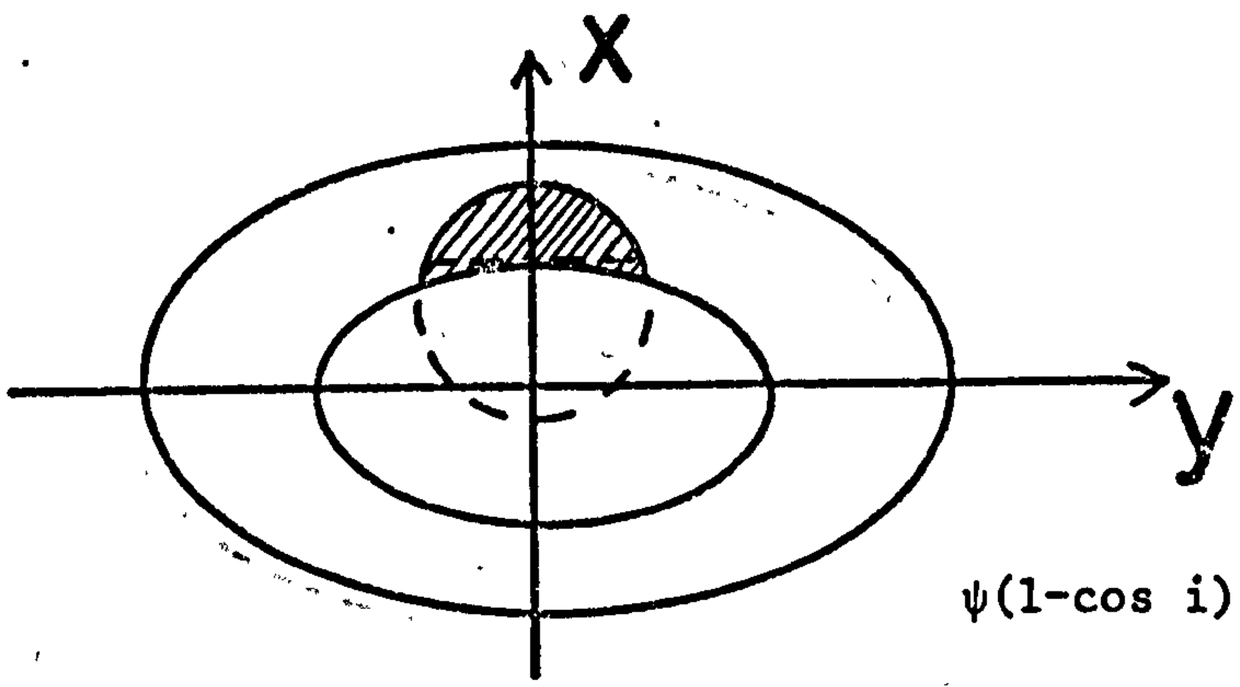

$\psi(1-\cos i) \lesssim \tau \lesssim (1-\cos i)$

(ii)

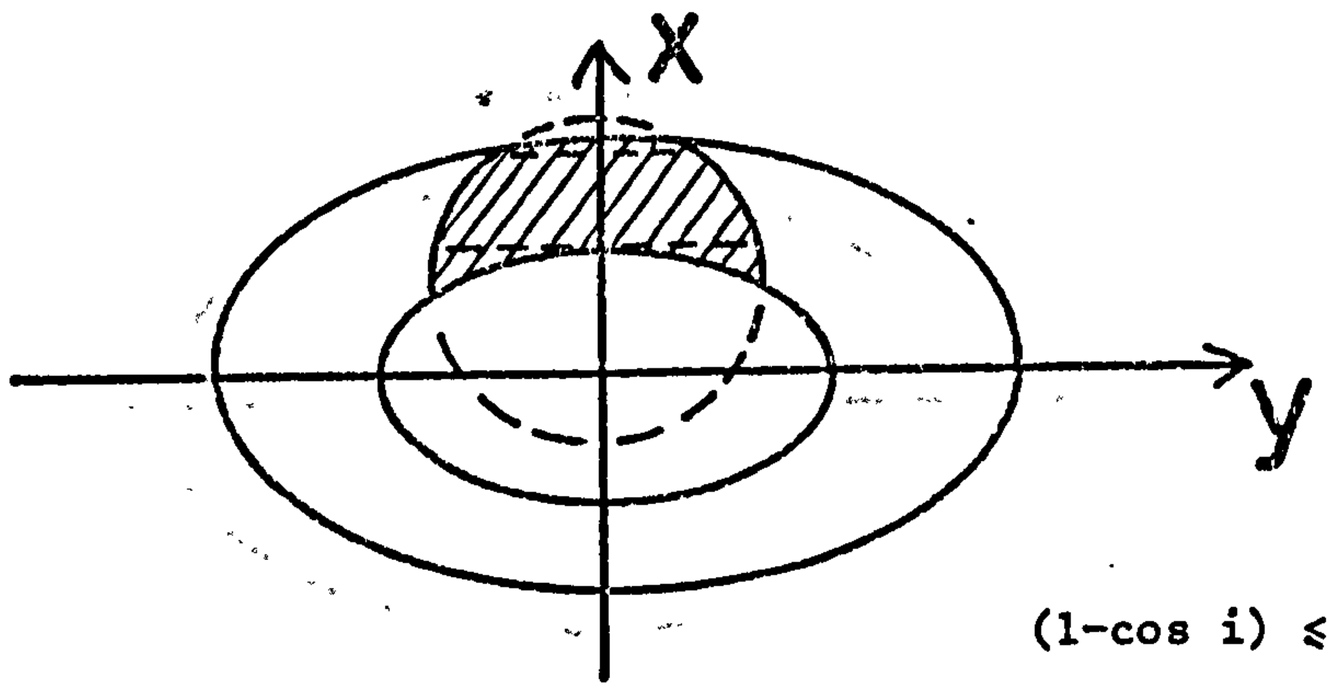

$(1-\cos i) \lesssim \tau \lesssim \psi\ (1+\cos i)$

(iii)

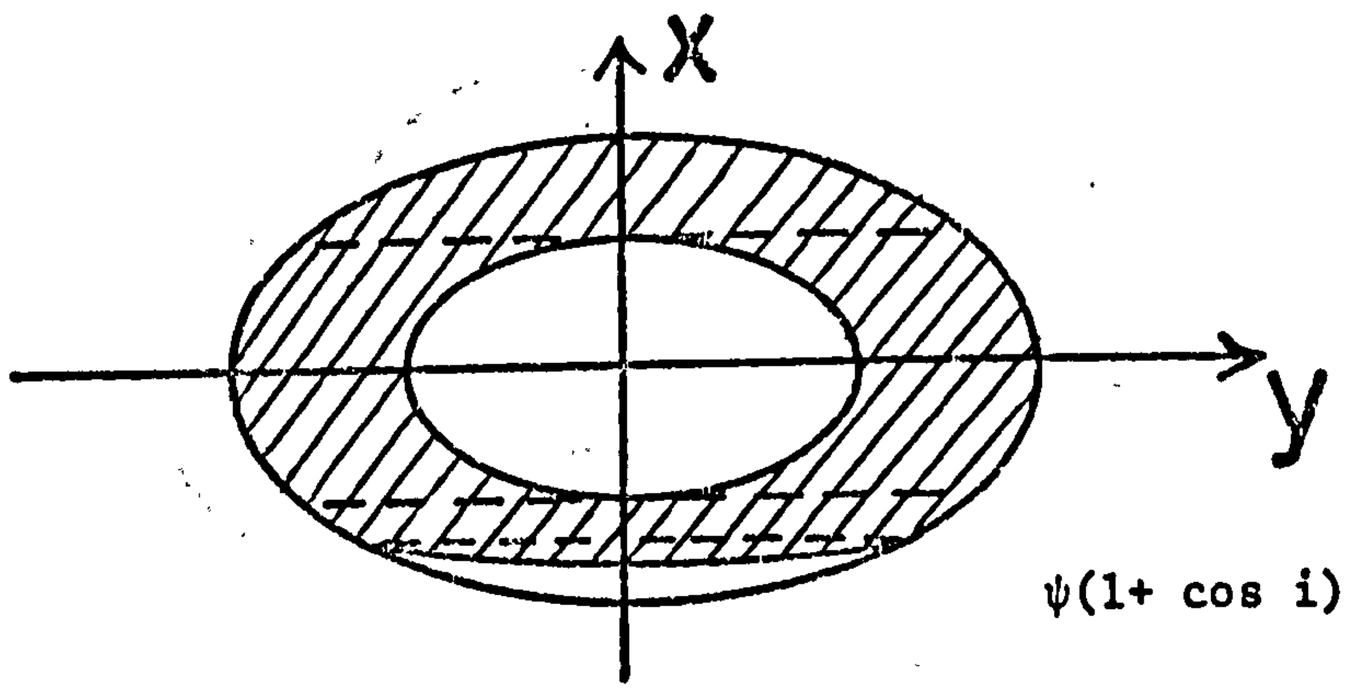

$\psi(1+\cos i) \lesssim \tau \lesssim (1+\cos i)$

Figure (6.3a) Inclined disc where $\psi \gtrsim \psi_{LIMIT}$ as seen by a distant observer. The development of the 'circle of emission' with time is shown (shaded portion of disc) broken lines are boundaries of emission regions.

(i)

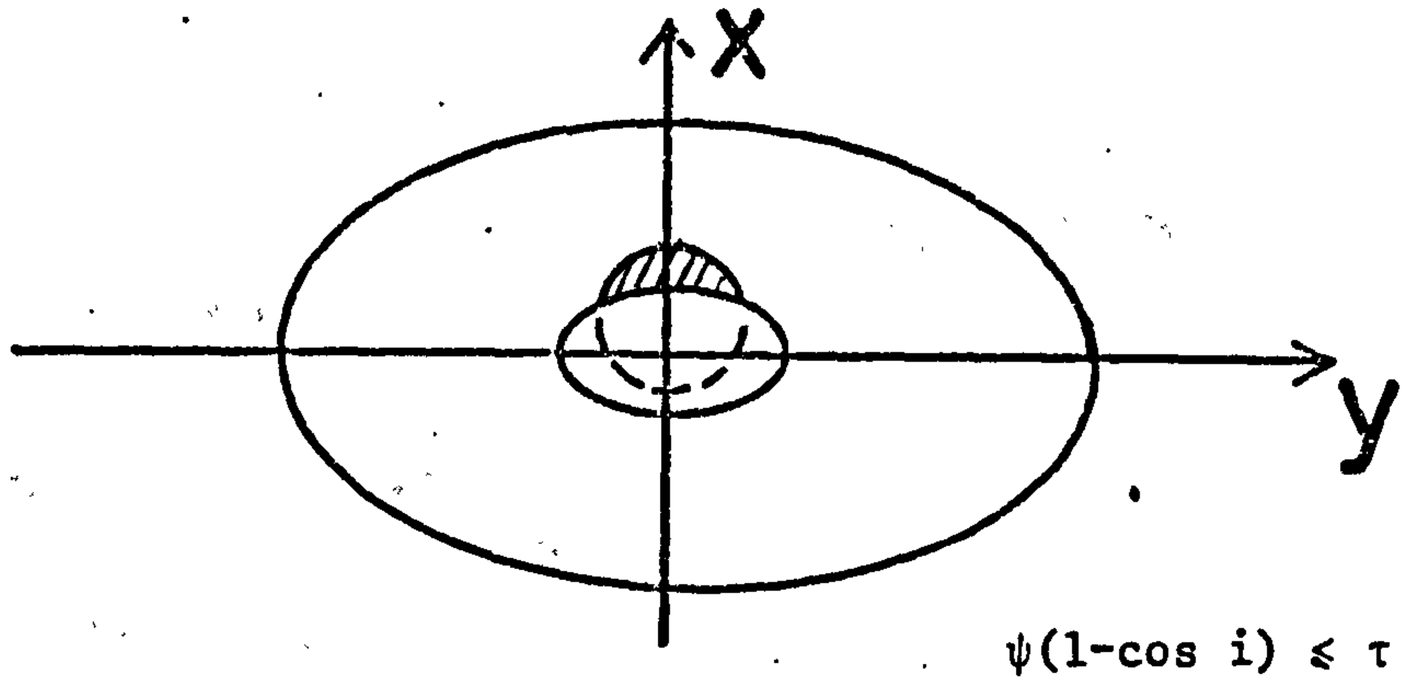

$\psi(1-\cos i) \leq \tau \leq \psi (1+\cos i)$

(ii)

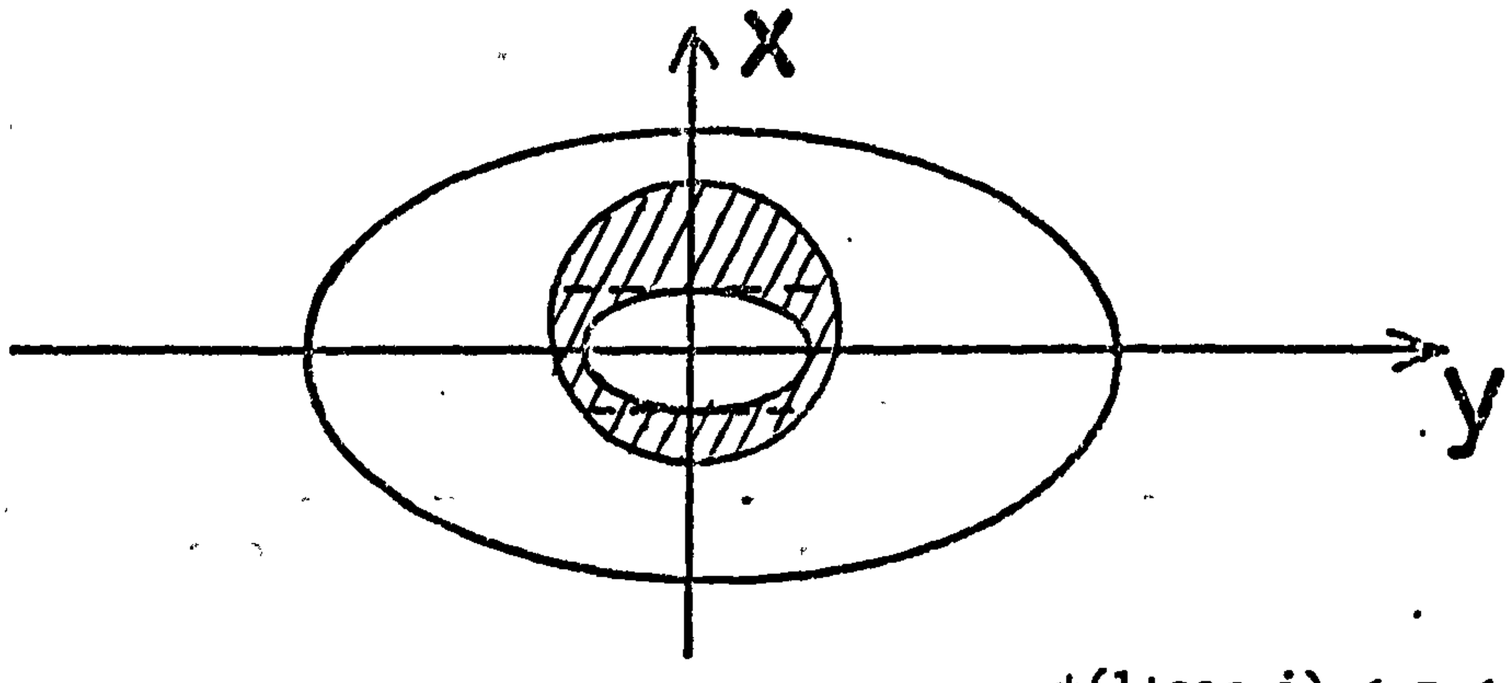

$\psi(1+\cos i) \leq \tau \leq (1-\cos i)$

(iii)

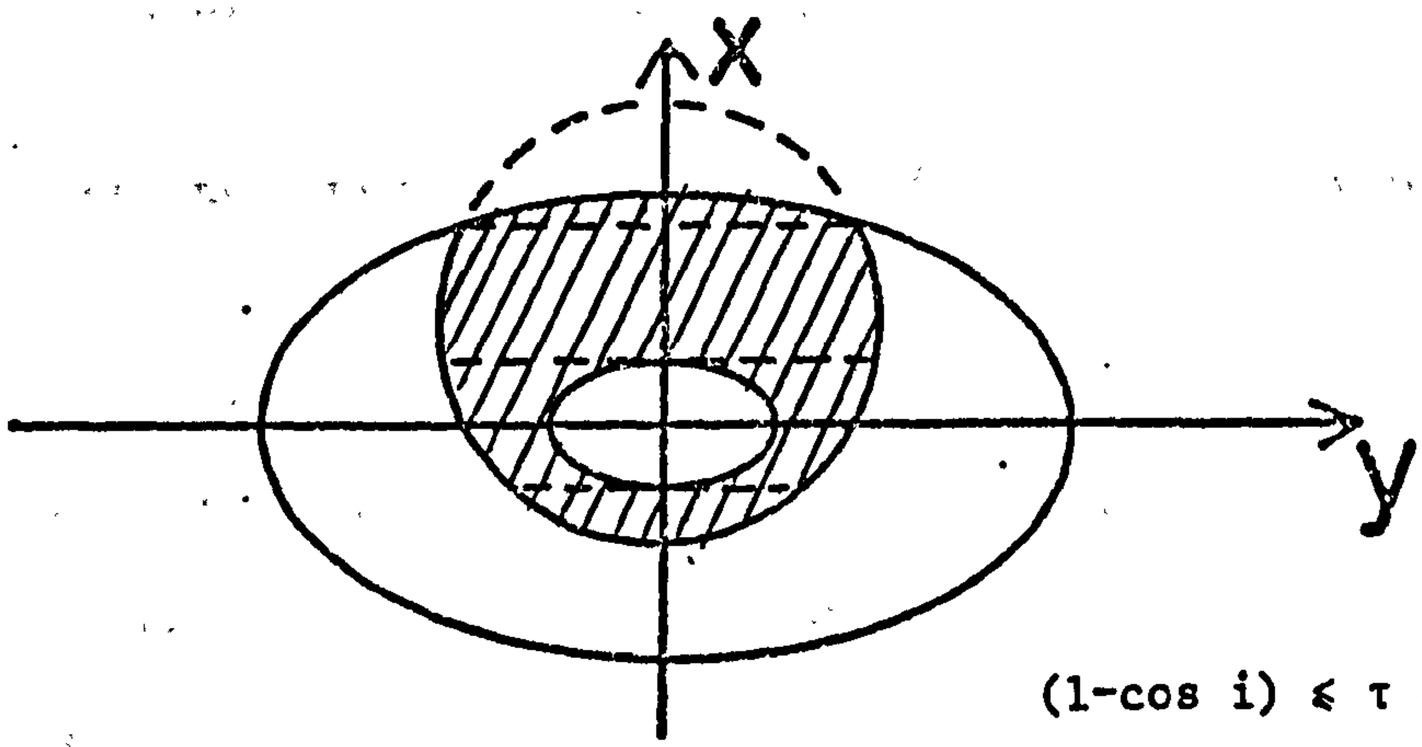

$(1-\cos i) \leq \tau \leq (1+\cos i)$

Figure (6.3b) Inclined disc where $\psi < \psi_{LIMIT}$ as seen by a distant observer. The development of the circle of emission is shown (shaded portion of disc) broken lines are boundaries of emission regions.

the form

$$f_\nu(\tau) = 2C_1' \int_{x=x_i(\tau)}^{R_1 \sin i} \int_{y=y_i(x)}^{y_c(x)} F(x, y)\, dy\, dx$$

$$+ \int_{x=R_1 \sin i}^{x_0(\tau)} \int_{y=0}^{y_c(x,\tau)} F(x, y)\, dy\, dx \quad +$$

$$\int_{x=x_0(\tau)}^{R \sin i} \int_{y=0}^{y_0(x)} F(x, y)\, dy\, dx \qquad (6.10)$$

where

$$F(x, y) = \frac{(x^2 \operatorname{cosec}^2 i + y^2)^{-\beta/2}}{\exp\left[\frac{h\nu}{kK_0 T} (x^2 \operatorname{cosec}^2 i + y^2)^{1/\alpha+4}\right] - 1} ,$$

$$y_c(x, \tau) = R(\tau^2 + 2\tau \cot i\, x/R - x^2/R^2)^{\frac{1}{2}}$$

By performing numerical integration of equations such as (6.10) for all cases and times illustrated in figures (6.3), the infra-red flux development of a disc at several inclinations for a step function central source light curve was determined. The results of these calculations are shown in figures (6.4a) - (6.4d) where the model parameters are

$$R = 2R_1 = 2 \times 10^{17} \text{ cm}$$

$$i = 90^o \quad \text{i.e. } \Delta t_0 \simeq 38\tfrac{1}{2} \text{ days}$$

$$a = 2 \times 10^{-6} \text{ cm}$$

$$\alpha = 1 \qquad \beta = 1$$

$$L = 5 \times 10^{38} \text{ erg s}^{-1} \quad \text{(step function)}$$

The results are of course purely qualitative as the disc thickness is not defined.

Figure (6.4a) Light curves at 3 wavelengths (numbers above curves are wavelengths in μm) observed from a disc of dust grains where $i = 90^{o}$, $R = 2R_1 = 2 \times 10^{17}$ cm, $\beta = 1$. The grains are assumed to be graphite spheres with $a = 2 \times 10^{-6}$ cm, $\alpha = 1$ surrounding a central source with a step function light curve ($L = 5 \times 10^{38}$ $ergs^{-1}$). The vertical scale is arbitrary.

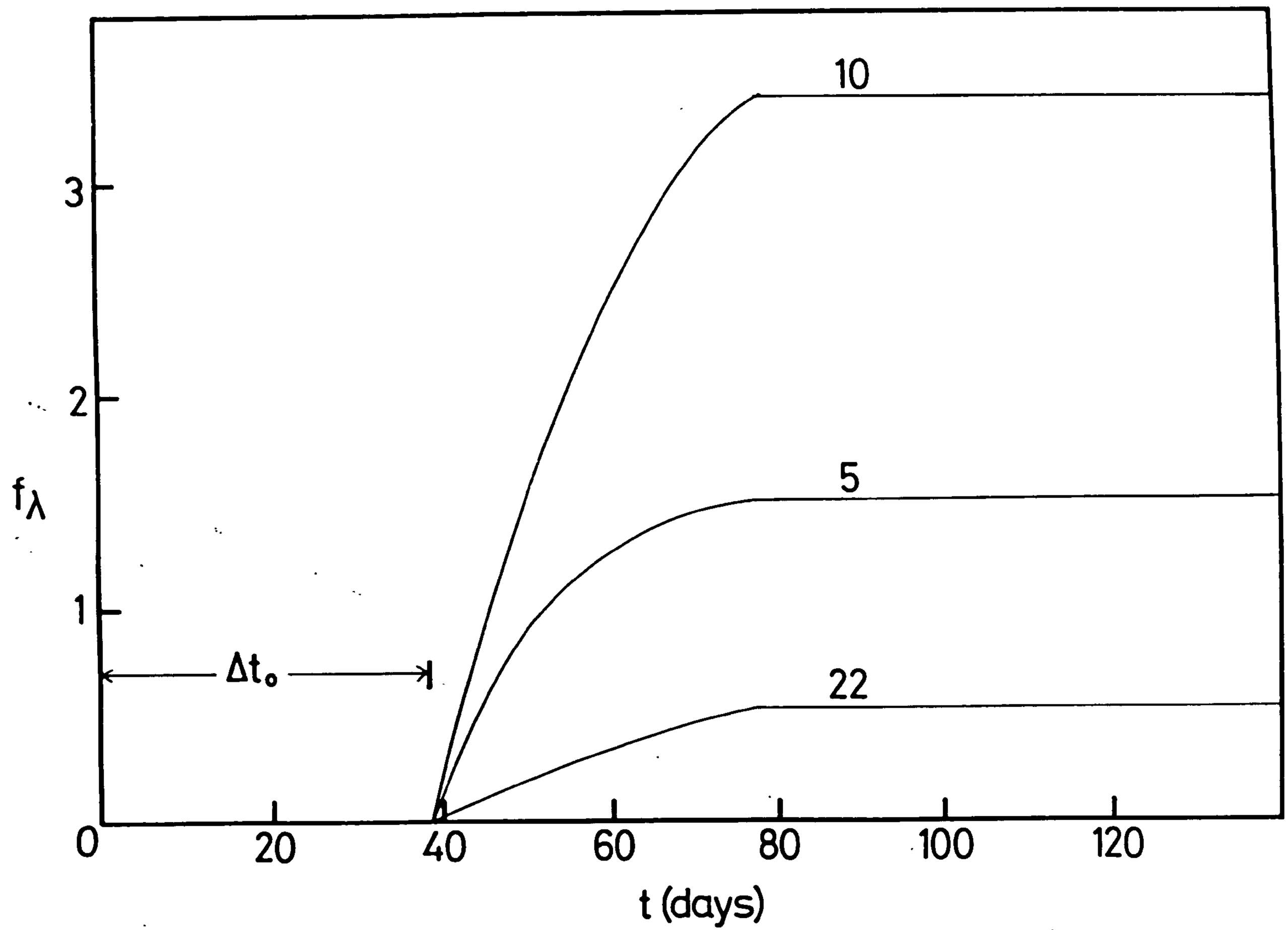
10
5
22
3
2
1
0
f_λ
Δt_o
20
40
60
80
100
120
t (days)

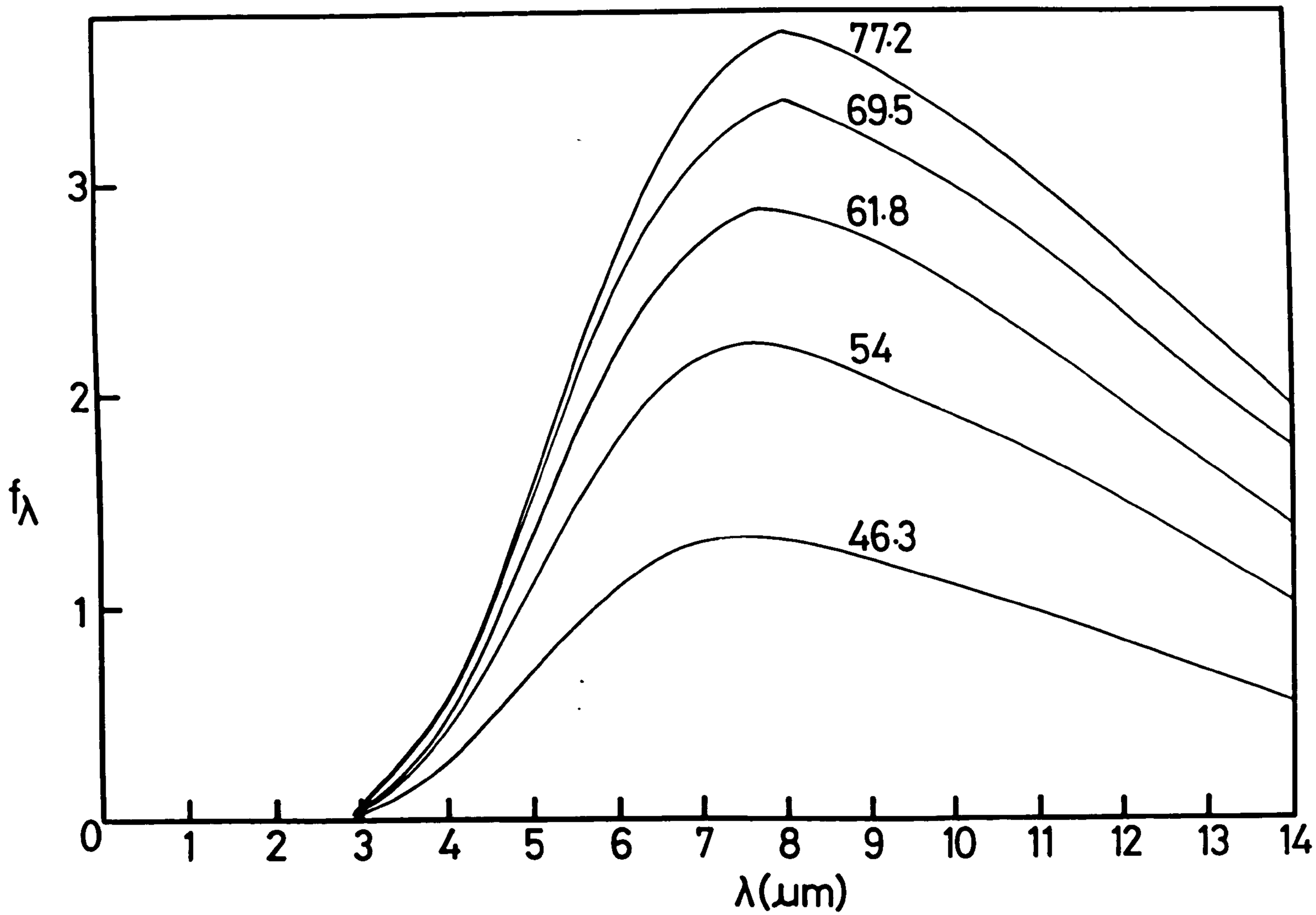

Figure (6.4b) Observed spectral development of a disc of dust grains heated by a step function central source light curve. Parameters as in figure (6.4a). Numbers over curves are time in days from central source outburst. Vertical scale arbitrary.

Figure (6.4c) Light curves observed at λ = 10 μm from a disc of dust grains at various values of inclination (given over curves). All other parameters are as in figure (6.4a). (Vertical scale arbitrary).

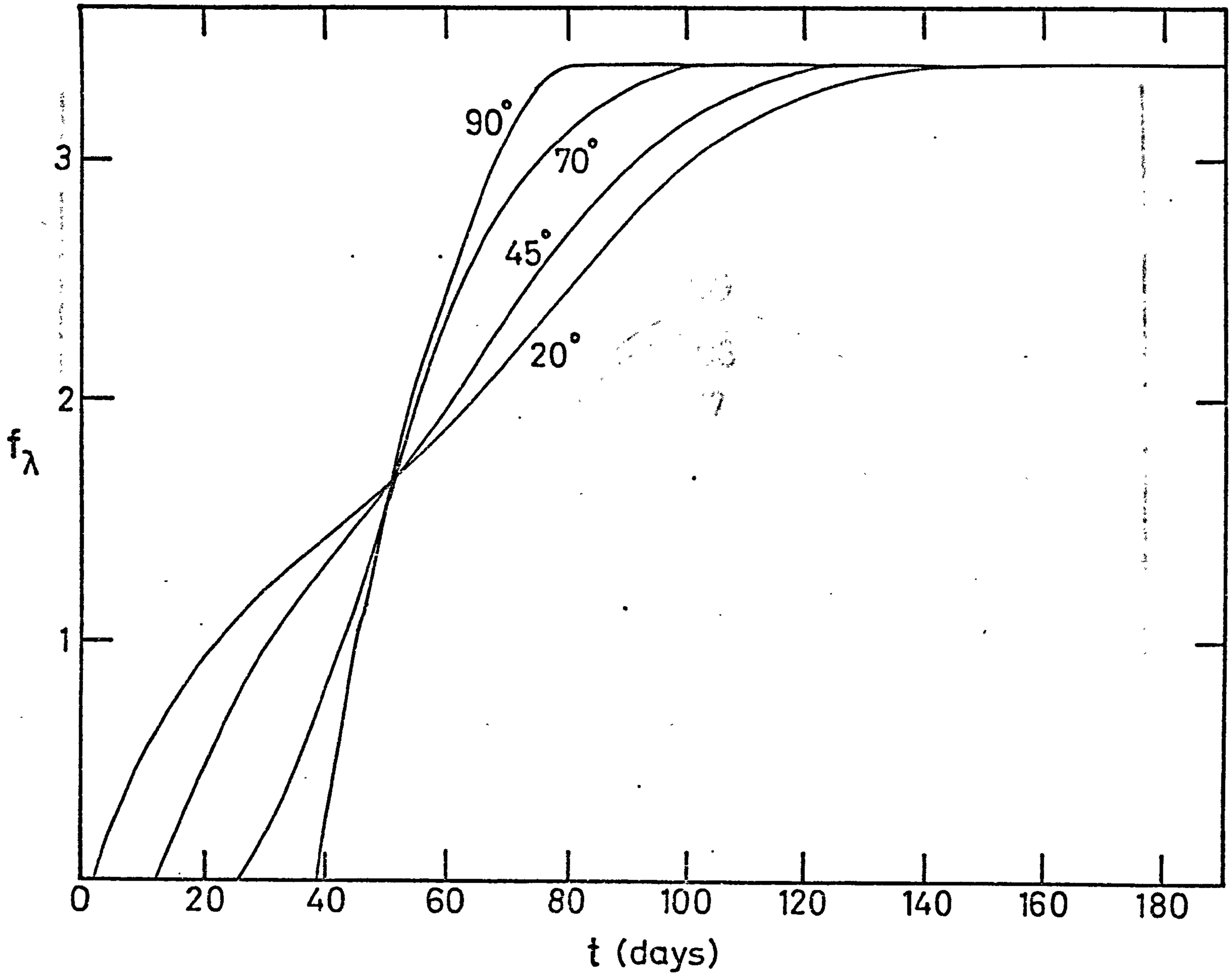
90°
70°
45°
20°
3
2
1
f_λ
0
20
40
60
80
100
120
140
160
180
t (days)

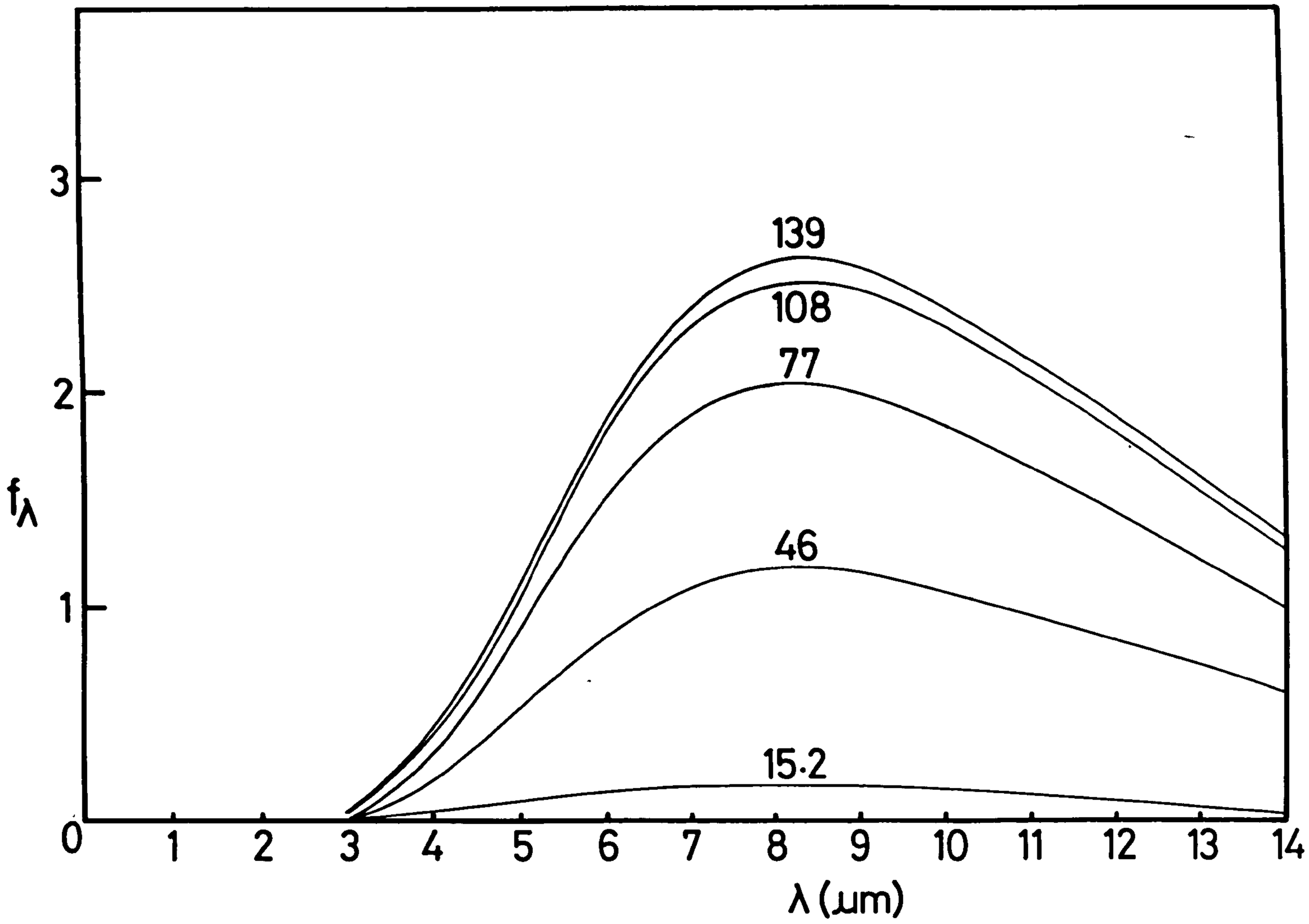

Figure (6.4d) Observed spectra from a disc with i = 45° at various times in days from outburst (numbers adjacent to curves). All other parameters are as in figure (6.4a). The vertical scale is arbitrary.

The light curves of figure (6.4a) clearly show the lag between the observation of the initial step in the central source and the response in the infra-red. There is also a clear levelling-out in the flux increase at a time corresponding to $\tau = 1$ ($i = 90^{o}$) where the emission parabola has completely filled the disc.

From the spectra of figure (6.4b) we can see that the spectrum peaks between 7 and 8.5 μm at any given time. As expected the peak shifts toward larger wavelengths with time as more distant grains are heated by the central object. Initially, for the parameters used, $T_g(R_1) = 320^{o}K$ and if the grains were perfect black bodies we would expect $\lambda_{max} \simeq 9.3$ μm. However, solution of equation (4.9) with $\alpha = 1$ gives $\lambda_{max} \simeq 7.5$ μm for the same temperature. It can be seen from the figure that at the earliest time, when emission arises mainly from grains near R_1, $\lambda_{max} \simeq 7.5$ μm as expected. The coolest grains at distance R from the central object are at a temperature $T_g(R) = 244^{o}K$. Again with $\alpha = 1$ the peak in f_λ would be expected to lie at $\lambda_{max} \simeq 9.8$ μm if all grains were at this temperature. Thus we would expect $7.5\ \mu m \lesssim \lambda_{max} < 9.8\ \mu m$ at all times which appears to be the case.

The numerically derived results were checked against the results achieved by analysis in section (6.3.1) for $10\ \mu m \lesssim \lambda \lesssim 30\ \mu m$. With 50 steps in x and y the numerical result differed by $\sim 2\%$ at 30 μm and $\sim 5\%$ at 10 μm for all values of τ used in the plots of figure (6.4a). This was taken to indicate that the numerical solution could now be used with some confidence for more complex situations.

Figure (6.4c) illustrates the effect on the infra-red curves of tilting the disc. The smaller the value of i the shorter is the interval between the initial step of the central source and the beginning of the rise in the infra-red. The peak infra-red flux is reached at later times for smaller values of i. The combination of these two effects means that the light curves must cross at a value $\psi < \tau < 1$.

Figure (6.4c) at first sight appears to imply that at t $\sim$ 50 days the flux at 10 μm will be the same for any disc inclination. However on an expanded horizontal scale the times of crossing of light curves may be seen to differ by several days.

Figure (6.4d) shows the spectral development when i = 45°. Note that although again 7.5 μm $\lesssim \lambda_{max} <$ 9.8 μm (see above) the shift in peak is less marked and the spectra are somewhat flatter than in figure (6.4b). This is to be expected as at all times there would be a greater number of more distant grains involved in emission than for larger i values.

In order to incorporate more general central source light curves into the solution, phase relationships between the central source and a grain at position (x, y) on the disc were derived. Previously we deduced in section (4.3.1) that the phase difference, Δt, between the observed flux from the central source and that from a grain at polar co-ordinates (r, θ) is given by

$$\Delta t = \frac{r}{c}(1 - \cos\theta) \qquad \text{(c.f. equation 4.19)}$$

Here $r\cos\theta \equiv x\cot i$ and $r \equiv (x^2 \operatorname{cosec}^2 i + y^2)^{\frac{1}{2}}$, therefore

$$\Delta t = \frac{x}{c}\left\{(\operatorname{cosec}^2 i + y^2/x^2)^{\frac{1}{2}} - \cot i\right\} \qquad (6.11)$$

Incorporation of the phase relation given by equation (6.11) into the numerical solution of the transfer equation enabled the qualitative models of the next section to be set up.

6.4.1 Possible Application of the Disc Model to the Infra-red Development of some Novae

As a test of the flexibility of the numerical integration programmes the central source is now given a light curve of the form $L = L_0 \exp(-\omega t)$ for all t > 0. As in chapter 5 this was used to simulate the possible

time dependence of the heating function of a nova. The resulting light curves of figure (6.5a) where $i = 45^{o}$ are qualitatively very similar to those observed in some novae such as Serpentis 1970, Aquilae 1975 and Vulpeculae 1976 (see Chapter 2). The most obvious similarity is the lag, Δt_0, between the heating function peak (taken in this case to coincide with $(M_v)_{min}$) and the initial rise in the infra-red flux.

Figure (6.5b) illustrates the spectral development in this case. As expected the flux builds up with time to a maximum and then falls away. The actual peak of emission shifts relatively rapidly to longer wavelengths giving the impression of a cooling 'black body'. Thus each wavelength dominates the emission at a specific time, which is of course later for longer wavelengths. Note that in figure (6.5b) we can also see the shallowing of the spectrum at later times. Here the most distant grains are brought within the emission circle at the same observer time as a few more of the nearer ones.

We have already suggested in chapter 5 that rapid condensation of dust grains may not be responsible for the late infra-red development of some novae. In this case we would require the grains to have condensed from previous outburst ejecta over the time interval between outbursts. Here however we require the formation of a disc of grains at a considerable distance from the nova.

It is well established that ejection of material from novae is not isotropic. The generally accepted model is that of ejecta in the form of an equatorial ring or disc and possibly polar blobs (e.g. Hutchings, 1972; see also figure (3.6)). If the grains subsequently condensed in the ejected ring or disc a situation geometrically similar to the one envisaged here would arise. With the ring or disc inclined at an angle i to the line of sight the infra-red lag would arise purely from the geometry of the situation as described above.

If we assume that the type of grain formed in nova ejecta is fairly

Figure (6.5a) Light curves at 3 wavelengths (numbers above curves are wavelengths in μm) as observed from a disc of graphite grains ($a = 2 \times 10^{-6}$ cm, $\alpha = 1$) where $R = 2R_1 = 2 \times 10^{17}$ cm, $\beta = 1$, $i = 45^{o}$. The central source is nova in form with $L_0 = 5 \times 10^{38}$ $ergs^{-1}$ and $\omega = 10^{-7}$ s^{-1}. The vertical scale is arbitrary.

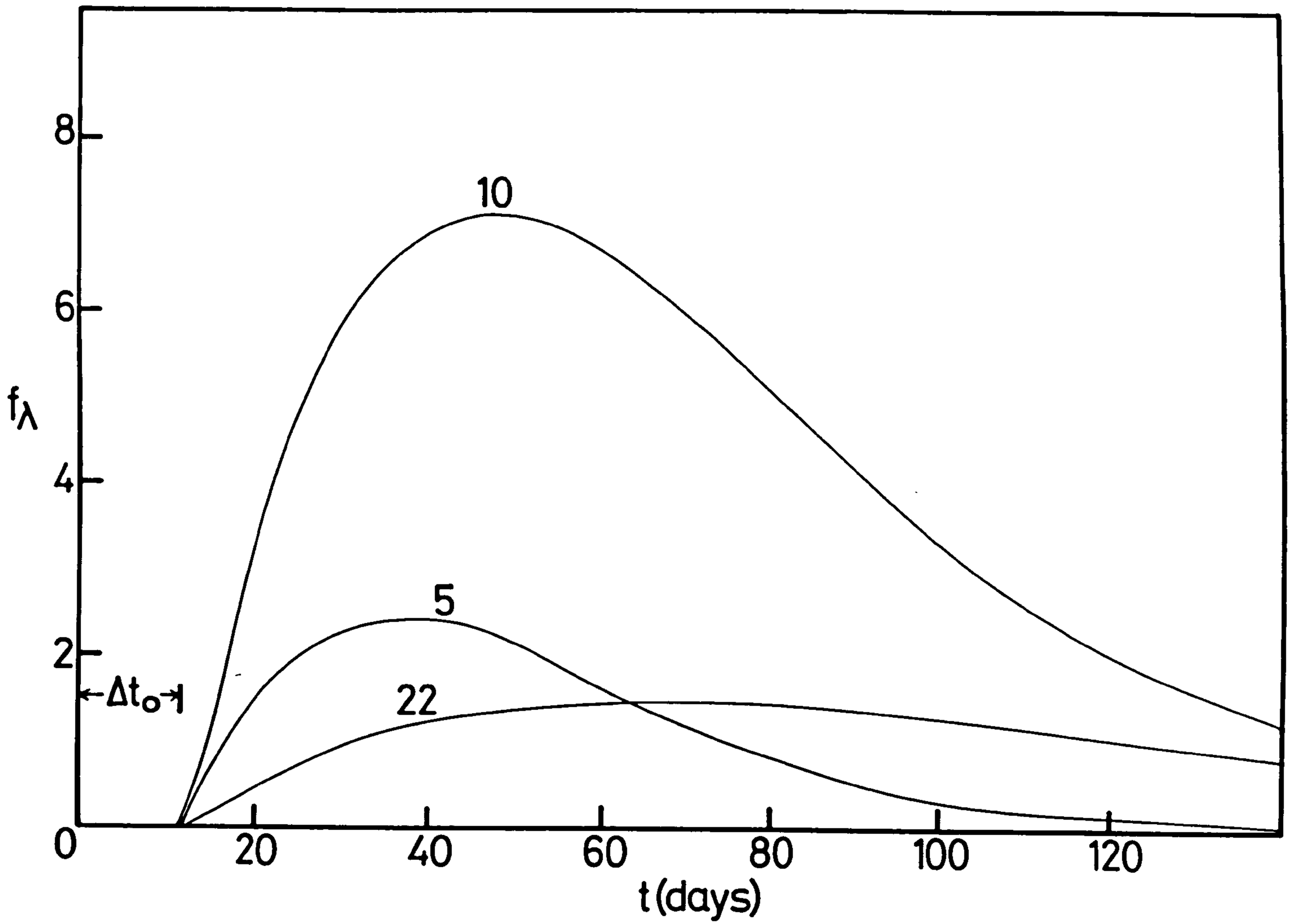
8
6
4
2
0
f_λ
$\leftarrow \Delta t_o \rightarrow$
10
5
22
20
40
60
80
100
120
t (days)

Figure (6.5b) Observed spectra from a disc with $i = 45^{o}$ and a nova-like central source light curve and other parameters as in figure (6.5a). The numbers adjacent to each curve refer to the time in days from the outburst. The vertical scale is arbitrary.

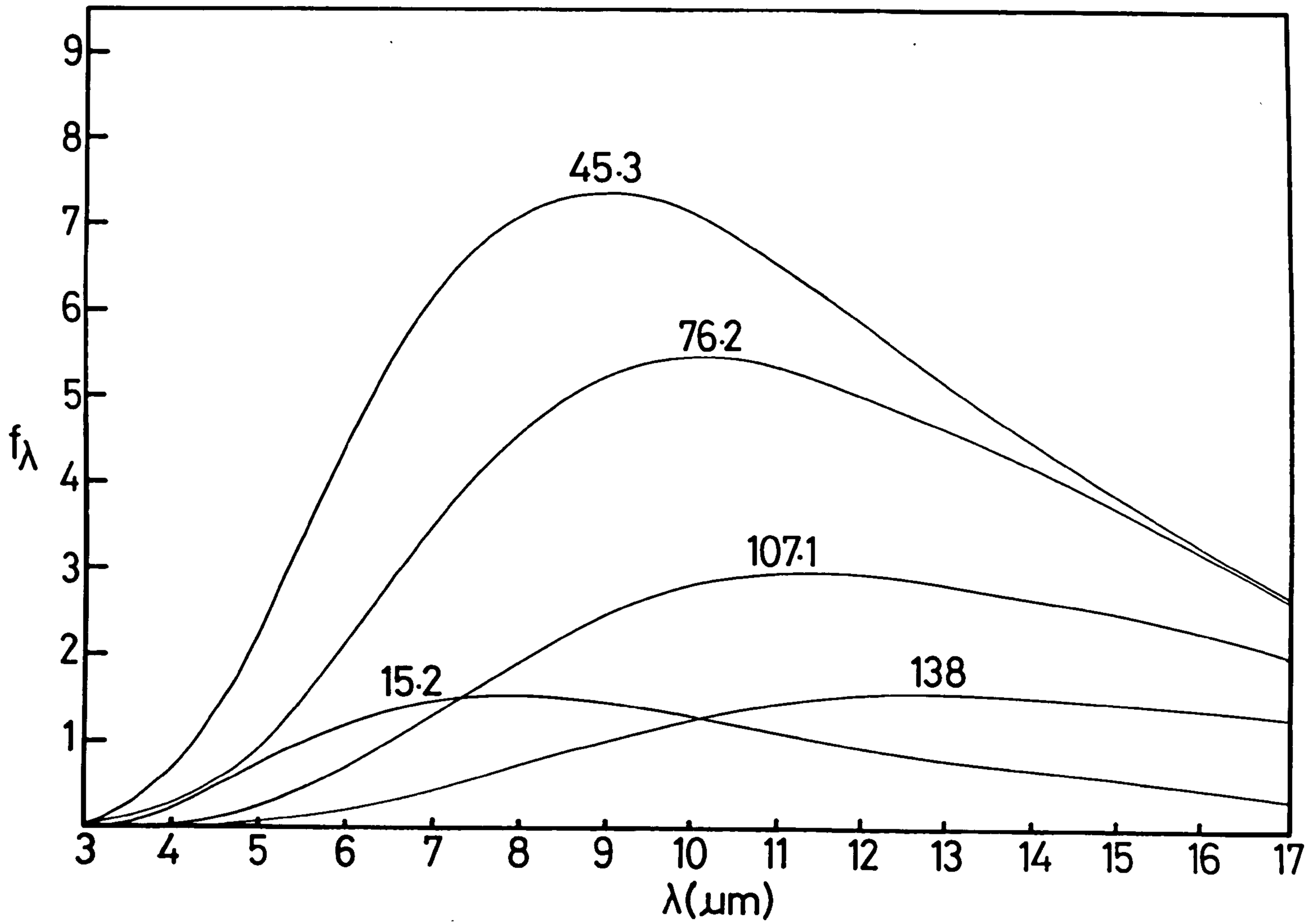
9
8
7
6
5
4
3
2
1
f_λ
45.3
76.2
107.1
15.2
138
3
4
5
6
7
8
9
10
11
12
13
14
15
16
17
λ(μm)

Figure (6.5c) Light curves at four wavelengths (numbers above curves are wavelengths in μm) as observed for the nova model parameters of figure (6.5a) except $i = 70^{o}$. The vertical scale is arbitrary.

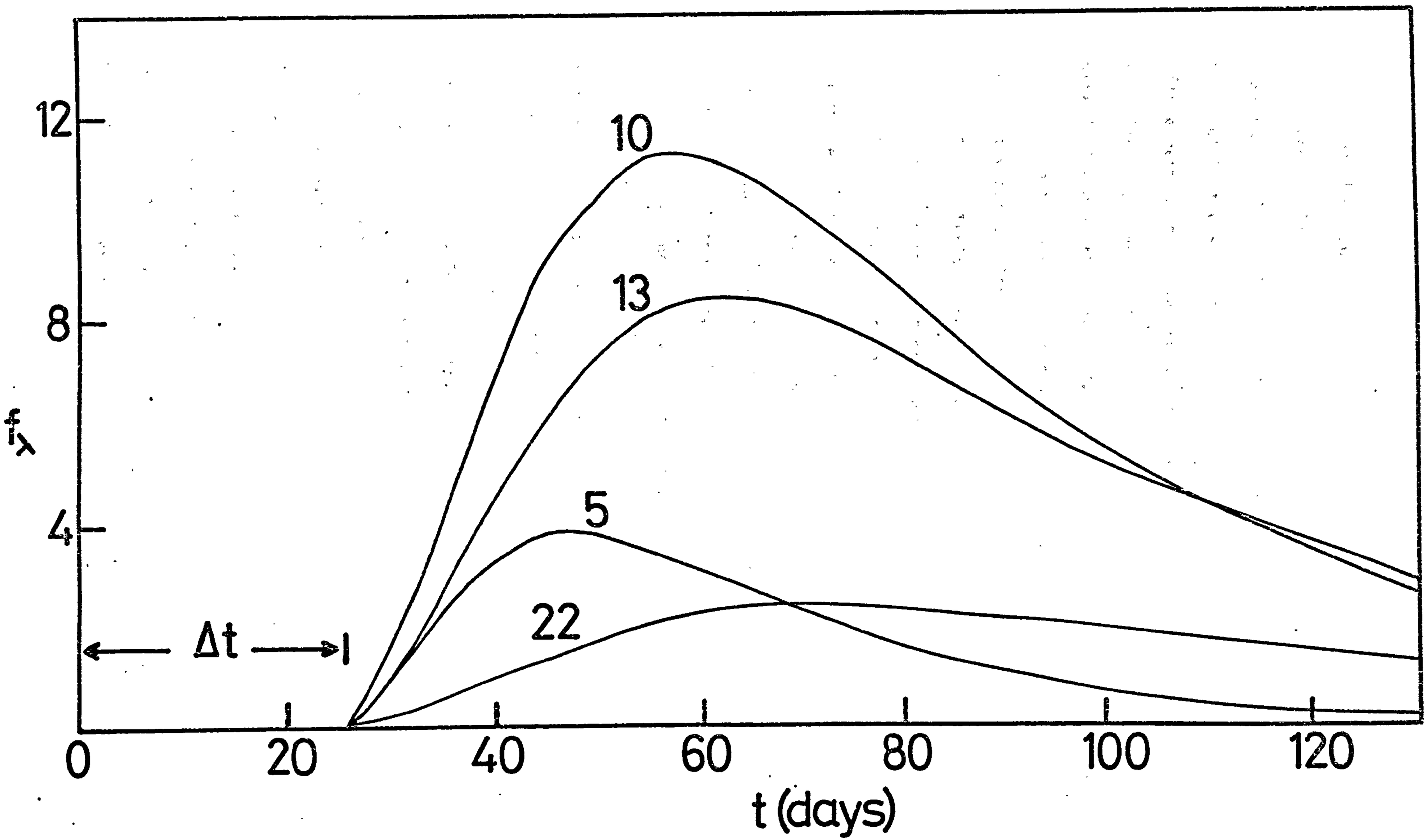
12
8
4
f_λ
10
13
5
22
Δt
0
20
40
60
80
100
120
t (days)

consistent between novae and that the emission at early times is dominated by that from the hottest grains situated at R_1 (see above) then with $T_g(R_1) \propto (L/R_1^2)^{1/\alpha+4}$ we can see that the grain temperature will not be too sensitive to L (which ranges over an order of magnitude between the novae considered here). Thus the wavelength of peak emission $\lambda_{max} \simeq$ const. $R^{2/\alpha+4}$ at early times. If the disc of grains were inclined at the same angle i for all novae then there would be a correlation between the spectral peak at early times and the lag, Δt_0. In other words the longer the wavelength λ_{max} the larger the value of Δt_0. This relationship would also emerge for a large enough sample of novae where disc inclinations would average out.

Table (6.1) contains the relevant data available on five novae. The values of Δt_0 were found from extrapolation of early infra-red observations at long wavelengths, where the central source contribution would be relatively small. The data in the table suggest there may be a correlation between the initial peak wavelength and the lag.

Closer examination however shows that there are several objections to this model for most infra-red novae. Firstly the clear correlation between transition and infra-red rise in Novae Serpentis 1970 and Vulpeculae 1976 is difficult to explain. Secondly even if $i \sim 90^o$ the inner cavity radius in the case of Nova Vulpeculae for example would have to be $\sim 1.5 \times 10^{17}$ cm; this, as we have seen, gives grain temperatures $\sim 300^oK$ for $L = 5 \times 10^{38}$ erg s^{-1} and $\alpha = 1$, $a = 2 \times 10^{-6}$ cm. This is far lower than the 900^oK of the 'isothermal' stage of this nova (Ney & Hatfield, 1976). To increase the grain temperature to this value either the luminosity of the central object would have to be increased by a factor of ~ 250 or the grain size reduced by the same amount. Even a combination of the two to achieve this increase would entail assuming rather unlikely values of a and L. It is in any case unlikely that $i = 90^o$ and for any value of $i < 90^o$ R_1 would need to be even larger.

Table 6.1

Nova	λ_{max} (μm)	Δt_0 (days)
Serpentis 1970	3.5 ± 1	56 ± 10
Aquilae 1975	3 ± 1	$\gtrsim 8$
Cygni 1975	$\gtrsim 4.8$	$\sim 100 \pm 20$
Vulpeculae 1976	3.5 ± 1	60 ± 10
Cygni 1978	$\lesssim 3.6$	30 ± 10

The third main objection to this model is that it assumes that grains and disc inclinations will be similar for this small sample of novae. Both of these assumptions will of course be erroneous. We would expect any correlation such as there may be in table (6.1) to be masked by the varying inclinations likely in this small sample.

Finally if the infra-red luminosity is of the order of the central object's luminosity then the shell of grains needs not only to be opaque but also to cover most of the 'sky' as seen from the central object; obviously the thin disc will not do this. As we make the disc thicker, or make it torroidal Δt_0 will decrease until for total 'sky' coverage $\Delta t_0 = 0$. It appears that in the case of Nova Serpentis 1970 at least $L_{IR} \sim L_{UV}$ and thus the disc model could not apply here.

6.4.1 Specific Application to Nova Cygni 1975

Of the five novae of table (6.1) only one may be adequately described by this model and that is Nova Cygni 1975. This nova apparently had a late developing infra-red excess of relatively small proportions (see Chapter 2). Although it is still uncertain whether this excess was thermal or not in nature (Ferland & Shields, 1978) we will assume for the present that it was.

If we refer to figure (2.8) we can see that the peak flux appears to have arisen at $\sim$ 10 μm. Extrapolating the 10 μm rise back in time it seems to have begun at $\sim$ 100 days from outburst, thus $R_1 \gtrsim 2 \times 10^{17}$ cm. With a peak luminosity of $\sim 2 \times 10^{39}$ erg s^{-1} (Wu & Kester, 1977) and grains similar to those already discussed in this chapter ($a = 2 \times 10^{-6}$ cm, $\alpha = 1$) the grain temperature at R_1 would be $\lesssim 300^{o}K$ which with $\alpha = 1$ gives $\lambda_{max} \gtrsim 8.3$ μm. Therefore we have an apparently self-consistent delay and grain temperature for this nova.

The luminosity of the infra-red component L_{IR} (if assumed to be thermal with $\lambda_{max} = 10$ μm) is $\sim 3 \times 10^{34}$ erg s^{-1}. Thus the ratio of

$L_{IR}/L_{UV} \sim 1.5 \times 10^{-5}$ and either the dust shell is optically thin or, as we assume here, it only covers a small fraction of the central object's sky.

As with many novae there is evidence that the outburst of Nova Cygni 1975 was not isotropic. Boyarchuk and Gershberg (1977) found that the ejecta of the 1975 outburst of this nova were distributed in an equatorial ring (inclination $\sim 60^{o}$ to the line of sight of the observer) and two polar blobs (see figure (3.6)). As we have seen in chapters 2 and 5 Brecher et al. (1977) ascribed the lack of thermal X-rays from the nova to the absence of pre-outburst circum-nova material. With condensed grains (and presumably other ejecta) at the distance we require for R_1 the concurrent ejecta would not encounter this material for $\sim$ 30 years (assuming ejection velocities $\sim$ 2000 kms^{-1}) and hence would not produce the expected X-ray flux at early times.

Because of this lack of evidence of pre-existing circum-nova material it has been conjectured that this was the first outburst of Nova Cygni 1975. Obviously we must presume for our purposes that it was at least its second and that some grains had condensed from a previous outburst. This model might well fit in with that of chapter 5 if the inclination of the disc at each outburst were slightly different. As time went on the material from successive outbursts would lead to grain condensations in many directions from the central object thus leading to spherical symmetry; hence the models of the previous chapter would then apply. A correlation between speed class and amount of circum-nova material would be expected if a nova becomes 'slower' with age.

6.5.1 Conclusion

We have seen in this chapter that with a disc of dust grains surrounding a variable central source the relative position of the observer to the disc is crucial in determining the behaviour of the

observed re-radiated infra-red flux. For example by increasing or decreasing the inclination of the disc, i, not only the light curves but also the observed spectra are noticeably altered.

The general model does not seem to adequately explain the infra-red development of most of the novae studied. It is believed that the heating function theory outlined in chapter 5 is more successful in fitting the observations except possibly in the case of Nova Cygni 1975 where the disc model may apply.

Again in this chapter we have assumed that the grains are static and not affected by evaporation. In the following chapter we will examine the effects of evaporation of grains on the dust distribution and on the subsequent infra-red flux.

Chapter 7

Grain Evaporation

7.1.1 Introduction

The theoretical models we have employed so far in this work have all assumed that the dust distribution from which the infra-red flux arises is composed of static, identical dust grains which suffer no changes in composition or size as the central source flux varies. In a real situation these assumptions will not be strictly valid. This chapter therefore briefly explores the effect of one grain destruction mechanism (i.e. evaporation) on the observed grain distribution and infra-red flux.

Section (7.2.1.) describes the evaporation rates of isolated small graphite spheres exposed to differing amounts of incident radiation from a constant luminosity source. The value $\alpha = 1$ is assumed throughout but the qualitative results are not sensitive to changes in α. This section includes an investigation of the inclusion of evaporation in the energy balance equation.

In section (7.3.1) we discuss the evaporation of grains in an optically thin cloud from the point of view of centrally and externally placed observers. From here onwards the central source is assumed to have a step function light curve with a nova-like luminosity ($L = 5 \times 10^{38}$ ergs^{-1}). The infra-red flux as observed by a distant observer is found for a spherical shell and expanding cavity with different grain density distributions in section (7.3.2). Comparison is then made qualitatively with the observed behaviour of Nova Vulpeculae 1976 in the infra-red.

7.2.1 Grain Evaporation Rate

For an isolated grain of radius a at temperature T_g the rate of decrease of grain radius with time, $\dot{a}$, is given by equation (3.8). Strictly the grain temperature should be derived from the energy balance between the absorbed incident flux, F_A, reradiated flux, F_E and the rate of energy loss in vaporising the surface layers of the grain P_V. Thus far we have neglected the latter for as we shall discover it only becomes important for grains at very high temperatures.

We may express the energy balance in the form

$$F_A = F_E + P_V \tag{7.1}$$

where F_A and F_E are given by the terms on the left and right hand sides of the equality in equation (3.9) respectively. The rate of change of grain energy by vaporisation is equivalent to $-\dot{m}_g H$ where $\dot{m}_g$ is the rate of grain mass loss and H is the heat of vaporisation of the grain material. Thus by expressing $\dot{m}_g$ in terms of $\dot{a}$ from equation (3.8) we can see that

$$P_V = 4\pi a^2 H \, p_{sat}(T_g) \left(\frac{m_c}{2\pi \, k \, T_g}\right)^{\frac{1}{2}} \tag{7.2}$$

(assuming an accommodation coefficient $\alpha_c = 1$).

For graphite grains the saturated vapour pressure of carbon with temperature is tabulated in Wickramasinghe (1967), p. 88. From these results the following relationship was derived

$$p_{sat}(T_g) \simeq p_0 \exp\left(-\frac{T_0}{T_g}\right) \tag{7.3}$$

where $p_0 = 1.322 \times 10^{14}$ dyne cm^{-2} and $T_0 = 8.575 \times 10^4$ ^oK.

In chapter 4 and subsequent chapters grain temperature has been derived from the energy balance $F_A = F_E$. This led to the derivation

of equation (4.3), which may be expressed as

$$T_g \simeq K_0 \left[\frac{L\, Q^*_{abs}}{r^2\, a} \right]^{1/\alpha+4} \qquad (7.4)$$

where

$$K_0 = \frac{c^2}{32\pi\, h\, Q_0^{\pi}} \left(\frac{h}{k} \right)^{\alpha+4} \left\{ \Gamma(\alpha+4)\ \zeta(\alpha+4) \right\}^{-1}$$

We can see from equation (7.4) that T_g is grain size dependent due to the dependence of Q_{abs} on a in the infra-red. We may also note that the product $L\, Q_{abs}$ is equivalent to the heating function HFN of chapter 5. Q_{abs} is thus effectively the Planck mean of absorption $\bar{Q}_{abs}$ as defined by Gilman (1974), which is also grain size dependent. However it would appear from Gilman's (1974) work that for $T_* >> 3 \times 10^4$ °K (as in the case of a nova beyond transition) $\bar{Q}_{abs} \simeq 1$ for all $a \gtrsim 10^{-7}$ cm in the case of graphite spheres.

In order to compare the effects of inclusion and exclusion of energy loss through vaporisation in the energy balance equations on the subsequent value of T_g, equation (7.1) was solved iteratively using Newton's method. A value of H = 170.4 k cal/g atom for graphite was taken from Ubbelohde and Lewis (1960) p. 53. This value of T_g was then compared with the solutions of equation (7.4) for $L = 5 \times 10^{38}$ $ergs^{-1}$, and $\alpha = 1$, several values of $10^{-7} \lesssim a \lesssim 2 \times 10^{-6}$ cm and three values of the central source-grain distance, r. These r values are differentiated by curves (a), (b) and (c) in figure (7.1). In this figure $T_g(2)$ is the grain temperature derived from the full treatment including vaporisation and $T_g(1)$ is derived from equation (7.4) neglecting vaporisation.

It can be seen from figure (7.1) that the smaller the value of r the greater is the discrepancy between $T_g(1)$ and $T_g(2)$. This is because

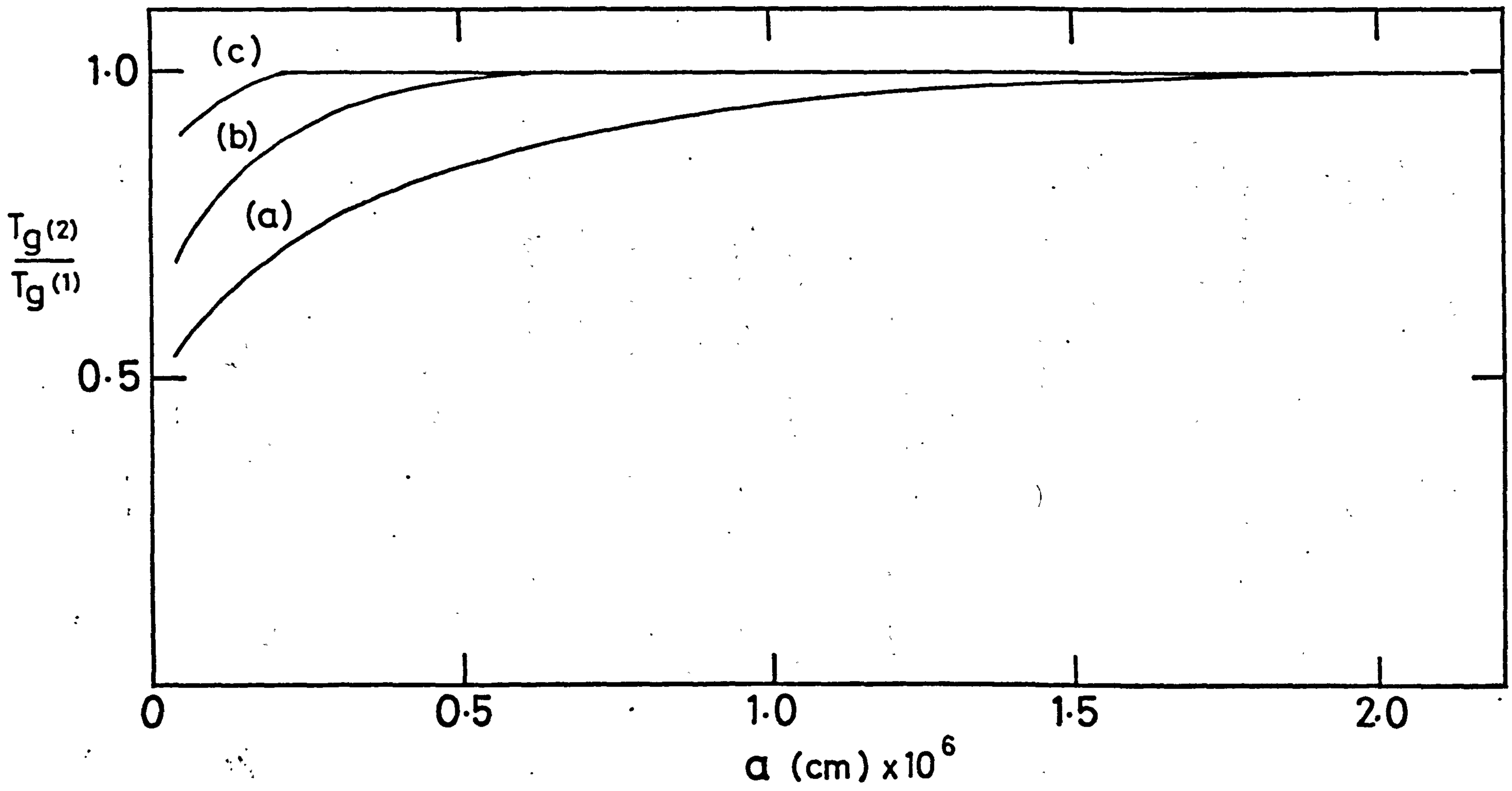

Figure (7.1) The ratio of grain temperatures derived from consideration of the energy balance including vaporisation (Tg(2)) and excluding vaporisation (Tg(1)). Curves (a), (b) and (c) refer to r = 5 x 10^{14} cm, 10^{15} cm and 2 x 10^{15} cm respectively from a central source with L = 5 x 10^{38} ergs^{-1}. The grains are assumed to be graphite spheres with α = 1.

the higher the grain temperature, the greater is the effect of the increased energy loss through vaporisation. This in turn lowers the temperature from that expected when vaporisation is neglected in the energy balance equation (7.1). For example at $r = 5 \times 10^{14}$ cm for 5×10^{-7} cm grains $T_g(1) = 3587^{o}K$ whereas $T_g(2) = 3015^{o}K$. At $r = 2 \times 10^{15}$ cm for the same grain size, $T_g(1) = 2061^{o}K$ and $T_g(2) = 2059^{o}K$. It would appear that for grain temperatures $\lesssim 2500^{o}K$, which we have so far considered, equation (4.3) is a very good approximation for T_g.

If we now substitute equation (7.3) into equation (3.8) we arrive at an expression for the evaporation rate of an isolated grain of the form

$$\dot{a} = - \frac{p_0}{s} \exp\left(- \frac{T_0}{T_g}\right)\left(\frac{m_c}{2\pi\ k\ T_g}\right)^{\frac{1}{2}} \qquad (7.5).$$

It will be appreciated that in the analysis that follows we are justified in taking the grain temperature derived from equation (7.4) as being correct as for $T_g \gtrsim 2500^{o}K$, $\dot{a} \gtrsim 6 \times 10^{-8}$ cms^{-1}. Thus for high temperatures where the difference between $T_g(1)$ and $T_g(2)$ is large evaporation is in any case very rapid.

If we now substitute equation (7.4) into equation (7.5) we have

$$\dot{a} \simeq - A_0' \, a^{1/2\alpha+8} \exp\left(- A_1' \, a^{1/\alpha+4} \right) \qquad (7.5)$$

where

$$A_0' = \frac{p_0}{s}\left(\frac{m_c}{2\pi\ k\ K_0}\right)\left(\frac{r^2}{L}\right)^{1/2\alpha+8},$$

$$A_1' = \frac{T_0}{K_0}\left(\frac{r^2}{L}\right)^{1/\alpha+4}$$

and Q^*_{abs} is taken to be equal to one.

The evaporation time t_{evap} of a grain from radius $a = a_0$ to $a = 0$ is thus given by

$$t_{evap} \simeq \frac{1}{A_0'} \int_0^{a_0} \exp\left\{A_1' a^{1/\alpha+4}\right\} a^{-1/2\alpha+8} \, da \qquad (7.7)$$

Equation (7.7) is solvable by the method of integration by parts for half integer values of α. This served as a check on the numerical solutions used extensively later.

For a given source the evaporation time of a grain will depend on several factors. If we assume (i) that the grains are graphite spheres (with $\alpha = 1$); (ii) that they are situated in a medium which is optically thin to ultra-violet radiation; (iii) that the ambient gas density is low enough for recondensation to be ignored (i.e. we can use equation (7.7) as it stands); then the evaporation rate will depend on r, L and a_0.

Numerical integration of equation (7.7) for a source with $L = 5 \times 10^{38}$ ergs^{-1} ('nova') and $L = 10^{44}$ ergs^{-1} ('Seyfert nucleus') for various values of a and r produced the results shown in figure (7.2). The dotted line shows the distance at which a black body would have $T_{BB} = 2000^{o}K$ (this is often taken as the maximum temperature at which graphite grains can exist).

We can see from figure (7.2) that a dust grain with $a = 10^{-6}$ cm for example would not survive for sufficient time at any distance $r \lesssim 2 \times 10^{15}$ cm to radiate continuously over the timescales of $\sim$ 100 days required in the nova models of chapter 5.

When the integration was performed to determine the evaporation time down to half mass it was found that a figure such as (7.2) would not show up any difference in the resulting evaporation distances.

Figure (7.2) Evaporation time, t_{evap}, against distance, r_1 from a 'nova' ($L = 5 \times 10^{38}$ ergs^{-1} - lower scale) and a 'Seyfert nucleus' ($L = 10^{44}$ ergs^{-1} - upper scale). The grains are assumed to be graphite spheres with $\alpha = 1$. Grain size in μm is given above each curve. The dashed line gives the equivalent distance of a black body at 2000°K.

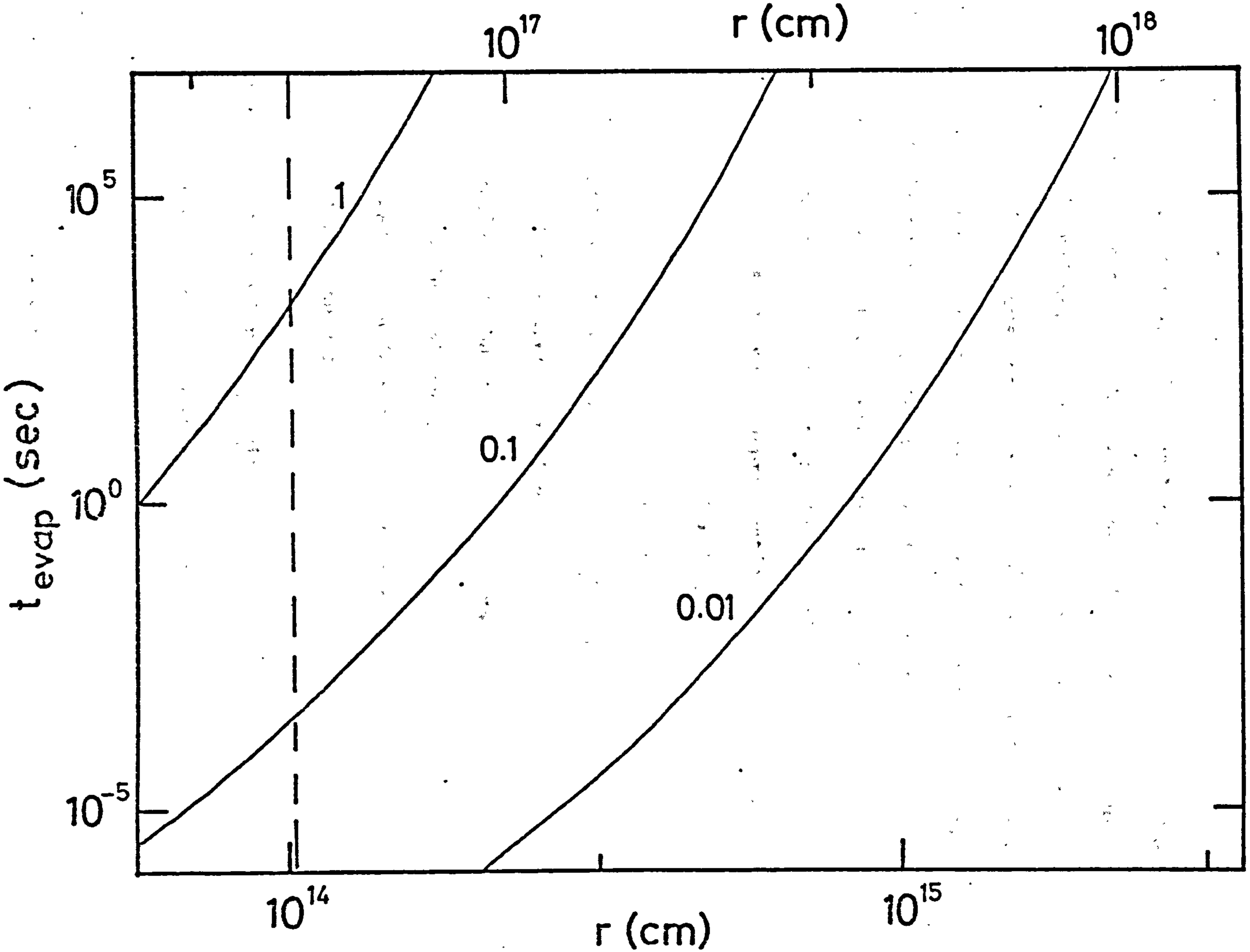
r (cm)
10^{17}
10^{18}
10^{5}
10^{0}
10^{-5}
t_{evap} (sec)
1
0.1
0.01
10^{14}
10^{15}
r (cm)

This suggested that the last part of evaporation is very rapid. We can see from the grain temperature equation (7.4) that as a decreases T_g increases thus increasing the evaporation rate, $\dot{a}$. The effect is that the grain retains effectively its initial radius then evaporation, once started, is very rapid.

Equation (7.7) was solved using Newton's method to give values of a for various values of t. This was repeated for several values of the initial grain radius, distance and α. As a general example of the results figure (7.3) shows those for $a_0 = 10^{-5}$ cm, $\alpha = 1.0$ at three values of r for a constant nova-like luminosity, $L = 5 \times 10^{38}$ ergs^{-1}, Obviously if the value of a_0 were smaller then complete evaporation would be more rapid. This fairly sudden disappearance of the grain once evaporation to $\sim 0.7a_0$ has taken place as illustrated in figure (7.3) enables us to use a useful approximation. If we consider

$$a = a_0 \quad , \quad 0 < t \lesssim t_{evap}$$

$$a = 0 \quad , \quad t > t_{evap}$$

then there is effectively no grain size distribution across any part of the shell except that present initially but truncated for $a \lesssim$ the radius of evaporated grains for that r. We will assume however that all grains have the same initial radius.

We now proceed to consider the effect of evaporation on the cavity as seen by a distant observer.

7.3.1 Evolution of the Central Cavity

We now consider the case where a dust cloud surrounds a source of high frequency radiation with a light curve as defined by equation (4.22) with $\dot{w} = 0$.

Obviously to a centrally placed observer an evaporating cavity which is increasing in size due to an instantaneously increased central source luminosity would be spherical. The cavity expansion would

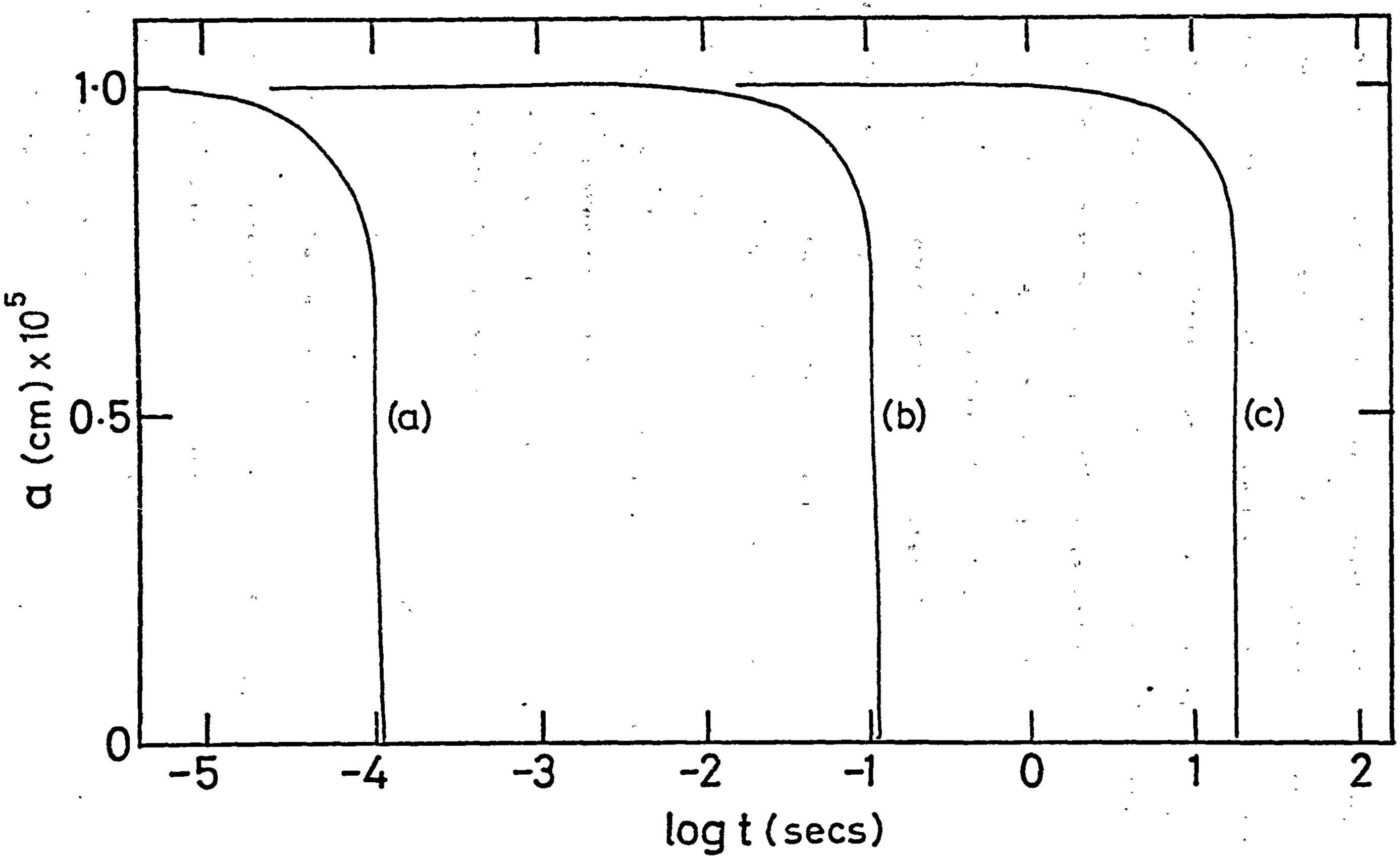

Figure (7.3) Evaporation curves for spherical graphite grains ($a_0 = 10^{-5}$ cm, $\alpha = 1.0$) at (a) $r = 10^{14}$ cm (b) $r = 2 \times 10^{14}$ cm and (c) $r = 3 \times 10^{14}$ cm from a central source with $L = 5 \times 10^{38}$ ergs^{-1}.

however not be observed to proceed with uniform velocity. The observer in this case would see the front of increased luminosity expanding through the dust shell at velocity c/2. The flux density (as seen by a grain) associated with this luminosity would obviously decrease with distance and hence so would the grain temperature at the inner boundary of the emitting sphere. Thus the further from the central object the grains were placed the longer they would take to evaporate.

The expansion of the cavity as seen by a centrally placed observer would at first appear to keep up with the expanding front of increased luminosity. However as the grains at greater distances took longer to evaporate so the cavity would lag behind allowing more grains to radiate.

The situation becomes more complex when the observer is positioned externally to the dust shell. In this case light travel time arguments lead to an observed cavity which is initially highly non-spherical but as time goes on the expanding cavity approximates more to a sphere, as we shall see below.

If we choose $L = 5 \times 10^{38}$ ergs^{-1}, $a_0 = 2 \times 10^{-6}$ cm, and $\alpha = 1$ for graphite spheres then from equation (7.7) the points (0) of figure (7.4) are derived. The solid curve in this figure is fitted to these points by the empirical expression

$$\log_{10}(t_{evap}) \simeq 5.156 \times 10^{-6}\, r^{0.4343} - 12.736 \qquad (7.8)$$

Any change in the luminosity can be compensated for by adjusting r to keep $(L/r2)$ constant. The error in the fit increases slightly towards larger values of r with an error of $\sim$ 6% at $r \simeq 1.4 \times 10^{15}$ cm.

If we now consider point H in figure (4.1) then we can see from equation (4.19) that a grain here at position (r", θ") is observed to have been heated for a time (t - t"), where t is measured from the observed onset of high luminosity of the central object and t" is given by

Figure (7.4) Evaporation time against distance from a constant 'nova' luminosity source for $a = 2 \times 10^{-6}$ cm (other parameters as in figure 7.2). The points marked Θ are from solution of equation (7.6). The solid line is an empirical fit to these points (see text).

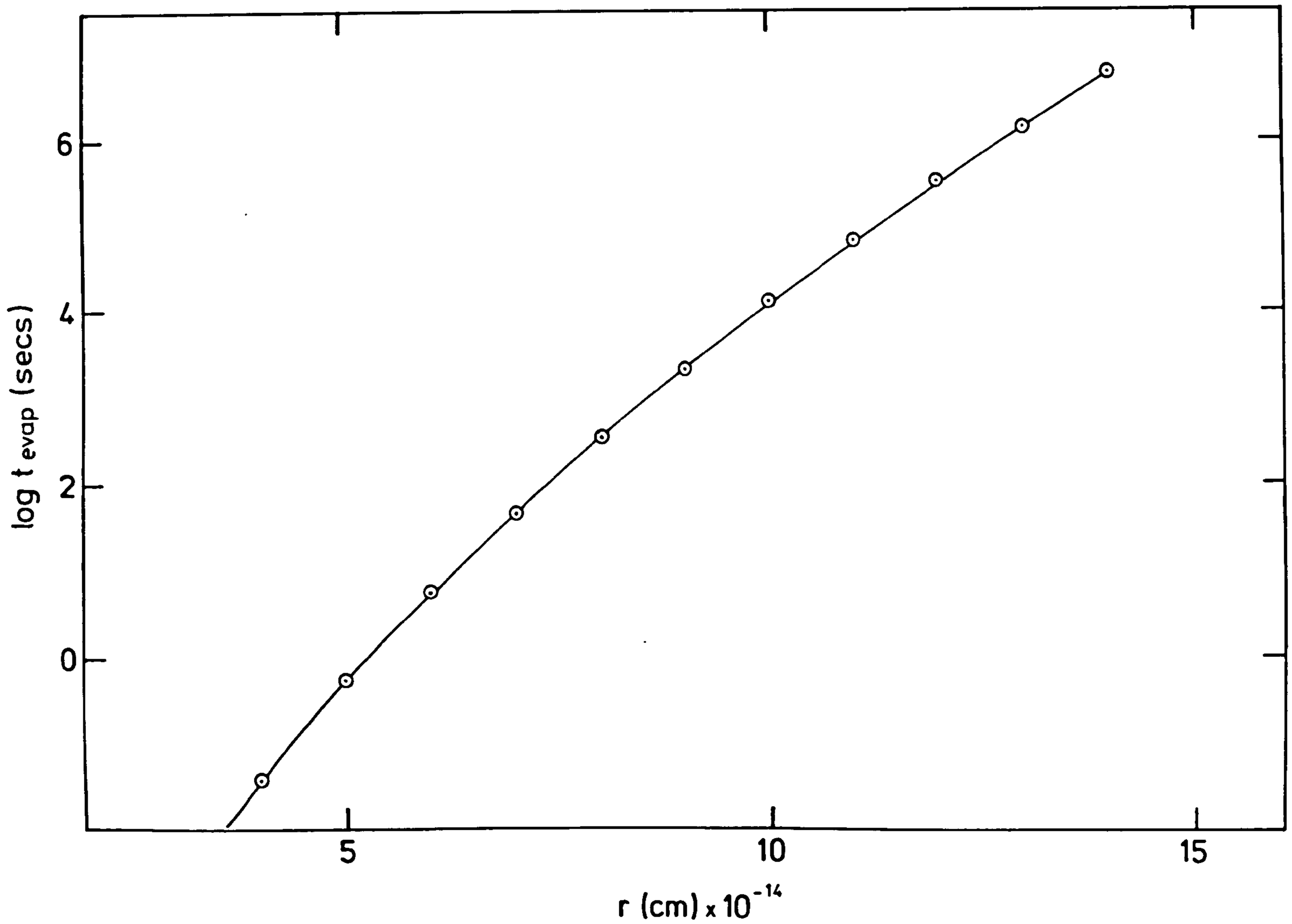
6
4
2
0
log t evap (secs)
5
10
15
r (cm) x 10^-14

$$t'' = (1 - \cos\theta'') \frac{r''}{c} \quad . \qquad (7.9)$$

Thus if we observe the central source and dust shell at t = 100s for example along line CO grains taking less than 100s to evaporate will have done so. Along QC in figure (4.1) however grains will be seen to have been exposed for times ranging from 0 to 100 seconds. The short distance travelled by the parabola at this time results in grain temperatures being very high and thus evaporation times very short. The rear of the parabola and evacuated cavity thus tend to coincide to all intents and purposes at early times. However as the cavity increases in size and the initial grain temperatures decrease so t_{evap} increases and the cavity 'lags' behind the parabola.

We set $t_{evap} = (t - t'')$ i.e. a grain at (r'', θ'') observed to have been exposed for a time $(t - t'')$ will have just evaporated. We then arrive at an expression which relates the observer's time to the co-ordinates $(\theta_{evap}, r_{evap})$ of the inner surface of the evaporated cavity for the parameters given above for equation (7.8), i.e.

$$\log_{10}(t - \frac{r_{evap}}{c} (1 - \cos\theta_{evap})) - 5.156 \times 10^{-6} r_{evap}^{0.4343} + 12.736 = 0 \qquad (7.10)$$

Equation (7.10) was solved at given times using Newton's method for r_{evap} as a function of θ_{evap}. The results were then plotted as figure (7.5). We can see from this figure that, as indicated above, the observed cavity is initially elongated toward the observer. The most distant parts from the observer follow the parabola of emission at these early times ($t < 10^5$s). As time goes on however the cavity lags behind the parabola and it is essentially spherical for $t \gtrsim 10^5$s although it will of course continue to grow at an ever-decreasing rate.

We now proceed to consider in the next section the evolution of the externally observed infra-red flux from a dust distribution in which

Figure (7.5) Evolution of the central cavity (solid lines) with time (associated figures) for parameters of the 'nova' case as in figure (7.2). At times $t > 10^5$ s the cavity is essentially spherical and only arcs of the spheres are shown. Dashed lines indicate the position of the parabola of emission.

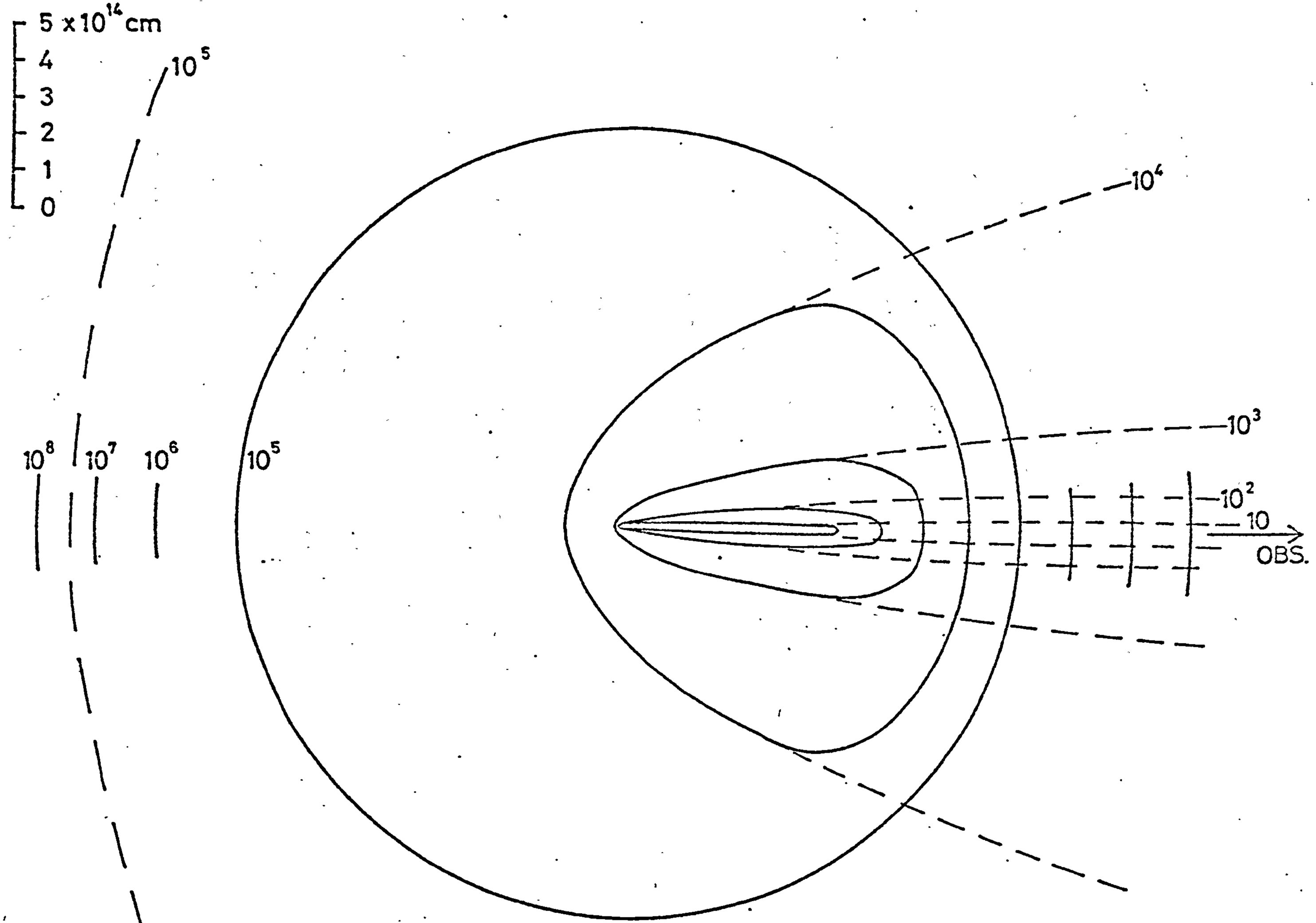
5 x10^14 cm
4
3
2
1
0
10^5
10^8
10^7
10^6
10^5
10^4
10^3
10^2
10
OBS.

this type of cavity growth is occurring.

7.3.2 Evolution of the Observed Infra-red Flux from a Dust Shell with an Expanding Evaporated Cavity

Obviously even before the central source reaches maximum luminosity, in any realistic situation there is bound to be an evacuated cavity where no grains reside between nova outbursts. As we have seen in chapter 5 Malakpour (1978) for example found that small grains would not be expected to approach a quiescent nova closer than $\sim 3 \times 10^{15}$ cm. To illustrate the effect of evaporation on the observed infra-red flux we will assume that the initial cavity size is 10^{15}cm. The central object is taken to be nova-like with a step function light curve and $L = 5 \times 10^{38}$ ergs^{-1}. The dust shell is composed of 2×10^{-6} cm graphite grains with $\alpha = 1$. The shell is taken to have an outer radius $R = 10^{16}$ cm and is optically thin at all wavelengths.

It can be seen from figure (7.5) that at time $t \sim 1$ day the cavity would already be approximately spherical by the time the radius $r_{evap} \simeq 10^{15}$ cm. At later times the cavity approximates even more closely to sphericity; the cavity is therefore assumed to be spherical at all times. The values of r_{evap} were thus derived from equation (7.10) which for $t >> 2r_{evap}/c$ has the same form as equation (7.8) above. These were then read into a programme such as that described in Appendix A1 as effectively time dependent values of the inner cavity radius previously called R_1. The resulting light curves and spectra for grain distributions with $\beta = 0$ and $\beta = 2$ are shown in figures (7.6) and (7.7) respectively.

In order to check the results of the programmes used to calculate the flux from the shell with an expanding cavity, programmes were run with the same parameters except that the inner cavity radius was fixed (i.e. $R_1 = 10^{15}$ cm cf. section (4.4.2) previously). The flux

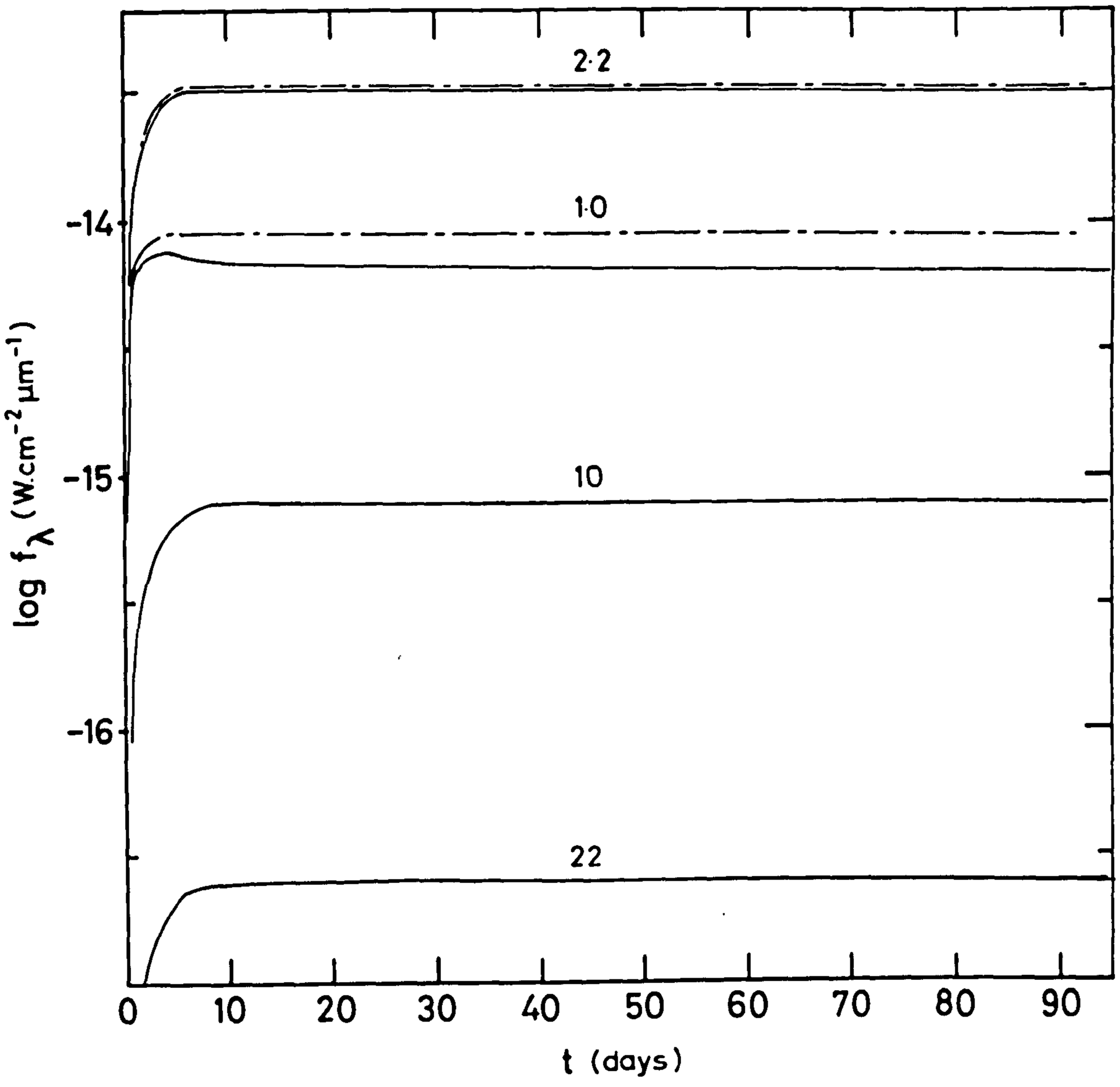

Figure (7.6a) Infra-red light curves from an evaporating dust shell with R = 10^{16} cm and step function central source light curve (L = 5 x 10^{38} ergs^{-1}). Initial grain mass $(Mg)_0$ = 1.2 x 10^{-7} $M_\odot$ with a = 2 x 10^{-6} cm, α = 1 β = 0. Figures over curves are wavelengths in μm. Dashed lines show flux behaviour in the absence of evaporation.

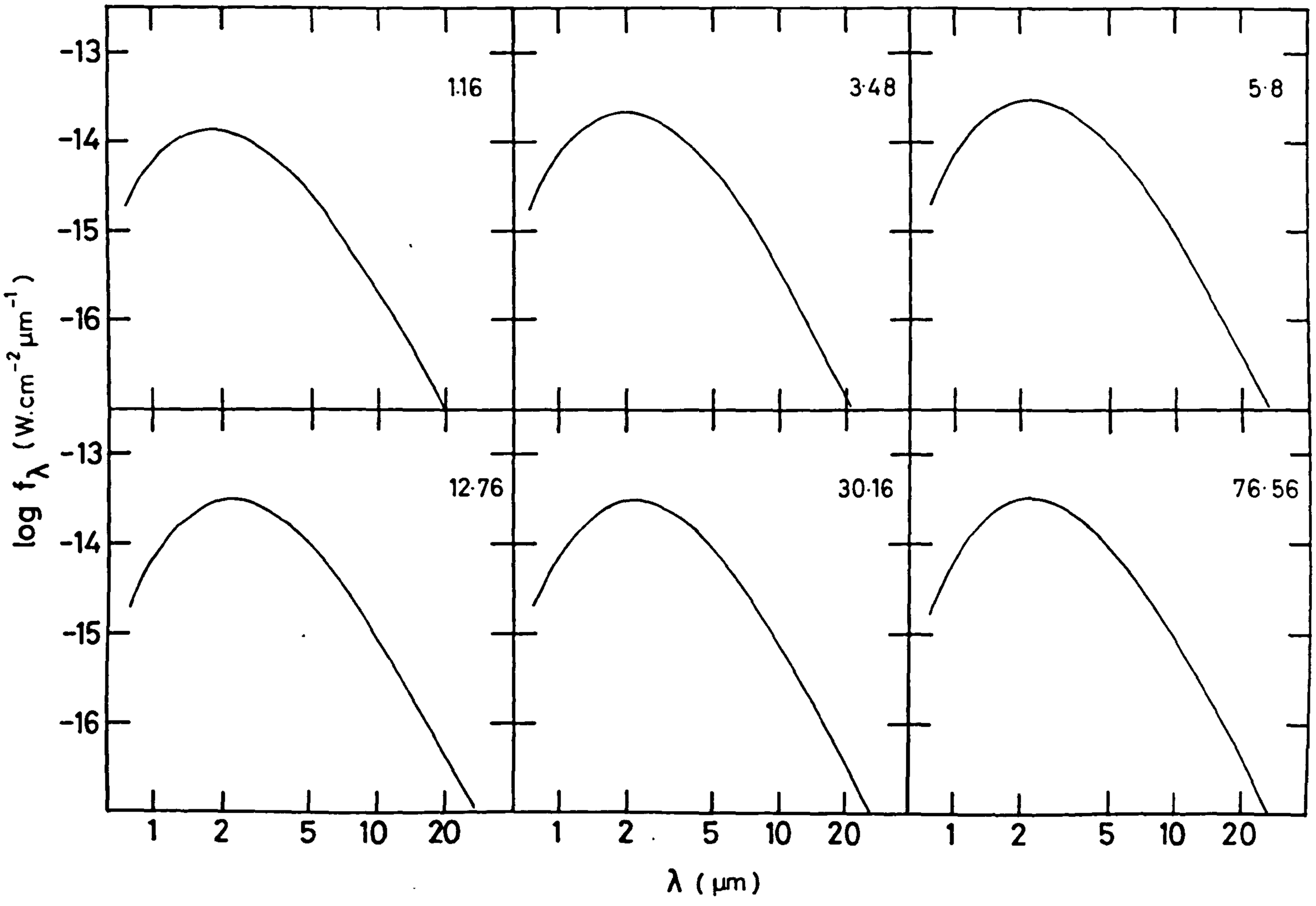

Figure (7.6b) Spectra observed to arise from a dust shell as in figure (7.6a). Figures at top right of each spectrum, refer to time in days from central source 'outburst'.

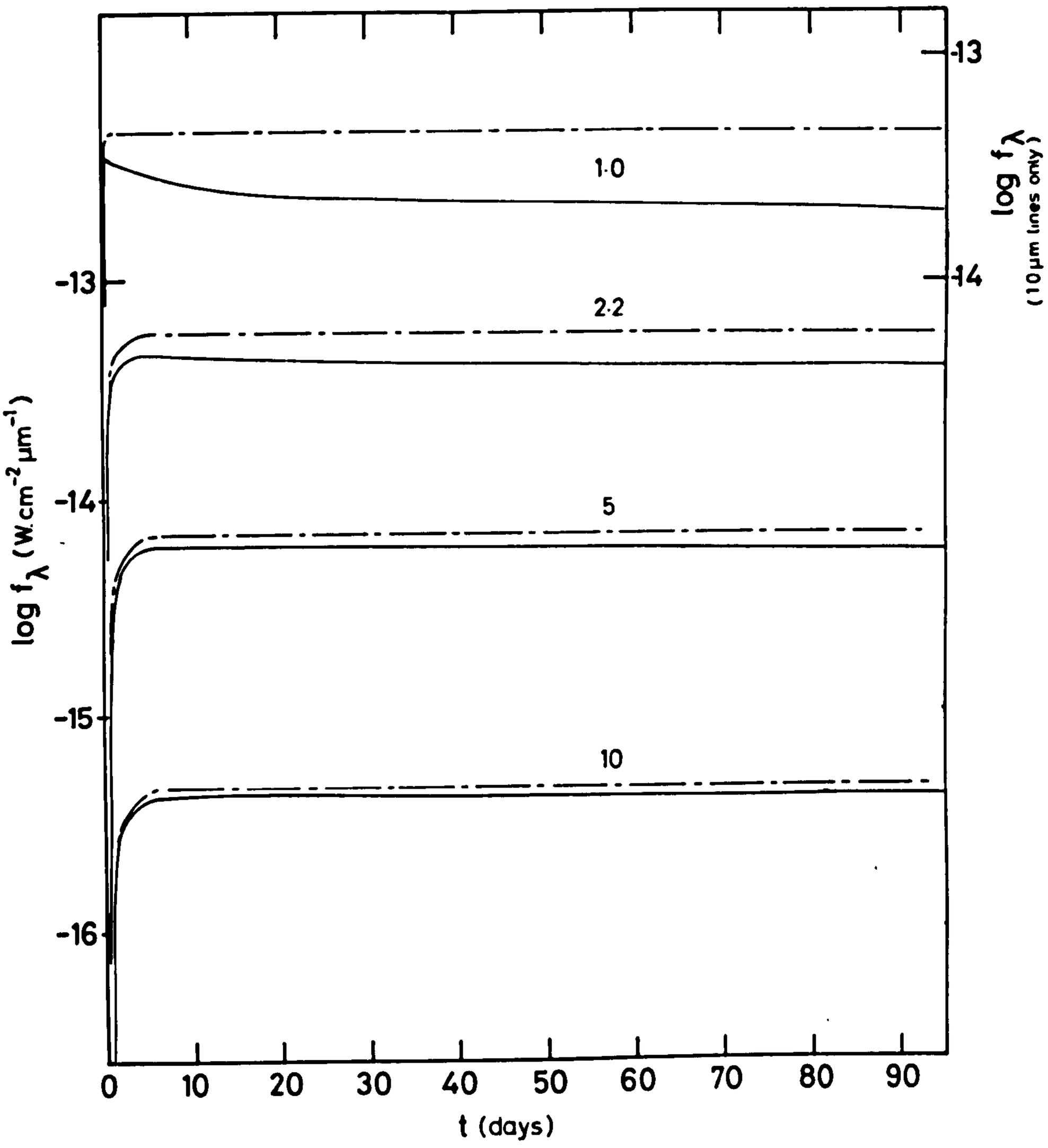

Figure (7.7a) Infra-red light curves from a dust shell with parameters as in figure (7.6a) except $(Mg)_0 = 4.8 \times 10^{-8}\ M_\odot$ and $\beta = 2$.

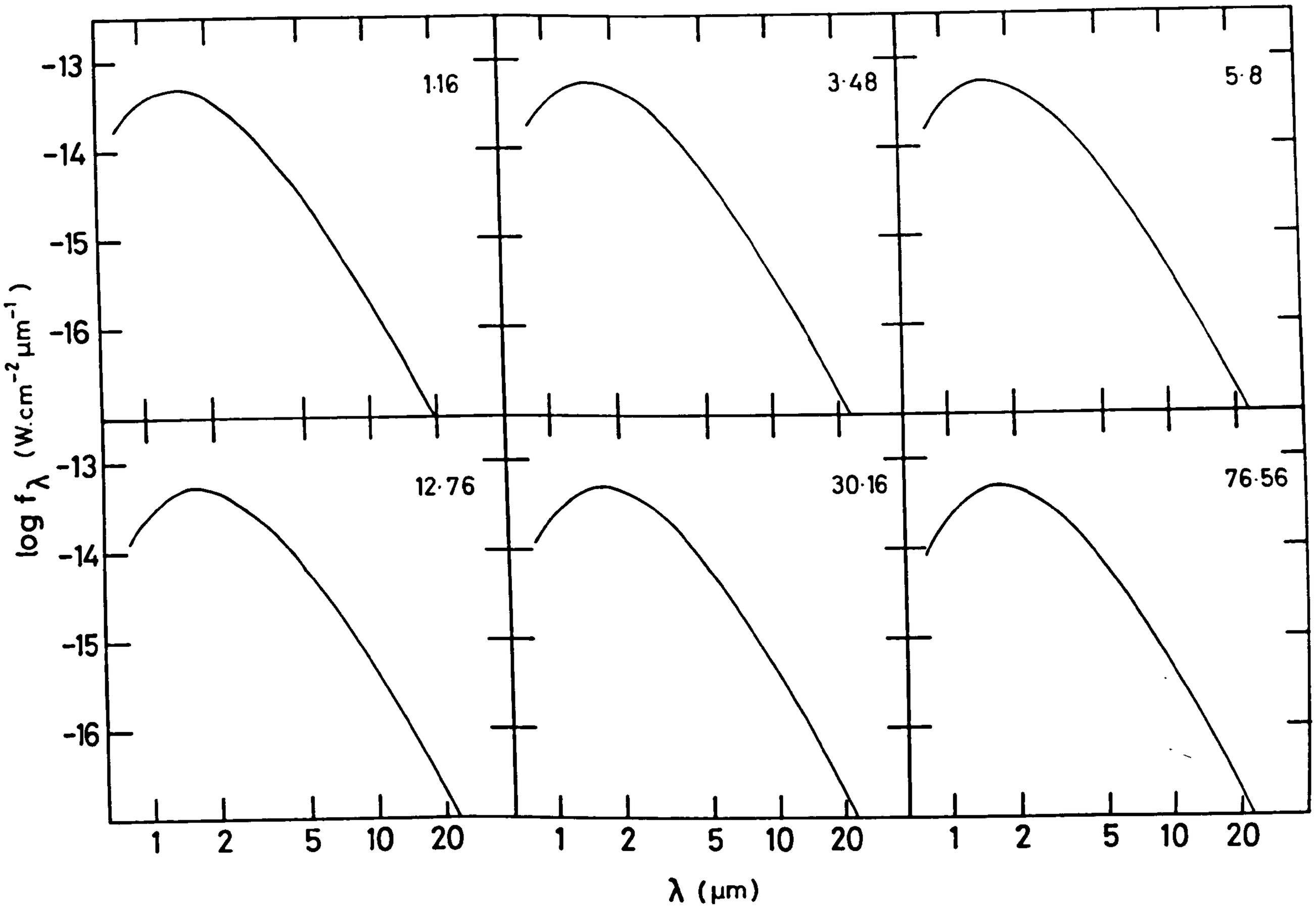

Figure (7.7b) Observed spectra from dust shell of figure (7.7a).

evolution thus derived is shown as dashed lines in figures (7.6a) and (7.7a).

If we now refer to figure (7.6a) we can see that at short wavelengths there is a noticeable difference in observed flux between the static and evolving cases. At 1 μm the flux falls away from a peak value at t ∿ 5 days in the case of an evaporating cavity even though the central object flux is steady. At longer wavelengths the major infra-red flux contribution for a $\beta = 0$ grain distribution is from grains more distant from the central source than those likely to be evaporated in the timescale that interests us here. The difference between the static and evolving cavity fluxes is so small as to not show up at 10 or 22 μm in the figure. Figure (7.6b) shows the resulting spectra for the evolving cavity case with $\beta = 0$. The greatest changes as expected from figure (7.6a) occur at early times (i.e. $\lesssim$ 10 days) where as we shall see later a rapid 'cooling' is taking place.

Figure (7.7a) shows the flux evolution for a similar shell but with $\beta = 2$. This of course tends to concentrate many grains into regions where they will be subject to evaporation within the timescale of observation. Thus even at long wavelengths there is a marked difference between the static and evolving shell fluxes: even at 10 μm the flux is falling with time. However the rate of decline at 1 μm is at all times greater than that at 10 μm.

Figure (7.7b) shows the spectral development of the flux from the same evolving shell. Direct comparison with figure (7.6b) reveals that at all times the temperature derived from the wavelength of the peak flux would be greater for the shell with $\beta = 2$ than for the shell with $\beta = 0$. This would be expected as there are more high temperature grains at higher values of β.

The development of the observed colour temperature T_{K-N} for each shell is shown in figure (7.8). As expected the shell with $\beta = 0$

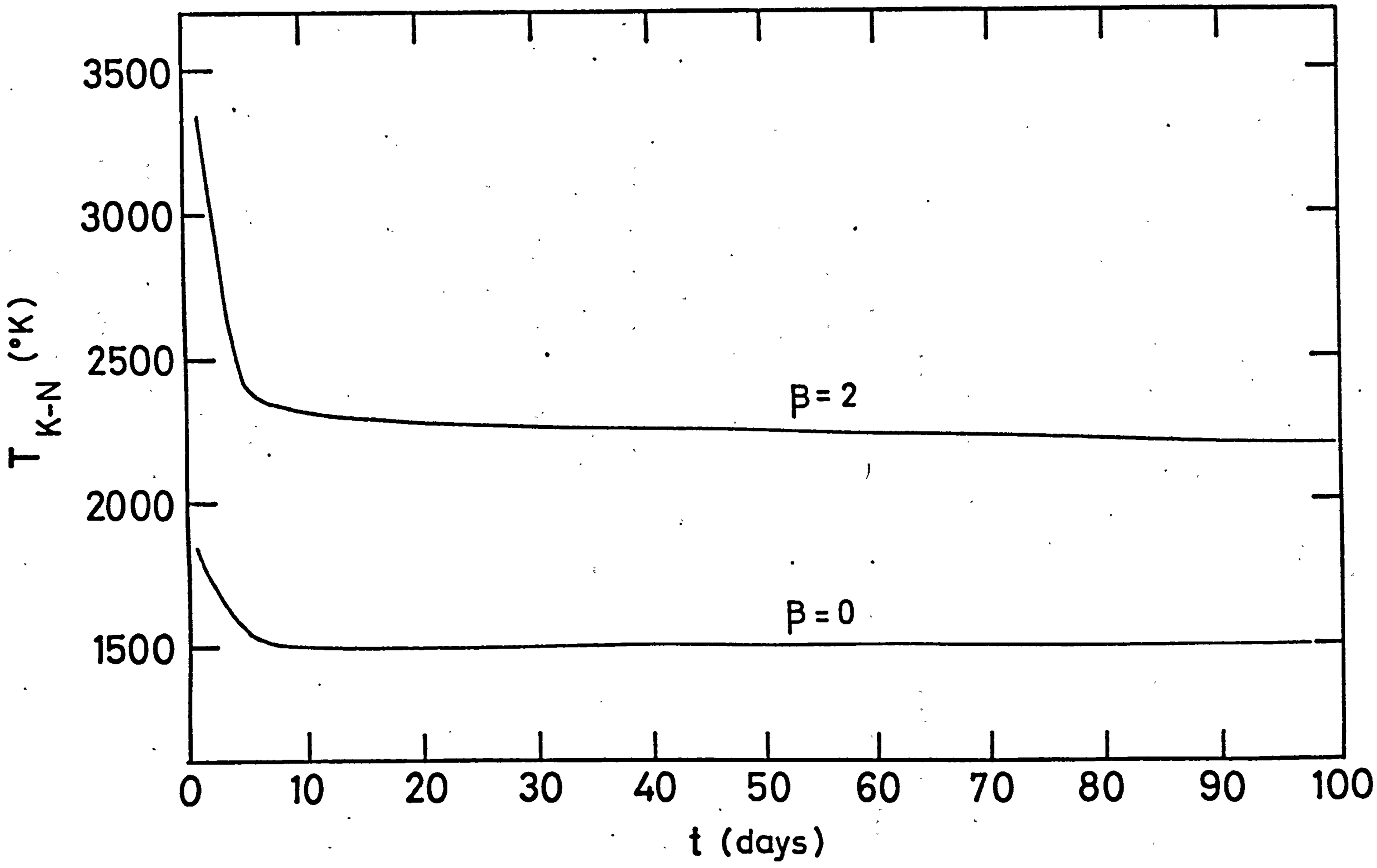

Figure (7.8) Infra-red colour temperatures deduced for dust shells with evaporating central cavities and parameters as in figures (7.6) and (7.7).

consistently yields a lower value of T_{K-N}. In both cases the temperatures are however much higher than observed from the dust shells of the novae studied so far in this work. The temporal behaviour of the temperature is however qualitatively very similar to that of Nova Vulpeculae 1976, particularly in the $\beta = 0$ case where an initial steep drop is followed by an 'isothermal' stage.

7.4.1 Conclusion

This chapter has briefly explored in an essentially qualitative way the effects of evaporation on the grain distribution and the subsequently evolved infra-red flux for nova-like sources. It has been shown that greater observed differences from a static shell occur for a grain distribution with $\beta = 2$ rather than for $\beta = 0$. For $\beta = 2$ the main contribution to the flux arises from centrally concentrated grains subject to evaporation within the timescales of interest.

Comparing the results qualitatively with the observations of Nova Vulpeculae 1976 it has been found that the temporal development of the observed colour temperature resembles that of this nova. However there is only a very small decline in overall observed flux over the 100 days covered by the calculations even for the $\beta = 2$ shell. This is unlike the nova where after $\sim$ 20 days from transition the decline in observed infra-red flux was much more rapid.

It would appear that as far as the colour temperature behaviour of the dust shell of Nova Vulpeculae 1976 is concerned the evaporation model gives a much closer qualitative description of the observations than the static model. However we can see from figure (7.8) that even for $\beta = 0$ the derived colour temperatures are higher than those observed (see chapters 2 and 5). It is perhaps unlikely therefore that graphite grains are responsible for the infra-red flux if we are correct in using the evaporation model. A grain type with a higher rate of evaporation

at a given temperature would of course generally yield consistently lower temperatures.

We now proceed to consider in the final chapter how further refinements to the basic models outlined so far in this work may achieve better fits to the observations. We also suggest how the work may be developed in the future.

CHAPTER 8

Discussion, Suggestions for Further Work and Conclusions

8.1.1 Introduction

It appears that the general field of infra-red variability of thermal cosmic sources is one in which little detailed theoretical work has previously been attempted. It is perhaps not surprising therefore that there are several sections of the work described herein which require further research or suggest entirely novel avenues of exploration.

After a general discussion of the results derived in the current work in section (8.2), this chapter continues with section (8.3) in which consideration of the ways research may be applied and extended in future is given.

Finally in section (8.4) the conclusion to the thesis as a whole is presented.

8.2.1 Discussion of Results

In chapter 4 the basic models of infra-red variability from dust shells were developed. This entailed the investigation of the reaction times of graphite grains to changes in incident flux. It was determined that, to all intents and purposes, the grains react instantaneously to those changes, certainly at the grain temperatures with which we were later concerned. The development of a general geometrical model for a distantly observed fluctuating source was then initiated and the idea of the 'parabola of emission' put forward for a central source with a step function light curve. The transverse velocity of expansion of the observed parabola was then shown to be superlight for a time $1 - {}^{1}/_{\sqrt{2}} \leq \tau \leq 1 + {}^{1}/_{\sqrt{2}}$.

In chapter 4 the equation of transfer was solved analytically for the special case of a central source with a step function light curve, an optically thin shell and calculated for $\beta < 2$. This led to the rather surprising result that at all values of wavelength the flux from the shell rose linearly for $\tau \leq 2\psi$. It then maximised at $\tau = 2$. The numerical solution was then used for more general models including rather simple 'nova' models. The similarity between the results here and the observations of novae with late-developing infra-red excesses led to the formulation of more-specific models in chapter 5.

First however this general model was utilised to make brief investigations of the variation of surface brightness due to re-emission across the face of the visible disc of the dust shell and an investigation was made of the optical depth through the shell to background radiation. The phase and amplitude relationships of central source and dust shell fluxes were also examined.

Detailed application of the principles outlined in chapter 4 was made in chapter 5 to three specific novae. It was found that by employing small ($\sim 10^{-6}$ cm) graphite grains in the circumnova cloud and

an increasing central source temperature the late developing infra-red excesses of Novae Serpentis 1970 and Aquilae 1975 could be accurately modelled. That of Nova Vulpeculae 1976 was less satisfactorily explained in this chapter but it prompted the investigations of grain evaporation considered later in chapter 7. The actual processes of grain cloud formation were also discussed at some length in chapter 5.

Chapter 6 investigated the situation in which a disc of dust grains surrounds a variable central source. It was shown that to a distant observer the re-radiation from the disc will appear to emanate from within a 'circle of emission' (if the central source light curve is a step function) which expands with a velocity greater than the velocity of light for all $i < \pi/2$. The evolved infra-red light curves and spectra also depend strongly on the angle of inclination of the disc to the observer. The model was qualitatively applied to Nova Cygni 1975 whose late-developing thermal excess is somewhat controversial even now.

Chapter 7 summarised the results of work on the evaporation of grains. The initial section gave the derivation of grain temperatures with the inclusion of energy loss via evaporation of surface layers. However this was shown to make a negligible difference with grains at $T_g \lesssim 2000^{o}K$ and the evaporation energy loss was subsequently ignored. Light travel time arguments were again employed to map the observed development of a central cavity. This gave the interesting result of an initially highly non-spherical cavity tending towards sphericity with time. When the equation of radiative transfer was solved numerically for the dust shell with an expanding cavity of this type the infra-red fluxes decayed at late times even though the central object had a step function light curve. The colour temperature behaviour of the source was qualitatively similar to Nova Vulpeculae 1976.

We now proceed to suggest how the work may be extended in future.

8.3.1 Suggestions for further work - Introduction

In this section we will briefly consider how the research described in this thesis may be improved and extended by future work. The suggestions contained herein include proposals not only for theoretical studies but for observational and experimental work as well.

8.3.2 Properties of Grains

The basic assumption throughout this work has been that the grains with which we are concerned are perfect spheres whose optical properties are similar to those of graphite. Some allowance for the uncertainties in experimentally and theoretically derived parameters for graphite has been made by introducing the variables α and ρ. It has long been recognised however that naturally occurring graphite is more likely to form platelets initially, and possibly cylinders or long 'whiskers' where time and ambient carbon gas density allow (Wickramasinghe, 1967, p. 59). It might therefore seem that any future work involving graphite grains should utilise the extinction properties of these non-spherical grains. Obviously where these grains are distributed about an object such as a nova some alignment of grains may occur due to electromagnetic or gas-streaming effects. The resulting polarisation of the central source flux would then indicate the presence of such grains.

Of course it is known that other grain types do exist in the vicinity of many astrophysical objects. The silicate spectral features at $\sim$ 10 μm are well known as are those of water ice (see for example, Martin, 1978, p. 199). Although neither of these grain types has been conclusively shown to exist near novae (and hence to give rise to the late infra-red excesses of certain classical novae) the possibility exists that a composite grain type may well be involved. For example graphite (or similar) grains may well between outbursts form ice mantles which 'insulate' the cores until the central source reaches high

luminosity at $\lesssim$ 1700Å where the ice absorption rises to a short wavelength plateau (Isobe, 1971). This composite core-mantle grain type is another important extension which will be required in more detailed future models.

It appears that there exists little experimental data on the temperature dependence of Q_{abs} (a point noted by Patashnick & Rupprecht, 1977 with regard to ice grains). Our inclusion of the temperature dependence, ρ, in the absorption efficiency of graphite was an attempt to accommodate this to some extent. However it is difficult to ascribe a single conductivity function as this not only varies with the type of graphite considered but also with the orientation of the grain relative to the direction of interest (Goldsmith et al., 1960). There appears to be a great deal of experimental and theoretical research required into the temperature dependence of the absorption efficiency therefore for all plausible grain types. Once these data were available the inclusion in the energy balance equations could have quite a marked effect.

8.3.3 Non-Static Dust Shells

It has been noted on several occasions in this work that the static dust shell models of chapter 5 and the static disc of dust grains outlined in chapter 6 will not be truly accurate representations of what is actually occurring. Chapter 7 has outlined the initial investigation of the effects of grain evolution (evaporation in this case) on the development of the source geometry and the subsequent infra-red flux. However even this model is somewhat idealised.

In any real situation the cloud of dust grains will not initially contain a homogeneous grain size (or even grain type). In the case of a nova the grains already extant before the concurrent outburst will at first be subject to evaporation alone. However once the

ejecta reach the innermost grains they will be sputtered by the out-flowing gas ions of the ejected nova envelope. The sputtering rates of grain materials would therefore need to be known fairly accurately for different incident atomic types and energies. Some data are already available on this (see for example, Draine, 1977); however it appears that more extensive work still has to be done to provide comprehensive information.

Condensation, or re-condensation of grains during and between outbursts would of course be another process tending to make the static shell model less accurate. Application of the data on evaporation, sputtering and grain growth rates would hopefully be made to the development of N(a, t), the time dependent grain radius distribution.

From considerations such as these it would be hoped to construct more realistic models of astrophysical objects and thus exact fits to observational data. Initially application to novae such as Nova Vulpeculae 1976 when grain destruction processes are indicated, might be envisaged. The situation would of course be complex as the heating function of each grain in the shell would be position dependent as would the size and composition of the grains (if the grains were initially composite core-mantle for example). As seen in chapter 7 the observed evaporation rate, and hence the grain size distribution at any instant, would also depend on the position of the observer. For sputtering, the velocity of propagation of the ejecta in a nova is far less than the velocity of light and thus the sputtering front would be essentially spherical as externally observed. Also, of course, grains outside the ejecta would be unaffected by sputtering, though still subject to evaporation.

In the realistic situation where the shell was not static studies of the 2200Å feature might show variability even in a pre-existing dust cloud associated with a nova. Detailed observational work in this

wavelength region should help to determine when a pre-existing cloud was subject to destructive forces and when a condensing cloud of grains was being observed.

8.3.4 Different Source Geometries

Chapter 6 explored the situation of a variable central source surrounded by a thin disc of dust grains. This yielded several interesting results including the qualitative application of the model to the late infra-red development of Nova Cygni 1975. As we saw in section (3.5.1) it is unlikely that at each outburst ejecta are distributed isotropically about the nova. Indeed we have seen that it is generally thought that the ejecta form an equatorial ring with two polar blobs after the outburst (see figure (3.6)). A disc thus approximates to the possible distribution of grains which may have condensed in the equatorial ring. However it would of course be more appropriate in future to explore the process of emission from torroidal grain shells and from isolated 'blobs'.

Throughout this work we have assumed the variable high frequency source to be placed centrally within the dust distribution. However it is likely that the high frequency primary source will in some cases be adjacent to an irregular dust cloud (cf. Couderc, 1939) or be placed out of the plane of a disc, or thin 'slabs', of dust grains for example. Further consideration will also have to be given to the instance where multiple shells of various geometries surround the central object. The complexity of the situation is potentially immense once grain size and number density distributions are also incorporated.

8.3.5 The Phase Relationship of Central Source and Dust Shell Emitted Fluxes

As was seen in section (4.4.5) the variability of a sinusoidally

varying centrally positioned primary source is mirrored by the variation in infra-red flux from the dust shell. The phase difference between central source and dust shell fluxes was shown to be dependent upon optical depth through the cloud and (more importantly) the size of the shell. It was also found that it is the inner radius, R_1, which has the major influence in determining the phase difference between the shell and central source fluxes.

Future work would involve the completion of the preliminary investigations. Once completed satisfactorily then application of the results to Mira variables and other periodically varying objects with dust associations would be undertaken. It is felt by the present author that this would be an extremely important extension of this work resulting in the direct determination of R_1. The next section details some of the expected results that might be gleaned from such a study.

8.3.6 Objects of Future Interest

The majority of the work described in this thesis has been devoted to the subject of the late-developing infra-red excess of classical novae. However the potential applications of this work are much more wide-ranging.

We saw in chapter 2 that recurrent novae have been shown to have dust shells which exist prior to the subsequent outburst. RS Oph is a prime example of this. In any future outbursts it would therefore be extremely important to monitor the infra-red development of these objects as they should, to some extent, behave in a similar fashion to classical novae. Dwarf novae may also be of interest in this respect; however the present author is not aware of evidence that any of these objects are associated with variable thermal infra-red emission from dust grains.

Within the Galaxy there are several other types of object of interest. Long period variables with dust associations would be of

particular importance. The evidence for phase lags between central source and dust shell fluxes was outlined in section (2.1.2) for certain Mira variables. By studying the phase difference Φ several values of χ might be inferred (see section (4.4.5)). By also studying the central source luminosity and the thermal spectrum of the dust shell (i.e. to determine its effective temperature) the most likely value of the dust shell radius could be suggested. Angular diameter determinations would therefore give an extinction-independent distance to the object. Ciatti and Rosino (1974) have observed Mira variables at UBV and near infra-red wavelengths. However, as with novae etc., longer term, more extensive observations at a wider range of wavelengths would be essential to enable the construction of detailed models.

As was mentioned earlier in sections (2.1.2) and (3.3.1) certain type II Seyfert galaxies show infra-red variability which may result from emission from dust grains near the variable central sources of these objects. There has been a good deal of controversy in recent years over the thermal nature of the infra-red emission of these objects. This usually arises because of the relatively short timescales of variation which have been thought in the past to be irreconcilable with the relatively cool (i.e. extensive) dust clouds required to produce the emission. However further work on the phase problem as outlined in the previous section may well yield cloud diameters which whilst large enough to give low observed temperatures will nevertheless be of the right order compared with the central source period to produce rapid fluctuations.

There are of course other more individual objects (e.g. HM Sge, CRL 3099 etc) as well as T Tauri stars and some Wolf Rayet stars to which future attention could usefully be given. It is hoped that individual models would be tailored for each source including suitable geometry and grain type.

In the long term the principles behind this work (i.e. travel times from a central source to a point of re-emission and the light travel time of that re-emission to a distant observer) could be applied to radio sources where a flux of charged particles is emitted from a central object and they subsequently emit via the synchrotron mechanism.

8.4.1 General Conclusions

We have endeavoured in this work to considerably expand the theoretical bakground on variability in thermal infra-red sources. To that end we have not only looked at the properties of individual grains but we have applied light travel time arguments to the large scale situation. The models we have developed have been applied with some success to certain classical novae although our assumptions concerning pre-existing grains have tended to go against many previously held beliefs.

We have begun work along more specific lines not only as far as particular cosmic sources are concerned but also for different geometries (i.e. the disc) and non-static shells (i.e. evaporation). The scope for future development and application of the work completed here would appear to be immense and it is hoped that the good fortune which led the author through only a minimal number of the inevitable 'blind alleys' will continue in the future.

APPENDIX A1

The Main Programme for Specific Dust Shell Models

A1.1.1 Introduction

It is obvious from what has already been stated, particularly in chapter 4 of this work, that analytical solution of the equation of transfer in more realistic situations than the optically thin shell and step function light curve case is unlikely; numerical methods were therefore utilised. This appendix describes in detail the form of the programme used to compute the observed infra-red flux from a dust shell in a more complex set of circumstances. Other programmes were of course developed in the course of this work, but on the whole they were either standard (as in the graph plotting routines) less complex (as in the Bernoulli number summation of the analytical solution) or similar to the one described herein (as in the case of the disc).

A1.2.1. FLOW CHART

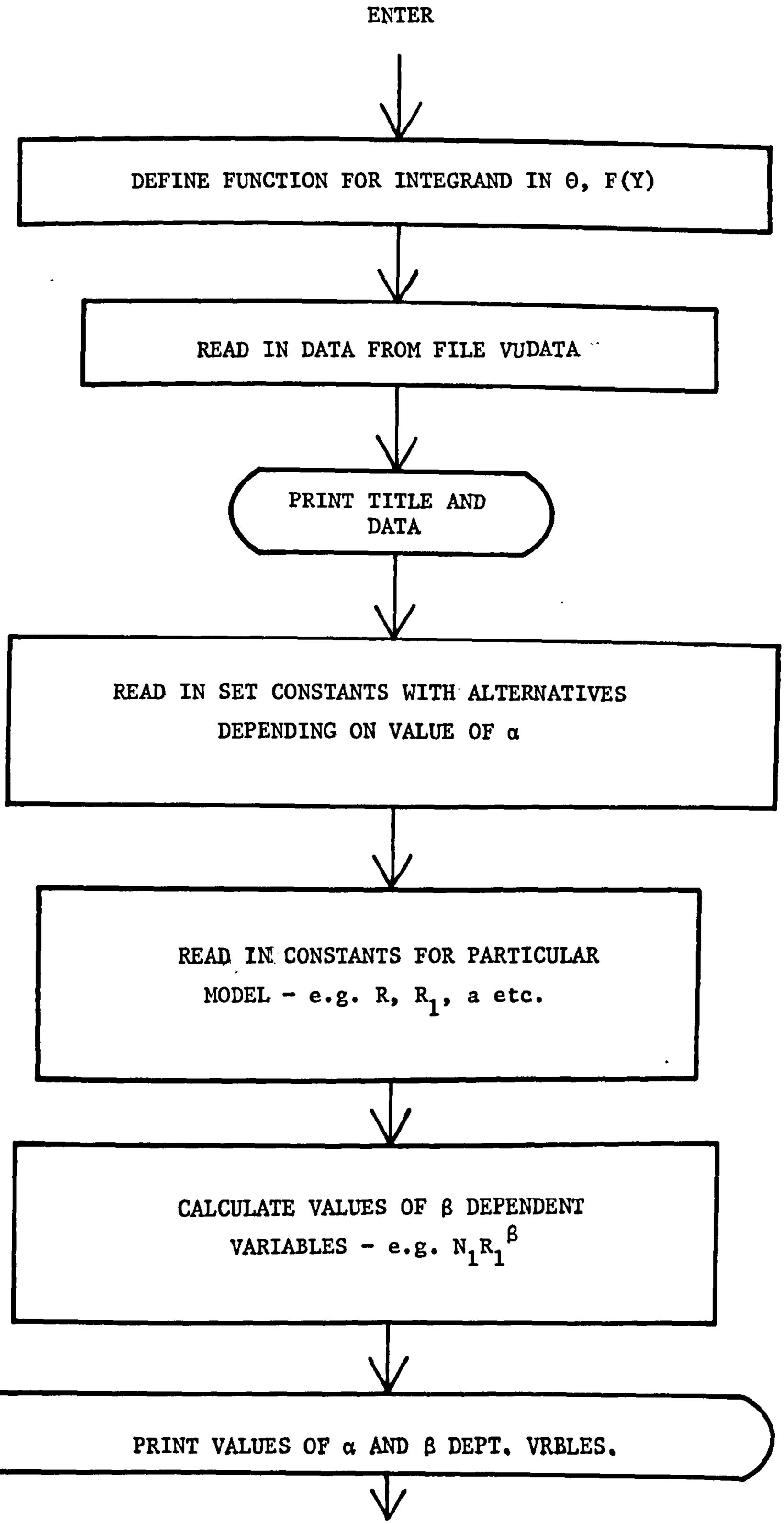

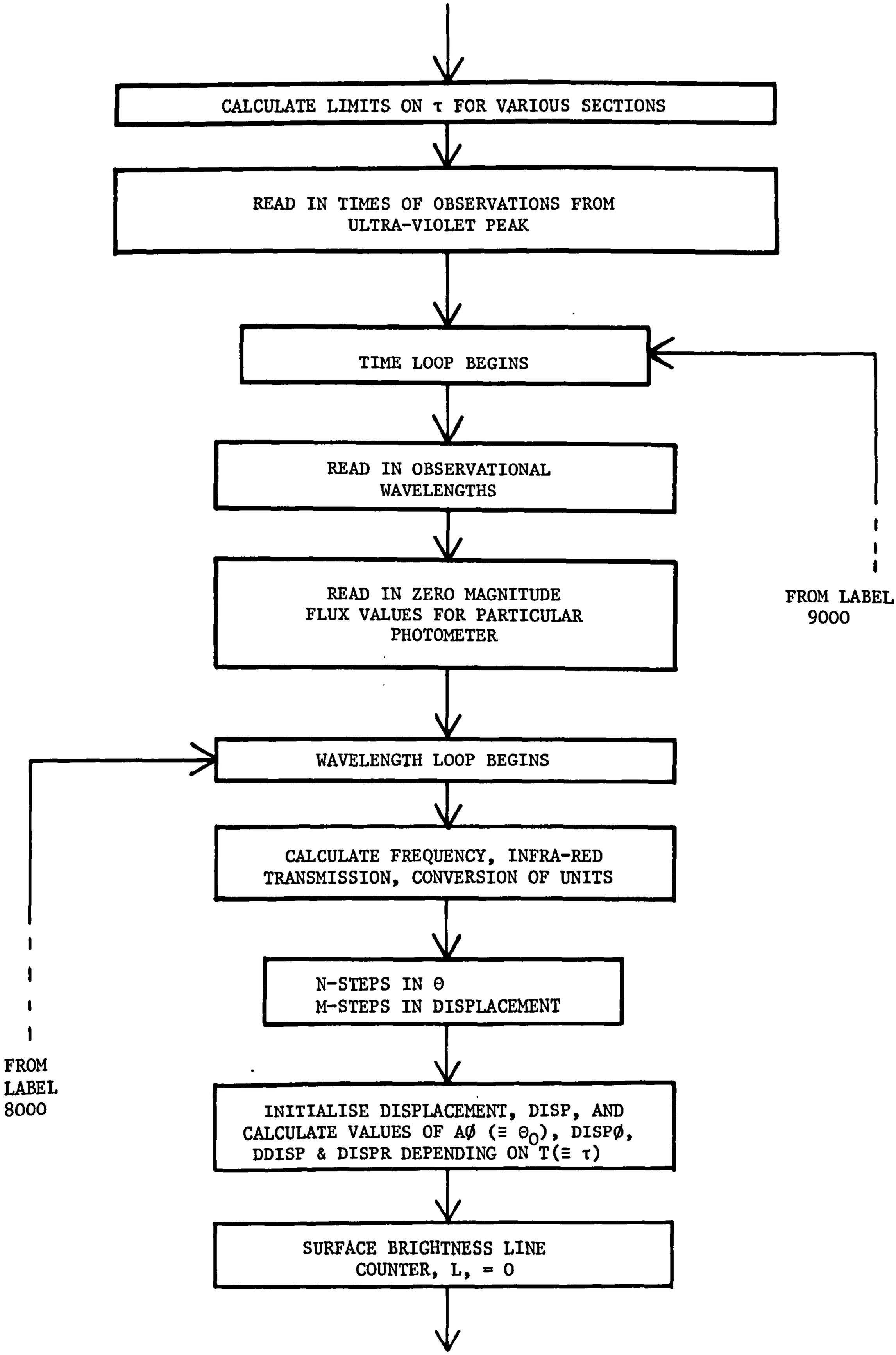
CALCULATE LIMITS ON τ FOR VARIOUS SECTIONS
READ IN TIMES OF OBSERVATIONS FROM ULTRA-VIOLET PEAK
TIME LOOP BEGINS
READ IN OBSERVATIONAL WAVELENGTHS
READ IN ZERO MAGNITUDE FLUX VALUES FOR PARTICULAR PHOTOMETER
FROM LABEL 9000
WAVELENGTH LOOP BEGINS
CALCULATE FREQUENCY, INFRA-RED TRANSMISSION, CONVERSION OF UNITS
N-STEPS IN Θ
M-STEPS IN DISPLACEMENT
FROM LABEL 8000
INITIALISE DISPLACEMENT, DISP, AND CALCULATE VALUES OF AØ (≡ Θ0), DISPØ, DDISP & DISPR DEPENDING ON T(≡ τ)
SURFACE BRIGHTNESS LINE COUNTER, L, = 0

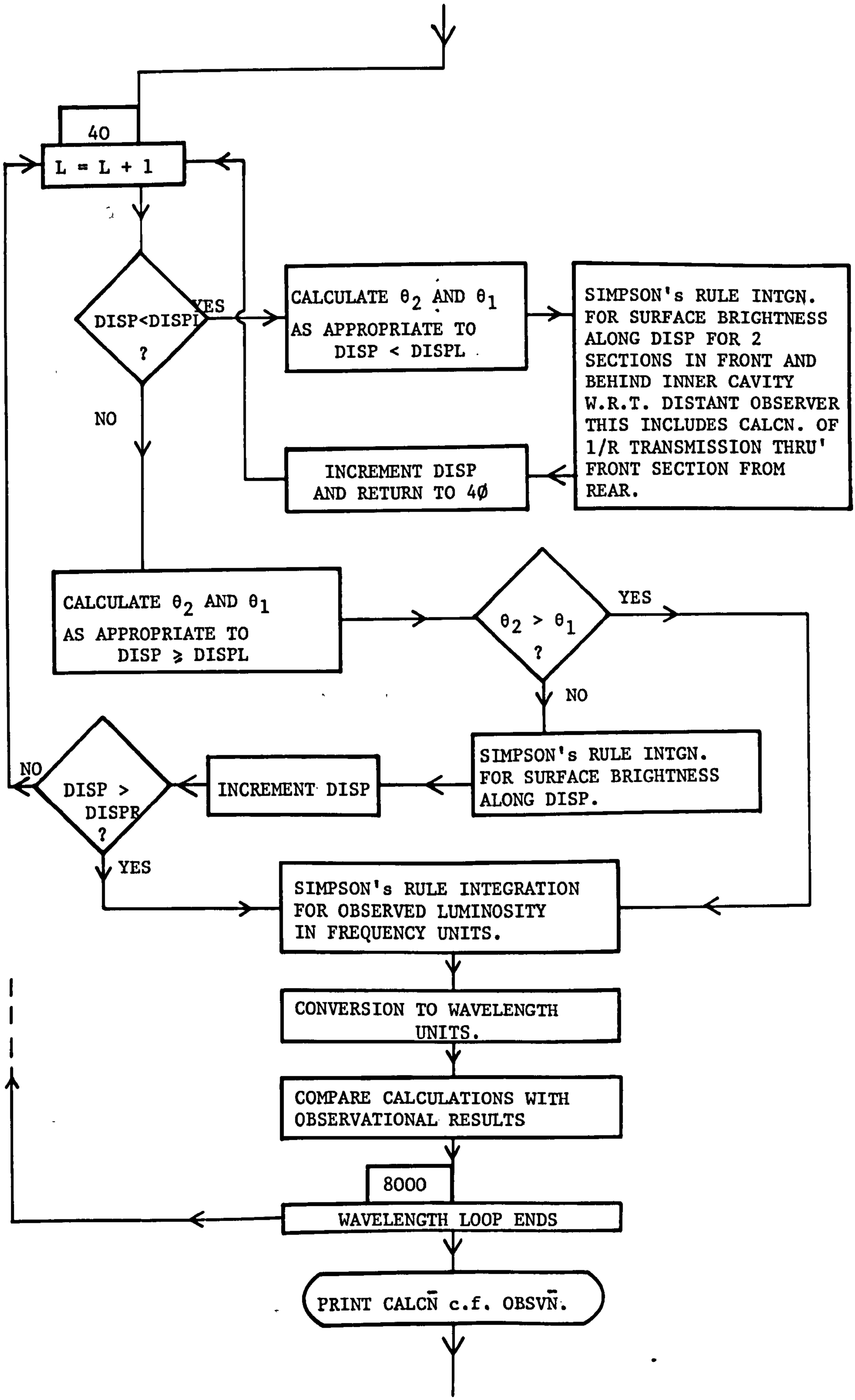
40
L = L + 1
DISP<DISPL ?
YES
NO
CALCULATE θ2 AND θ1
AS APPROPRIATE TO
DISP < DISPL
SIMPSON's RULE INTGN.
FOR SURFACE BRIGHTNESS
ALONG DISP FOR 2
SECTIONS IN FRONT AND
BEHIND INNER CAVITY
W.R.T. DISTANT OBSERVER
THIS INCLUDES CALCN. OF
1/R TRANSMISSION THRU'
FRONT SECTION FROM
REAR.
INCREMENT DISP
AND RETURN TO 4Ø
CALCULATE θ2 AND θ1
AS APPROPRIATE TO
DISP ≥ DISPL
θ2 > θ1 ?
YES
NO
SIMPSON's RULE INTGN.
FOR SURFACE BRIGHTNESS
ALONG DISP.
INCREMENT DISP
DISP > DISPR ?
NO
YES
SIMPSON's RULE INTEGRATION
FOR OBSERVED LUMINOSITY
IN FREQUENCY UNITS.
CONVERSION TO WAVELENGTH
UNITS.
COMPARE CALCULATIONS WITH
OBSERVATIONAL RESULTS
8000
WAVELENGTH LOOP ENDS
PRINT CALCN̄ c.f. OBSVN̄.

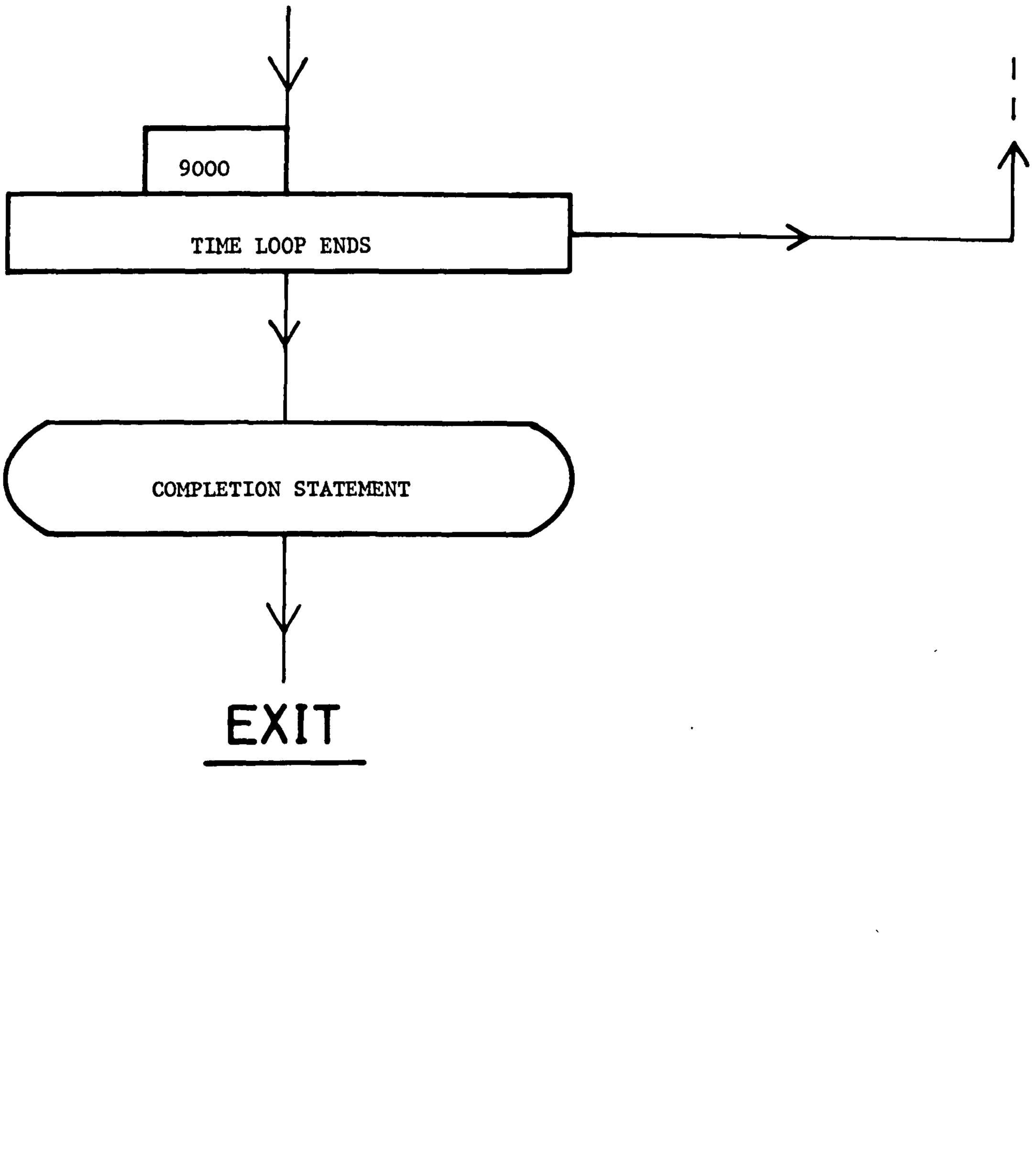
9000
TIME LOOP ENDS
COMPLETION STATEMENT
EXIT

A1.3.1 Programme Structure

This sub-section describes the main functioning of the numerical integration programme with reference particularly to section (A1.2.1) and chapter 4. A copy of the programme is shown in figure (A1.1). We will now proceed to work through this figure (note that this is only one version of the programme specific to Nova Vulpeculae 1976, although the basic form is similar for other nova models).

After declaring real and integer variables and setting up the arrays to be used, section (i) of the programme establishes the function, $f(\theta)$, to be integrated along lines of sight at displacements, DISP, ($\equiv R \sin \theta_2$) from the centre of the observed emission. F(Y) ($\equiv f(\theta)$) is composed of various sub-functions, including the observed luminosity a grain receives at any instant at any point within the cloud, GLUM (Y); the transmissions of ultra-violet and infra-red radiation, TUV (Y) and TIR (Y) and the resulting temperature a grain is observed to possess, GTEMP (Y). In this case the functions are defined for $\beta = 2$.

Section (ii) of the programme reads in the observational data which are stored in magnitude form in the file VUDATA. The values are then printed out in the form of a table so that any faults at this most important point can easily be detected.

We now proceed to read in the set constants including α and β. In the case of the Reimann Zeta and Gamma functions an alteration in α is accommodated by conditional statements. Section (iii) also contains the derivation of $N_1 R_1^{\beta}$ ($\equiv$ NØRØX) from total grain mass depending upon the value of β. As in the rest of the programme integer values of $0 \leqslant \beta \leqslant 3$ can be accommodated. We define Q^*_{abs} ($\equiv$ QUVABS) and the constant of proportionality, Kl, in the calculation of Q_{abs} ($\equiv$ QIRABS) later as well as the light curve parameters and the limits on τ ($\equiv$ T) utilised in following sections. The absolute limit on τ ($\equiv$ ABSLIM) sometimes imposed is also included.

After printing the values of α and β, (iv) (a) calculates parameters such as the grain number density at R (≡ RDENS); ultra-violet transmission (≡ TAUUV) and the temperature of the grains at the outer edge of the shell (TEMPG, r = R). TEMR1 is the grain temperature at the inner radius ($r = R_1$). These, and other important parameters are then printed out. Section (iv) (b) in which again transmission through the shell at r = R (DISP = 0) is calculated necessarily comes after the definition of the observational wavelengths etc. in section (v).

In section (v) the days after the discovery of the object on which observations were made are read in. Statement number 1Ø allows the value of Δt_u (= 63.5 here) to be read in. Also defined here are the observational wavelengths plus others which enable spectra to be more accurately drawn and the standard (zero magnitude) fluxes relative to the particular photometer used in the observations (Strecker & Ney, 1974).

The observational wavelength loop begins in (vi) (a) where the absorption efficiency in the infra-red is calculated. Section (vi) (b) includes the conversion factor to $Wcm^{-2}\ \mu m^{-1}$ from $ergs^{-1}\ cm^{-2}\ Hz^{-1}$.

We now proceed in (vii) to define the parameter DISP and certain limiting values of this parameter.

DISP is initially given a very small value compared with the shell size. Giving DISP an initial value of zero - as would strictly be correct - would lead to possible overflow later in the programme. The angle AØ (≡ Θ_0, see Figure 4.1) defines the maximum displacement, DISPØ except when $\tau \geq 1$ when $(DISP)_{max} = R$. Once the shell has been filled by the central source radiation $\Theta_0 = \Pi$ (statement 4ØØ).

The upper limit on displacement is set as slightly less than the real value (i.e. DISPR < DISPØ) again to prevent possible overflow. These approximations have negligible effect on the final results however. The incremental value of displacement (≡ DDISP) is then defined.

DISPL is the displacement at which the paraboloid of emission cuts the inner cavity. For times $\tau \geq 2\psi$ (where $\psi \equiv$ RATIO) therefore, DISPL $\equiv$ 0.

The final part of section (vii) initialises the surface brightness integration counter, L. This labels a particular surface brightness to allow the programme to use it in the computation of total observed flux.

In order to follow the logic of sections (viii) and (ix) reference should be made to figure (4.1). Section (viii) is divided into two parts a) and b) by section (ix). (ix) performs the integrations required to derive surface brightness at displacements DISPL < DISP < R1 for $\tau \geq \psi$.

As the Fortran IV compiler does not possess the functions $\sin^{-1}x$ and $\cos^{-1}x$ the angle A2 (initially $\equiv \theta_2$ in figure (4.1)) is found in terms of $\tan^{-1}$(function of DISP). The initial value of A1 is equivalent to the angle $\widehat{OCM}$ of figure (4.1). If the displacement is greater than DISPL however, A1 is set equal to θ_1 (as defined in Chapter 4., section 4.4.2) unless $\theta_1 < \theta_0$ in which case A1 $\equiv \Pi - \theta_2$. Care was taken, by use of conditional statements, to ensure that no errors emerged due to the fact that the function ATAN always gives angles between 0 and $\Pi/2$.

If $\tau < \psi$ or if DISPL $\not<$ DISP $\not<$ R1 for $\tau \geq 2\psi$ we proceed into section (viii) (b). This is where the integration along lines of sight to give the surface brightness at the observed surface of the shell is performed within the above limits.

First the increment in A ($\equiv \theta$) is calculated and then a summation is performed following Simpson's rule, the values of A being substituted in F (Y) above each time. SURFB(L) is thus the surface brightness corresponding to the line or right at displacement DINC + L x DDISP. If DISP $\leq$ DISPR the programme returns control to label 40 having

incremented the displacement and to increment L for the next loop.

If however $\tau \geq 2\psi$ and DISPL < DISP < R1 as in figure (4.5a)C) for example then control passes into section (ix). A1 is initially defined as θ_1 above (cf. $\overset{\frown}{OCA}$ of figure 4.1) unless the displacement is such that A1 $\equiv \Pi - \theta_2$. A2 is re-defined as initially equivalent to angle $\overset{\frown}{OCB}$ of figure (4.1). Increments in A ($\equiv \theta$) along line AB are calculated and a Simpson's rule integration performed. The resulting surface brightness is labelled CONT1. This flux will of course be diminished by extinction in its passage through the front portion of the shell (i.e. along line ML). The optical depth to infra-red radiation along a line such as ML is defined in equation (4.38a). Here the dependence of the equation on the β value is taken into account. The final contribution of the rear portion (AB) to the surface brightness from the surface element at L is given by CONT2 = CONT1* DIM (where DIM is the transmission of infra-red along ML).

Angles A1 and A2 are redefined as equivalent to $\overset{\frown}{OCM}$ and $\overset{\frown}{OCL}$ respectively and control transferred back to label 57. The integration is now performed for the front portion (line ML) and the resulting surface brightness from the element at L is the sum of the new value of CONT1 and CONT2 as already found. Displacement is incremented and control returned to label 4Ø where the next loop in DISP and L begins.

Having completed calculation of surface brightnesses across a radius of the observed disc for one wavelength at a given time, control passes to statement label 1ØØ and thence into section (x). Here the integration is in terms of DISP for all the surface. Again Simpson's rule is used with the appropriate integral dependent upon the value of β. This is where the value of SURFB(L) related to a particular value of DISP is utilised from those calculated above.

Once the theoretical observed luminosity is calculated and converted to the alternative wavelength units it is compared with actual

observations in the function TEST(G). The remainder of the observational wavelengths are then run through the programme before the next value of T is assumed. This final section (xi) then prints the results out on the line printer and also places them into a disc file in such a way that they are acceptable to the SPSS package of routines on the UMRCC 1906A/7600. This enables 'scattergrams' of both the observational data and theoretical model to be output on the line printer at the same time as the numerical results are returned. Thus reasonably fast comparisons of the fit of the model to the observations can be made. Figure (A1.2) shows a scattergram returned from computations based on Nova Vulpeculae 1976.

Figure (A1.1) Copy of a computer programme to model the behaviour of Nova Vulpeculae 1976.

```
      PROGRAM VURES(FLASH,OUTPUT,FILE1,TAPE7=FLASH
     1,TAPE2=OUTPUT,TAPE5=FILE1)
C PROGRAMME TO CALCULATE THE OBSERVED LUMINOUS FLUX FROM I/R RADIATION
C RERADIATED FROM DUST GRAINS SURROUNDING A FLUCTUATING SOURCE
C
C SPHERICALLY SYMMETRIC DUST SHELL MODEL
C
C THE LATE I/R DEVELOPMENT OF NOVAE
C
C NOVA VULPECULAE 1976(SEE NEY AND HATFIELD 1978)
C
C
      DIMENSION WAVLEN(50),SURFB(100),FREQ(4),DAY(33),ED(33,5)
     1,FLUX0(30),OBSLUM(5),TEST(5),OFLUX(5)
      INTEGER G,P
      REAL NORMX,K1,L0,M,LIMIT1,LIMIT4,LIMIT5
C-----------------------------------------------------------------------
C
C FUNCTION FOR INTEGRATION TO GIVE SURFACE BRIGHTNESS ALONG LINES AT
C PARTICULAR DISPLACEMENTS 'DISP'
      SMALLR(Y)=DISP/SIN(Y)
      TUV(Y)=EXP(-SECTU*(1./R1-1./SMALLR(Y)))
      TIR(Y)=EXP(-SECTI*DISP**(1.-BETA)*(Y-A2))
      GLUM(Y)=L0*EXP(-OMEGA*R/C*(T-SMALLR(Y)/R*(1.-COS(Y))))
      GTEMP(Y)=PK*(GLUM(Y)*C*C*TUV(Y)*QUVABS/(ZETA6*GAMMA6*32*PI*
     1SMALLR(Y)**2.*K1*PH))**(1./(ALPHA+4.))
      PLANCK(Y)=C1/(EXP(PK*FREQ/GTEMP(Y))-1.)
      F(Y)=PLANCK(Y)*TIR(Y)                                    B=2
C
C-----------------------------------------------------------------------
C TITLE TO DATA PRINTOUT
      WRITE(2,2501)
C
C READ IN DATA FROM STORED ARRAY OF I/R OBSERVATIONS
C
      READ(7,2502)((ED(P,G),G=1,5),P=1,33)
C
C PRINT OUT DATA
      WRITE(2,2502)((ED(P,G),G=1,5),P=1,33)
C
2501  FORMAT(//23H DATA FROM FILE VUDATA //)
2502  FORMAT(5F8.2)
C
C SET CONSTANTS
      ALPHA=1.0
      BETA=2.0                                                 *****
C
      ZETA6=1.01734
      IF(ALPHA.EQ.1.0)ZETA6=1.03693
      IF(ALPHA.EQ.0.0)ZETA6=1.08232
      GAMMA6=120
      IF(ALPHA.EQ.1.0)GAMMA6=24.0
      IF(ALPHA.EQ.0.0)GAMMA6=0.0
C
      BK=1.380626E-16
      PH=6.626205E-27
      C=2.997925E+10
```

(i)

(ii)

(iii)

```
      PI=4.*ATAN(1.)
      PK=PH/BK
60    C
      R=0.8E+16
      RATIO=0.75/0.8
      R1=RATIO*R
      D=3.0E+21
65    C
      C CALCULATE 'NORUX' FROM GRAIN MASS
      C
      AG=2.E-06
      XSECT=PI*AG*AG
70    GMASS=1.0E-06
      SOLARM=1.99E+33
      SGRAPH=2.5
      NORUX=GMASS*SOLARM*3./(16.*PI*PI*AG**3.*SGRAPH*(R-R1))
      IF(BETA.EQ.1.0)NORUX=GMASS*SOLARM*6.0/
     1(16.*PI*PI*AG**3.*SGRAPH*(R*R-R1*R1))
75    IF(BETA.EQ.0.0)NORUX=GMASS*SOLARM*3.0/
     1(16.*PI*PI*AG**3.0*SGRAPH*(R**3.-R1**3.))
      SECT=NORUX*XSECT
      QUVABS=1.0
80    SECTU=SECT*QUVABS
      K1=0.135/(1.E-05*(1.3626E+14)**ALPHA)*AG
      C
      C LIGHT CURVE PARAMETERS
      C
85    LO=4.E+38
      OMEGA=1.5E-07
      C INTEGRATION LIMITS ETC.
      LIMIT1=RATIO
      LIMIT4=2.*RATIO
90    LIMIT5=2.0
      ABSLIM=1.5
      C----------------------------------------------------------------------
      C
      C WRITE IMPORTANT PARAMETERS
95    C
      WRITE(2,20)ALPHA,BETA
      20 FORMAT(//8H ALPHA= ,F8.2,7H BETA= ,F8.2)
      C
      C CALCULATE DENSITY OF GRAINS AT OUTER RADIUS AND PRINT IMPORTANT RESULTS
100   RDENS=NORUX/(R*R)
      IF(BETA.EQ.1.0)RDENS=NORUX/R
      IF(BETA.EQ.0.0)RDENS=1.*NORUX
      C
      C CALCULATE TRANSMISSION ALONG RADII FOR U/V AND I/R
105   TAUUV=EXP(-SECTU*(1./R1-1./R))
      IF(BETA.EQ.0.0)TAUUV=EXP(-SECTU*(R-R1))
      IF(BETA.EQ.1.0)TAUUV=RATIO**(SECTU)
      C
      C CALCULATE TEMPERATURE AT OUTER RADIUS (PEAK LUM.) AND PRINT RESULTS
110   TEMPG=PH/BK*(LO*C*C*TAUUV*QUVABS/(ZETA6*GAMMA6*32.*PI*R**2.*K1*PH)
     1)**(1./(ALPHA+4.))
      TEMR1=TEMPG*(RATIO*TAUUV)**(-1./(ALPHA+4.))
      WRITE(2,30)D,LO,OMEGA,R1,R,AG,GMASS,RDENS,TEMR1,TEMPG,TAUUV
      30 FORMAT(5X,3H D=,E10.4/4X,4H LO=,E10.4,8H  OMEGA=,E10.4/
```

(iii) (cont.)

(iv) (a)

```
      14X,4H R1=,E10.4,5X,3H R=,E10.4/4X,4H AG=,E10.4,1X,
      17H GMASS=,E10.4,1X,7H RDENS=,E10.4/1X,7H TEMR1=,
      1E10.4,1X,7H TEMPG=,E10.4/1X,7H TAUUV=,E10.4///)
       WRITE(2,37)
37     FORMAT(54H  CALC    TEST    CALC    TEST    CALC    TEST  CALC    TEST /
      102H  3.5     3.5     4.8     4.8     8.6     8.6   10.6    10.6     DAY )
C++++++++++++++++++++++++++++++++++++++++++++++++++++++++++++++++++++++++++++++++
C TIME LOOP STARTS
C
C OBSERVATION TIMES (FROM DISCOVERY) FOR NOVA VULPECULAE 1976
C SET UP TIME LOOP
      DO 10 P=1,33
10     DAY(P)=-63.5
       DAY(1)=DAY(1)+64.9
       DAY(2)=DAY(2)+67.8
       DAY(3)=DAY(3)+70.5
       DAY(4)=DAY(4)+71.9
       DAY(5)=DAY(5)+78.8
       DAY(6)=DAY(6)+80.8
       DAY(7)=DAY(7)+82.8
       DAY(8)=DAY(8)+84.8
       DAY(9)=DAY(9)+87.8
       DAY(10)=DAY(10)+88.8
       DAY(11)=DAY(11)+98.8
       DAY(12)=DAY(12)+103.75
       DAY(13)=DAY(13)+108.75
       DAY(14)=DAY(14)+112.75
       DAY(15)=DAY(15)+118.7
       DAY(16)=DAY(16)+124.7
       DAY(17)=DAY(17)+131.7
       DAY(18)=DAY(18)+132.6
       DAY(19)=DAY(19)+138.6
       DAY(20)=DAY(20)+147.6
       DAY(21)=DAY(21)+152.25
       DAY(22)=DAY(22)+153.6
       DAY(23)=DAY(23)+165.4
       DAY(24)=DAY(24)+170.5
       DAY(25)=DAY(25)+172.5
       DAY(26)=DAY(26)+186.4
       DAY(27)=DAY(27)+191.4
       DAY(28)=DAY(28)+194.35
       DAY(29)=DAY(29)+198.35
       DAY(30)=DAY(30)+213.4
       DAY(31)=DAY(31)+225.3
       DAY(32)=DAY(32)+232.4
       DAY(33)=DAY(33)+235.4
       DO 9000 P=1,33
       T=C/R*DAY(P)*86400.
C-------------------------------------------------------------------------------
C OBSERVATIONAL WAVELENGTHS
C
       DO 1 G=1,30
       FLUX0(G)=0.0
1      WAVLEN(G)=0.0
       WAVLEN(1)=3.5E-04+WAVLEN(1)
       WAVLEN(2)=4.80E-04+WAVLEN(2)
       WAVLEN(3)=8.60E-04+WAVLEN(3)
```

(iv)(a) (cont.)

(v)

(v) (cont)

```
      WAVLEN(4)=10.70E-04+WAVLEN(4)
      WAVLEN(5)=12.20E-04+WAVLEN(5)
      WAVLEN(6)=18.00E-04+WAVLEN(6)
      WAVLEN(7)=4.00E-04+WAVLEN(7)
      WAVLEN(8)=4.50E-04+WAVLEN(8)
      WAVLEN(9)=5.00E-04+WAVLEN(9)
      WAVLEN(10)=5.50E-04+WAVLEN(10)
      WAVLEN(11)=6.00E-04+WAVLEN(11)
      WAVLEN(12)=6.50E-04+WAVLEN(12)
      WAVLEN(13)=7.00E-04+WAVLEN(13)
      WAVLEN(14)=7.50E-04+WAVLEN(14)
      WAVLEN(15)=8.00E-04+WAVLEN(15)
      WAVLEN(16)=8.50E-04+WAVLEN(16)
      WAVLEN(17)=9.00E-04+WAVLEN(17)
      WAVLEN(18)=9.50E-04+WAVLEN(18)
      WAVLEN(19)=10.0E-04+WAVLEN(19)
      WAVLEN(20)=10.5E-04+WAVLEN(20)
      WAVLEN(21)=11.0E-04+WAVLEN(21)
      WAVLEN(22)=2.75E-04+WAVLEN(22)
      WAVLEN(23)=3.25E-04+WAVLEN(23)
      WAVLEN(24)=3.75E-04+WAVLEN(24)
      WAVLEN(25)=4.25E-04+WAVLEN(25)
      WAVLEN(26)=5.25E-04+WAVLEN(26)
      WAVLEN(27)=5.75E-04+WAVLEN(27)
      WAVLEN(28)=6.75E-04+WAVLEN(28)
      WAVLEN(29)=7.25E-04+WAVLEN(29)
      WAVLEN(30)=7.75E-04+WAVLEN(30)
C
C FLUX VALUES AT ZERO MAGNITUDE
C(SEE STRECKER AND NEY,1974)
      FLUX0(1)=FLUX0(1)-14.15
      FLUX0(2)=FLUX0(2)-14.66
      FLUX0(3)=FLUX0(3)-15.62
      FLUX0(4)=FLUX0(4)-16.01
      FLUX0(5)=FLUX0(5)-16.18
      FLUX0(6)=FLUX0(6)-16.89
C-----------------------------------------------------------------------
C
C
```

(vi) (a)

```
C\\\\\\\\\\\\\\\\\\\\\\\\\\\\\\\\\\\\\\\\\\\\\\\\\\\\\\\\\\\\\\\\\\\\\\\\\\\\\\\\
C WAVELENGTH LOOP STARTS
      DO 8000 G=1,4
C CALCULATE 1/R EXTINCTION PARAMETERS
      FREQ=C/WAVLEN(G)
      CI=2.*PH*FREQ**3./(C*C)
      QIRABS=K1*FREQ**ALPHA
      SECTI=SECT*QIRABS
C
```

(iv) (b)

```
      TAUIR=EXP(-SECTI*(1./R1-1./R))
      IF(BETA.EQ.0.0)TAUIR=EXP(-SECTI*(R-R1))
      IF(BETA.EQ.1.0)TAUIR=(R1/R)**(SECTI)
```

(vi) (b)

```
C CALCULATE CONVERSION FACTOR FOR FLUX TO W/CM/MICRON
      SICONV=FREQ*FREQ*1.E-11/C
C
C-----------------------------------------------------------------------
C NUMBER OF STEPS
C N-SURFACE BRIGHTNESS
```

(vi) (b) (cont)

```
      C M-LUMINOSITY
            M=50
            N=64
      C-----------------------------------------------------------------------------
```

(vii)

```
      C
      C
      C CALCULATE DISPLACEMENTS
      C
      C INITIAL DISPLACEMENT
            DINC=1.E+13
            DISP=DINC
            IF(T.GT.LIMIT5)GO TO 400
            A0=ATAN(SQRT(2*T-T*T)/(1-T))
            IF(T.GT.1.00001)A0=A0+PI
            DISP0=R*SIN(A0)
            DDISP=(DISP0-DISP)/M
            DISPR=DISP0-5.E+13
      400   IF(T.GT.LIMIT5)A0=PI
            IF(T.GT.1.0)DDISP=(R-DISP)/M
            IF(T.GT.1.0)DISPR=R-5.E+13
            IF(T.GE.LIMIT4)GO TO 401
            DISPL=SQRT(T*(2.*R1/R-T))*R
      401   IF(T.GT.LIMIT4)DISPL=0.0
      C
      C INITIALSE SURFACE BRIGHTNESS INTEGRATION COUNTER-(L)
            L=0
      40    L=L+1
      C
```

(viii)(a)

```
      C CALCULATE ANGLES FOR S.B. INTEGRATION
            A2=ATAN((DISP/R)/(SQRT(1-(DISP/R)**2.)))
            B=2*T*SIN(A2)/(T*T+SIN(A2)**2.)
            IF(DISP.GE.DISPL)GO TO 51
            A1=ATAN(DISP/(R1*SQRT(1.-(DISP/R1)**2.)))
            GO TO 56
      51    CONTINUE
            B1=ATAN(B/SQRT(1.-B*B))
            A1=PI-B1
            IF(DISP.LT.DISPL)GO TO 406
            IF(A1.LT.A0)GO TO 56
      406   CONTINUE
            IF(T.GT.1.0)GO TO 56
            A3=ATAN(T/SQRT(1.-T*T))
            IF(A2.GT.A3)A1=B1
      56    CONTINUE
            IF(DISP.LT.DISPL)GO TO 506
            IF(A1.LT.A0)A1=PI-A2
      506   CONTINUE
            IF(T.LT.LIMIT1)GO TO 59
            DD=DISPL/R
            IF(A2.LT.ATAN(DD/SQRT(1.-DD*DD)))GO TO 59
            IF(A2.GT.ATAN(RATIO/SQRT(1.-RATIO*RATIO)))GO TO 59
      C
      C
```

(ix)

```
      C*****************************************************************************
      C THIS SUBSECTION'S CONCERNED WITH TOTAL S.B. CONTRIBUTION FROM EMITTING
      C VOLUME AT REAR OF SPHERE WHEN T.GT.LIMIT2
      C
```

```
                A1=PI-B1
                IF(A1.LT.A0)A1=PI-A2
                A2=PI-ATAN(DISP/(R1*SQRT(1.-(DISP/R1)**2.)))
                STEP1=(A1-A2)/N
290             KX=0
          C
          C SET SUMMING VARIABLES FOR BACK END S.B. INTGN..
          57    BSUM4=0.0
                BSUM2=0.0
295             STEP2=STEP1+STEP1
                KX=KX+1
          C GIVE 'A' INITIAL VALUE IN LOOP
                A=A2+STEP1
          C INITIALISE LOOP COUNTER
300             KZ=1
          C
          C THE SUMMING LOOP
          58    BSUM4=BSUM4+F(A)
                BSUM2=BSUM2+F(A+STEP1)
305             IF(KZ.GE.N-3)GO TO 43
                KZ=KZ+2
                A=A+STEP2
                GO TO 58
          43    FRED1=4.*BSUM4
310             FRED2=BSUM2*2.
                FRED3=F(A1)
                FRED4=F(A1-STEP1)*4.
                FRED5=F(A2)
                FRED(KX)=FRED1+FRED2+FRED3+FRED4+FRED5
315             CONT1=STEP1/3.0*FRED(KX)
          C
          C CALCULATE THE I/R OPTICAL DEPTH THROUGH FRONT PORTION
                DIM=EXP(-SECTI
               1*(ATAN((DISP/R1)/SQRT(1.-(DISP/R1)**2.))
320            1-ATAN(DISP/(R*SQRT(1.-(DISP/R)**2.))))/DISP)
                IF(BETA.EQ.1.0)DIM=(RATIO*(1.+SQRT(1.-(DISP/R1)**2.))/(1.+COS(ATAN
               1((DISP/R)/SQRT(1.-(DISP/R)**2.)))))
               1**SECTI
                IF(BETA.EQ.0.0)DIM=EXP(-SECTI*(SQRT(R**2.-DISP**2.)
325            1-R1*SQRT(1.-(DISP/R1)**2.)))
                IF(KX.EQ.1)CONT2=CONT1*DIM
          C
          C FRONT PORTION ANGLES
                A1=PI-A2
330             A2=ATAN((DISP/R)/SQRT(1.-(DISP/R)**2.))
                STEP1=(A1-A2)/N
                IF(KX.EQ.1)GO TO 57
                SUMFB(L)=CONT1+CONT2
          C INCREMENT DISP AND RETURN TO 40
335             DISP=DISP+DDISP
                GO TO 40
          C*****************************************************************************
          C
          C
342       59    CONTINUE
                IF(A2.GT.A1)GO TO 100
          C
```

(ix) (cont)

(viii) (b)

```
      C INTEGRATION BY SIMPSON'S RULE FOR SURFACE BRIGHTNESS
            H=(A1-A2)/N
      345   TWOH=H+H
      C
      C SET SUMMING VARIABLES.
      C
            SUM4=0.0
      350   SUM2=0.0
      C GIVE 'A' INITIAL VALUE IN LOOP
            A=A2+H
      C INITIALISE LOOP COUNTER
            I=1
      355   C THE SUMMING LOOP
      C
      60    SUM4=SUM4+F(A)
            SUM2=SUM2+F(A+H)
            IF(I.GE.N-3)GO TO 70
      360   I=I+2
            A=A+TWOH
            GO TO 60
      70    CONST3=4.*SUM4
            CONST4=2.*SUM2
      365   CONST5=F(A1)
            CONST6=F(A1-H)*4.
            CONST7=F(A2)
            CONST2=CONST3+CONST4+CONST5+CONST6+CONST7
      C
      370   C COMPUTE AND PRINT SURFACE BRIGHTNESS
      C AND GRAIN TEMPS AND OPTICAL DEPTHS AT THE EXTREMES
      C (PRINT OPTIONAL)
            SURFB(L)=H/3.0*CONST2
      C
      375   C INCREMENT DISP AND RETURN TO 40
            DISP=DISP+DDISP
            IF(DISP.GT.DISPR)GO TO 100
            GO TO 40
      100   CONTINUE
      380   C
      C-----------------------------------------------------------------------
      C
      C INTEGRATION BY SIMPSON'S RULE FOR OBSERVED LUMINOSITY
      C
      385   OMEG=2.*PI*SECTI/(D*D)
      C SET SUMMING VARIABLES
            DSUM4=0.
            DSUM2=0.
            DISP=DINC+DDISP
      390   DISP2=DDISP+DDISP
      C INITIALISE LOOP COUNTER
            J=2
            K=1
      C THE SUMMING LOOP
      395   1112  CONTINUE
            IF(BETA.LT.2.0)GO TO 1112
            DSUM4=DSUM4+SURFB(J)
            DSUM2=DSUM2+SURFB(J+1)                                    *****
      1112  IF(BETA.EQ.1.0)DSUM4=DSUM4+DISP*SURFB(J)
```

(viii)(b) (cont)

(x)

```
      IF(BETA.EQ.0.0)DSUM4=DSUM4+DISP*DISP*SURFB(J)
      IF(BETA.EQ.1.0)DSUM2=DSUM2+(DISP+DDISP)*SURFB(J+1)
      IF(BETA.EQ.0.0)DSUM2=DSUM2+(DISP+DDISP)*(DISP+DDISP)*SURFB(J+1)
      IF(K.GE.M-3)GO TO 132
      K=K+2
      J=J+2
      DISP=DISP+DISP2
      GO TO 112
C
C-------------------------------------------------------------------------------
C
C COMPUTE AND PRINT OBSERVED LUMINOSITY
132   OBSLUM=OMEG*(DDISP/3.)*(4.*DSUM4+2.*DSUM2+4.*SURFB(M-1)+SURFB(1)  *****
     1+SURFB(M))                                                        *****
      IF(BETA.EQ.1.0)OBSLUM=OMEG*(DDISP/3.0)*(4.*DSUM4+2.*DSUM2+4.*
     1(DISPO-DISP2)*
     1SURFB(M-1)+DINC*SURFB(1)+(DISPO-DDISP)*SURFB(M))
      IF(BETA.EQ.0.0)OBSLUM=OMEG*(DDISP/3.0)*(4.*DSUM4+2.*DSUM2+
     14.*(DISPO-
     1DISP2)**2.*SURFB(M-1)+DINC*DINC*SURFB(1)+(DISPO-DDISP)**2.*
     1SURFB(M))
      COBSLU=SICONV*OBSLUM
      OBSLUF=ALOG10(OBSLUM)
      OBSLUW(G)=ALOG10(COBSLU)
C
C TEST CALCULATED VALUES AGAINST OBSERVATION
      OFLUX(G)=FLUXO(G)-ED(P,G)/2.5
      TEST(G)=OBSLUW(G)-OFLUX(G)
C
      IF(OBSLUW(G).LT.-18.5)GO TO 9000
C
8000  CONTINUE
C END OF WAVELENGTH LOOP
C
C+++++++++++++++++++++++++++++++++++++++++++++++++++++++++++++++++++++++++++++++
C
      WRITE(2,2500)OBSLUW(1),TEST(1),OBSLUW(2),TEST(2),
     1OBSLUW(3),TEST(3),OBSLUW(4),TEST(4),DAY(P)
2500  FORMAT(9F7.2)
      WRITE(5,5200)OBSLUW(1),OFLUX(1),OBSLUW(2),OFLUX(2),
     1OBSLUW(3),OFLUX(3),OBSLUW(4),OFLUX(4),DAY(P)
5200  FORMAT(9F7.2)
9000  CONTINUE
C END OF TIME LOOP
C
C\\\\\\\\\\\\\\\\\\\\\\\\\\\\\\\\\\\\\\\\\\\\\\\\\\\\\\\\\\\\\\\\\\\\\\\\\\\\\\\\
C
2101  CONTINUE
C
C COMPLETION STATEMENT AND PROGRAMME END
      WRITE(2,3101)
3101  FORMAT(33H COMPUTATION COMPLETE OR INVALID )
C-------------------------------------------------------------------------------
C-------------------------------------------------------------------------------
C-------------------------------++++++++++<<<<<<<<<<>>>>>>>>>>++++++++++--------
      STOP
      END
```

X (cont)

(xi)

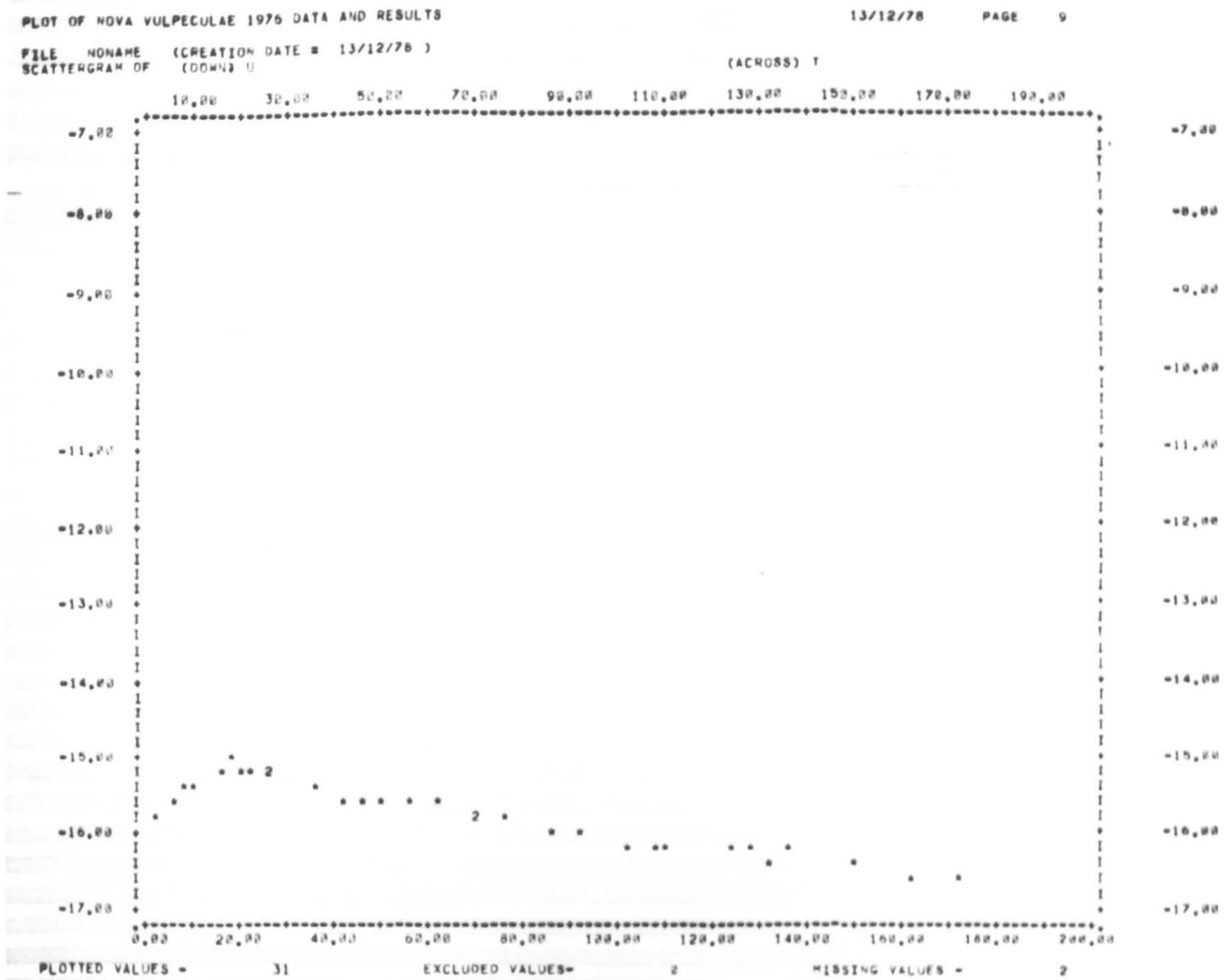

Figure (A1.2) Scattergram of the observed flux at 10.6 μm with time for Nova Vulpeculae 1976 derived from a programme similar to that shown in figure (A1.1).

APPENDIX A2

Glossary of Variables and Constants

A2.1.1 Introduction

This appendix contains an alphabetical listing of the main variables and constants used several times during this work together with a brief explanation of each. Greek and Roman letters are listed separately. Variables and terms in common usage have on the whole been omitted unless some confusion may arise by their omission.

A2.2.1 The Greek Variables and Constants

α	Exponent of frequency relating frequency of emitted and incident radiation to the absorption efficiency of the grain material.
α_c	Carbon atom sticking coefficient.
β	Exponent of the dependence of grain number density on distance from a central object.
Γ	The gamma function
γ	$\equiv\left(\frac{\alpha+4}{2}\right)\left(3-\beta\right)-1$
γ'	$\equiv \gamma - \left(\frac{\alpha+4}{2}\right)$
γ_G	The Universal constant of gravitation.
δ_λ	Optical depth at wavelength λ.
δ_{BG}	Optical depth to background radiation.
ζ	The Reimann-Zeta function.
Ⓗ	Debye temperature of grain material
θ, θ_0, θ_1, θ_2	Angles as defined in figure (4.1).
θ_{BB}	Black body angular diameter.
θ_{evap}	Angle defined as θ above of a grain which has just been observed to evaporate.
λ	Wavelength.
λ_B	Limiting wavelength of the analytical solution of the equation of transfer.

λ_c	Cut-off wavelength of a filter
λ_{max}	Wavelength of maximum luminous flux.
ν	Frequency.
ρ	Exponent in the temperature dependence of grain material electrical conductivity.
Σ_ν, Σ_λ	Surface brightness of an object at frequency ν and wavelength λ respectively.
Σ_{BG}	Background radiation surface brightness.
σ	Electrical conductivity of grain material.
σ_s	Stefan's constant.
τ, τ_1	Time measured in units of light travel time across the external radius of the dust shell and the radius of the internal cavity respectively.
Φ	Phase difference between fluctuations from the central source and dust shell as observed externally.
χ	$\equiv \frac{\omega R}{C}$.
ψ	Ratio of cavity radius to external dust shell radius.
ψ_0	Value of ψ at time $t = t_0$.
Ω	Solid angle subtended by a source.
ω	Angular frequency.

A2.2.2 The Roman Variables and Constants

a	Grain radius.
a_0	Initial grain radius prior to evaporation or further growth.
a_∞	Maximum grain radius on grain growth model.
$B(\nu, T)$	Planck function at frequency ν, temperature T.
B_n	nth Bernoulli number.
C_v	Specific heat at constant volume.
D	Distance from observer to central source.
D_r	Drag force.
F_λ, F_ν	Observed luminous flux at wavelength λ and frequency ν respectively.
G	Gravitational force.
g	Asymmetry factor for scattering.
H	Latent heat of Vaporisation of grain material.
HFN	The Heating Function defined by the product of the efficiency factor for absorption and the central source luminosity integrated over all wavelengths.
I_λ	Intensity of radiation at wavelength λ.
i	Inclination of a disc of dust grains to the line of sight of a distant observer.
L	Luminosity.

L_{CL}	Luminosity of the constant luminosity phase of a moderate speed nova.
L_{IR}, L_{UV}	Infra-red and ultra-violet luminosities respectively.
M_{ej}	Total mass ejected by a nova.
M_g	Total mass of dust grains in a dust shell.
M_v	Absolute visual magnitude.
m	Refractive index of grain material.
m_C, m_H	Masses of carbon and hydrogen atoms respectively.
m_g	Mass of an individual grain.
m_v	Observed visual magnitude.
N	Grain number density.
N_C, N_H	Gas number densities of carbon and hydrogen atoms respectively.
N_{TOTAL}	Total number of grains formed per outburst of a nova.
N_1	Grain number density at the inner radius, R_1.
P	Period of fluctuation of a source.
PFN	Radiation pressure function.
P_r	Radiation pressure force on a grain.
P_v	Rate of energy loss through vaporisation.
p_c	Partial pressure of free carbon.
P_{sat}	Saturated vapour pressure.

Q_{abs}, Q_{sca}, Q_{ext}, Q_{pr}	Efficiency factors for absorption, scattering, extinction and radiation pressure respectively.
Q''_0	Constant of proportionality relating absorption efficiency of a grain to grain temperature, radius and the frequency of incident radiation.
$\bar{Q}$	Planck mean of the efficiency factors.
R	External radius of dust distribution.
R_1	Cavity radius in dust distribution.
R_c	The gas constant.
R_{gas}	Radius of the ejected shell of gas from a nova.
r	Central source - grain distance.
r'	Displacement of a point in the dust shell from the central source as observed externally.
r_c	Radius of circle of emission in the case of a disc of dust grains surrounding a variable central source.
r_{evap}	The observed radius vector of a grain which has just evaporated.
r_0	The condensation distance of grains after ejection from a central source.
s	Grain bulk density.
T	Gas temperature.
T_{BB}	Black body temperature.

T_c	Condensation temperature of dust grains.
T_g	Grain temperature.
T_{rad}	Temperature of a perfect black body if placed at distance r from a central source.
T_*	Effective stellar surface temperature.
t	Time as measured from a given origin.
t_c	Time of cessation of expansion of the infra-red emitting region of a dust shell as externally observed.
t_{cool}	Cooling time of a grain.
t_{evap}	Evaporation time of a grain.
t_i	Time taken for complete ionisation of a nova gas shell.
t_0	Time from outburst of a nova to the onset of dust formation.
$t_{3,v}$	Time in days for the observed visual magnitude of a nova to fall by 3 magnitudes.
Δt_u	Time from peak visual luminosity of a nova to the transition slope break.
Δt_0	Time interval between heating function maximum and the start of infra-red emission from a disc of dust grains surrounding a variable central source.
U	Internal energy of a grain.
u	Relative grain-gas velocity.

u_T Terminal velocity of a grain moving in a gas.

v Ejection velocity of matter from a nova.

v_d Apparent transverse velocity of expansion of the emitting region of a dust shell relative to the central source.

$v_{d.e.}$ Velocity of the Diffuse-Enhanced spectrum of a nova.

v_p Velocity of the Principal spectrum of a nova.

$\bar{v}_{th}$ The mean thermal velocity of gas atoms or molecules.

v_r Velocity of expansion of the emission circle in the case of a disc of dust grains surrounding a variable central source.

APPENDIX A3

The Visibility of Pregalactic Fluctuations and the Consequences for the Value of the Deceleration Parameter, q_o

A3.1.1 General Introduction

The work described in this appendix was carried out during the tenure of the University of Keele Research Studentship at a time when the paper summarising the basis of the main part of this thesis was under review (Bode and Evans, 1979a). This appendix is not however directly related to the preceeding chapters although it is concerned in part with the same extinction properties as those of the interstellar dust already considered.

N.B. The notation used in this appendix is independent of that used earlier in this work.

A3.1.2 Introduction to Theory and Observation

It is generally accepted that the cosmic microwave background radiation first observed by Penzias and Wilson (1965) is one of the strongest pieces of evidence in favour of there having been a hot dense phase in the early history of the universe. At early times radiation and matter were in thermal equilibrium. However, as soon as the point in the expansion was reached when the equilibrium temperature fell below about $4000^{o}K$, the dilute hydrogen gas ceased to be completely ionised and opaque due to Thomson scattering from electrons. This 'era of recombination' occurred at a time t_r corresponding to a red-shift Z_r given by

$$\frac{T(t_o)}{T(t_r)} = \frac{1}{1 + Z_r}$$

where $T(t_o)$ is the present temperature of the microwave background and $T(t_r)$ is the temperature at recombination.

Observations of the cosmic background radiation have shown that the spectrum follows closely that of a black body with temperature $T(t_o)$ $2.7^{o}K$ (Peebles, 1974). This leads to a value of Z_r of about 1500.

Although it is not yet clear how inhomogeneities arose in the early universe before recombination, the fact that galaxies are observed now is taken to indicate that the hot dense phase up to time t_r was not homogeneous but contained density fluctuations presumably of the order of a galactic mass. These density fluctuations would give rise to temperature fluctuations and therefore it is expected that the microwave background should, on a small enough scale, appear anisotropic. Present theories indicate that these temperature anisotropies should give $\Delta T(t_o)/T(t_o) \sim 10^{-4} - 10^{-3}$ over angles given approximately by Weinberg, (1972) as

$$\phi \simeq \frac{2H_o}{c}\left[\frac{3Mq_o^2}{8\pi p_c}\right]^{1/3}$$

where H_o is the Hubble parameter value at time t_o (this being the constant of proportionality between the cosmic scale factor $R(t_o)$ and its rate of change $\dot{R}(t_o)$ at time t_o); M is the fluctuation mass; c is the velocity of light; ρ_c is the critical or closure density of the universe and q_o is the deceleration parameter defined in terms of the scale factor as

$$q_o \equiv -\ddot{R}(t_o)\,\frac{R(t_o)}{\dot{R}^2(t_o)}$$

It can be seen that even for small values of q_o, ϕ is of the order of several seconds of arc for m = 10" $M_\odot$ (an average galactic mass), $\rho_c \simeq 5 \times 10^{-30}$ gcm^{-3} and $H_o = 50$ km s^{-1} Mpc^{-1} .

Because of the great significance attached to observation of small-scale anisotropy in the background radiation numerous attempts have been undertaken in recent years to detect any that might be present (Weinberg, 1972; Carpenter et al., 1973). No significant anisotropy appears to exist down to limits of at most $\Delta T/T \sim 3.2 \times 10^{-4}$ over angles of less than $\phi \sim 1$" according to these observations. All this applies if the universe is completely transparent to the cosmic background radiation. We now consider the effects of various obscuring materials beginning with intergalactic dust.

A3.2.1 Obscuration by Dust

It was suggested by Alfvèn and Mendis (1977) that dust already existing in galaxies at any epoch might make the universe optically thick to the background radiation. This would effectively smooth-out any fluctuations and render the observed background highly isotropic.

However Pollaine (1978) has subsequently shown that a more detailed treatment, including evolutionary effects etc., indicates that galactic dust makes virtually no contribution to the opacity of the universe from the epoch of galaxy formation to the present.

Although primarily concerned with galactic dust, Alfvèn and Mendis refer to the possible existence of intergalactic dust. Numerous other authors have presented evidence from which they derive upper limits to dust density (Nickerson and Partridge, 1971; McKee and Petrosian, 1974) or actual values for the density (Nandy et al., 1974; Schmidt, 1974). The question thus arises as to whether intergalactic dust could make the universe optically thick, effectively smearing out any fluctuations in the microwave background radiation. It will be shown that if dust between galaxies is responsible for making the universe optically thick then very severe constraints are placed upon the deceleration parameter, q_o .

If intergalactic dust does exist, the main questions which must be asked are

(i) How did it get there?

(ii) When was it formed?

(iii) What is its composition?

(iv) What is its density?

Chiao and Wickramasinghe (1972) have shown that the radiation pressure of starlight upon charged conducting grains in galaxies is sufficient to expel sub-micron interstellar grains along magnetic field lines into intergalactic space. Estimates of the density of material in the form of grains ejected in this way in intergalactic space agree well with the observed limits quoted above.

If this mechanism is the dominant one then grains will have existed only since galaxies contained dust producing stars. The time at which galaxies formed is given approximately by the time for the

matter density of the universe to reach that presently in galaxies. This time we denote as t_g.

Field (1974) looks at this problem in a slightly more detailed way by considering the original perturbations in a way similar to that for the whole universe. In other words the scale and mass of the perturbation determine whether it will expand forever with the universe or undergo expansion to a maximum and then contract (which is analogous with the universe as a whole for different values of q_o). From this he deduces that galaxies were formed at a time later than $3.5 \times 10^7 (M_{11})^{\frac{1}{4}}$ years, where $M_{11} = M/10^{11} M_\odot$, otherwise they would be more tightly bound than observed. The best estimate of t_g given by Field is 7×10^7 years. This is slightly less than the value calculated by Partridge and Peebles (1967) of 1.5×10^8 years.

The value of Z_g, the observed redshift corresponding to time t_g, will of course depend on the cosmological model we use.

If we assume zero cosmological constant and that the universe is on a large scale isotropic, homogeneous, and has negligible pressure (at the epochs of interest) then we may describe it using a Friedmann model. Equation (A3.1) below is the so-called Friedmann equation where this model universe is described in terms of the cosmic scale factor, R(t); the universal gravitation constant, G; the matter density, $\rho(t)$ and the curvature index, k (Weinberg, 1972)

$$\frac{\dot{R}^2(t)}{R^2(t)} = \frac{8\pi G\rho(t)}{3} - \frac{kc^2}{R^2(t)} \qquad \text{(A3.1)}$$

If the energy density of the universe is dominated by nonrelativistic matter with negligible pressure p, then

$$\rho(t) = \rho_o \left[\frac{R(t)}{R_o}\right]^{-3} \qquad \text{for } p \ll \rho c^2 \qquad \text{(A3.2)}$$

By taking equation (A3.2) and writing ρ_o and k/R_o^2 in terms of q_o and H_o, where R_o is the present scale factor, equation (A3.1) can be expressed in the form

$$\frac{\dot{R}^2(t)}{R_o^2} = H_o^2 \left[1 - 2q_o + 2q_o \left[\frac{R_o}{R(t)} \right] \right] \qquad \text{(A3.3)}$$

Equation (A3.3) can be solved parametrically (Weinberg, 1972). In the case of $q_o > \frac{1}{2}$

$$\theta - \sin\theta = \frac{t\, H_o\, (2q_o - 1)^{3/2}}{q_o} \qquad \text{(A3.4a)}$$

$$\frac{R_o}{R(t)} = 1 + Z = \frac{2q_o - 1}{q_o} \quad \frac{1}{(1 - \cos\theta)} \qquad \text{(A3.4b)}$$

where θ is the so-called development angle of the universe at time t. For any values of H_o, q_o and t_g we can therefore find the value of Z_g.

For $0 < q_o < \frac{1}{2}$ equation (A3.4) is valid with $\theta = i\psi$ (ψ real), i.e.:-

$$\text{Sinh}\,\psi - \psi = \frac{t\, H_o\, (1 - 2q_o)^{3/2}}{q_o} \qquad \text{(A3.5a)}$$

$$\frac{R_o}{R(t)} = 1 + Z = \frac{1 - 2q_o}{q_o} \quad \frac{1}{(\text{Cosh}\,\psi - 1)} \qquad \text{(A3.5b)}$$

In the case of flat space ($q_o = \frac{1}{2}$) Z is simply given by

$$\frac{R_o}{R(t)} = 1 + Z = \left[\frac{2}{3\, H_o\, t} \right]^{2/3} \qquad \text{(A3.6)}$$

Having obtained a value for Z_g from our chosen values of H_o, q_o and t_g, we can then calculate the optical depth to the cosmic microwave background for intergalactic dust. At this stage however we must make

certain assumptions.

It is assumed that no dust existed prior to the epoch of galaxy formation and that the major part of the dust we see now was formed at time t_g when rapid evolution of high mass stars with resultant ejection of condensibles in the form of heavier elements was taking place (Schmidt, 1974). If we further assume, following Chioa and Wickramasinghe (1972), that intergalactic dust originated as interstellar dust then it can be shown that virtually all this dust will survive from t_g until the present epoch (Margolis and Schramm, 1977).

If τ is the optical depth between a source emitting radiation of frequency ν at time t, and an observer receiving the radiation at time t_o at frequency ν_o, and if $\sigma(\nu)$ is the extinction cross-section and n(t) is the proper member density of scatters then

$$\tau(\nu_o) = \int_t^{t_o} n(t) \quad \sigma(\nu)\ c\ dt \qquad \text{(A3.7)}$$

(Nandy et al., 1974)

By employing the assumptions made above, the number density per unit proper volume is given by

$$\begin{aligned} n(t) &= n(t_o)(1 + Z)^3 && \text{for } Z \leq Z_g \\ n(t) &= 0 && \text{for } Z > Z_g \end{aligned} \qquad \text{(A3.8)}$$

Thus the optical depth can be expressed by using equations (A3.3) and (A3.7) since $dt = dR/\dot{R}(t)$

$$\tau(\nu_o) = \frac{n_g(t_o)\ c}{\nu_o\ H_o} \int_{\nu_o}^{\nu} \frac{\nu}{\nu_o} \left[1 - 2q_o + 2q_o \frac{\nu}{\nu_o}\right]^{-\frac{1}{2}} \sigma(\nu)\ d\nu \qquad \text{(A3.9)}$$

where $n_g(t_o)$ is the present intergalactic grain number density.

Assuming that the wavelength dependence for intergalactic dust is the same as that for interstellar dust, the extinction cross-section is given by (Nandy et al., 1974).

$$\sigma(\lambda) = \frac{1}{1.086} \frac{A(\lambda)}{Ln_s} \qquad (A3.10)$$

where $A(\lambda)$ is the interstellar extinction law normalised with L = normalisation distance of 1 kpc and n_s the average number density of interstellar grains.

If we write (A3.9) in terms of $f = \nu/c$ and use (A3.10) we obtain (Nandy et al., 1974)

$$\tau(f_o) = \frac{c}{1.086\ L\ f_o\ H_o} \mu \int_{f_o}^{f} \frac{f}{f_o} \left[1 - 2q_o + 2q_o \frac{f}{f_o}\right]^{-\frac{1}{2}} A(f).df \qquad (A3.11)$$

where $\mu = n_g(t_o)/n_s$.

The interstellar extinction is of the form $A(f) = A_o f$ for $f \lesssim 3.6\ \mu m^{-1}$. This is useful as for an observing wavelength $\lambda_o = 1$ cm, f will indeed be less than $3.6\ \mu m^{-1}$ for every epoch after recombination. Thus (A3.11) becomes

$$\tau(f_o) = \frac{A_o c}{1.086 L f^2_o\ H_o} \mu \int_{f_o}^{f} f^2 \left[1 - 2q_o + 2q_o \frac{f}{f_o}\right]^{-\frac{1}{2}}.df$$

and this integrates to give

$$\tau(f_o) = \frac{A_o\ c}{1.086L\ H_o} \mu \frac{f_o}{15q^3_o} \left[(1 + 2q_o\ Z_g)^{\frac{1}{2}} \left\{3q^2_o\ (1 + Z_g)^2 + 2q_o\ (2q_o - 1)(1 + Z_g) + 2\ (1 - 2q_o)^2\right\} - 15q_o^2 + 10q_o - 2\right] \qquad (A3.12)$$

Here $A_o = 0.55$ and $\mu = 10^{-7}\ (H_o/75\ kms^{-1}\ Mpc^{-1})$ from a fit of quasar colour against red shift (Nandy et al., 1974). The value of intergalactic dust mass density at the present epoch would therefore be of the order of $1.5 \times 10^{-33}\ gcm^{-3}$. This in itself would have no significant effect on q_o for $q_o \gtrsim 10^{-3}$ (for $H_o \lesssim 100\ kms^{-1}\ Mpc^{-1}$).

A plot of q_o against $\tau_g(\nu_o)$ is shown in figure (A3.1). This is for an observing wavelength of 1 cm, $\mu = 6.67 \times 10^{-8}$, $H_o = 50\ kms^{-1}\ Mpc^{-1}$,

Figure (A3.1) The dependence of optical depth at $\lambda_0 = 1$ cm on the deceleration parameter, q_0 for intergalactic dust (curve A) and free electrons (curve B). Broken vertical line is the lower limit on q_0 derived from the known amount of observable matter in the form of galaxies.

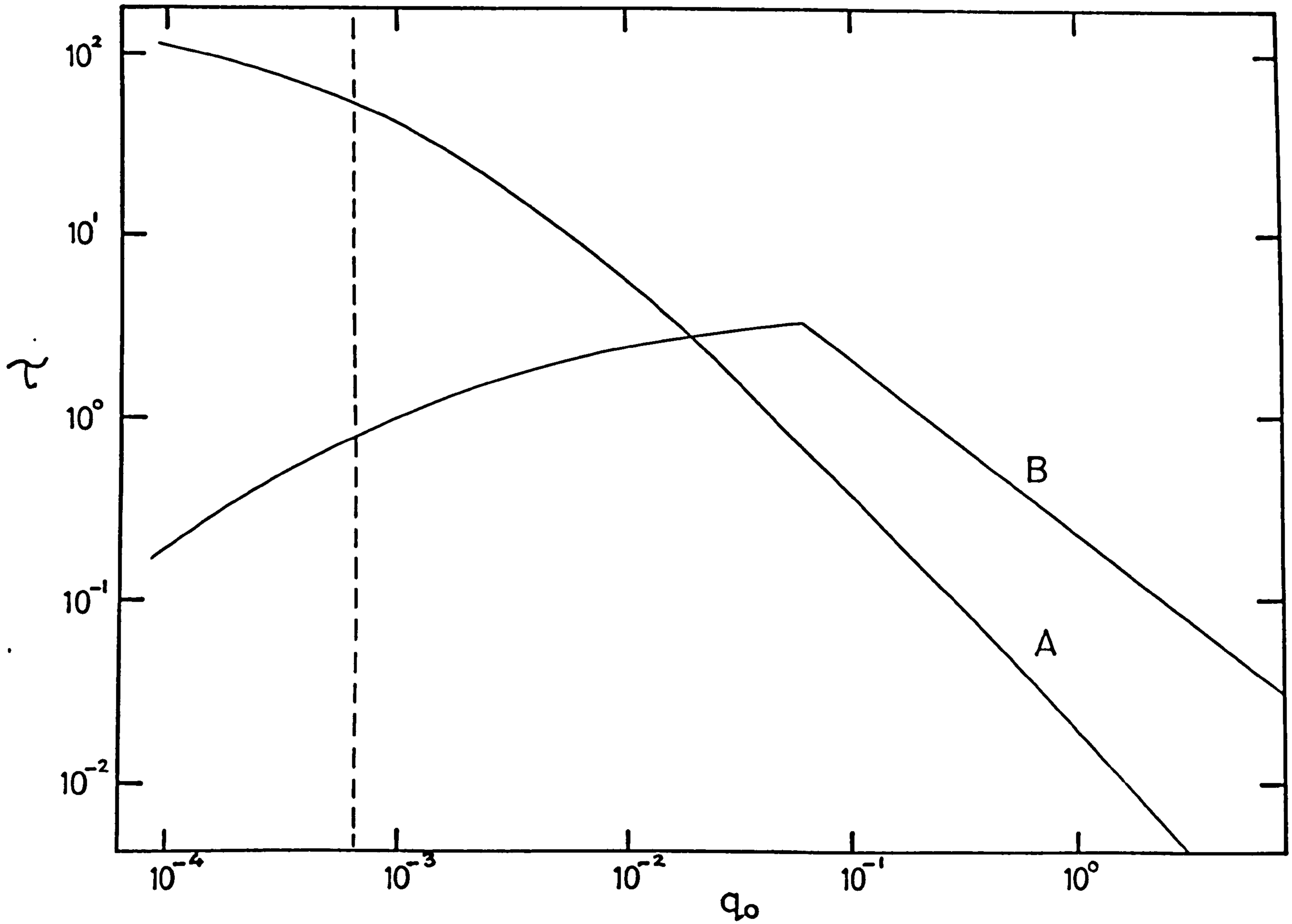
10^{2}
10^{1}
10^{0}
10^{-1}
10^{-2}
τ
B
A
10^{-4}
10^{-3}
10^{-2}
10^{-1}
10^{0}
q_0

$t_g = 7 \times 10^7$ yr. It can easily be seen that the universe is not optically thick to the cosmic microwave background with values of $q_o \gtrsim 0.05$.

This limit is strengthened if (i) the dust density is less than Nandy *et al.* suggest, giving fewer scatterers.

(ii) much of the grain density now observed has been produced since galaxy formation, giving fewer scatterers at early times.

(iii) a higher value of H_o is assumed giving a light ray a shorter path length from any epoch corresponding to a redshift Z to the present.

(iv) galaxies formed much later than expected (i.e. Z_g is decreased).

In other words, to compensate for the effects of any of these possibilities, q_o would have to be reduced so that a light ray would spend a longer time in each epoch in order for $\tau_g(\nu_o)$ to remain large.

The value of μ used so far has been taken from Nandy, Morgan and Reddish (1974) and is above the upper limits quoted by McKee and Petrosian (1974) of 1.5×10^{-34} gcm^{-3} ($H_o = 50$ kms^{-1} Mpc^{-1}, $q_o = \frac{1}{2}$). The latter also assumed that the dust was similar to interstellar dust in their studies of quasar spectra. Obviously lower values of q_o would lead to lower limits on the density in the case discussed by McKee and Petrosian who were looking for absorption features.

If the dust density were decreased then extremely low values of q_o would be required to keep the universe optically thick. The lowest value q_o can take is now considered to be $\sim 6.5 \times 10^{-4}$ from what we know to exist locally. In a study by Gott *et al.* (1974) limits on q_o were found by consideration of a number of different methods. They determined the range of values q_o can take to be $0.025 < q_o < 0.045$.

A3.2.2 Obscuration by Thomson Scattering by Free Electrons

Our reasoning thus far is based on the assumption that the small scale isotropy of the microwave background might be due to smoothing out by intergalactic dust grains. There are however other factors which might contribute to making the universe opaque to this radiation (see also table 3.1).

(a) Pollaine (1978) has already discounted galaxian dust and it seems unlikely that very much grain formation could occur in intergalactic space itself.

(b) Atoms, molecules or nonconducting particles with radii far less than the wavelength of the radiation at any given epoch would of course follow a λ^{-4} scattering (or extinction) law. Studies of Lyman-α in QSO spectra have however failed to detect any intergalactic neutral hydrogen to a redshift $Z \lesssim 2.9$ (Field, 1972) and the mechanism suggested by Chiao and Wickramasinghe (1972) for the origin of dust is not efficient for very small non-conducting grains.

(c) The possibility has been examined (Peebles, 1974) that intergalactic 'asteroids' of solid hydrogen could exist and not be detected as the scatter would be wavelength independent. However as this is only considered as an example of a possible stable state and as no evidence exists even for interstellar asteroids we discount it.

(d) The main alternative to dust is of course Thomson scattering by free electrons. This again is a wavelength independent process and therefore has no effect onthe shape of the spectrum of the background radiation. However there do exist methods to at least determine upper limits to the density of ionized hydrogen in intergalactic space.

Previous authors have assumed that the number density of electrons at the present epoch $n_e(o)$ is dependent upon q_o (e.g. Weinberg, 1972; Sunyaev, 1977). This pre-supposes that most of the material content of the universe is intergalactic and also fully ionized. The value of

$n_e(o)$ is thus given by

$$n_e(o) = \frac{3H_o^{\,2}\, q_o}{4\pi G m_H} \cdot x \qquad \text{(A3.13)}$$

where m_H is the mass of the hydrogen atom and $x(\leq 1)$ allows for the fact that a certain percentage of the intergalactic medium will be non hydrogenic (e.g. if we have 75% hydrogen, 25% helium by weight, $x = 0.88$, as we shall assume here).

In the absence of any great 'missing mass' problem however it is more relevant to take $n_e(o)$ independent of q_o and to ascribe to it the upper limit of 3×10^{-7} cm^{-3} consistent with that derived by Arons and Wingert (1972) and Cousik and Lerche (1975). This is of course only reasonable until the value of $n_e(o)$ exceeds the maximum allowable from equation (A3.13); for $q_o < 0.06$ we derive equation (A3.14a) from (A3.13):-

$$n_e(o) < 4.9 \times 10^{-6} \cdot q_o \text{ cm}^{-3} \qquad (q_o < 0.06) \qquad \text{(A3.14a)}$$

$$n_e(o) < 3 \times 10^{-7} \text{ cm}^{-3} \qquad (q_o \geq 0.06) \qquad \text{(A3.14b)}$$

(Assuming of course that $n_e(o) \equiv n_p(o)$, the local proton density).

Obviously before decoupling, the universe was optically thick to radiation but after recombination at an epoch corresponding to a redshift $Z_r \simeq 1500$ the electron density would have been very small and until some re-ionization process occurred the universe would effectively have been transparent.

It has been suggested (Arons and Wingert, 1972) that re-ionization occurred after the first quasars formed at an epoch corresponding to a redshift of $Z \simeq 8$ (Sunyaev, 1971). However other work has associated re-ionization with the time at which bright, young galaxies appeared which was earlier than this (Tinsley, 1972; Sunyaev, 1977) and therefore at larger values of redshift Z.

Sunyaev (1977) considers that there was a time, t_m, corresponding

to a redshift Z_m from when all the intergalactic gas would have been ionized. This occurred when the number of ionizing photons emitted by bright young galaxies exceeded the number of recombinations in any unit volume per unit time, i.e.

$$\int_{\nu_o}^{\infty} \frac{N(Z)\ L_\nu . d\nu}{h\nu} > (\alpha_t - \alpha_1) n_e^{\ 2}(Z) \qquad \text{(A3.15)}$$

where ν_o is the frequency of radiation above which ionization can occur; $N(Z)$ is the mean space density of sources at redshift Z; L_ν is the average source lumnosity per unit frequency at frequency ν; $(\alpha_t - \alpha_1)$ is the recombination coefficient to all levels except the first and $n_e(Z)$ is the electron number density at redshift Z.

Sunyaev (1977) also assumes a power law spectrum for the ultraviolet sources

$$L_\nu = L_o \left[\frac{\nu}{\nu_o}\right]^{-\alpha}.$$

Upon integration of equation (A3.15) above we find

$$\frac{N(Z)}{h\alpha} L_o > (\alpha_t - \alpha_1) n_c^{\ 2}(Z)$$

where $N(Z) \simeq 0.03\ (1 + Z)^3\ Mpc^{-3}$ (assuming that the number of sources remains constant), $L_\nu \simeq 3 \times 10^{29}\ ergs^{-1}\ Hz^{-1}$, $(\alpha_t - \alpha_1) = 2.5 \times 10^{-13}\ T_4^{-\frac{1}{2}}\ cm^3 s^{-1}$ and $T_4 = T/10^4\ ^oK$ (Sunyaev, 1977).

We can therefore determine the red-shift Z_m corresponding to the epoch of reionization from the expression

$$1 + Z_m \leq \frac{N_o\ L_o}{h\alpha} \cdot \frac{1}{(\alpha_t - \alpha_1)} \cdot \frac{1}{n_e(o)^2}$$

which gives (from Sunyaev, 1977)

$$Z_m \simeq 5.38 \times 10^{-3} \left[n_e(o)\right]^{-2/3} \qquad \text{(A3.16)}$$

Using a value of $n_e(o) = 3 \times 10^{-7}$ cm^{-3} in (A3.16) Z_m exceeds Z_g for $q_o \gtrsim 0.01$. This means that for higher values of q_o the intergalactic medium became completely ionized as soon as galaxies were formed (if their number density and luminosity were high enough) for this value of $n_e(o)$.

The optical depth to Thomson scattering is obtained from equation (A3.7) above where $\tau(\nu_o) = \tau_T$, the wavelength independent optical depth to Thomson scattering, $\sigma(\nu) = \sigma_T$ the Thomson cross-section ($= 0.6652 \times 10^{-24}$ cm^2), again wavelength independent, and $n(t) = n_e(t)$ the electron proper number density at any epoch. Having substituted in (A3.7) and integrated we arrive at an expression for the optical depth (see Weinberg, 1972):

$$\tau_T = \frac{\sigma_T \, n_e(o) \, c}{H_o \, 3q_o^{\,2}} \left\{ (1 + 2q_o \, Z_u)^{\frac{1}{2}} \, |3q_o + q_o Z_u - 1| + 1 - 3q_o \right\} \qquad \text{(A3.17)}$$

Here $n_e(o)$ is given by equation (A3.14), $Z_u = Z_g$ for $Z_m > Z_g$ and $Z_u = Z_m$ for $Z_m \lesssim Z_g$. Again Z_g is given by equations (A3.4), (A3.5) or (A3.6) above as applicable.

A plot of τ_T against q_o is shown as curve B in figure (A3.1) where again $H_o = 50$ kms^{-1} Mpc^{-1} and $t_g = 7 \times 10^7$ yrs. It can be seen that the q_o independent $n_e(o)$ portion gives a decreasing extinction as q_o increases. The reverse is true for the q_o dependent portion where extinction increases with increasing q_o toward a maximum value of $\tau_T \sim 3.3$ at $q_o \sim 0.06$. If the universe is optically thick to Thomson scattering by free electrons then it can be seen that $8.4 \times 10^{-4} \lesssim q_o \lesssim 0.2$. The upper limit on q_o is made even stronger if (i) Re-ionization occurred later than an epoch corresponding to a redshift Z_u as defined above.

(ii) Ionized hydrogen in intergalactic space has a number density of less than

3×10^{-7} cm^{-3}.

(iii) H_o is greater than 50 kms^{-1} Mpc^{-1} (it is certainly not much smaller (Gott et al., 1974)).

(iv) Galaxy formation occurred later than t_g (i.e. Z_g is smaller).

A3.3.1 Conclusion

The lack of observation of small scale anisotropy in the cosmic microwave background radiation could of course be due to the fact that the fluctuations, if they exist, are so small as to be below the present limits of detection. However it would seem more likely that the lack of observation is due to 'washing out' by scatterers between us and the epoch of recombination.

The two scattering media considered most likely to be the cause of opacity are Thomson scattering by free electrons and by interstellar-like intergalactic dust. The former would make the universe opaque to the cosmic background radiation only if $8.4 \times 10^{-4} \lesssim q_o \lesssim 0.2$ and the density of electrons locally, $n_e(o)$, is not much less than the upper limit derived from observation (Arons and Wingert, 1972). The latter would provide obscuration for all $q_o \lesssim 0.05$ and it becomes more effective with decreasing values of q_o. It seems likely therefore that the obscuration is due to dust and thus $q_o << 0.1$ making the universe open by a large margin.

Appendix A4 Reprints

Astron. Astrophys. 73, 113–120 (1979)

ASTRONOMY AND ASTROPHYSICS

Infrared Emission by Dust Grains near Variable Primary Sources

I. General Considerations

M. F. Bode and A. Evans

Department of Physics, University of Keele, Staffordshire, ST5 5BG, U.K.

Received March 24, revised June 30, 1978

Summary. In this paper we consider the infrared emission by an assembly of identical static dust grains distributed with spherical symmetry about a centrally-located variable source of short wavelength radiation. We describe the distribution of grain temperatures as seen by a distant observer for several simple light curves and we conclude that the angular diameter derived on the assumption that the source radiates as a black body is not a reliable measure of the actual angular diameter of an optically thin dust source. General expressions are given for the flux density at infrared frequencies; explicit expressions are given for the case in which the central source has a step function light curve and the dust distribution is optically thin and the density of which has power-law dependence on distance from the central source. The possibility that superluminal effects might be observed at infrared wavelengths shortly after the outburst of a nova is briefly discussed.

Key words: dust sources – variable sources – infrared sources – novae – Seyfert galaxies

I. Introduction

A wide variety of objects are known to emit strongly at infrared frequencies and these include both galactic (e. g. novae) and extragalactic (e. g. Seyfert nuclei) sources. In many cases, particularly among the extragalactic sources, there is strong evidence that the radiating mechanism at all observing frequencies is nonthermal, while in others the evidence is equally strong that thermal emission by dust grains is responsible for the observed infrared flux (e. g. Ade et al., 1976). In addition it is known that the primary short wavelength ($h\nu \gtrsim 2$ eV) fluxes associated with these thermal infrared sources are variable. As it is this primary radiation that is thermalized by dust grains it would be natural to expect corresponding variability at infrared frequencies also, provided of course that the light travel time across the relevant portion of the dust assembly is less than the typical variation timescale of the primary source of radiation, measured in the rest frame of the source.

The emission by dust grains surrounding non-variable sources has been very thoroughly investigated (e. g. Rowan-Robinson, 1975), but this does not seem to be the case where variable sources are concerned. For example, Rees et al. (1969) considered the dependence of the timescales of the infrared variability of Seyfert nuclei on wavelength and on the luminosity of the primary short wavelength source; while Burbidge and Stein (1970) concluded that variations in the primary source might give rise to corresponding variability in the infrared, down to timescales of a few seconds.

We consider here the infrared emission from an assembly of dust grains surrounding a variable source of short wavelength radiation, the source being at rest relative to the observer. We do not, at present, compare our results with any particular source, although parameters typical of various classes of objects will be used to give numerical estimates of the effects that emerge from our analysis. We defer detailed comparisons with, and specific models for, particular sources until later.

II. Grain Temperature

The bulk properties of the grain material are obviously crucial in determining the nature not only of the re-radiated spectrum but also the infrared variability. The optical properties of the grain material determine, among other things, the equilibrium grain temperature and the cooling time of a grain and we define in the usual way Q_{ext}, Q_{sca} and Q_{abs} as the extinction, scattering and absorption efficiencies in the infrared. The same notation carrying an asterisk (*) refers to the values of these quantities at short wavelengths. Also we may write $Q_{ext} = Q_{abs}(1-A)^{-1}$, where A is the albedo of the grain material.

For generality, we follow Rees et al. (1969) and write

$$Q_{abs} = Q_0(\nu/\nu_0)^{\alpha} \tag{1a}$$

where ν_0 is a suitable fiducial frequency, and Q_0 and α are taken to be frequency independent. For example, if we assume spherical grains, of radius $a \ll \lambda/2\pi$, where λ is the wavelength of the incident radiation, the asymptotic form of the Mie formulae for spherical, conducting grains gives Q_{abs} as a function of frequency ν (Wickramasinghe, 1967):

$$Q_{abs} \approx (12\pi a/c\sigma)\nu^2 \tag{1b}$$

where σ is the electrical conductivity of the grain material. Evidently for small ideal grains – whether dielectric or metallic – and long infrared wavelengths, $\alpha = 2$, but for grains with impurities etc., a weaker dependence on ν is likely (e. g. Rees et al., 1969).

We note from Eq. (1b) that $Q_0 \propto a/\sigma$; consequently Q_{abs} is a function of temperature by virtue of the temperature dependence of the conductivity of the grain material (Greenberg, 1968), a factor that is generally ignored by most workers. We write

$$Q_0 = Q_0'(T/T_0)^{\rho} \tag{1c}$$

where T_0 and ρ are constants and $Q_0' \propto a$ [cf. Eq. (1b)]. For example, from data summarized by Goldsmith et al. (1961),

Send offprint requests to: A. Evans

$\rho \approx -0.5$ for natural graphite and $\rho \approx 2$ for iron, for temperatures in the range of interest.

Also we note the possibility that the conductivity of the grain material may not be isotropic. For example, the conductivity of graphite parallel to the cleavage plane is significantly higher than that perpendicular to the same plane. However, provided that the grains in our model, whatever their composition and structure, are randomly orientated, the effect of anisotropic conductivity on our numerical results will not be more than a factor of order unity.

As is well known (e. g. Wickramasinghe, 1967), the temperature of a grain, T_g, is determined by the equilibrium between the absorption of short wavelength radiation (the effect of the infrared radiation field being negligible) and its subsequent re-radiation. We neglect the process described by Greenberg (1976), in which T_g fluctuates erratically on the absorption of individual photons. This process is likely to be significant if the internal energy of a grain is not much greater than the photon energy and may be ignored if $a \gtrsim 10^{-1}$ μ as will be the case here.

In what follows, we neglect the motion of grains, although some motion is to be expected as a result of gravitation, radiation pressure etc. We also neglect the fact that the dust distribution is likely to be time dependent as grains evaporate and (perhaps) recondense as the luminosity of the central object as observed by the grains attains a threshold value that takes grain temperatures past their temperature of evaporation and recondensation. We further assume here that the dust distribution is gas-free and that scattering by the grains at all frequencies is isotropic. These added complications are to be considered elsewhere.

We define $N(r)$ as the number density of grains at distance r from the primary source of radiation; for simplicity we assume that all grains have the same radius and are identical in every respect. For a spherical dust distribution, radius R, having an empty concentric cavity of radius R_1 [i.e. $N(r)=0$ for $r<R_1$ and $r>R$; see Fig. 1] the mass of grains is obviously

$$M_{gr} = (16\pi^2 a^3 s/3) \int_{R_1}^{R} N(r) r^2 dr$$

where s is the bulk density of the grain material. Also at distance r from the central source, the optical depth for short wavelength radiation is

$$\tau^* = \int_{R_1}^{r} Q^*_{abs} \pi a^2 N(r) dr.$$

In the case of a non-variable central source, the equilibrium grain temperature is given in the usual way by the expression (valid for a dust distribution that is optically thin to its own radiation):

$$\int_0^\infty (L_\nu/4\pi r^2) \exp(-\tau^*) Q^*_{abs}(\nu) \pi a^2 d\nu = 4\pi a^2 \int_0^\infty Q_{abs}(\nu) B(\nu, T_g) d\nu \tag{2}$$

for a grain distant r from the central source. In Eq. (2), L_ν is the luminosity of the primary source (assumed to radiate isotropically) and $B(\nu, T_g)$ is the Planck function. Neglecting as usual the dependence of Q^*_{abs} on frequency, and using Eqs. (1a) and (1c), we have

$$T_g^{\alpha+\rho+4} = (L/4\pi r^2) \exp(-\tau^*) (Q^*_{abs}/Q''_0) \nu_0^\alpha \cdot (c^2/2h) (h/k)^{\alpha+4} \{\Gamma(\alpha+4)\zeta(\alpha+4)\}^{-1} \tag{3a}$$

where $L = \int_0^\infty L_\nu d\nu$, h, k and c are the usual physical constants and Γ and ζ are gamma and Riemann zeta functions respectively; also $Q''_0 = Q'_0 T_0^{-\rho}$. We note that our expression for T_g differs from that given by Rees et al. (1969) because these authors did not take into account the temperature dependence of σ; obviously Eq. (3a) reduces to the form given by Rees et al. (1969) for $\rho = 0$.

We note that, to a very good approximation, the temperature dependence of σ may be allowed for by setting $\rho = 0$ and making the appropriate adjustment in the value of α. We follow this procedure here and our numerical results in subsequent sections are given for several values of α.

We now incorporate the time dependence of L, the magnitude and time dependence of which will clearly depend on the nature of the central object (e. g. nova, Seyfert nucleus). Although the essence of the models to be described is the finite and position-dependent light travel time from primary source to dust grain to observer, we shall for simplicity assume a point central source, across which light travel time may be neglected. Also at this stage we make no distinction between source and observer time, which differ only by a constant when source and observer are relatively at rest.

If the grain temperature assumes the equilibrium value corresponding to the instantaneous value of L (as observed by the grain) with negligible delay, the temperature of a grain at time t in the grain reference frame is given by

$$T_g(t) \propto [L(t-r/c) \{r(t)\}^{-2} \exp\{-\tau^*(t)\} P(t)]^{1/(\alpha+4)} \tag{3b}$$

where $P = P(Q(t), \alpha(t))$ is a function of the optical efficiencies and of α as defined by Eq. (3a). We include in Eq. (3b) the possible time dependence of the optical properties of the grain material (appropriate, for example, in the case of core-mantle grains, from which the mantle might evaporate in a time $\lesssim$ the timescale of variation of the primary source) and of $N(r)$ and r, as already noted. However we assume for the present that changes in T_g are caused entirely by the variations in the luminosity of the central source; i. e. we are neglecting grain motion, as well as changes in grain radius and composition.

We note from Eq. (3a) that infrared radiation of wavelength λ comes largely from a region with dimensions

$$\sim \text{const } \lambda^{(\alpha+4)/2} \exp(-\tau^*/2).$$

Thus we would expect more rapid variability at shorter than at longer wavelengths [see also Rees et al. (1969)]. We note also that if the dust assembly is optically thin to primary radiation, the timescale of variability at wavelength λ is $\propto \lambda^{(\alpha+4)/2}$, but is $\propto \lambda^{(\alpha+4)/2} \exp(-\tau^*/2)$ if the distribution is optically thick; i. e. we may expect to see more rapid variations at wavelength λ in an optically thick source than in a source that is optically thin to short wavelength radiation.

How valid is our assumption that the grain temperature reacts to changes in L with negligible delay? To consider this two parameters of particular interest are (a) the time taken for the absorbed energy to diffuse through the grain and (b) the grain cooling time $\tau_{cool} \simeq |U/\dot{U}|$, where U is the internal energy of a grain. Greenberg (1976) estimated that the former is $\sim 10^{-10}$ s (for $a \sim 0.1$ μ), and is therefore completely negligible. Burbidge and Stein (1970) estimated τ_{cool} on the assumption that U is given in terms of the classical value $3R_g T_g$, R_g being the universal gas constant. These authors further assumed that the grains radiate as blackbodies and hence found that $\tau_{cool} \propto a T_g^{-3}$. Thus $\tau_{cool} \sim 1$ s for graphite grains of radius 0.1 μ and having $T_g \sim 100$ K.

This estimate of τ_{cool} may not be reliable because (a) grains in astrophysical environments are unlikely to have temperatures sufficiently high for the classical form of U to be valid and (b) grains do not radiate as blackbodies. In the case of isotropically

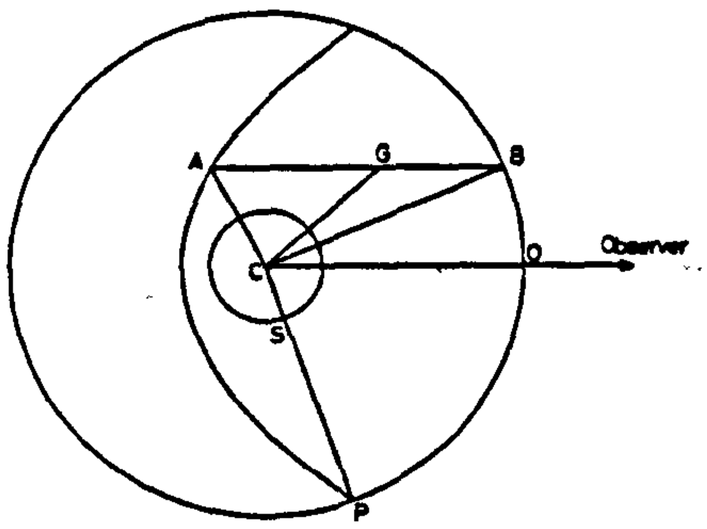

Fig. 1. Geometry of spherically symmetric dust distribution, centre C, with concentric empty cavity. Radius of dust assembly $=CO=R$; radius of cavity $=CS=R_1$; radius vector from C to arbitrary point A on parabola $=r_1$; radius vector from C to grain $G=r$. $\widehat{OCP}=\theta_0$; $\widehat{BCO}=\theta_1$; $\widehat{GCO}=\theta$; $\widehat{ACO}=\theta_1$. Short wavelength source at C

structured materials, for example, we find that $\tau_{cool} \propto T^{-\alpha}$, independent of a, if we take these factors into account. [We note that, for non zero ρ, the exponent of T in this expression for τ_{cool} would have been $-(\alpha+\rho)$ rather than $-\alpha$.] Although the energy content of grains is now smaller, their radiating efficiency is also diminished with the result that the cooling time estimates of Burbidge and Stein are about an order of magnitude too low.

However, these timescales are sufficiently short that we may assume that the grain temperature reacts instantaneously to changes in the luminosity of the primary short wavelength source. The only situations that would not comply with this assumption would be those in which changes in luminosity occur over timescales (in the source rest frame, when appropriate) $\lesssim \tau_{cool}$. Thus, for example, our analysis would not apply to emission by dust grains near a young pulsar – even if grains could exist in such an environment. The objects with which we shall be concerned may always be considered to have fluctuation timescales $\gg \tau_{cool}$.

We now proceed to consider the observed distribution of grain temperatures within a source.

III. The Distribution of Grain Temperatures

In the reference frame of an infinitely distant observer, the distribution of grain temperatures, observed at any given instant of time, within an assembly of dust grains depends on (a) the location of individual grains in relation to the central source and (b) the light curve of the latter. In the reference frame of the primary short wavelength source, the distribution of grain temperatures clearly has spherical symmetry, centred on the primary source. However, this is not the situation experienced by a distant observer (see Fig. 1, which serves to define all geometrical factors for the spherically symmetric case). The dependence of grain temperature on time is given essentially by Eq. (3a). In the reference frame of the central source in which the luminosity varies as $L(t)$, the temperature – at time t' – of a grain located a distance r from the source is given by $T_g(t'-2r/c)$. The corresponding result in the observer's frame gives the temperature of the grain G (see Fig. 1) as $T_g(t'-r(1-\cos\theta)/c)$.

We consider a source the luminosity of which varies as

$$\left.\begin{aligned} L(t)&=0 \quad (t\leqq 0)\\ &=L_0 \quad (t\geqq 0)\end{aligned}\right\}$$

where L_0 is a constant. Obviously such a light curve is unlikely to arise in many astrophysical situations. However we shall often use Eq. (4) for illustrative purposes; also it is one of the few cases for which the equation of radiative transfer may be solved analytically.

In the reference frame of the central source C the light pulse at $t=0$ spreads out with spherical symmetry and would be observed to have radius $ct/2$ at time t by an observer at C. In the reference frame of an infinitely distant observer, the pulse has the form, at time t, of a paraboloid of revolution having focus C and semilatus rectum ct:

$$r_1 = ct/(1-\cos\theta_1). \tag{5}$$

Here r_1 and θ_1 are defined in Fig. 1 and t is now measured by the distant observer from the moment the pulse is first observed. To illustrate the distribution of grain temperatures, as seen at time t by a distant observer, for a spherically symmetric distribution of grains, we consider in addition to Eq. (4) light curves of the form

$$\left.\begin{aligned} L(t)&=0 \quad (t\leqq 0)\\ &=L_0\exp(-\omega t) \quad (t\geqq 0)\end{aligned}\right\} \tag{6a}$$

and

$$L(t)=L_0+L_1\sin\omega t \tag{6b}$$

where ω, L_0 and L_1 are constants, $L_0>L_1$ and $\omega^{-1}\gg\tau_{cool}$. Equation (6a) could, for example, give a reasonable description of the pretransition stage of a nova light curve.

[We note here that, strictly, the discontinuity in $L(t)$ at $t=0$ in Eqs. (4) and (6a) violates the condition specified at the end of the previous section, namely that fluctuation timescales be $\gg\tau_{cool}$. However, provided that $\tau_{cool} \ll$ (rise time at $t=0$) $\ll\omega^{-1}$, Eqs. (4) and (6a) are valid to a high degree of accuracy and at the same time, satisfy the condition on τ_{cool} specified in the previous section.]

Figure 2 shows the distribution of grain temperatures as seen at the times indicated by a distant observer for the light curves given in Eqs. (4), (6a), and (6b), together with that for a non-variable primary source (in all cases the dust distribution is optically thin). Evidently the temperature distribution is extremely inhomogeneous, even in the case of a non-variable source, and the distribution increases in complexity even for the simple light curves considered thus far.

We note here that, if it is assumed that the source under consideration radiates as a black body, its angular diameter ϕ is sometimes estimated from

$$\phi_{BB}=\text{const}\,(\lambda f_\lambda)_{max}^{1/2}T_{BB}^{-2}; \tag{7}$$

here f_λ is the flux density in wavelength units and T_{BB} the equivalent blackbody temperature, both quantities being estimated from spectral data (e.g. Gallagher and Ney, 1976). Clearly this expression cannot be valid if the dust distribution is optically thin (cf. Fig. 2). In making the blackbody assumption it is assumed that the observed radiation originates essentially at the surface of the dust source and clearly, if the source is transparent to its own radiation ϕ_{BB} must be less than ϕ. Indeed we shall see in Sect. V below that ϕ_{BB} can be several orders of magnitude less than the actual angular diameter of an optically thin source.

IV. Spectra and Light Curves at Infrared Wavelengths

(4) The time dependence of the flux density of the assembly of dust grains observed at infinity is given by solving the equation of

116

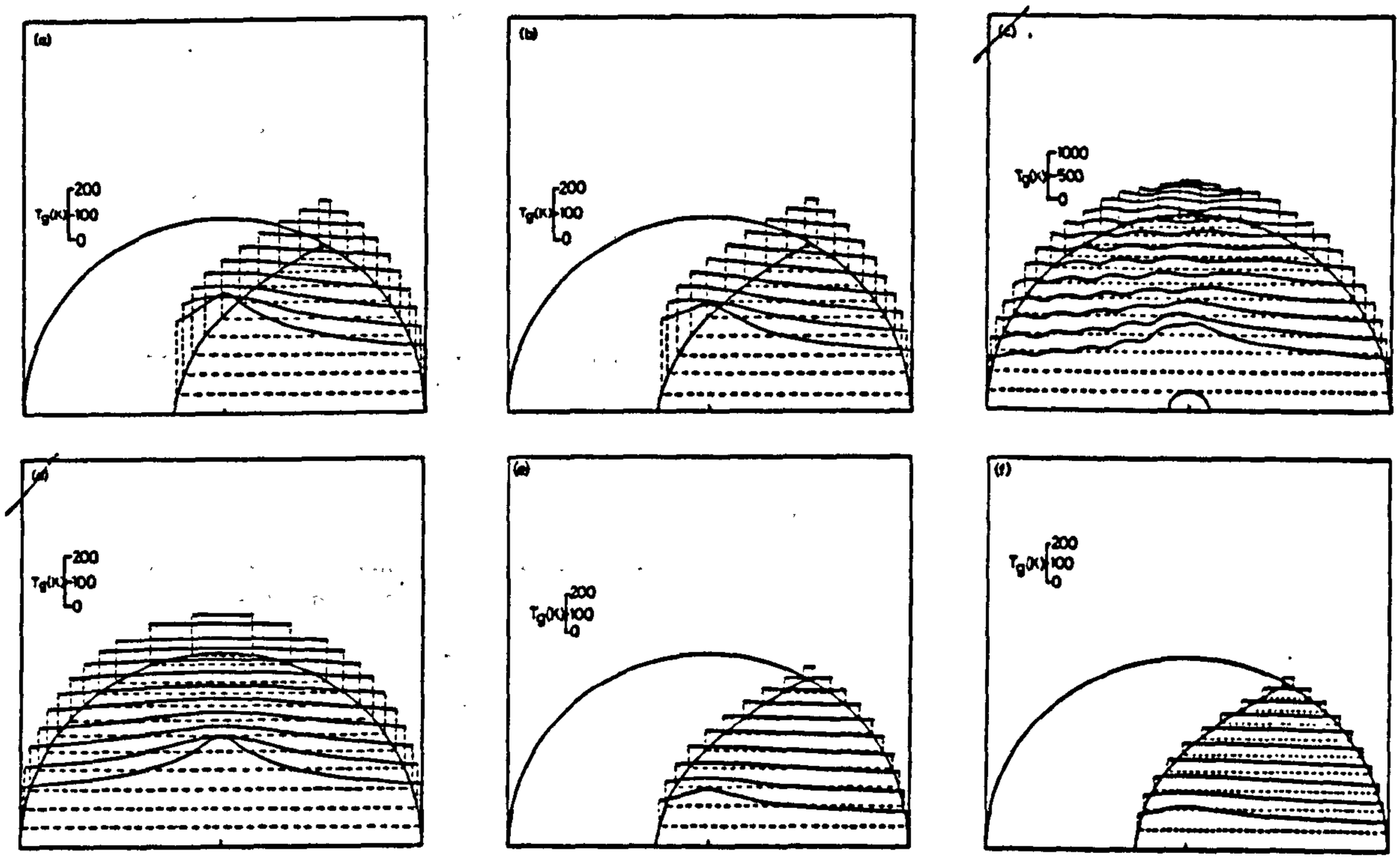

Figs. 2a–f. Distribution of grain temperatures in a spherical dust source as seen by a distant observer; centre of dust distribution is located at tick mark in each case. Location of observer as in Fig. 1. Cavity negligible in size unless specifically included. In this and all subsequent figures, $a=0.1\,\mu$. Each curve gives the observed temperature along the corresponding broken line, with temperature scale as indicated. a Light curve given by Eq. (4); $R=500\,R_1=5\,10^{17}$ cm; $L_0=5\,10^{38}$ erg s^{-1}; $M_{gr}=3.3\,10^{-6}\,M_\odot$; $t=0.5\,R/c$. b Light curve given by Eq. (6a); $\omega=0.1$ mag d^{-1}; all other parameters as a. e Light curve given by Eq. (6b); $R=10\,R_1=5\,10^{18}$ cm; $L_1=0.3\,L_0=3\,10^{43}$ erg s^{-1}; $M_{gr}=3\,10^{-4}\,M_\odot$; $\omega=0.1$ mag d^{-1}. d Constant luminosity source; parameters as a. e as a. f as a. For a–d $\alpha=2$; for e $\alpha=1$; for f $\alpha=0.5$. $\beta=2$ in all cases

radiative transfer in the usual way; this we do shortly. However we consider first some geometrical aspects of an assembly of dust grains surrounding a primary source having the light curve given by Eq. (4). As already noted, the pulse at $t=0$ has, in the reference frame of a distant observer, the form of a paraboloid of revolution and for brevity, we measure time in units of R/c; we set $ct/R=\tau$.

While $\tau<1$ the observer will see a disc the apparent radius of which increases at the rate

$$v=c(1-\tau)\{\tau(2-\tau)\}^{-1/2},$$

which is superluminal if $\tau<1-2^{-1/2}$. This kind of effect is not, of course, new (e.g. Couderc, 1939) and is referred to in the literature as "optical reverberation" (e.g. Morrison and Sartori, 1969) and "light echo" (e.g. Lynden-Bell, 1977). It is frequently encountered in radio astrophysics (e.g. Blandford et al., 1977), although as far as we are aware, it has not been applied to infrared emission by dust grains.

We may note that superluminal effects of this kind might be observable at infrared wavelengths in novae, which climb rapidly to maximum light (the form of the post-maximum light curve has obviously no bearing on this discussion), provided that the nova progenitor is surrounded by an assembly of dust grains. It is generally accepted that grains might form in the ejecta of *some* novae (e.g. Clayton and Wickramasinghe, 1976) and in view of the recurrent nature of novae (Ford, 1978) one might expect to find grains already in existence near nova progenitors, either as a result of previous outbursts or, less likely, as a result of grain formation by the cooler component of the nova system. We do not consider here the details of whether or not grains exist in the vicinity of pre-nova systems but if they do, superluminal effects should be observable for a time $\sim 0.3\,R/c$ (if the visibility of the nova against the background etc, is taken into account, we would expect this upper limit on the duration of superluminal effects to be frequency dependent). While a large assembly of dust grains would tend to smear out any variation, it would on the other hand prolong the effect discussed here and the duration of the effect would contain information about the extent of the dust distribution. Also superluminal effects would not occur if grains formed only in the ejecta of the concurrent outburst and so a search for superluminal effects in the infrared could test whether grains are formed in concurrent ejecta or are already present in the vicinity of nova systems. (We note that this violation of causality is not a consequence of the assumed light curve, which, because of the finite dimensions of the central object, itself violates causality at $t=0$).

This apparent lack of causality can also be illustrated in the following way. Notwithstanding the remarks made in Sect. III

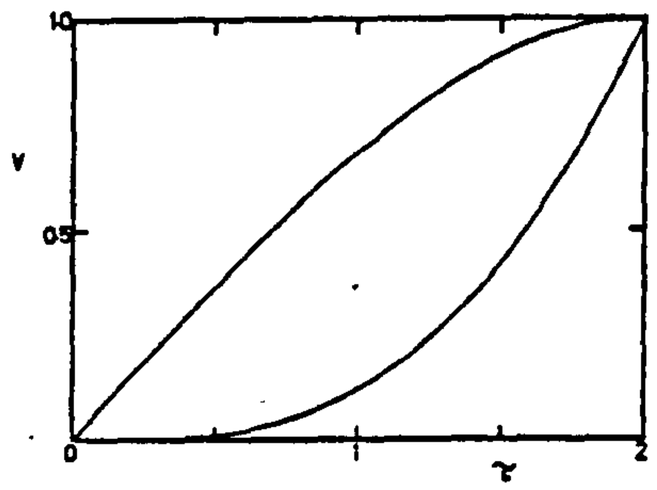

Fig. 3. Variation of emitting volume V with time as observed at central source (lower curve) and by distant observer (upper curve) for spherical dust distribution with negligible cavity. Dust distribution has unit volume and central source has step function light curve

concerning the distribution of grain temperatures in a dust source, we assume for illustrative purposes that all grains have the same temperature and radiate as blackbodies. If the dust distribution is optically thin and uniform, we would naively expect the infrared luminosity to be $L_{IR}(t) \propto N'(t) \propto V'(t)$, where N' and V' are respectively the number of radiating grains and emitting volume observed at time t. In the reference frame of the source, we clearly have $L_{IR} \propto \tau^3$, whereas in the reference frame of a distant observer, $L_{IR} \propto \tau(1-\tau^2/12)$. Figure 3 compares the emitting volumes (i.e. the infrared luminosities) as observed in each reference frame at corresponding times, for an assembly of unit volume. We note that, when $\tau \ll 1$ and the apparent rate of increase of radius is superluminal, we have $R \gg c(L_{IR}/\dot{L}_{IR})$, in contrast to the usual result $R \lesssim c(L_{IR}/\dot{L}_{IR})$ (e.g. Terrell, 1967), which applies to emission from the surface of a source which has no bulk relativistic motions and which applies to the present case when $\tau \gtrsim 1$. We note also that the result $R \gg c(L_{IR}/\dot{L}_{IR})$ also applies in the reference frame of the source, in which the observed velocity of expansion, while not superluminal, is relativistic ($v = c/2$).

We now consider the flux density of a spherical distribution of dust grains surrounding a variable source of short wavelength radiation, the luminosity of which varies with time as $L = L(t)$. The distribution of grain temperatures as seen at a given instant of observer time has already been discussed in Sect. III.—

The surface brightness of the source is given by

$$\Sigma_{source}(\theta_2) = \int_0^{s} \exp(-\tau_{abs}) N(r) \pi a^2 Q_{abs} B(\nu, T_g) ds'$$

where

$$\tau_{abs} = \int_0^{s'} N(r) \pi a^2 Q_{abs} ds'$$

and where s and s' are measured along a line of sight like AGB (see Fig. 1). It is convenient to divide the expression for Σ_{source} into two parts, depending on whether τ lies in the ranges $0 \leqq \tau \leqq 1$ or $\tau \geqq 2$; the latter case obviously includes that in which the central source is continuously variable, while the former refers to cases in which the primary source "switches on" spontaneously (e.g. novae). For each case we have

$$\Sigma_{source}(\theta_2) = \int_{\theta_2}^{\theta_1} \exp(-\tau_{abs}(\theta)) N(R \sin\theta_2/\sin\theta) \pi a^2 Q_{abs} \cdot B(\nu, T_g(\theta)) R \sin\theta_2 \operatorname{cosec}^2\theta d\theta \quad (0 \leqq \tau \leqq 1) \tag{8a}$$

$$\Sigma_{source}(\theta_2) = \int_{\theta_2}^{\pi-\theta_2} \exp(-\tau_{abs}(\theta)) N(R \sin\theta_2/\sin\theta) \pi a^2 Q_{abs} \cdot B(\nu, T_g(\theta)) R \sin\theta_2 \operatorname{cosec}^2\theta d\theta \quad (\tau \geqq 2). \tag{8b}$$

In the Eqs. (8)

$$\theta_1 = \sin^{-1}\{2\tau \sin\theta_2/(\tau^2 + \sin^2\theta_2)\}$$

or

$$\theta_1 = \sin^{-1}\{(R/R_1)\sin\theta_2\}$$

depending on whether $\theta_2 >$ or $< \sin^{-1}\{(R_1/R)(2\tau_1 - \tau_1^2)^{1/2}\}$, where $\tau_1 = ct/R_1$. For $1 \leqq \tau \leqq 2$, $\Sigma_{source}(\theta_2)$ is given by Eq. (8a) or (8b) according as $\theta_2 <$ or $> \pi - \theta_0$, where θ_0 is given by Eq. (5) as $\theta_0 = \cos^{-1}(1-\tau)$. We note that the time dependence of Σ_{source} is incorporated in the time dependence of $T_g \propto \{L(t)\}^{1/(\alpha+4)}$.

In addition to the observed flux density from the source itself, we also include the effects of background radiation, which are likely to be significant at infrared frequencies. If Σ_0 is the surface brightness of the background, its contribution to the observed surface brightness of the source is given by

$$\Sigma_{BG}(\theta_2) = \Sigma_0 \exp\{-\tau_{BG}(\theta_2)\},$$

where

$$\tau_{BG}(\theta_2) = 2\pi a^2 Q_{abs}\left\{N(R) R\cos\theta_2 - \int_{R\sin\theta_2}^{R} (r^2 - R^2\sin^2\theta_2)^{1/2} \frac{\partial N}{\partial r} dr\right\} \quad (\theta_2 > \sin^{-1}(R_1/R))$$

$$= 2\pi a^2 Q_{abs}\left\{N(R) R\cos\theta_2 - N(R_1)(R_1^2 - R^2\sin^2\theta_2)^{1/2} - \int_{R_1}^{R} (r^2 - R^2\sin^2\theta_2)^{1/2} \frac{\partial N}{\partial r} dr\right\} \quad (\theta_2 < \sin^{-1}(R_1/R))$$

for an isotropic dust distribution.

The observed flux density in frequency units is given by

$$\left.\begin{aligned} f_\nu &= \int_\Omega \Sigma d\Omega \\ &= \frac{2\pi R^2}{D^2} \int_0^{\theta_0} \Sigma(\theta_2) \sin\theta_2 \cos\theta_2 d\theta_2 \quad (0 \leqq \tau \leqq 1) \\ &= \frac{2\pi R^2}{D^2} \int_0^{\pi/2} \Sigma(\theta_2) \sin\theta_2 \cos\theta_2 d\theta_2 \quad (\tau \geqq 1) \end{aligned}\right\} \tag{9}$$

in which $\Sigma = \Sigma_{source} + \Sigma_{BG}$, θ_2 and θ_0 are defined by Fig. 1 and Ω is the solid angle subtended by the source, at distance D.

Clearly there will be very few cases in which Eqs. (8) and (9) may be solved analytically. One such case is that of the light curve given by Eq. (4), for a grain distribution that is optically thin to both infrared and primary radiation and for which $N(r) = N_1(r/R_1)^{-\beta}$, where N_1 and β are constants. For this case, we may write Eq. (3a) in the form $T_g(r) = T_1(r/R_1)^{-2/(\alpha+4)}$, where T_1 is a constant. Equations (8) and (9) become (with $\Sigma_{BG} = 0$)

$$f_\nu = K_1 \nu^3 \left(\frac{\alpha+4}{2}\right) \tau \sum_{n=0}^{m} \frac{B_n}{n!(n+\gamma)} (K_2\nu)^{n-1} \left(\frac{m}{m-1}\right) (1 - y^{m-1})$$

$$(0 \leqq \tau \leqq 2y) \tag{10a}$$

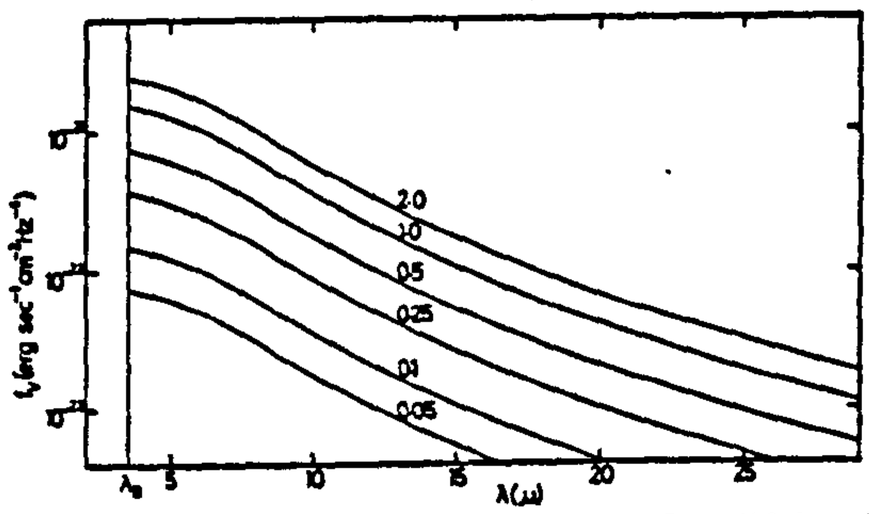

Fig. 4. Re-radiated spectra calculated using Eqs. (10a) and (10b) for dust shell having $R=2.5\,10^{16}$ cm, $y=0.64$, $\alpha=2$, $\beta=1$, and $M_{gr}=2.2\,10^{-7}\,M_\odot$; central source has step function light curve with $L_0=5\,10^{38}$ erg s^{-1}. Spectra are identified according to values of τ. See text for significance of λ_s. Vertical scale arbitrary

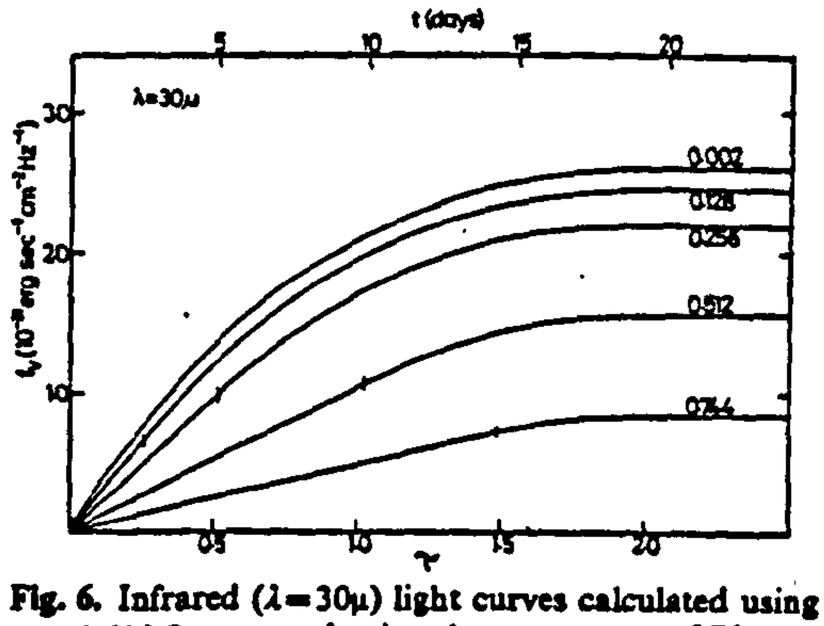

Fig. 6. Infrared ($\lambda=30\mu$) light curves calculated using Eq. (10a) and (10b) for source having the parameters of Fig. 4; curves are identified according to value of $y=R_1/R$. Light curves are linear for times earlier than those indicated by tick marks. Upper scale gives time in days after event is observed at short wavelengths. Vertical scale arbitrary

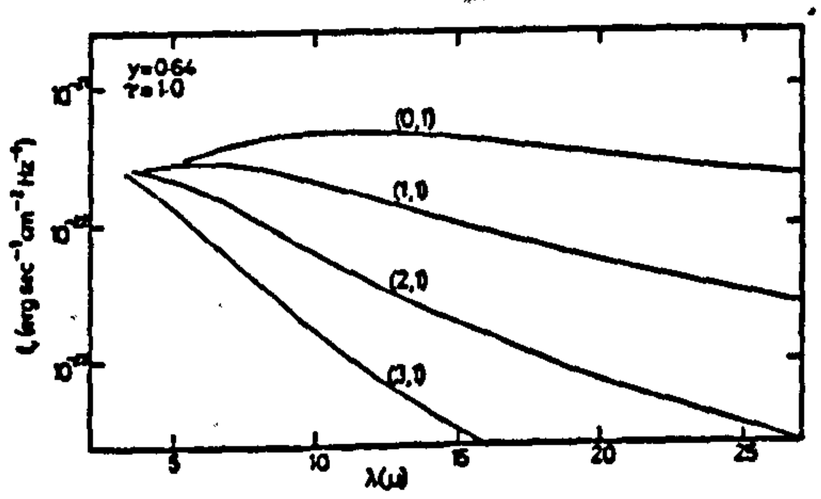

Fig. 5. As Fig. 4, for $\tau=1$ and several values of α. Spectra are labelled in the form (α, β) and terminate at short wavelengths at the appropriate value of λ_s (see text). Vertical scale arbitrary

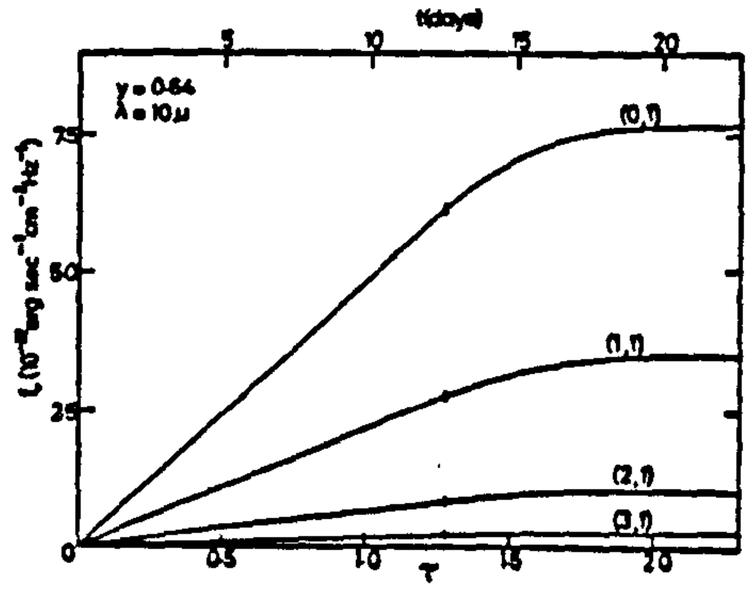

Fig. 7. As Fig. 6, for $\lambda=10\,\mu$ and several values of α. Light curves are labelled in the form (α, β). Vertical scale arbitrary

$$f_\nu = K_1 \nu^3 \left(\frac{\alpha+4}{2}\right) \tau \cdot \sum_{n=0}^{\infty} \frac{B_n}{n!(n+\gamma)} (K_2\nu)^{n-1} \left\{\left(\frac{m}{m-1}\right)\left(1-\frac{1}{m}\left(\frac{\tau}{2}\right)^{m-1}\right)-\frac{2y^n}{\tau}\right\} \qquad (2y \leqq \tau \leqq 2). \qquad (10b)$$

The following notation is used in Eqs. (10a) and (10b):

$K_1 = (2\pi R^3/D^2)\,(2h/c^2)\,N_2 y^\beta \pi a^2 Q_{abs}$
$K_2 = (h/kT_1)\,y^{-2/(\alpha+4)}$
$\gamma = (3-\beta)\,(\alpha+4)/2-1$
$m = 2(n-1)/(\alpha+4)+3-\beta$
B_n = Bernoulli number of order n
$y = R_1/R$.

The series in Eqs. (10a) and (10b) converge if $K_2\nu<2\pi$, i.e. for wavelengths exceeding

$$\lambda_s = (c/2\pi)\,\{(16\pi R^2/L_0)\,(Q_0/Q^*_{abs})\,\nu_0^{-\alpha} \cdot (2h/c^2)\,\Gamma(\alpha+4)\,\zeta(\alpha+4)\}^{1/(\alpha+4)};$$

this lower limit on λ arises because, in the derivation of Eqs. (10a) and (10b) we have used the identity

$$\frac{x}{e^x-1} = \sum_{n=0}^{\infty} \frac{B_n x^n}{n!}$$

which is defined only for $|x|<2\pi$ (we note that our result is *not* equivalent to taking the Rayleigh-Jeans limit of the Planck function).

According to Eq. (10a), the flux density rises linearly with time for all frequencies when $\tau \leqq 2y$, i.e. when $t \leqq 2R_1/c$. During the early stages the form of the re-radiated spectrum is therefore independent of time and consequently so is the value of T_{BB}. The re-radiated spectrum is shown in Fig. 4 for $y=0.64$, $\alpha=2$ and several values of τ. At long wavelengths, f_ν is approximately proportional to $\lambda^{-3.3}$ and so the source cannot be approximated by a blackbody at any time. Figure 5 illustrates the effect of changing α on the re-radiated spectrum; we note that, for $y \sim 1$, as is the case here, changing β has little effect because the number of high temperature grains is not significantly affected. We note further that when $\alpha=0$ we do not recover a blackbody spectrum

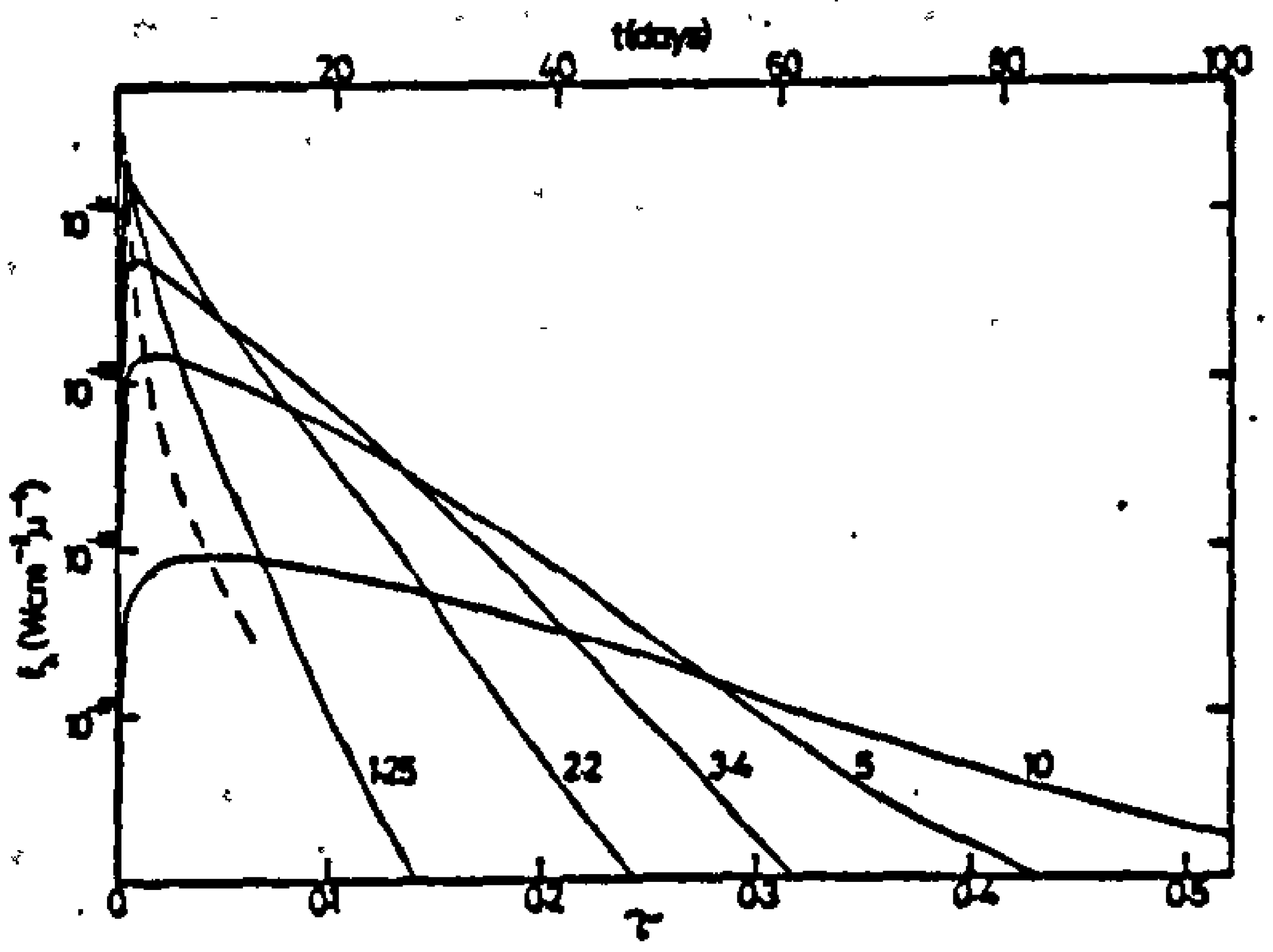

Fig. 8. Infrared light curves for dust assembly and nova as described in text; curves are identified by wavelength, in μ. Broken curve is the approximate locus of time of maximum flux. Upper scale gives time in days after nova event is observed at short wavelengths. Vertical scale arbitrary

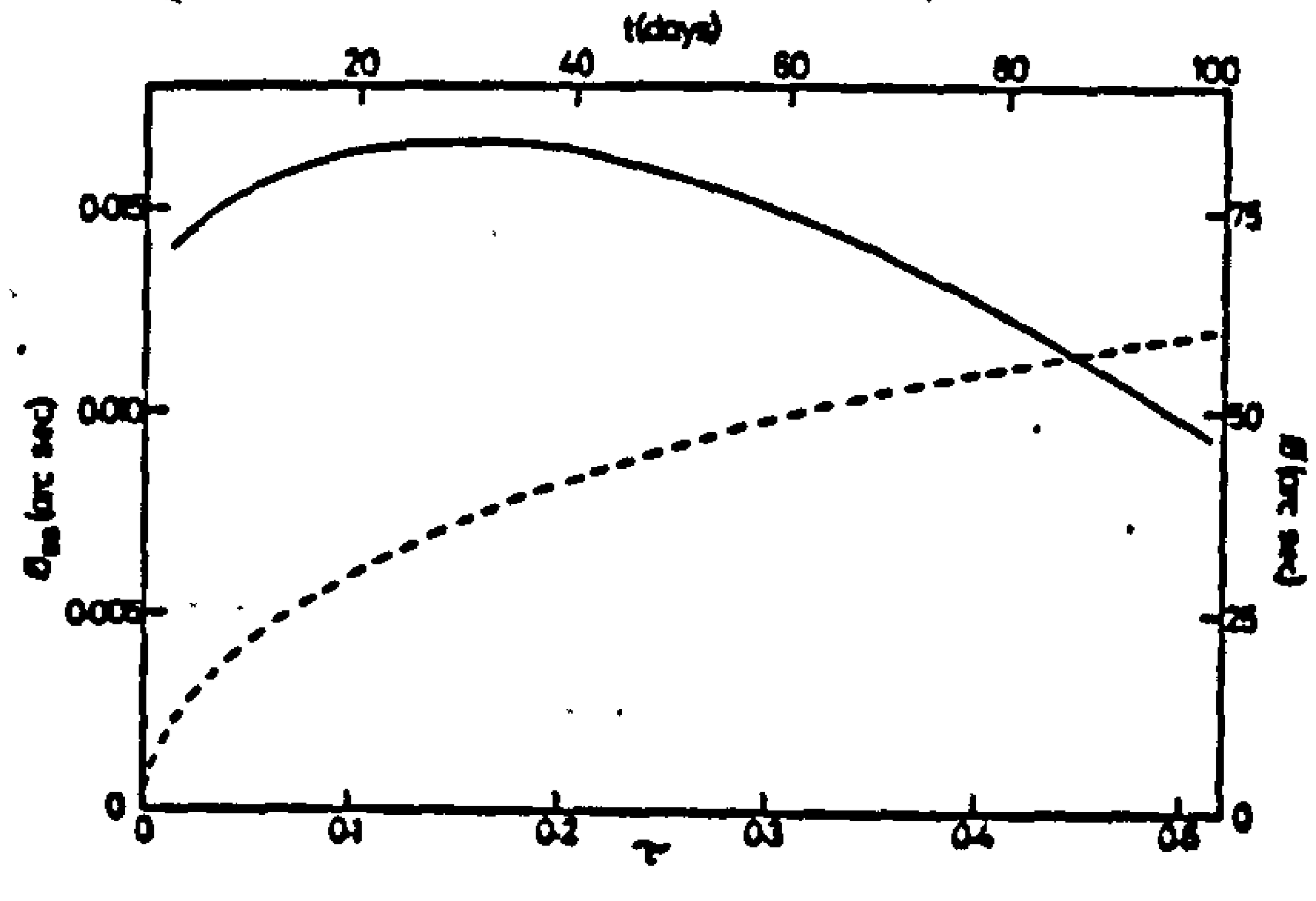

Fig. 11. Variation of ϕ_{BB} with time for dust assembly and nova as described in text. Solid curve and left vertical scale refer to ϕ_{BB}; broken curve and right vertical scale refer to ϕ. Upper scale gives time in days after nova event is observed at short wavelengths

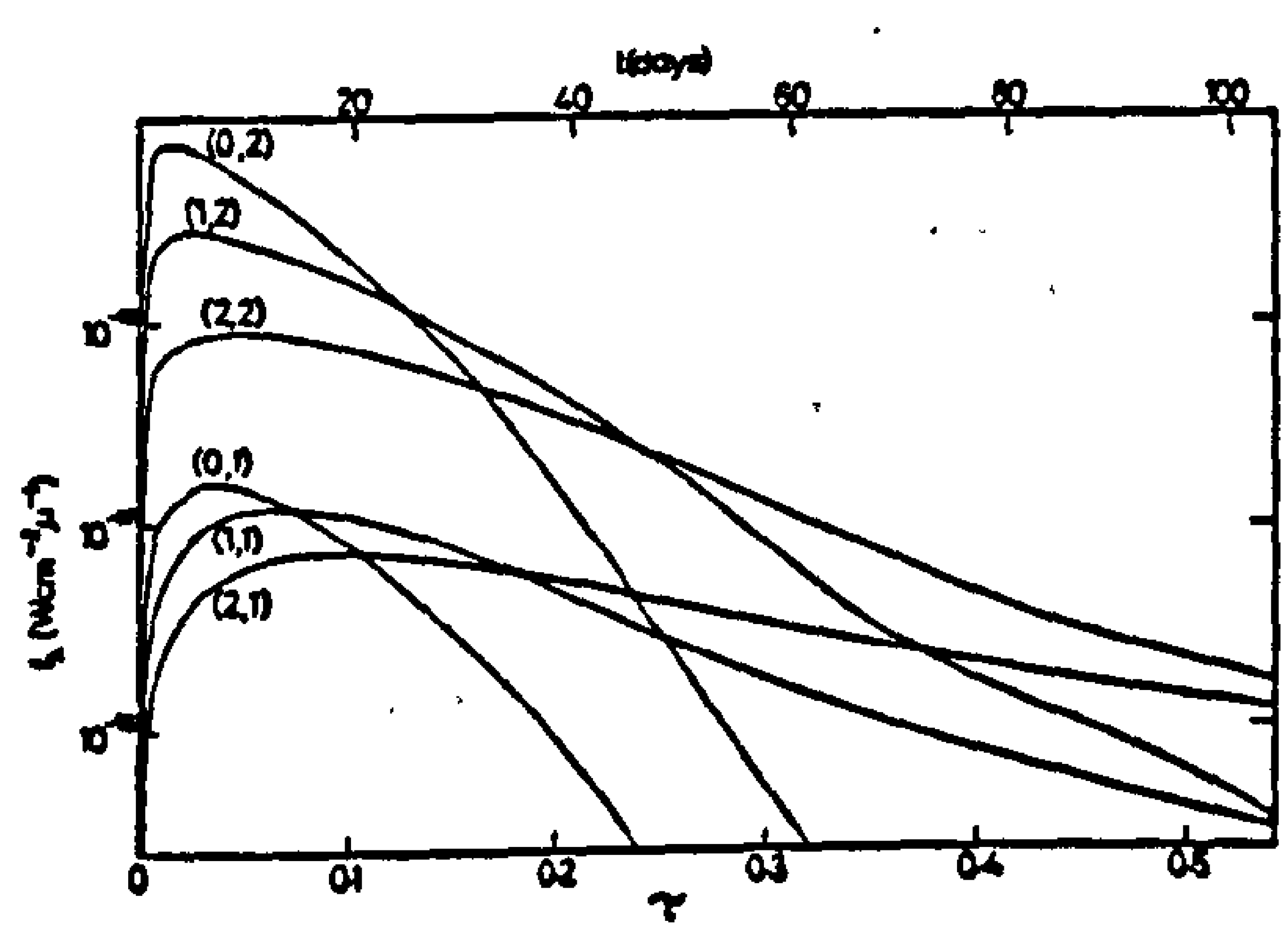

Fig. 9. As Fig. 8, for $\lambda = 10$ μ and several values of α and β. Light curves are labelled in the form (α, β). Upper scale gives time in days after nova event is observed at short wavelengths. Vertical scale arbitrary

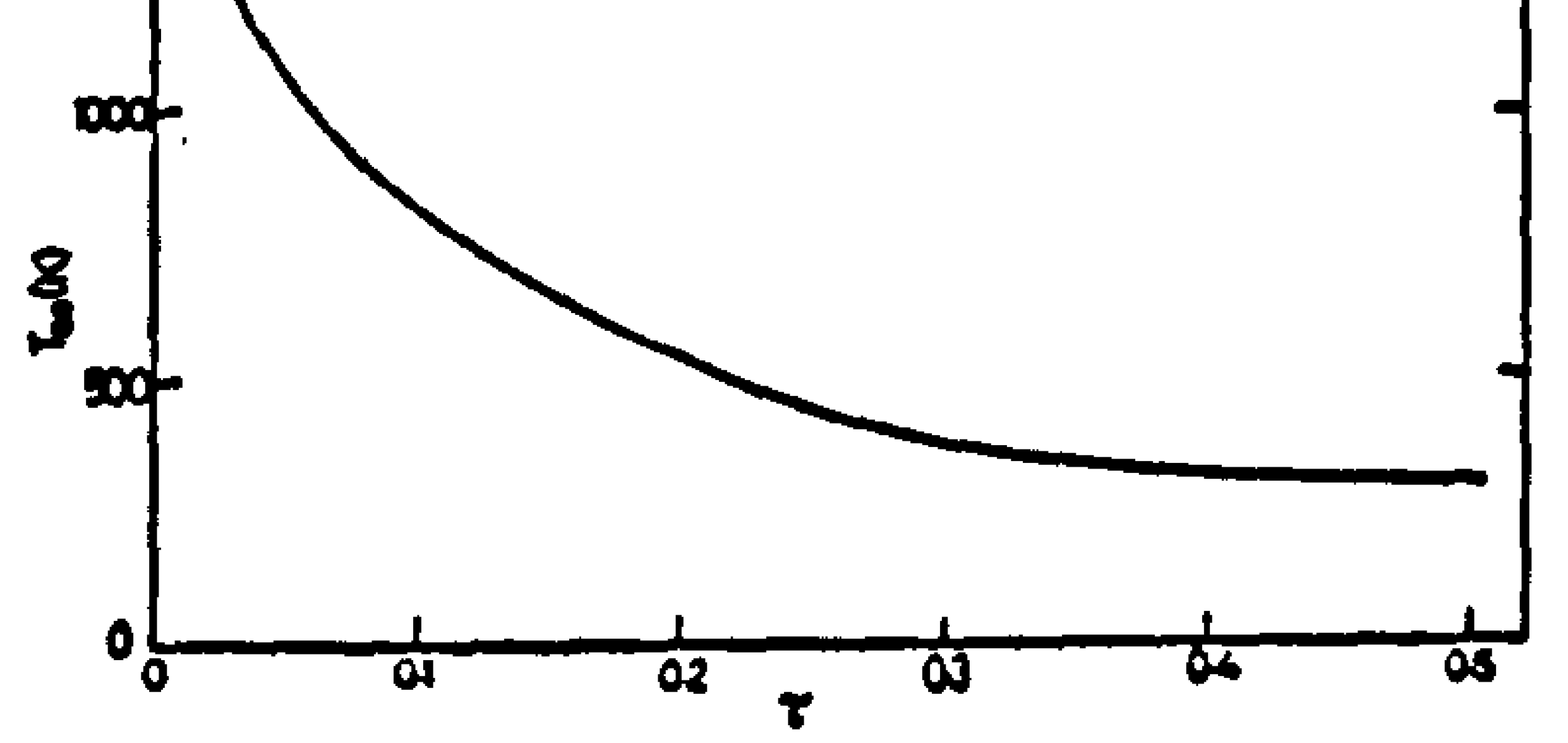

Fig. 10. Variation of blackbody temperature with time for dust assembly and nova as described in text. Upper scale gives time in days after nova event is observed at short wavelengths

because the source under consideration is optically thin; also increasing α has the effect of steepening the spectrum because $K_1 \propto \lambda^{-\alpha}$ [cf. Eq. (10a)].

The light curves for $\lambda = 30$ μ, $\alpha = 2$ and several values of y are illustrated in Fig. 6. Figure 7 illustrates the effect of changing α on the form of the light curves at $\lambda = 10$ μ.

When $\tau \gtrsim 2$, Eq. (12a) gives the flux density of an optically thin dust distribution having $N(r) \propto r^{-\beta}$ surrounding a non-variable (luminosity L_0) source as

$$f_\nu = K_1 \nu^3 (\alpha+4) \sum_{n=0}^{\infty} \frac{B_n}{n!(n+\gamma)} (K_2 \nu)^{n-1} (1-y^n).$$

V. Application to Novae

In order to illustrate an application of the results derived above, we consider a dust shell having the following parameters:

$R = 5\ 10^{17}$ cm	$R_1 = 10^{15}$ cm
$\alpha = \beta = 2$	$D = 1$ kpc
$a = 0.1$ μ	$M_{gr} = 3.3\ 10^{-6}\ M_\odot$

surrounding a nova the luminosity of which declines at the rate $\omega = 0.1$ mag. per day. We assume that the radiation responsible for heating the dust grains has the same dependence on time as the visual light curve, although there is no a priori reason why this should be so.

The assumed rate of decay, together with the well-known relationship between ω and L_0 (e.g. McLaughlin, 1960) gives the peak luminosity of the nova as $L_0 = 5\ 10^{38}$ erg s^{-1} [cf. Eq. (6a)]. Also we take $Q_0 = 0.135$ at $\nu_0 = 1.36\ 10^{14}$ Hz for 0.1 μ grains. The value $\beta = 2$ corresponds to isotropic emission of grains (or of grain forming material) by the prenova system, with no braking etc., by the interstellar medium. The dust distribution is optically thin to both primary and infrared radiation with the above values of R_1, R, β, and M_{gr}. (We again take $\Sigma_{g0} = 0$). We repeat here that we are not, at this stage, attempting to construct models for specific sources; the results to be described in this Section are for illustrative purposes only.

The light curves obtained from Eq. (9) are shown in Fig. 8 for several infrared wavelengths. There are several noteworthy

features in this figure, which we shall discuss at greater length elsewhere. For the present we merely note that the infrared light curves reach maximum flux with a delay that increases with increasing wavelength; this behaviour is of course well known to occur in some novae (e.g. Geisel et al., 1970).

Figure 9 illustrates the effect of changing α and β on the light curves at $\lambda = 10$ μ (when varying β, the number of grains was adjusted to maintain constant grain mass). We note that, for the case under consideration, decreasing β decreases the observed flux and delays the time of maximum flux; the latter effect also results from increasing α, which also causes a steepening of the light curves.

Returning to Fig. 8, we note that the light curve for each wavelength predominates at one time only, this time increasing with increasing wavelength. This latter behaviour is, of course, a manifestation of the cooling of the grains, also illustrated in Fig. 10, in which the blackbody temperature T_{BB} is defined as usual by the relationship $\lambda_{max} T_{BB} = \text{const}$ (λ_{max} is the wavelength of maximum flux at any time).

As noted in Sect. III, the blackbody temperature may be used (Gallagher and Ney, 1976) to evaluate ϕ_{BB}, the angular diameter of an equivalent blackbody [cf. Eq. (7)]. The variation of ϕ_{BB} with time for the case under consideration is illustrated in Fig. 11, together with the time dependence of the actual angular diameter ϕ. We note that, unless τ is close to zero, $\phi_{BB}/\phi \sim 10^{-4}$ so that, as remarked earlier, ϕ_{BB} is not a reliable guide to the angular diameter of an optically thin dust source.

The reason for this discrepancy arises from the fact that, when the source is optically thin, the bulk of the observed radiation comes from the hottest grains – i.e. those closest to the central source (for the case discussed here, for example, $\phi_{BB}/\phi \sim R_1/R$) – and indeed we would expect ϕ_{BB} to be virtually independent of ϕ for an optically thin source. For an optically thick dust distribution, the only grains contributing to the observed flux are those at $r \sim R$. Consequently the inferred blackbody temperature will be greatly reduced from its value in the optically thin case [cf. Eq. (3a)] so we would expect to find that $\phi_{BB} \sim \phi$. Evidently an estimate of the opacity of the dust distribution is essential before it can be judged whether or not the quantity ϕ_{BB} is meaningful.

VI. Concluding Remarks

The general theory developed here can be applied to a wide variety of situations. Any astrophysical system that has among its constituent parts (a) a dust producing component and (b) a variable source of short wavelength radiation, should be described by the analysis given here, with appropriate modifications, including the case in which one has a non-variable source the location of which relative to the dust distribution is variable. The general arguments would also apply, for example, to synchrotron radiation sources in which the radiating electrons are produced by pion production in material surrounding a variable source of relativistic protons, provided that the electrons "cool" in a suitably short time.

However, for the time being, we restrict ourselves to consideration of dust sources and further papers will deal with the application of the results obtained here to various cosmic sources of infrared radiation.

Acknowledgements. We thank Drs D. Dugdale and T. Markvart for helpful discussions and the referee for his constructive criticisms. Computations were performed on the CDC 7600 at the University of Manchester via the University of Keele link. One of us (M.F.B.) is in receipt of a University of Keele Research Studentship.

Refereaces

Ade, P.A.R., Rowan-Robinson, M., Clegg, P.E.: 1976, *Astron. Astrophys.* 53, 403
Blandford, R.D., McKee, C.F., Rees, M.J.: 1977, *Nature* 267, 211
Burbidge, G.R., Stein, W.A.: 1970, *Astrophys. J.* 160, 573
Couderc, P.: 1939, *Ann. Astrophys.* 2, 271
Clayton, D.D., Wickramasinghe, N.C.: 1976, *Astrophys. Space Sci.* 42, 463
Ford, H.C.: 1978, *Astrophys. J.* 219, 595
Gallagher, J.S., Ney, E.P.: 1976, *Astrophys. J. Letters* 204, L35
Geisel, S.L., Kleinmann, D.E., Low, F.J.: 1970, *Astrophys. J. Letters* 161, L101
Goldsmith, A., Waterman, T.E., Hirschhorn, H.J.: 1961, Handbook of Thermophysical Properties of Solid Materials, 1, MacMillan Co., New York
Greenberg, J.M.: 1968, in *Stars and Stellar Systems*, 7, ed. B. M. Middlehurst and L. H. Aller, p. 221, Univ. Chicago Press
Greenberg, J.M.: 1976, in *Far Infrared Astronomy*, ed. M. Rowan-Robinson, p. 299, Pergamon Press
Lynden-Bell, D.: 1977, *Nature* 270, 396
McLaughlin, D.B.: 1960, in *Stars and Stellar System* 6, ed. J. L. Greenstein, p. 585, Univ. Chicago Press
Morrison, P., Sartori, L.: 1969, *Astrophys. J.* 158, 541
Rees, M.J., Silk, J.I., Werner, M.W., Wickramasinghe, N.C.: 1969, *Nature* 223, 788
Rowan-Robinson, M.: 1975, *Monthly Notices Roy. Astron. Soc.* 172, 109
Terrell, J.: 1967, *Astrophys. J.* 147, 827
Wickramasinghe, N.C.: 1967, Interstellar Grains, Chapman and Hall

Astron. Astrophys. 78, 78–81 (1979)

ASTRONOMY AND ASTROPHYSICS

Visibility of Pregalactic Fluctuations and an Upper Limit on q_0

M. F. Bode and A. Evans

Department of Physics, University of Keele, Staffordshire, ST5 5BG, U.K.

Received May 12; revised November 13, 1978

Summary. We consider the effect of intergalactic dust and free electrons on the visibility of small-scale anisotropy in the cosmic microwave background and we show that failure to detect these fluctuations implies that the deceleration parameter q_0 is very much less than the value required to close the universe. We also show that, whether the intervening medium obscures fluctuations or not, Thomson scattering does not contribute significantly to the opacity of the intergalactic medium.

Key words: cosmology — intergalactic medium — cosmic microwave background

I. Introduction

The cosmic microwave background is generally, though not universally, accepted to be radiation emitted at the "surface of last scattering", observed at redshift $z = z_s \sim 1500$ (e.g. Weinberg, 1972). Apart from providing this evidence of a hot, dense phase of the universe, the microwave background can provide other information of cosmological interest. For example, density enhancements that are destined to condense into galaxies should show up as temperature fluctuations with $\Delta T/T \sim 10^{-3}$ and an angular scale $\sim 1'$ on an otherwise isotropic background (e.g. Weinberg, 1972).

We consider here the effect of intergalactic dust and free electrons on the visibility of these pregalactic fluctuations. We show that failure to detect them – and limits on $\Delta T/T$ are already quite restrictive (e.g. Boynton, 1974) – may set significant upper limits on the deceleration parameter q_0, if we assume that they are obscured by an intervening medium.

II. Transparency of the Intergalactic Medium

The fluctuations in the microwave background are observable only if the universe is transparent out to redshift z_s and obviously if the intergalactic medium is optically thick this potentially accessible evidence of galaxy formation will be fogged out. The fact that pregalactic fluctuations have not been observed in the background suggests that they are being obscured by material lying "between" us and the surface of last scattering. Plausible values of $\Delta T/T$ are estimated to lie in the range $\sim 10^{-4} - 3\,10^{-3}$ (e.g. Weinberg, 1972). However, in work summarized by Boynton (1974), upper limits on $\Delta T/T$ are already at the lower end of this range and although there might still be room for observational and theoretical manoeuvre we proceed on the assumption that any fluctuations in the microwave background are indeed obscured by intervening material.

The possible material content and resultant transparency of the intergalactic medium have been discussed by several authors (see e.g. Weinberg (1972) and Peebles (1974) for reviews) and the various possibilities considered have been as follows: (a) intergalactic "asteroids"; (b) atoms and molecules; (c) small dielectric particles; (d) "conventional" dust; (e) free electrons.

There appears to be no way at present of confirming or refuting the presence in the intergalactic medium of solid particles having dimensions $\gg\lambda$, the wavelength of incident radiation. Nevertheless, following other workers (e.g. Margolis and Schramm, 1977), we dismiss possibility (a). Also (b) must be negligible at the epochs of interest, which include those during which the intergalactic gas has been completely reionized. We do not consider that small ($\ll\lambda$) dielectric grains (c) contribute to the opacity of the intergalactic medium for reasons that will emerge below. In any case, we may note that even if (b) and (c) are present to any extent, their scattering efficiency ($\propto\lambda^{-4}$) at the long wavelengths of interest here is extremely low. As is well known, the only plausible candidates for rendering the intergalactic medium optically thick are "conventional" (interstellar-like) dust grains and free electrons.

If either dust or free electrons exist in the intergalactic medium, the optical depth to redshift z is given by (for zero cosmological constant)

$$\tau(z) = c/H_0 \int_0^z n(z')\sigma(\lambda(z'))(1+z')^{-2}(1+2q_0z')^{-1/2}dz' \qquad (1)$$

where it is assumed that the relevant material is uniformly and isotropically distributed on a sufficiently large scale (Weinberg, 1972). In Eq. (1), n is the proper number density of either dust grains or of free electrons as appropriate, σ the extinction cross-section and c, H_0 ($=50$ km/s/Mpc), z and q_0 have their usual meanings.

We consider the effect of intergalactic dust and free electrons in turn.

III. Intergalactic Dust

The possibility that there might exist detectable quantities of dust distributed between galaxies has been considered by several

Send offprint requests to: A. Evans

authors (see Margolis and Schramm (1977) and references therein). A novel aspect of this possibility has recently been discussed by Alfvén and Mendis (1977), who argued that the universe is transparent only out to $z \sim 40$, interstellar dust in galaxies rendering the universe optically thick to background radiation at this redshift. However, a more rigorous treatment (Pollaine, 1978) of this problem showed their conclusion to be erroneous. Although these authors were primarily concerned with dust in galaxies, Alfvén and Mendis (1977) briefly considered uniformly distributed intergalactic dust, specifically the "whiskers" proposed by Wickramasinghe et al. (1975) to provide a local origin for the background radiation. We consider here however the effect on the opacity of the intergalactic medium of intergalactic dust having extinction properties similar to those of interstellar dust.

The existence of intergalactic dust has been proposed by Nandy et al. (1974) and Schmidt (1974) on the basis of the variation of quasar colours with redshift; we use here the formalism of Nandy et al. As pointed out by several authors (e.g. Gott et al., 1974) it is extremely unlikely that grain forming material existed at any time in the intergalactic medium. However, as shown by Chiao and Wickramasinghe (1972), spiral galaxies may eject significant quantities of their interstellar dust into the intergalactic medium, this process being most efficient for graphite grains of radius $\sim 0.1\ \mu$m. These authors have also shown that this mechanism can give rise to a local intergalactic dust density $\sim 10^{-34}$ g cm^{-3}, which is of the same order as that suggested by Nandy et al. (1974) and Schmidt (1974), allowing for adjustment of the H_0 values assumed and the uncertainties involved. We may also note that the process described by Chiao and Wickramasinghe is not particularly efficient for small dielectric particles, so they would not be expected to be an important constituent of any intergalactic dust that originated in galaxies.

If intergalactic dust is produced in this way there can certainly be no dust beyond redshift z_a, corresponding to the epoch of galaxy formation t_a (taken here to be 7×10^7 yr (Field, 1975), independent of the value of H_0), where

$$1 + z_a = R(t_0)/R(t_a) \tag{2}$$

(cf. Alfvén and Mendis, 1977; Pollaine, 1978); here $R(t)$ is the cosmic scale factor and t_0 the epoch of observation. Obviously z_a is a function not only of t_a but also of the deceleration parameter q_0.

Once present in the intergalactic medium, dust grains would be virtually indestructible (Margolis and Schramm, 1977) and if grain number is conserved during the expansion the proper number density of grains n_d at redshift z is given as usual by

$$\begin{aligned} n_d(z) &= n_d(0)(1+z)^3 \qquad (z \leq z_a) \\ &= 0 \qquad\qquad\qquad (z > z_a) \end{aligned} \tag{3}$$

where $n_d(0)$ is the local number density of intergalactic dust grains. This dependence of n_d on z would apply if each galaxy capable of grain formation experienced during its early evolution a phase of rapid and short-lived heavy element production, grain formation and ejection. The latter would be particularly effective if, at the relevant time, grain producing galaxies were more luminous than they presently appear to be (cf. Schmidt, 1974). Furthermore, we assume that the proper number density of grain producing galaxies also increases as $(1+z)^3$ and that the ejected grains partake in the expansion. If grain production and ejection have been proceeding continuously since time t_a, a somewhat weaker dependence on z would be appropriate in Eq. (3).

In the expression for n_d we have neglected the possibility that grains may have formed before time t_a, for example from condensible material produced in pregalactic stars (e.g. Schmidt, 1974; Pollaine, 1978). However, an estimate of the likely abundance of heavy elements from such objects (Pollaine, 1978) shows that even if grain formation from heavy elements is 100% efficient the grain density at times corresponding to $z > z_a$ was negligible by comparison with that in more recent epochs.

In order to compute the optical depth for intergalactic dust we assume as usual (e.g. Nandy et al., 1974; Schmidt, 1974; Alfvén and Mendis, 1977; Pollaine, 1978) that at long wavelengths, $\sigma \propto \lambda^{-1}$. Thus, using the normalization of Nandy et al. (1974) for the intergalactic extinction law, we have

$$\begin{aligned} \tau_d(f_0, q_0) = \frac{A_0}{1.086}\frac{c/H_0}{L}\frac{n_d(0)}{n_e}\frac{f_0}{15q_0^3} \\ \cdot\{(1+2q_0z_a)^{1/2}[3q_0^2(1+z_a)^2 \\ + 2q_0(2q_0-1)(1+z_a) + 2(1-2q_0)^2] \\ - 15q_0^3 + 10q_0 - 2\}. \end{aligned} \tag{4}$$

Here $z_a = z_a(q_0)$ is given by Eq. (2), $f_0 = \lambda_0^{-1}$, λ_0 being the observing wavelength in μm, $A_0 = 0.55$, n_e is the number density of interstellar grains and L is a normalization distance on 1 kpc. Throughout we take $\lambda_0 = 1$ cm (cf. Boynton, 1974). Following Nandy et al. (1974),

$$\frac{n_d(0)}{n_e} = \mu = 10^{-7}\left\{\frac{H_0}{75\ \text{km/s/Mpc}}\right\},$$

which leads to a grain density of 10^{-33} g cm^{-3}. This amount of grains ($\sim 2\,10^{-4}$ times the closure density) has negligible effect on the dynamics of the universe. It should be noted that, in arriving at this value for μ, Nandy et al. assumed $q_0 = 1$, but their choice of q_0 should not have a significant effect on their derived value of μ.

From Eq. (4), we may regard τ_d as a function of q_0 (including, of course, the q_0-dependence of z_a, as given by Eq. (2)). The variation of τ_d with q_0 is shown in Fig. 1 (curve A), in which we note that τ_d increases with decreasing q_0, for reasons discussed by Pollaine (1978). The largest optical depth is found in the "empty" Milne ($q_0 = 0$) universe, in which

$$\tau_d(q_0 = 0) = \frac{A_0}{1.086}\frac{c/H_0}{L}\mu\frac{f_0}{3}[(H_0t_0)^{-2} - 1].$$

From Fig. 1 we see that for the amount of intergalactic dust proposed by Nandy et al. (1974), and with conservation of grain number, the universe is transparent to the background radiation only if $q_0 > 0.05$. Thus if dust grains are present in the intergalactic medium to the extent proposed by Nandy et al. (1974) and Schmidt (1974), any fluctuations in the microwave background would be visible only if $q_0 > 0.05$. If intergalactic dust is responsible for obscuring pregalactic fluctuations, then $q_0 \leq 0.05$.

This upper limit on q_0 applies if pregalactic fluctuations are hidden by intergalactic dust, with local density 10^{-33} g cm^{-3} and proper number density obeying Eq. (3). However, it is quite likely that Eq. (4) over-estimates the optical depth τ_d for a number of reasons.

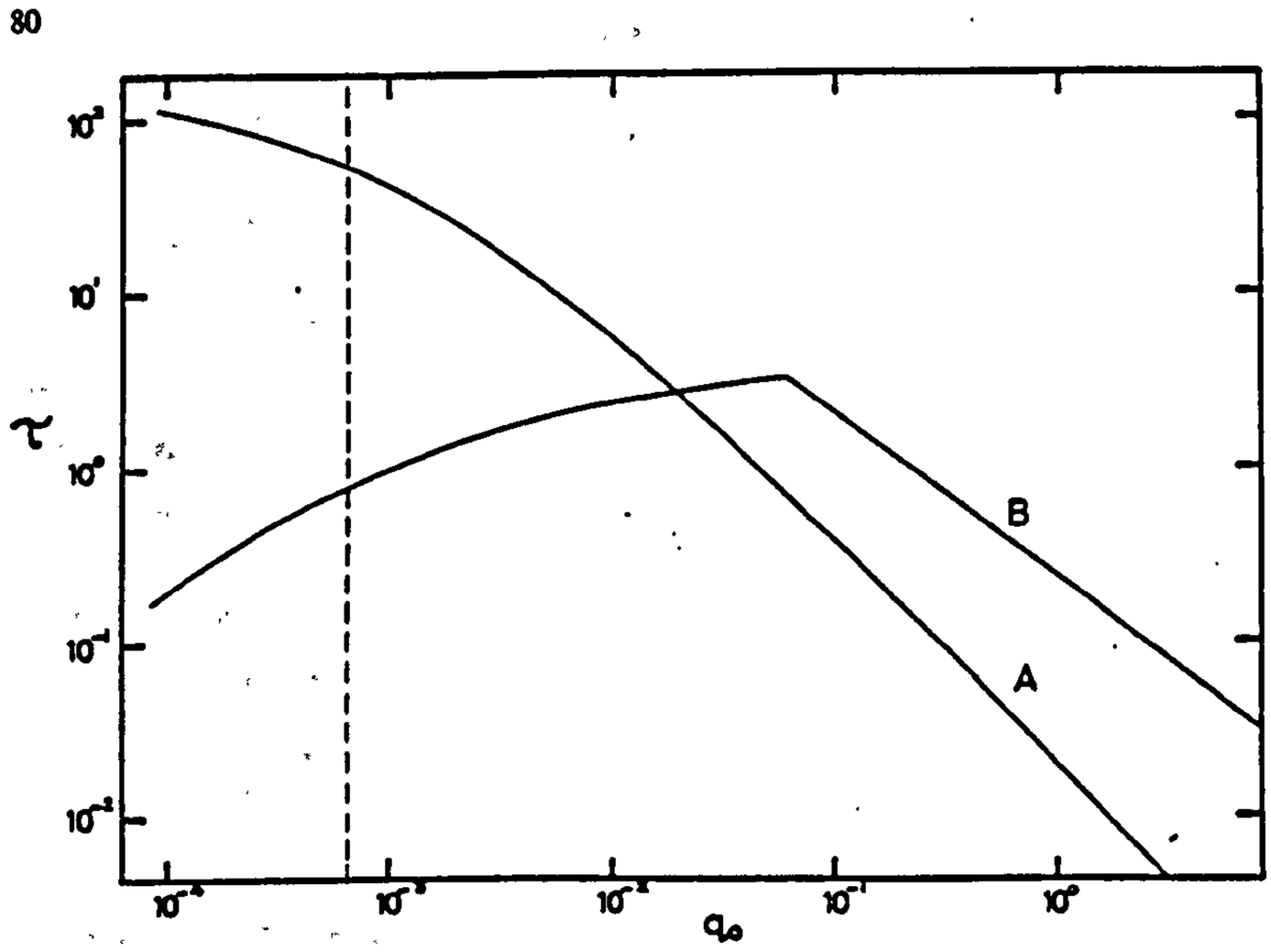

Fig. 1. Dependence of optical depth, at 1 cm observing wavelength, on deceleration parameter q_0 for intergalactic dust (curve A) and free electrons (curve B); see text for details. Broken vertical line is known lower limit on q_0 from the amount of matter observed in the form of galaxies

Firstly, the values assumed for H_0 and t_G, while acceptable in themselves, may also be lower limits on these quantities (Gott et al., 1974; Field, 1975). If the product $H_0 t_G$ were larger than we have assumed, τ_d would be correspondingly smaller, because of Eq. (2). [We note that, since $\mu \propto H_0$, changing H_0 has no effect on the factor outside the brackets in Eq. (4).]

Secondly, there is no evidence that intergalactic dust exists beyond $z \sim 2.2$, the limiting redshift in the data of Nandy et al. (1974) and Schmidt (1974). It may therefore be too liberal an extrapolation to populate the intergalactic medium with dust grains to redshift z_G (~ 100 for $q_0 \sim 0.01$). For example, even if grain producing galaxies did form at time t_G, grain production may not have commenced until some time later.

Thirdly, if we do suppose that grain production and ejection have proceeded continuously since time t_G – and the mechanism of Chiao and Wickramasinghe (1972) suggests that the process is an ongoing one – the optical depth to intergalactic dust would be considerably less than that expected from Eq. (4) even if the local grain density were as high as 10^{-33} g cm^{-3}, as suggested by Nandy et al. (1974) and Schmidt (1974). This is because there would be fewer grains at very large redshifts than Eq. (3) and the assumed value of $n_d(0)$ would imply, as already noted.

For these reasons, curve A in Fig. 1 represents an upper limit on the opacity of intergalactic dust to the background radiation. Hence whatever the values of H_0 and t_G, and whatever the distribution of intergalactic dust, $q_0 \leq 0.05$ if dust is responsible for obscuring pregalactic fluctuations.

We now consider Thomson scattering by free electrons.

IV. Thomson Scattering

The possibility that embryonic galaxies might be obscured by intergalactic electrons has of course been discussed by several authors (see e.g. Weinberg (1972) and Sunyaev (1977) and references therein). However, previous workers have assumed that the local number density of electrons $n_e(0)$ is given in terms of q_0 by the expression

$$n_e(0) = \frac{3H_0^2 q_0}{4\pi G m_H} x \qquad (5)$$

where G is the constant of gravitation, m_H is the mass of a hydrogen atom and x ($\lesssim 1$) allows for possible nonhydrogenic content of the intergalactic medium (e.g. $x = 0.88$ for a helium abundance of 25% by weight, as we shall assume here). Obviously this assumption presupposes that all dynamically significant matter is ionized and uniformly distributed between galaxies. However evidence available at present seems to indicate that there is in fact little matter between galaxies (e.g. Gott et al., 1974) and so the usual assumption $n_e(0) \propto q_0$ is not entirely justified.

Although equation (5) provides an extreme upper limit on $n_e(0)$, a more meaningful limit $n_e(0) < 3\,10^{-7}$ cm^{-3} has been suggested by the work of Gott and Gunn (1972), who considered the consequences of the infall of intergalactic gas into the Coma cluster. Their argument has been criticized by, amongst others, Field (1974), on the grounds that they assumed the intergalactic gas to be cool, whereas X-ray evidence points to its being hot. However, as shown by Cowsik and Lerche (1975), the effect of hot intergalactic gas on the rotation of galaxies also implies $n_e(0) < 3\,10^{-7}$ cm^{-3}. Also we may note that a similar upper limit on $n_e(0)$, based on photoionization of intergalactic hydrogen by quasars, has been set by Arons and Wingert (1972).

For $q_0 < 0.06$, the upper limit $n_e(0) < 3\,10^{-7}$ cm^{-3} exceeds the maximum allowable by Eq. (5). Accordingly we assume for $n_e(0)$ the upper limit

$$n_e(0) < 4.9\,10^{-6} q_0 \text{ cm}^{-3} \qquad (q_0 < 0.06) \qquad (6a)$$

$$n_e(0) < 3\,10^{-7} \text{ cm}^{-3} \qquad (q_0 > 0.06) \qquad (6b)$$

where Eq. (6a) derives directly from Eq. (5). We use the Eqs. (6) for $n_e(0)$ to compute the opacity of the intergalactic medium to Thomson scattering.

The optical depth to Thomson scattering is given by equation (1) with $\sigma = \sigma_T$, the Thomson cross-section:

$$\tau_e(q_0) = \frac{c}{H_0}\sigma_T n_e(0)\int_0^{z_m}(1+z')(1+2q_0z')^{-1/2}dz'$$

$$= \frac{c}{H_0}\sigma_T\frac{n_e(0)}{3q_0^2}$$

$$\cdot\{(1+2q_0z_m)^{1/2}(3q_0+q_0z_m-1)+1-3q_0\}, \quad (7)$$

where

$$z_m = z_e \quad (z_e < z_0) \quad (8a)$$

$$= z_0 \quad (z_e > z_0) \quad (8b)$$

and

$$z_e = 5.4\,10^{-3}\{n_e(0)\}^{-2/3}.$$

Equation (8a) gives the redshift at which complete reionization of the intergalactic gas by strong sources of ultraviolet radiation occurs, determined by the method of Sunyaev (1977); while Eq. (8b) expresses the fact that these sources did not exist before galaxy formation. Also we have assumed that the dependence of the proper number density of electrons on redshift obeys Eq. (3).

The dependence of τ_e on q_0, computed by means of Eqs. (6), (7), and (8), is shown in Fig. 1 (curve B). Curve B is, like curve A, an upper limit, not only by virtue of the upper limit on $n_e(0)$ but also in view of the remarks made in the previous section concerning the values of H_0 and t_0.

We note that, with the q_0-independent limit on $n_e(0)$, Eq. (6b), τ_e increases with decreasing q_0 (cf. curve A); whereas when the limit on $n_e(0)$ is q_0-dependent, as in Eq. (6a), τ_e *decreases* with decreasing q_0. Consequently we have the upper limit

$$\tau_e < 3.3 \quad (9)$$

on the optical depth of the intergalactic medium to Thomson scattering.

If we take curve B at face value, the intergalactic medium is optically thick to Thomson scattering for

$$8.4\,10^{-4} < q_0 < 0.2.$$

We note that the lower limit on q_0 is of the same order as the extreme lower limit ($q_0 > 6.5\,10^{-4}$) derived by Gott et al. (1974) on the basis of the amount of matter observed in individual Supercluster galaxies; while the upper limit is of the same order as that derived in the previous section. We note, however, that in view of the upper limit (9), Thomson scattering is unlikely to be effective in obscuring embryonic galaxies and that if it is to contribute to the opacity of the intergalactic medium at all, the local number density of electrons cannot be significantly below the limits set by the Eqs. (6).

V. Concluding Remarks

If we ascribe the failure to detect small scale fluctuations in the microwave background to the opacity of the intervening medium, the only plausible agencies are intergalactic dust and Thomson scattering by free electrons. The former is capable of rendering the intergalactic medium opaque – and hence of hiding young galaxies – if $q_0 < 0.05$; while the latter can do so – but not particularly effectively – if $q_0 < 0.2$. In view of the fact that both curves in Fig. 1 are upper limits, failure to observe fluctuations in the microwave background would imply $q_0 \ll 0.1$ if we are correct in assuming that such failure is a result of the opacity of the intervening medium. [Obviously q_0 cannot be arbitrarily small as the *extreme* lower limit $q_0 > 6.5\,10^{-4}$ (Gott et al., 1974) must be satisfied.] Such a low value of q_0 would be contrary to that recently derived from the Hubble diagram (Kristian et al., 1978) and its uncertain evolutionary corrections, but would be in line with values obtained without reference to the Hubble diagram (e.g. Gott et al., 1974; Sandage and Tammann, 1975).

If fluctuations in the microwave background are not observable as a result of intervening material, then we may conclude that the universe must certainly be open ($q_0 < 0.5$), and is probably so by a fairly comfortable margin.

Acknowledgement. One of us (M.F.B.) is in receipt of a University of Keele Research Studentship.

References

Alfvén, H., Mendis, A.: 1977, *Nature* 266, 698
Arons, J., Wingert, D.W.: 1972, *Astrophys. J.* 177, 1
Boynton, P.E.: 1974, in *Confrontation of Cosmological Theories with Observational Data*, ed. M. S. Longair, D. Reidel Publ. Co., 163
Chiao, R.Y., Wickramasinghe, N.C.: 1972, *Monthly Notices Roy. Astron. Soc.* 159, 361
Cowsik, R., Lerche, I.: 1975, *Astrophys. J.* 199, 555
Field, G.B.: 1974, in *Confrontation of Cosmological Theories with Observational Data*, ed. M.S. Longair, D. Reidel Publ. Co., 13
Field, G.B.: 1975, in *Stars and Stellar Systems. IX. Galaxies and the Universe*, eds. A. Sandage, M. Sandage, and J. Kristian, Univ. Chicago Press, 359
Gott, J.R., Gunn, J.E., Schramm, D.N., Tinsley, B.M.: 1974, *Astrophys. J.* 194, 543
Gunn, J.E., Gott, J.R.: 1972, *Astrophys. J.* 176, 1
Kristian, J., Sandage, A., Westphal, J.A.: 1978, *Astrophys. J.* 221, 383
Margolis, S.H., Schramm, D.N.: 1977, *Astrophys. J.* 214, 339
Nandy, K., Morgan, D.H., Reddish, V.C.: 1974, *Monthly Notices Roy. Astron. Soc.* 169, 19P
Peebles, P.J.E.: 1974, Physical Cosmology, Princeton Univ. Press, 2nd Edition
Pollaine, S.: 1978, *Nature* 271, 426
Sandage, A., Tammann, G.A.: 1975, *Astrophys. J.* 197, 265
Schmidt, K.H.: 1974, *Astron. Nachr.* 295, 163
Sunyaev, R.A.: 1977, in *Radio Astronomy and Cosmology*, ed. D.L. Jauncey, D. Reidel Publ. Co., 327
Weinberg, S.: 1972, Gravitation and Cosmology, J. Wiley and Sons, Inc.
Wickramasinghe, N.C., Edmunds, M.G., Chitre, S.M., Narlikar, J.V., Ramadurai, S.: 1975, *Astrophys. Space Sci.* 35, L9

REFERENCES

Abramowitz, M. & Stegun, I., 1972. 'Handbook of Mathematical Functions' (Dover, New York).

Alcock, G. E. D., 1976. I.A.U. Circ. No. 2997.

Alfven, H. & Mendis, A., 1977. Nature, 266, 698.

Allen, C. W., 1973. Astrophysical Quantities, 3rd Edn. (Athlone, Press, London).

Andersen, P. H., Borra, E. F. & Dubas, O. V., 1971. P.A.S.P., 83, 491.

Antipova, L. I., 1978. Sov. Astron. Lett., 4, 45.

Arp, H., 1956. A. J., 61, 15.

Arons, J. & Wingert, D. W., 1972. Ap. J., 177, 1.

Bath, G. T. & Shaviv, G., 1976. M.N.R.A.S., 175, 305.

Bath, G. T., 1978(a). Q.J.R.A.S., 19, 442.

Bath, G. T., 1978(b). M.N.R.A.S., 182, 35.

Bath, G. T. & Shaviv, G., 1978. M.N.R.A.S., 183, 515.

Bath, G. T., 1979. Private Communication.

Blandford, R. D., McKee, C. F. & Rees, M. J., 1977. Nature, 267, 211.

Bode, M. F. & Evans, A., 1979(a). Astron. Astrophys., 73, 113.

Bode, M. F. & Evans, A., 1979(b). Astron. Astrophys., 78, 78.

Borra, E. F. & Andersen, P. H., 1970. P.A.S.P., 82, 1070.

Bosma, P. B., 1975. Astron, Astrophys., 40, 185.

Boyarchuk, A. A. & Gershberg, R. E., 1977. Astron. Zh., 54, 488.

Brecher, K., Ingham, W. H. & Morrison, P., 1977. Ap. J., 213, 492.

Burbidge, G. R. & Stein, W. A., 1970. Ap. J., 160, 573.

Burkhead, M. S. & Seeds, M. A., 1970. Ap. J. (Letters), 160, L51.

Burkhead, M. S., Penhallow, W. S. & Honeycutt, R. K., 1971. P.A.S.P., 83, 338.

Carpenter, R. L., Gulkis, S. & Sato, J., 1973. Ap. J. (Letters), 182, L61.

Cassatella, A., Bevenuti, P., Clavel, J., Heck, A., Penston, M., Selvelli, P. L. & Macchetto, F., 1979. Astron. Astrophys., 74, L18.

Chiao, R. Y. & Wickramasinghe, N. C., 1972. M.N.R.A.S., 159, 361.

Ciatti, F. & Rosino, L., 1974. Astron. Astrophys. Suppl., 16, 305.

Ciatti, F., Mammano, A. & Vittone, A., 1977. Astron. Astrophys., 61, 459.

Clayton, D. D. & Hoyle, F., 1976. Ap. J., 203, 490.

Clayton, D. D. & Wickramasinghe, N. C., 1976. Astrophys. and Sp. Sci., 42, 463.

Code, A. D., 1972. In 'Scientific Results from OAO - 2', ed. A. D. Code (NASA, SP310), p. 535.

Cohen, M., Barlow, M. J. & Kuhi, L. V., 1975. Astron. Astrophys., 40, 291.

Collin-Souffrin, S., 1977. In 'Novae and Related Stars', p. 123 (D. Reidel, Dordrecht).

Cottrell, M. J. & Smith, S. E., 1978. P.A.S.P., 90, 615.

Couderc, P., 1939. Ann. d'Astrophys., 2, 271.

Cowsik, R. & Lerche, I., 1975. Ap. J., 199, 555.

Davidson, K., Humphreys, R. M. & Merrill, K. M., 1978. Ap. J., 220, 239.

Draine, B. T., 1977. "Sputtering", Cornell Univ. Centre for Radiophysics and Space Research, preprint no. CRSR 669.

Draine, B. T. & Salpeter, E. E., 1979. Ap. J., 231, 438.

Dunlop, S., 1979. Private Communication of B.A.A.V.S.S. observations.

Ennis, D., Becklin, E. E., Beckwith, S., Elias, J., Gatley, I., Matthews, K., Neugebauer, G. & Willner, S. P., 1977. Ap. J., 214, 478.

Evans, A., 1979. Private Communication.

Faulkner, J., 1974. In 'Late Stages of Stellar Evolution', I.A.U. Symp. No. 66, Ed. Taylor, (D. Reidel, Dordrecht).

Feast, M. W. & Glass, I. S., 1974. M.N.R.A.S., 167, 81.

Ferland, G. J. & Sheild, G. A., 1978. Ap. J. (Letters), 224, L15.

Ferland, G. J., Lambert, D. L., Netzer, H., Hall, D. N. B. & Ridgway, S. T., 1979. Ap. J., 227, 489.

Field, G. B., 1972. Ann. Rev. Astron. Astrophys., 10, 227.

Field, G. B., 1974. In 'Stars and Stellar Systems', Vol. IX, Eds. A. & M. Sandage & J. Kristian (Chicago, Chicago Univ. Press).

Forrest, W. J., Gillett, F. C. & Stein, W. A., 1975. Ap. J., 195, 423.

Friedjung, M., 1977. In 'Novae and Related Stars', Ed. M. Friedjung (D. Reidel, Dordrecht), p. 95.

Gallagher, J. S. & Holm, A. V., 1973. Bull. Am. Astron. Soc., 5, 387.

Gallagher, J. S. & Code, A. D., 1974. Ap. J., 189, 303.

Gallagher, J. S., 1977. A. J., 82, 209.

Gallagher, J. S. & Ney, E. P., 1977. Ap. J. (Letters), 204, L35.

Gehrz, R. D., Grasdalen, G. L., Hackwell, J. A. & Ney, E. P., 1978. I.A.U. Circ., No. 3296.

Gehrz, R. D., Hackwell, J. A. & Briotta, D., 1978. Ap. J. (Letters), 221, L23.

Geisel, S. L., Kleinmann, D. E. & Low, F. J., 1970. Ap. J. (Letters), 161, L101.

Geisel, S. L., 1970. Ap. J. (Letters), 161, L105.

Gilman, R. C., 1972. Ap. J., 178, 423.

Gilman, R. C., 1973. M.N.R.A.S., 161, 3P.

Gilman, R. C., 1974. Ap. J. Supplement, No. 268, p. 397.

Gilra, D. P., 1971. Nature, 229, 237.

Goldsmith, A., Waterman, T. E. & Hirschorn, H. J., 1961. In 'Handbook of Thermophysical Properties of Solid Materials', Vol. 1 (MacMillan Co., New York).

Gorynya, N., 1976. I.A.U. Circ. No. 3008.

Gott, J. R., Gunn, J. E., Schramm, D. N. & Tinsley, B. M., 1974. Ap. J., 194, 543.

Gradshteyn, I. S. & Ryzhik, I. M., 1965. 'Tables of Integrals, Series and Products' (Academic Press, London).

Greenberg, J. M., 1968. In 'Stars and Stellar Systems', Vol. VII, Ed. B. M. Middlehurst & L. Aller, p. 221 (Chicago, Univ. Chicago Press).

Greenberg, J. M., 1973. In 'Interstellar Dust and Related Topics', I.A.U. Symp. No. 52, Eds. Greenberg & van de Hulst (D. Reidel, Dordrecht).

Greenberg, J. M., 1976. In 'Far Infra-red Astronomy', Ed. M. Rowan-Robinson, p. 299, (Pergamon Press, London).

Greenberg, J. M., 1978. In 'Cosmic Dust', Ed. J. A. M. McDonnell (Wiley, London).

Greenberg, J. M., 1979. Private Communication.

Grenfell, T. C., 1971. P.A.S.P., 83, 66.

Grygar, J., Smolinski, J. & Hutchings, J. B., 1971. P.A.S.P., 83, 15.

Harvel, C. M., 1974. 'Radiative Transfer in Circumstellar Dust', Ph.D. Thesis, Univ. Florida.

Harvey, P. M., Harley, A. T. & Gatley, T., 1979. Ap. J., 231, 115.

Hirose, H., 1970. I.A.U. Circ. No. 2212.

Hjellming, R. M. & Wade, C. M., 1970. Ap. J. (Letters), 162, L1.

Hoyle, F. & Wickramasinghe, N. C., 1962. M.N.R.A.S., 124, 418.

Huffman, D. R. & Stapp, J. L., 1973. In 'Interstellar Dust and Related Topics', I.A.U. Symp. No. 52, Ed. J. M. Greenberg (D. Reidel, Dordrecht).

Hutchings, J. B., 1972. M.N.R.A.S., 158, 177.

Hutchings, J. B. & Fisher, W. A., 1973. P.A.S.P., 85, 122.

Hyland, A. R. & Neugebauer, G., 1970. Ap. J. (Letters), 160, L177.

Isobe, S., 1971. Ann. Tokyo Astron. Obs., 12, 263.

Jones, T. W., Leung, C. M., Gould, R. J. & Stein, W. A., 1977. Ap. J., 212, 52.

Joseph, R. D., 1979. Private Communication.

Klare, G. & Wolf, B., 1978. Astron. Astrophys. Suppl., 33, 327.

Kleinmann, D. E. & Low, F. J., 1967. Ap. J. (Letters), 149, L1.

Kohoutek, L. & Klawittler, P., 1973. Astron. Astrophys. Suppl., 11, 347.

Kraft, R. P., 1963. Adv. Astron. Astrophys., 2, 43.

Krelowski, J., 1978. Private Communication.

Larson, R. B., 1969. M.N.R.A.S., 145, 297.

Lefèvre, J., 1979. Astron. Astrophys., 72, 61.

Lindblad, B., 1935. Nature, 135, 133.

Livio, M., Salzman, J. & Shavin, G., 1979. M.N.R.A.S., 188, 1.

Low, F. J., 1978. Private Communication.

Malakpour, I., 1973. Astron. Astrophys., 28, 393.

Malakpour, I., 1977. Astrophys. & Sp. Sci., 47, 49.

Malakpour, I., 1978. In 'The Interaction of Variable Stars with their Environment' (I.A.U. Coll. No. 42, Bamberg), p. 214, Ed. R. Kippenhahn and J. Rahe (Bamberg: Remeis Sternwarte).

Margolis, S. H. & Schramm, D. N., 1977. Ap. J., 189, 17.

Martin, P. G., 1978. "Cosmic Dust" (Oxford Univ. Press).

McCarthy, D. W., Howell, R. & Low, F. J., 1978. Ap. J. (Letters), 223, L113.

McKee, C. F. & Petrosian, V., 1974. Ap. J., 189, 17.

McLaughlin, D. B., 1960. In 'Stars and Stellar Systems', Vol. VI, Ed. Kuiper (Chicago, Chicago Univ. Press).

Mie, G., 1908. Ann. Physik., 25, 377.

Morrison, P. & Sartori, L., 1969. Ap. J., 158, 541.

Nandy, K., Morgan, D. H. & Reddish, V. C., 1974. M.N.R.A.S., 169, 19.

Nandy, K., Thompson, G. I., Cornochan, D. J. & Wilson, R., 1978. M.N.R.A.S., 184, 733.

Nariai, K., 1974. Astron. Astrophys., 36, 231.

Neugebauer, G., 1978. Physica Scripta., 17, 149.

Ney, E. P. & Hatfield, B. F., 1978. Ap. J. (Letters), 219, L111.

Nickerson, B. G. & Partridge, R. B., 1971. Ap. J., 169, 202.

Pacholczyk, A. G., 1970. "Radio Astrophysics", (Freeman & Co., San Francisco).

Papousek, J. & Vetesnik, M., 1977. Astron. Zh., 54, 600.

Partridge, R. B. & Peebles, P. J. E., 1967. Ap. J., 147, 868.

Pataschnick, H. & Rupprecht, G., 1977. Icarus, 30, 402.

Payne-Gaposchkin, C., 1957. 'The Galactic Novae', (Dover, New York).

Peebles, P. J. E., 1974. 'Physical Cosmology', (Princeton, Princeton Univ. Press).

Penston, M. V., Penston, M. J., Selmes, R. A., Becklin, E. E. & Neugebauer, G., 1974. M.N.R.A.S., 169, 357.

Penzias, A. A. & Wilson, R. W., 1965. Ap. J., 142, 419.

Pesch, P., 1975. I.A.U. Circ. No. 2835.

Phillips, J. P., Wade, R., Selby, M. J. & Sanchez Magro, C., 1979. M.N.R.A.S., 187, 45.

Pollaine, S., 1978. Nature, 271, 426.

Pottasch, S. R., 1967. Bull. Astron. Inst. Neth., 19, 227.

Pottasch, S., Wesselius, P. R., Wu, C. -C. & van Duinen, R. J., 1977. Astron. Astrophys., 54, 435.

Puetter, R. C., Russell, R. W., Soifer, B. T. & Willner, S. P., 1978. Ap. J. (Letters), 223, L93.

Rees, M. J., Silk, J. I., Werner, M. W. & Wickramasinghe, N. C., 1969. Nature, 223, 788.

Reimers, D., 1975. Mem. Soc. Roy. Sci. Liege, Ser. 6, 8, 369.

Robinson, E. L., 1973. Ap. J., 186, 347.

Rowan-Robinson, M., 1974. M.N.R.A.S., 172, 109.

Salpeter, E. E., 1974. Ap. J., 193, 585.

Salpeter, E. E., 1977. Ann. Rev. Astron. Astrophys., 15, 267.

Samus, N. N., 1975. I.A.U. Circ. No. 2828.

Sanduleak, N. & Chen, P., 1975. I.A.U. Circ. No. 2835.

Sanyal, A., 1974. Ap. J. Suppl., 28, 115.

Sato, S., Maihara, T. & Okuda, H., 1973. Pub. Astron. Soc. Japan, 25, 571.

Sato, S., Kawara, K., Kobayashi, Y., Maihara, T., Oda, N. & Okuda, H., 1978. Pub. Astron. Soc. Japan, 30, 419.

Schmidt, K. -H., 1974. Astron. Nachr., Bd., 295, 163.

Sparks, W. M., Starrfield, S. & Truran, J. W., 1977. In 'Novae and Related Stars', p. 189, Ed. M. Friedjung (D. Reidel, Dordrecht.)

Starrfield, S., Sparks, W. M. & Truran, J. W., 1974. Ap. J. Suppl., 28, No. 261, 247.

Stebbins, J., Huffer, C. H. & Whitford, A. E., 1939. Ap. J., 90, 209.

Stratton, F. J. M., 1928. Handbook of Astrophys., 6, 251.

Strecker, D. W. & Ney, E. P., 1974. Ap. J., 79, 797.

Sunyaev, R. A., 1971. Astron. Astrophys., 12, 190.

Sunyaev, R. A., 1977. "Radio Astronomy and Cosmology", I.A.U. Symp. No. 74, p. 327, Ed. Jauncey (D. Reidel, Dordrecht).

Svolopoulos, S., 1966. P.A.S.P., 78, 157.

Szkody, P., 1977. Ap. J., 217, 140.

Terrell, J., 1967. Ap. J., 147, 827.

Tinsley, B. M., 1972. Ap. J., 178, 319.

Ubbelohde, A. R. & Lewis, F. A., 1960. 'Graphite and its Crystal Compounds' (Oxford Univ. Press, London).

Van de Hulst, H. C., 1957. 'Light Scattering by Small Particles' (Wiley, New York).

Van Genderen, A. M. & Uiterwaal, G. M., 1979. Astron. Astrophys. Suppl,, 36, 265.

Vrba, F. J., 1978. Private Communication.

Vrba, F. J., Schmidt, G. D. & Burke, E. W., 1977. Ap. J., 211, 480.

Wade, C. M. & Hjellming, R. M., 1971. Ap. J. (Letters), 163, L65.

Wallerstein, G., 1968. P.A.S.P., 81, 157.

Warner, B., 1976. In 'Structure and Evolution of Close Binary Systems', I.A.U. Symp. No. 73, Eds. P. Eggleton et al. (D. Reidel, Dordrecht).

Weinberg, S., 1972. 'Gravitation and Cosmology; Principles and Applications of the General Theory of Relativity', (John Wiley and Sons, New York).

Wickramasinghe, N. C., 1967. 'Interstellar Grains' (Chapman & Hall).

Wickramasinghe, N. C., 1972. M.N.R.A.S., 159, 269.

Wickramasinghe, N. C., 1973. 'Light Scattering Functions for Small Particles', (Hilger, London).

Wild, P., 1975. I.A.U. Circ. No. 2788.

Williams, P. H., Beattie, D. H., Lee, T. J. & Stewart, J. M., 1978. M.N.R.A.S., 185, 467.

Witt, A. N., 1973. In 'Interstellar Dust and Related Topics', I.A.U. Symp. No. 52, Ed. J. M. Greenberg (D. Reidel, Dordrecht).

Wright, E. L., 1979. Private Communication.

Wu, C. -C. & Kester, D., 1977. Astron. Astrophys., 58, 331.

Yamamoto, T. & Nishida, S., 1977. Progress Th. Phys., 57, 1939.

Zellner, B., 1971. A. J., 76, 651.

Zellner, B. & Morrison, N. D., 1971. A. J., 76, 645.